NASA
Reference
Publication
1208

August 1988

Present State of Knowledge of the Upper Atmosphere 1988: An Assessment Report

R. T. Watson and Ozone Trends Panel,
M. J. Prather and Ad Hoc Theory Panel,
and M. J. Kurylo and NASA Panel for
Data Evaluation

NASA

NASA Reference Publication 1208

1988

Present State of Knowledge of the Upper Atmosphere 1988: An Assessment Report

R. T. Watson and Ozone Trends Panel,
M. J. Prather and Ad Hoc Theory Panel,
and M. J. Kurylo and NASA Panel for
Data Evaluation
NASA Office of Space Science and Applications
Washington, D.C.

National Aeronautics
and Space Administration

**Scientific and Technical
Information Division**

TABLE OF CONTENTS

SECTION A

INTRODUCTION

In compliance with the Clean Air Act Amendments of 1977, Public Law 95-95, the National Aeronautics and Space Administration (NASA) has prepared a report on the state of our knowledge of the Earth's upper atmosphere, particularly the stratosphere. The report is composed of two parts. The first part which was issued earlier summarized the objectives, status, and accomplishments of the research tasks supported under the NASA (UARP). Part II is the present document and summarizes the evidence for changes in the chemical composition and physical structure of the stratosphere, in particular the abundance and distribution of ozone; the results of theoretical model calculations of how ozone may change in the future in response to increased atmospheric abundances of trace gases, primarily methane, carbon dioxide, nitrous oxide, halons, and chlorofluorocarbons (CFCs); and a review of the photochemical and chemical kinetics data that are used as input parameters for the atmospheric models.

For more than a decade scientists have postulated that man-made pollutants could cause harmful effects by reducing the amount of stratospheric ozone. In recognition of the importance of understanding such perturbations, Congress directed NASA in June 1975 to "develop and carry out a comprehensive program of research, technology, and monitoring of the phenomena of the upper atmosphere so as to provide for an understanding of and to maintain the chemical and physical integrity of the Earth's upper atmosphere". Responding to this Congressional mandate, NASA implemented a long-range upper atmospheric science program aimed at developing a comprehensive body of knowledge of upper atmospheric processes. In the near term NASA has a mandate to provide biennial reports to the Congress and concerned regulatory agencies on the status of upper atmospheric research, including scientific assessments of potential effects of human activities on the atmosphere, and particularly, on stratospheric ozone.

Many governments around the world, including the United States, have recognized that the ozone layer must be protected in order to protect human health and aquatic and terrestrial ecosystems from damage due to enhanced levels of ultraviolet radiation. In particular, it was recognized that the use of chlorine (chlorofluorocarbons (CFCs)) and bromine (halons) containing chemicals constitute a potential threat to the stability of the ozone layer. More than twenty nations, including the United States, signed the Vienna Convention for the Protection of the Ozone Layer in Vienna, Austria, in March 1985, and the Montreal Protocol on Substances that Deplete the Ozone Layer, in Montreal, Canada, in September 1987. The United States has also ratified both the Vienna Convention and the Montreal Protocol. The Vienna Convention and the Montreal Protocol both call for all regulatory decisions to be based on a scientific understanding of the issues, and specifically the Montreal Protocol calls for an international scientific assessment in 1989 in preparation for the 1990 policy review.

NASA recognizes the need for timely international scientific assessments when important new information becomes available as has occurred since the last major international scientific assessment (WMO, 1986). Reports based on Nimbus 7 satellite Solar Backscatter Ultraviolet (SBUV) and Total Ozone Mapping Spectrometer (TOMS) data claimed that large global decreases have occurred since 1979 in the total column of ozone

(about 1% per year) and in its concentration near 50 km altitude (about 3% per year). Data from the ground-based Dobson network also indicated that the total column content of ozone had decreased on a global scale significantly since 1979, although to a lesser extent than suggested by the satellite data. Further, there has been a significant amount of new research focussed on understanding the extent and cause of the depletion of ozone in the spring-time over the Antarctic.

NASA and the rest of the scientific community believed that it was imperative to evaluate whether the Nimbus 7 satellite data had been analyzed correctly, and if so, whether the reported decreases were due to natural causes such as a decrease in solar radiation (from solar maximum in 1979 to solar minimum in 1986), the 1982 volcanic eruption of El-Chichon, or the 1982 El-Nino event, or whether it was due to human activities such as the use of chlorofluorocarbons (CFCs). Therefore, during the fall of 1986 NASA decided to coordinate and cosponsor with the Federal Aviation Administration (FAA), the National Oceanic and Atmospheric Administration (NOAA), the World Meteorological Organization (WMO), and the United Nations Environmental Program (UNEP) a major review of all ground-based and satellite ozone data. A panel (the Ozone Trends Panel) composed of eminent scientists from federal agencies, research institutions, private industry, and universities was selected.

The Ozone Trends Panel report critically assessed whether the chemical composition and physical structure of the stratosphere has changed over the last few decades and whether our current understanding of the influence of natural phenomena and human activities is consistent with the observed change. The report is different from most previous national and international scientific reviews in that it did not simply review the published literature but performed a critical reanalysis and interpretation of nearly all ground-based and satellite data for total column ozone and the vertical profiles of ozone. To aid in the interpretation of the results of the re-analysis of the data a series of theoretical calculations for comparison with the reanalyzed ozone data was performed.

The executive summary of the Ozone Trends report was issued on March 15, 1988 and covered: (a) Spacecraft Instrument Calibration and Stability; (b) Information Content of Algorithms; (c) Trends in Total Column Ozone; (d) Trends in Ozone Profile Measurements; (e) Trends in Stratospheric Temperatures; (f) Comparison of Observed and Theoretically Predicted Trends of Ozone; (g) Trends in Source Gases; (h) Trends in Stratospheric Minor Constituents; (i) Trends in Aerosol Abundances and Distribution; (j) Observations and Theories Related to the Antarctic Ozone Hole; and (k) Statistical Procedures used to Analyze Trend Data.

This present NASA report is the sixth ozone assessment report submitted to Congress and the concerned regulatory agencies. Part 1 of this report contained an outline of the NASA Upper Atmospheric Research Program and summaries of the individual research efforts supported by it. This second part of the report has five sections, each written by a different group of scientists:

(A) Introduction;
(B) Key Findings
(C) The executive and chapter summaries of the international Ozone Trends Panel report;
(D) Model predictions of future ozone changes by a panel of theoreticians;
(E) A review by the NASA Panel for Data Evaluation of the status of kinetics and photochemistry.

SECTION B

KEY FINDINGS

B.1. Ozone Trends Panel Report

Source and Trace Gases

(1.1) There is undisputed observational evidence that the atmospheric concentrations of source gases important in controlling stratospheric ozone levels (chlorofluorocarbons, halons, methane, nitrous oxide, and carbon dioxide) continue to increase on a global scale because of human activities.

Global Ozone

(1.2) Calculations using two-dimensional photochemical models predict that increasing atmospheric concentrations of trace gases would have caused a small decrease in ozone globally between 1969 and 1986. Predicted decreases between 30 and 60 degrees latitude in the Northern Hemisphere for this period ranged from 0.5 to 1.0% in summer and 0.8 to 2.0% in winter, where the range reflects the results from most models.

(1.3) Analysis of data from ground-based Dobson instruments, after allowing for the effects of natural geophysical variability (solar cycle and the quasi-biennial oscillation (QBO)), shows measurable decreases from 1969 to 1986 in the annual average of total column ozone ranging from 1.7 to 3.0%, at latitudes between 30 and 64 degrees in the Northern Hemisphere. The decreases are most pronounced, and ranged from 2.3 to 6.2%, during the winter months, averaged for December through March, inclusive. Dobson data are not currently adequate to determine total column ozone changes in the tropics, sub-tropics, or Southern Hemisphere outside Antarctica.

(1.4) The model calculations are broadly consistent with the observed changes in column ozone, except that the mean values of the observed decreases at mid and high latitudes in winter are larger than the mean values of the predicted decreases. The observed changes may be due wholly, or in part, to the increased atmospheric abundance of trace gases, primarily chlorofluorocarbons (CFCs).

(1.5) Satellite instruments on Nimbus 7 (Solar Backscatter Ultraviolet (SBUV) and Total Ozone Mapping Spectrometer (TOMS)) have provided continuous global records of total column ozone since October 1978. Unfortunately they suffer from instrumental degradation of the diffuser plate, the rate of which cannot be uniquely determined. Thus, the data archived as of 1987 cannot be used alone to derive reliable trends in global ozone.

(1.6) The SBUV and TOMS satellite data have been normalized by comparison with nearly coincident ground-based Dobson measurements in the Northern Hemisphere. The resulting column ozone data, averaged between 53 degrees south and 53 degrees north latitudes, show a decrease of about 2 to 3% from October 1978 to October 1985. This period is approximately coincident with the decrease in solar activity from the maximum to the minimum in the sunspot cycle.

(1.7) Theoretical calculations predict that the total column ozone would decrease from solar maximum to solar minimum by an amount varying between 0.7 and 2% depending upon the model assumed for solar ultraviolet variability. Thus, the observed decrease in ozone from the satellite data between late 1978 and late 1985 is predicted to have a significant contribution from the decrease in solar activity during this period.

(1.8) Theoretical calculations predict that local ozone concentrations near 40 km altitude should have decreased between 1979 and 1985 by 5 to 12% in response to the decrease in solar ultraviolet output and the increased atmospheric abundance of trace gases. This range represents the decreases predicted from the different models for the latitude belt 30° to 60°N for all seasons.

(1.9) Analyses of satellite (SAGE) and ground-based (Umkehr) data taken since 1979 show small decreases in ozone concentrations; these decreases peak near 40 km altitude with mean values of 3 and 9%, respectively. These observational values agree within the range of their errors.

(1.10) Stratospheric temperatures between 45 and 55 km altitude have decreased globally by about 1.7°K since 1979, consistent with decreases in upper stratospheric ozone of less than 10%.

(1.11) Thus, this assessment does not support the previous reports based on SBUV and TOMS data of large global decreases since 1979 in the total column of ozone (about 1% per year) or in the ozone concentration near 50 km altitude (about 3% per year). These reports used data archived as of 1987, and the trends obtained were erroneously large because of unjustified and incorrect assumptions about the degradation of the diffuser plate common to both the SBUV and TOMS satellite instruments.

Antarctic Ozone

(1.12) There has been a large, sudden, and unexpected decrease in the abundance of spring-time Antarctic ozone over the last decade. Ozone decreases of more than 50% in the total column, and 95% locally between 15 and 20 km altitude have been observed.

(1.13) The total column of ozone in the Austral spring of 1987 at all latitudes south of 60 degrees south, was the lowest since measurements began 30 years ago.

(1.14) In 1987 a region of low column ozone over Antarctica lasted until late November - early December, which is the longest since the region of low ozone was first detected.

(1.15) While the column ozone depletion is largest in the Antarctic springtime, ozone appears to have decreased since 1979 by 5% or more at all latitudes south of 60 degrees south throughout the year.

(1.16) The unique meteorology during winter and spring over Antarctica sets up the special conditions of an isolated air mass (polar vortex) with cold temperatures required for the observed perturbed chemical composition.

(1.17) The weight of evidence strongly indicates that man-made chlorine species are primarily responsible for the observed decrease in ozone within the polar vortex.

B.2. Model Predictions of Future Ozone Changes By Ad-Hoc Panel

(2.1) Growth in trace gases other than chlorinated species is expected to have major impact on stratospheric ozone. An increase in CH_4 reduces the rate of chlorine-catalytic destruction of ozone and also generates ozone in the lower stratosphere and troposphere. Growth in CO_2 reduces stratospheric temperatures which leads in turn to increases in ozone. The solar cycle is also predicted and observed to influence column ozone on an 11-year cycle (see Ozone Trends Report, section C); its variations were not included in these long-term predictions by the Ad-Hoc panel.

(2.2) Current predictions of future changes in global ozone are not significantly different from the previous assessment (WMO, 1986). Changes in the chemical kinetic and atmospheric models that have occurred in the meantime have not altered the basic predictions.

(2.3) Two-dimensional models were used to perform (1) a time-dependent scenario, calculating year-to-year changes in composition and ozone, and (2) a traditional steady-state calculation for an atmospheric composition expected to be reached between the years 2040 and 2080. Both types of scenarios are described in Table B-1 and result in similar predictions.

(2.4) The expected decline in column ozone over the next 30 years from time- dependent simulations should be moderate over the tropics, -0.25 to -1.5 %, and largest at high latitudes during late winter and early spring, -2 to -4 %. All models predict large depletions in ozone concentrations near 40 km altitude with changes ranging from -6 % in the tropics to more than -15 % at high latitudes by the year 2015. Only two of the models continued the time-dependent scenario beyond 2015: in one case global ozone continued to decline but at a slower rate; in the other case, global ozone began to increase. Results at this point are dominated by CO_2 and CH_4 increases, for which the models have differing sensitivities.

(2.5) The steady-state scenario described in Table B-1 is based on previous assessments (WMO, 1986, Chapter 13) and predicts column ozone depletions of -1 to -2 % in the tropics by the middle of the 21st century. Column changes at mid- latitudes range from -3 to -6 % with a maximum value in early spring. In one model the inclusion of the temperature feedback on ozone tends to reduce these depletions by a factor of two. Large decreases in ozone concentrations predicted near 40 km altitude range from a minimum of -15 % in the tropics to more than -50 % at high latitudes.

(2.6) Several models discussed in section D have included feedbacks between the predicted ozone change and the transport of trace gases. Differences are apparent among these models, especially at high latitudes, emphasizing that predicting changes in stratospheric circulation and temperatures is still a research topic.

(2.7) The current assessment models do not adequately simulate the chemistry believed to be responsible for the Antarctic ozone hole. Thus, they cannot answer critical questions such as whether the Antarctic ozone hole will spread over the Northern Hemisphere or whether the unusual chemistry associated with the Antarctic hole will appear in the Arctic.

Table B-1

Model Scenarios

TIME-DEPENDENT SIMULATION (TD)

Trace Gas	1985-2015
N_2O	0.25% per yr
CH_4	1.0 % per yr
CO_2	0.5 % per yr
$CFCl_3$ (CFC-11)	265 Gg per yr
CF_2Cl_2 (CFC-12)	412 Gg per yr
CH_3CCl_3	454 Gg per yr
CCl_4	131 Gg per yr
CH_3Br	20 ppt unchanged
CH_3Cl	700 ppt unchanged

This calculation is a continuation of the simulations for the period 1955-1985 which are discussed in the Ozone Trends Report. The total stratospheric chlorine abundance in 1985 was approximately 3 ppb. Gg = 10^9 g.

STEADY-STATE PERTURBATION (SS)

Atmosphere:	"1980"	"20xx"
N_2O	300 ppb	360 ppb
CH_4	1.6 ppm	3.2 ppm
$CFCl_3$ (CFC-11)	170 ppt	800 ppt
CF_2Cl_2 (CFC-12)	285 ppt	2200 ppt
CH_3Br *	20 ppt	40 ppt
CO_2 *	340 ppm	680 ppm
CH_3Cl	700 ppt	unchanged
CH_3CCl_3	100 ppt	unchanged
CCl_4	100 ppt	unchanged
H_2O (tropopause)	3.0 ppm	unchanged
CO	100 ppb	unchanged

(*) The changes in CH_3Br (only source of Brx) and CO_2 were not able to be included in all models.

B.3. Evaluation of Kinetic and Photochemical Data

Most changes in, and additions to, the recommended kinetic and photochemical data base since the previous evaluation (JPL Publication 85-37) have been minor. Among the more important findings and revisions are the following.

(3.1) The most significant advances in laboratory studies of atmospheric chemistry have occurred in the area of heterogeneous chemical kinetics (specifically the studies of the reactions of chlorine and nitrogen containing species with stratospheric aerosols). For example, there is now direct experimental evidence of the efficient conversion of stable chlorine reservoir species ($ClONO_2$ and HCl) into more photochemically active forms of chlorine (HOCl, Cl_2, and Cl_2O) on ice and nitric acid/ice surfaces at 185°K. In addition, N_2O_5 has been observed to react with ice and HCl/ice surfaces to produce HNO_3 and $ClNO_2 + HNO_3$ respectively. These results have significant bearing on our understanding of the perturbed chemistry which may be associated with springtime Antarctic ozone loss.

(3.2) The rate constant for the $OH + HO_2$ reaction has been revised on the basis of results from a recent study which appears to resolve the differences between low and high pressure experimental data. Earlier low pressure studies may have systematically underestimated the rate constant due to the occurrence of secondary reactions. The new pressure independent recommendation and revised temperature dependence results in a 20% increase in the rate constant at the stratopause.

(3.3) Two recent laboratory investigations have resulted in a slight revision in the recommended temperature dependence for the $O + NO_2$ reaction. The recommended rate constant in the middle stratosphere is thus increased by approximately 15%.

(3.4) New measurements of the absorption cross-sections for O_3 photolysis between 185 and 225 nm have been incorporated into the recommendations. Over the wavelength range 185 to 204 nm the recommended cross-sections have been lowered between 0% and 5%. From 204 to 225 nm, the recommended values have been increased between 0% and 10%.

(3.5) The recommended quantum yield for the production of O atoms in the photolysis of NO_2 has been increased by approximately 20% (primarily in the 365 to 400 nm region where most photolysis occurs in the atmosphere).

SECTION C

THE OZONE TRENDS REPORT

Chapter 1: Summary

C-1.1. Introduction

In 1985 two important reports of changes in atmospheric ozone were released. The first report was of a large, sudden, and unanticipated decrease in the abundance of springtime Antarctic ozone over the last decade. The second report, based on satellite data, was of large global-scale decreases since 1979 in both the total column content of ozone and in its concentration near 50 km altitude. In October of 1986, the National Aeronautics and Space Administration (NASA), in collaboration with the National Oceanic and Atmospheric Administration (NOAA), the Federal Aviation Administration (FAA), the World Meteorological Organization (WMO), and the United Nations Environment Program (UNEP), formed an Ozone Trends Panel, that involved over one hundred scientists, to study the question of whether carefully re-evaluated ground-based and satellite data would support these findings. This report critically assesses our present knowledge of whether the chemical composition and physical structure of the stratosphere has changed over the last few decades and whether our current understanding of the influence of natural phenomena and human activities is consistent with any observed change. This report is different from most previous national and international scientific reviews in that we did not simply review the published literature, but performed a critical reanalysis and interpretation of nearly all ground-based and satellite data for total column and vertical profiles of ozone. To aid in the interpretation of the results of this re-analysis we also performed a series of theoretical calculations for comparison with the reanalyzed ozone data. In addition, a uniform error analysis was applied to all the data sets reviewed that contained information on the vertical ozone distribution.

C-1.2. Source and Trace Gases

There is undisputed observational evidence that the atmospheric concentrations of a number of the gases that are important in controlling atmospheric ozone and climate are increasing at a rapid rate on a global scale because of human activities. Such gases include nitrous oxide (N_2O), methane (CH_4), carbon tetrachloride (CCl_4), methyl chloroform (CH_3CCl_3), and several chlorofluorocarbons (CFCs) and halons (bromine-containing compounds, e.g $CBrF_3$, $CBrClF_2$). These gases are important sources of the stratospheric nitrogen, hydrogen, chlorine, and bromine species that are predicted to photochemically control the abundance of ozone. The increasing atmospheric concentration of carbon dioxide (CO_2) is also predicted to affect the abundance of stratospheric ozone, but indirectly, by modifying the temperature structure of the atmosphere and hence the rates of ozone destruction.

Ground-based measurements of hydrochloric acid (HCl) and hydrofluoric acid (HF) indicate that, between 1976 and 1987, their column abundances increased annually by rates of 2 -3 % for HCl and 5 - 10% for HF. Within the limits of experimental uncertainty, these rates are consistent with those expected from the increased tropospheric abundances of their source gases that contain chlorine and fluorine. There are currently an

insufficient number of measurements of the chlorine monoxide radical (ClO) to determine an accurate trend in this key stratospheric ozone-altering species.

A critical analysis of all nitrogen dioxide (NO_2) data from ground-based, aircraft and satellite instruments indicates that, if there has been any increase in NO_2 at all since 1979, it is less than 20%. Therefore, this assessment cannot support the recent report [1] of an approximately 60% increase in the stratospheric abundance of NO_2 between 1979 and 1986.

C-1.3. Total Column Ozone

Total column ozone measurements have been made for more than 30 years at many locations around the world using ground-based Dobson spectrophotometers. Satellite measurements suitable for detecting long-term changes in ozone began only in the late 1970's. Hence, at present, long-term changes and trends over decades can only be assessed using ground-based data. However, changes since late 1978 may be examined using both ground-based and satellite data. This assessment found that all of the ground-based and satellite data had to be critically reanalyzed before being used for the accurate determination of trends. The Dobson data were re-analyzed taking more fully into account instrument calibration changes. Furthermore, data from certain stations were deemed unusable because of questionable quality. The accuracy of the reevaluated data from a "good" Dobson station is estimated to be better than 0.7% per decade.

The quantity and quality of ground-based observations in the tropics and subtropics are such that the determination of trends is far less precise there than for northern midlatitudes. In addition, reliable data are sparse in the Southern Hemisphere outside of Antarctica. Thus, the Dobson data are not adequate to determine total column ozone changes in the tropics, sub-tropics, or Southern Hemisphere. The satellite data, while providing global coverage, are affected by long-term drifts in instrument calibration. The ground-based stations furnish these needed calibration standards for assuring stable performance in the satellite assessment of contemporary global changes in total column ozone. In this report, the determination of such changes since 1979 was made using satellite data normalized against the Dobson data.

Comparisons were made between simultaneous measurements of total column ozone by ground-based Dobson stations and by the SBUV and TOMS instruments on the Nimbus 7 satellite. These show that the column ozone amounts derived from satellite data have drifted downward with respect to the values derived from Dobson measurements by $3.5 \pm 0.5\%$ in the nine year period since the launch of the instruments in October 1978. An accurate determination of the trend in total column ozone using SBUV or TOMS data alone requires precise knowledge of the rate of degradation of the diffuser plate, which is a key optical component shared by both instruments. An incorrect estimate of the magnitude of the wavelength dependence of the degradation manifests itself as an erroneous change in ozone. There is insufficient information from the instruments themselves to determine this, and a model of the diffuser plate degradation had to be assumed in the production of the SBUV and TOMS data sets archived as of 1987. We find that this model is not unique, and that there is a wide range of models consistent with the available diffuser plate information. Consequently, we conclude that it is not possible to obtain a sufficiently accurate trend in total ozone using Nimbus 7 satellite data alone because the rate of degradation of the diffuser plate cannot be uniquely determined. Therefore, the ozone trends reported based on archived SBUV and TOMS data[2, 3] cannot stand alone as a

unique data set. The data can, however, be normalized by comparisons with ground-based instruments and then used for trend determinations, as is described in section C-4.2.

C-1.3.1 Total Column Ozone Changes Since 1960 Derived Using Ground-Based Dobson Data

C-1.3.1a Statistical Analysis of Data

Total column ozone abundances at individual ground-based stations are known to be affected by at least three natural cyclic geophysical changes, namely the annual cycle of the seasons, the quasi-biennial oscillation (QBO) of the stratospheric winds with a repeating cycle of about 26 months, and the 11-year solar sunspot cycle. There might also be natural effects from other irregular transient phenomena, such as the El Nino Southern Oscillation (ENSO), or sporadic events such as volcanic eruptions. In addition, strong theoretical reasons exist for believing that the injection of the oxides of nitrogen from the atmospheric nuclear bomb tests of the late 1950's and early 1960's caused a reduction in total column ozone at that time. A statistical analysis of the ground-based ozone data from the Dobson stations was made to assess whether, after allowance for the perturbations from seasonal cycles, the QBO, the solar sunspot cycle, and nuclear tests, a residual linear trend existed in the measurements after 1970. Any residual trend can then be compared to theory to test our understanding of the impact of the increased abundance of trace gases or other poorly understood natural phenomena such as the effects of the volcanic eruption of El Chichon.

The analysis of the ground-based ozone data can be carried out either through examination of the individual results on a station-by-station basis or by averaging the data over broad latitudinal bands in the Northern Hemisphere where sufficient high quality data are available. Both procedures have been used to analyze the data for the period 1965 to 1986. The scarcity of ground stations with long verified records make latitudinal band averages for the sub-tropics and Southern Hemisphere less reliable. Table C-1.1 shows the magnitude of the residual linear trends for individual months that correspond to ozone changes since 1969 over several latitude zones with the effects of the QBO and solar cycle effects removed. The data were also analyzed using only those values measured before the volcanic eruption of El Chichon and the large ENSO event of 1982. The residual linear trends obtained from this analysis were not significantly different from those obtained using data through 1986. Based on this result it appears that the trends are not significantly affected by these natural events. The magnitude of the QBO and solar cycle effects are shown at the bottom of Table C-1.1. The standard errors shown in Table C-1.1 should be combined with an estimated systematic error for each latitude belt, which would be undetected by the statistical regression procedure, of 0.3% per decade (0.5% for period 1969 to 1986). This would increase the magnitude of the standard errors shown in Table C-1.1 by about 0.2% or less.

The correlation of ozone change with the QBO is known to be dependent on latitude and this conclusion is confirmed in Table C-1.1. The ozone response to the solar cycle varies from negligible to about 2% peak-to-peak for different latitude belts, with the largest column ozone occurring at the sunspot maximum (winter 1979-1980). The remaining linear trends show that there has been a measurable decrease in the annual average total column ozone of 1.7 to 3.0% in all latitude bands from 30 to 64 degrees in the Northern Hemisphere from 1969 to 1986 (Table C-1.1). The decreases are largest during the winter months (2.3 to 6.2%), averaged for December through March, inclusive. These contrast to the smaller changes in column ozone during the summer months (+0.4 to -2.1%), averaged for June through August, inclusive. Although there are insufficient stations to determine an accurate trend in the latitudinal band average of total column ozone at latitudes higher than

TABLE C-1.1

Coefficients of Multiple Regressions to Re-analyzed Dobson Total Ozone Measurements Collected into Band Averages (total percent changes for period 1969-1986)+

	LATITUDE BAND		
	53°-64°N	40°-52°N	30°-39°N
MONTH			
JAN	- 8.3±2.2	- 2.6±2.1	- 2.2±1.5
FEB	- 6.7±2.8	- 5.0±2.2	- 1.2±1.9
MAR	- 4.0±1.4	- 5.6±2.3	- 3.5±1.9
APR	- 2.0±1.4	- 2.5±1.7	- 1.7±1.3
MAY	- 2.1±1.2	- 1.3±1.1	- 1.7±0.9
JUN	+1.1±0.9	- 1.8±1.0	- 3.3±1.0
JUL	+0.0±1.1	- 2.2±1.0	- 1.3±1.0
AUG	+0.2±1.2	- 2.4±1.0	- 1.0±1.0
SEP	+0.2±1.1	- 2.9±1.0	- 1.0±0.9
OCT	- 1.1±1.2	- 1.5±1.5	- 0.9±0.8
NOV	+1.5±1.8	- 2.4±1.3	- 0.1±0.8
DEC	- 5.8±2.3	- 5.5±1.7	- 2.1±1.1
ANNUAL AVERAGE	- 2.3±0.7	- 3.0±0.8	- 1.7±0.7
WINTER AVERAGE**	- 6.2±1.5	- 4.7±1.5	-2.3±1.3
SUMMER AVERAGE***	+0.4±0.8	- 2.1±0.7	- 1.9±0.8
QBO*	- 2.0±0.6	- 1.3±0.6	+1.9±0.6
SOLAR*	+1.8±0.6	+0.8±0.7	+0.1±0.6

* per cycle minimum to maximum.

** winter months include December to March, inclusive.

*** summer months include June to August, inclusive.

+ All uncertainties given in this table and throughout this report represent one standard error. The total uncertainty in the linear trends for total column ozone (1969 - 1986) can be calculated by combining the standard errors given in this Table with a systematic error of 0.5% by taking the square root of the sum of their squares. The uncertainties shown in this Table increase by 0.2% or less.

64°N the limited data suggest that there has been a decrease comparable in magnitude to that observed between 53° and 64°N. It should be noted that there are observational balloon-sonde data suggesting that tropospheric ozone may have increased at mid-latitudes in the Northern Hemisphere by as much as 1% per year over the last twenty years. Because about one tenth of the total column ozone is in the troposphere this would be equivalent to an increase in total column ozone of about 2%, possibly offsetting a decrease in stratospheric ozone. The reliability and hemispheric significance of these tropospheric data is currently a subject of debate.

Theoretical calculations of the expected changes in the total column ozone over the last thirty years were performed especially for this study. These calculations were carried out using two-dimensional models, which predict ozone changes with season and latitude. These calculations took into account variations in the solar output, the input of the oxides of nitrogen due to the nuclear bomb tests around 1960, and the increase in trace gas abundances, but they could not take into account the impact of the QBO, the ENSO, or the 1982 volcanic eruption of El-Chichon since there is inadequate understanding of how to model the various possible associated effects. These calculations predict that the total column ozone should have varied over the solar cycle by at least 0.7% and up to 2% and should have decreased between 30°-60°N by about 0.5 to 1.0% in summer and 0.8 to 2.0% in winter from 1969 to 1986 in response to the increased abundances of trace gases. One model predicts anomalous increases to summertime total column ozone that are inconsistent with other model results. The calculated changes in total column ozone caused by variations in solar output are broadly consistent with those observed. However, while the predicted decreases in total column ozone caused by the increased abundances of trace gases are consistent with the observed decreases in summer, the mean values of the predicted decreases are less than the mean values of the observed decreases in winter, especially at high latitudes. The residual linear trends in total column ozone might be caused wholly, or in part, by the increased abundance of trace gases, primarily CFCs.

C-1.3.1b Comparison of Two Consecutive 11-Year Solar Cycle Periods

The Dobson data were subjected to a second type of analysis. Namely, the change in total column ozone between two consecutive 11-year solar cycles, i.e. 1965-1975 and 1976-1986 inclusive, was assessed. This analysis has the advantage that averaging over 11-year time periods reduces ozone changes attributable to variations in solar output and the QBO. Measured changes in ozone between the two periods can then be compared to theoretical predictions of the effects due to increases in the abundance of the trace gases, primarily CFCs. The ground-based Dobson measurements of the total column ozone show an average decrease of $1.4 \pm 0.7\%$ between the periods 1965-1975 and 1976-1986 in the 30°-60°N latitude zone. This decrease was not uniform throughout the year, but was smaller in summer, $0.5 \pm 0.6\%$, and larger in winter, $2.5 \pm 1.0\%$. The decrease was also not uniform with latitude in winter, but was largest at high latitudes.

Model calculations of the expected changes in the total column ozone caused by an increase in the abundance of the trace gases between these same two periods predict greater depletions at mid and high latitudes in winter than in summer. The predicted decreases for the summer period (0.2 to 0.6%) are similar to those obtained from the Dobson data. Total column ozone was calculated to decrease in winter between these two time periods by about 0.5% at 30°N and about 1.0% at 60°N: these predicted decreases are less than half as large as the observed decreases during the winter period at mid to high latitudes..

C-1.3.2 Total Column Ozone Changes From Late 1978 to Late 1985 Using Satellite Data

As we have emphasized in this report, there is no way to correct the SBUV and TOMS measurements of total column ozone without comparison to other more stable records, such as Dobson measurements. One of the several possible models of the degradation of the SBUV diffuser plate that is consistent with available diffuser information leads to satellite total column ozone measurements that show no drift in time with respect to the ground-based measurements made when the satellite passed almost directly over the ground stations. Because the Dobson data are believed to be stable to better than 0.5% over the period 1979 to 1987, we decided to normalize the SBUV and TOMS total ozone data to the mid-latitude Northern Hemisphere Dobson data. This normalization procedure assumes that there is no significant latitudinal bias in the satellite degradation. The normalized TOMS satellite data show a decrease of total column ozone between October 1978 and October 1985 in all latitude zones in both the northern (1.1 to 3.7%) and southern (1.1 to 9.0%) hemispheres, as shown in Table C-1.2.

As noted, model calculations of total column ozone from 1979 to 1985 predict a decrease caused both by the increased abundance of trace gases and by the declining phase of the solar cycle. In response to the observed increase in trace gases, the models predict that the total column ozone should have shown a greater decrease at mid to high latitudes in winter (0.5 to 1.5%) than in summer (0.2 to 0.6%). The impact of decreasing solar output on total column ozone is predicted to be relatively invariant with latitude and season, and the range of predicted decreases varies from 0.7 to 2.0% over this period. Thus, the solar cycle may have had a comparable or larger impact on total column ozone than that of the trace gases over the period 1979 to 1985. Because of the short time period covered by the satellite data, less than one solar cycle, it is difficult to separate unambiguously the effects of solar variability and increased trace gas abundance on ozone. The predicted change in total column ozone in the Northern Hemisphere is broadly consistent with the observations for the period 1979 to 1985, although the satellite measurements possibly suggest largest changes at mid-latitudes whereas the models predict largest changes at high latitudes. The models do not have the ability to simulate the spring-time Antarctic ozone hole phenomenon and its possible impact at other seasons and latitudes in the Southern Hemisphere. Consequently, a comparison between observed and calculated changes in the Southern Hemisphere must be interpreted with caution. Because of the short time period and relatively small changes in ozone, a more detailed analysis of the accuracy of the measured data is required before any firm conclusions regarding a discrepancy between theory and observations can be drawn.

C-1.3.3 Predicted Changes For Total Column Ozone From 1986 Through 1991

The next maximum in the solar sunspot cycle is expected in 1991, and theoretical calculations predict that the natural response of ozone to this cycle will be to increase toward a maximum at that time. During the 1986-1991 time period, this natural response to the solar cycle may offset or even reverse the predicted decrease in total column ozone that would be due to the increasing abundances of atmospheric trace gases alone. With the possible exception of high latitude winter, where decreases may continue to be evident, total column ozone is predicted to exhibit very little change or small increases up to 1991. After 1991, when the solar ultraviolet output begins to decline, the total column ozone is again predicted to decrease.

Comparison of the normalized TOMS satellite data given in columns 2 and 3 in Table C-1.2 suggests that total column ozone, as predicted, has not continued to decrease in the Northern Hemisphere since passing the solar minimum in 1986 and the very intensive QBO

TABLE C-1.2

TOMS Total Column Ozone Changes+

(total percent changes)

Latitude Band	Total Change From 11 / 78 - 10 / 85	Total Change From 11 / 78 - 11 / 87
53S - 53N	-2.6 ± 0.5	-2.5 ± 0.6
0 - 53S	-2.6 ± 0.9	-2.9 ± 0.9
0 - 53N	-2.1 ± 1.5	-1.8 ± 1.4
53S - 65S	-9.0 ± 1.8	-10.6 ± 1.6
39S - 53S	-5.0 ± 1.8	-4.9 ± 1.8
29S - 39S	-3.2 ± 2.4	-2.7 ± 2.1
19S - 29S	-2.5 ± 1.9	-2.6 ± 1.5
0 - 19S	-1.1 ± 0.8	-2.1 ± 0.8
0 - 19N	-1.1 ± 1.5	-1.6 ± 1.3
19N - 29N	-3.5 ± 2.2	-3.1 ± 1.9
29N - 39N	-3.7 ± 2.0	-2.5 ± 1.7
39N - 53N	-2.7 ± 1.7	-1.2 ± 1.5
53N - 65N	-2.4 ± 1.6	-1.4 ± 1.4

This analysis represents a linear trend using an autoregressive model through the normalized TOMS data.

+ All uncertainties given in this table represent one standard error.

of 1985. However, the rate of change of total column ozone averaged over the Southern Hemisphere appears to have remained more constant through 1987, possibly because of the additional ozone losses associated with the Antarctic ozone hole phenomenon, especially in high latitudes in the Southern Hemisphere. A meaningful interpretation of the observations must await more data.

C-1.4. Vertical Distribution of Ozone

The vertical distribution of ozone has been measured globally using several satellite instruments including the Nimbus 7 SBUV instrument, the Stratospheric Aerosol and Gas Experiment (SAGE) I and II visible spectrometers, and the Solar Mesospheric Explorer (SME) infra-red and ultra-violet spectrometers. Long-term ground-based measurements of ozone up to altitudes of 50 km are restricted to just a few locations around the world using the Umkehr technique at Dobson Stations. As in the case of the total column ozone data, the vertical ozone profile data had to be fully reanalyzed before using them to assess changes or derive small trends. These reanalyzed data were used to evaluate changes in the vertical distribution of ozone since the late 1970's and were compared to the model simulations of the period 1979 to 1986 described above.

Our analysis of the different satellite data sets suggests that the determination of changes in the vertical distribution of ozone currently obtained using SAGE I and SAGE II data is the least sensitive to changes in the performance of the instruments over time. These data were combined to set limits on a possible ozone decrease in the altitude range 25 to 50 km in both the 20° to 50°N and 20° to 50°S latitude belts between the periods 1979-1981 and 1985-1987. At an altitude of 40 km, this change had a mean value of -3% with a standard error of about 1% and a possible systematic error of 4%. Consequently, the change in ozone near 40 km is between +1% to -7%. The SAGE data also indicate a decrease in ozone near 25 km that is comparable in magnitude to that observed near 40 km. However, the SAGE data show no change, $0 \pm 1\%$, (+4% to -4%, including the possible systematic error) near 50 km.

An earlier analysis of the SBUV data archived as of 1987 suggested that the vertical distribution of ozone changed dramatically between late 1978 and 1985 with a decrease of over 20% occurring near 50 km altitude. However, the determination of the vertical distribution of ozone from SBUV is even more dependent upon the corrections applied for the degradation of the diffuser plate than is the determination of total column ozone. The reported analysis[1] used data derived with the same SBUV diffuser plate model that was later found to be unsuitable for reliable determination of changes in total column ozone. A diffuser plate model that eliminates the bias between the SBUV and Dobson measurements of total column ozone also leads to a change in the ozone distribution that shows an increase near 50 km altitude, with a decrease that peaks at about 7% near 40 km altitude. Because of the arbitrary assumptions and uncertainties in the model, the results should be regarded as only suggestive, although generally supporting the SAGE I - SAGE II differences.

Measurements at low sun angles with the ground-based Dobson instrument (Umkehr technique) can be used to estimate the vertical distribution of stratospheric ozone. The Umkehr method suffers from the difficulties of the Dobson instrument, and the Umkehr measurements require a higher degree of operator skill. In addition, there are only a small number of Umkehr stations with an extended record, some stations suffer from sparse data records and have periods of noisy data, and the "Umkehr technique" is very sensitive to the

presence of stratospheric aerosols because these particles affect the transmission of the ultraviolet radiation used for the ozone measurements. The volcanic eruption of El Chichon in April of 1982 injected very large quantities of dust into the stratosphere, causing major interferences with attempts to apply the Umkehr technique for the determination of vertical ozone profiles. Theoretically, corrections for aerosol contamination can be made to the Umkehr data, but only if the atmospheric abundance, size distribution, and optical properties of the aerosols are accurately known. Therefore, the historical Umkehr record is questionable during volcanically disturbed periods because instrumentation for aerosol measurements has only recently begun to be installed at some of the locations where Dobson Umkehr measurements have been taken. Umkehr data from five northern mid-latitude stations, corrected using the best available data and theory for the effect of volcanic aerosols, suggest that ozone decreased between 1979 and 1986 by 8 ± 3%, and 9 ± 4%, at altitudes between 33-38 km (Umkehr level 7) and 38-43 km (Umkehr level 8), respectively. The uncertainty estimate includes the one standard uncertainty for random errors and a term for the uncertainty in the aerosol corrections, but there is no term for possible systematic errors. The decrease in ozone near 40 km is consistent within the stated experimental uncertainties with that obtained using SAGE I and SAGE II data, (and the SBUV data that has been corrected approximately for a diffuser plate model with more degradation), but is smaller than the decrease obtained using the SBUV data archived as of 1987. Because of the small number of stations, these figures cannot be regarded as a global estimate nor even as an average for the northern mid-latitude zone. Although an aerosol correction can be applied to the Umkehr data, concern remains due to the unquantified sensitivity of the analysis to the assumed aerosol properties, particularly following major volcanic eruptions. The Umkehr technique cannot be used as a primary tool for the continuous monitoring of the vertical distribution of ozone because of the several limitations cited above.

The analysis of stratospheric temperature trends can also be used to assess ozone changes in the upper stratosphere because the absorption of ultraviolet radiation by ozone is the primary heat source. A critical analysis of stratospheric temperature data from a variety of sources show a greater consistency than previously believed. Satellite radiance measurements corresponding to an altitude range from 45 to 55 km show a decrease in stratospheric temperature from 1979 to 1986 of 1.7 ± 1K globally, and 1.3 ± 1K in the tropics. If the archived SBUV data that indicated an ozone decrease of 20% near 50 km are inserted into radiative transfer models, satellite-measured temperature changes of -4 to -5K are predicted. The observed temperature changes are substantially less than the predicted values, providing an indirect confirmation that the SBUV data archived as of 1987 do not provide a reliable estimate of changes in ozone in the upper stratosphere. The observed temperature changes are, however, broadly consistent with those determined using SAGE I and II ozone data, and those predicted by the theoretical photochemical models (-1.8 ± 0.4K between 45 and 55 km altitude).

Therefore, the weight of observational evidence from SAGE, Umkehr, and temperature data thus indicates that the reported 50 km ozone decreases between 1979 and 1985 that were based on SBUV data archived as of 1987 cannot be supported. We conclude that these large SBUV ozone trends are a result of unjustified and incorrect assumptions about the degradation of the diffuser plate .

As noted, predicted changes in the vertical distribution of ozone over the period 1979-1985 indicate a maximum depletion near 40 km. Ozone near 40 km is predicted to have decreased by 5 - 12%: a 4 - 9% decrease in response to the increased abundances of the trace gases, and a 1 - 3% decrease in response to the reduced solar ultraviolet output over the time period. These ranges represent the decreases predicted from the different models for the latitude belt 30° to 60°N for all seasons. According to the theoretical models, the

dominant effect due to trace gases over this period comes from the increase in the atmospheric abundance of CFCs. These predicted changes in ozone are consistent with the observations, although somewhat greater than the mean value obtained using SAGE I and SAGE II data. In particular, the overall shape of the predicted changes in the vertical distribution of ozone is consistent with the SAGE data.

Unambiguous separation of the impact upon the vertical distribution of ozone by the two major perturbations, solar cycle and trace gases, awaits continued observation over the remainder of this solar cycle and perhaps beyond. Model forecasts for the period 1985 - 1991, as we approach the next solar maximum, predict that ozone near 40 km will continue to decrease as a result of increases in stratospheric chlorine, despite the rise in solar ultraviolet output, which by itself would lead to an increase in ozone amounts.

C-1.5. The Antarctic Ozone Phenomenon

Ground-based and satellite data have shown conclusively that the spring-time Antarctic column ozone decreased rapidly after the late 1970's. The high degree of interannual variability and the lack of satellite based ozone measurements precludes an accurate assessment of the magnitude of any ozone decreases prior to the late 1970's. The Antarctic ozone hole develops primarily during September, and the rate of loss of ozone within a given year appears to be increasing. Total column ozone (at all latitudes south of 60 degrees) was lower in the Antarctic springtime in 1987 than in any previous year since satellite measurements began (late 1978). In October 1987, the monthly zonal mean amount of total ozone at latitudes 60, 70, and 80 degrees south was about 20%, 40%, and 50% lower, respectively, than in October 1979. In 1987, a region of low ozone over Antarctica lasted until late November / early December, which is the longest since the region of low ozone was first detected. While the ozone depletion is largest in the Antarctic spring-time, normalized TOMS data indicate that total column ozone has decreased since 1979 by more than 5% at all latitudes south of 60 degrees throughout the year. At this time it is premature to judge if this is caused by a dilution of the air from the region of very low ozone, a changed meteorology, or some other unidentified phenomenon. However, at least some of the decrease is likely due to dilution. The magnitude of ozone changes during the polar night are uncertain because there are no TOMS satellite data during this period as the instrument depends upon reflected sunlight for its measurement. Balloon ozonesonde and SAGE II satellite data indicate that the ozone decrease over Antarctica is mainly confined to an altitude region between about 12 km and 24 km. The ozone concentrations between 15 and 20 km in October of 1987 have decreased by more than 95% from their values two months earlier.

Polar stratospheric clouds (PSCs) form during the winter as the stratospheric air over Antarctica becomes very cold with the long absence of sunlight. The persistence of PSCs, which are thought to play a key role in the formation of the Antarctic ozone hole, has increased since 1984. The 1985 observations showed that for the first time PSCs persisted at 16 km throughout the month of September and into October. Furthermore, PSCs lasted into October 1987 at altitudes as high as 18 km.

Temperatures during August and September in the lower Antarctic stratosphere show little or no change over the 1979-1986 period. However, there is substantial evidence that temperatures during October and November are now colder than in 1979. A decrease of about 8K has occurred near 15 km altitude in November.

From the ground-based observations made at the McMurdo station in 1986 and from the ER-2 and DC-8 aircraft campaign based in Punta Arenas in 1987, the weight of observational evidence very strongly suggests that chemical mechanisms involving man-made chlorine are the primary cause of the rapid decline of ozone during September within the polar vortex. The unique meteorology of the region sets up the special conditions of an isolated air mass (polar vortex) with very cold temperatures that is believed to be required for the unusual chemical mechanisms.

Previous attempts to model the spring-time Antarctic ozone decline solely as a response to changed transport processes required that ozone-poor air be moved into the lower stratosphere from below. Such a movement of air would also require local increases of long-lived trace species of tropospheric origin such as N_2O, CCl_3F (CFC-11), and CCl_2F_2 (CFC-12). Data from instruments aboard the ER-2 aircraft show that these trace species remain relatively constant during September as ozone declines significantly, indicating that it is very unlikely that such a transport mechanism could contribute significantly to the overall decline of ozone within the polar vortex. These data support the hypothesis that a chemical sink for ozone is required within the polar vortex.

The ground-based and aircraft data demonstrated that the chemical composition of the Antarctic stratosphere in springtime is highly perturbed compared to that expected at these latitudes based on measurements at mid-latitudes and predictions using chemical models that predate these new data. The distribution of chlorine among various molecular species is very different from that observed at mid-latitudes, as is the abundance and distribution of nitrogen species. In addition, regions of the polar vortex are severely dehydrated.

The data show, that while the summed abundance of chlorine in all chemical forms within the polar vortex is probably consistent with that expected (about equal to the summed abundance in the rest of the stratosphere), the balance was dramatically shifted from inactive forms of chlorine towards reactive species that might catalytically destroy ozone. The concentration of ClO within the region of very low ozone was enhanced by a factor of 100 to 500 compared with that measured at comparable altitudes at mid-latitudes, reaching about 1 ppbv at altitudes near 18.5 km by the end of September. These measured abundances of ClO appear to be sufficient to account for the destruction of ozone within the region of low ozone if our current understanding of the chlorine catalytic cycle involving ClO and the ClO dimer (Cl_2O_2) is correct. However, there are large uncertainties associated with that understanding and improved laboratory data are needed.

Low abundances of the bromine monoxide radical (BrO) were measured and imply that this species plays a minor role (less than 10%) in the catalytic destruction of ozone at ER-2 flight altitudes.

The stratosphere was both dehydrated and denitrified within the region of low ozone. The low abundances of nitrogen oxides (NO_x) that were measured clearly contradict any theories requiring elevated levels of NO_x.

C-1.6. Postscript

The conclusions of this report regarding global ozone trends would have been aided if the NOAA National Environmental Satellite and Data Information Service (NESDIS) had been able to provide any validated data from the SBUV-2 instrument launched in late 1984. Reliable SBUV-2 data should enable an improved recalibration of the Nimbus 7 SBUV data and provide a system for determining future changes in ozone that does not rely so

critically on the long-term stability of the absolute calibration of the Dobson network. There is an urgent need for NOAA NESDIS to increase the priority given for the timely processing and validation of SBUV-2 ozone data if the United States is to have a viable national program for monitoring ozone. Validated SBUV-2 data are absolutely necessary for the international scientific assessment scheduled for 1989 in preparation for the 1990 policy review in accordance with the Montreal Protocol.

The ground-based Dobson, and to a lesser extent the filter ozonometer, measurements play very important roles in a global ozone monitoring system both through direct determinations and as partial ground-truth calibrations for the satellite systems. Continued re-evaluations and corrections of the archived ground-based data by the various national meteorological services are necessary to make the existing 25-30 year records even more useful for trend determinations. The reevaluation will be most effective if the WMO should exercise its traditional role in assisting the implementation of the Global Ozone Observing System by guiding these activities.

NASA must vigorously pursue the new insights into the Nimbus 7 SBUV and TOMS instruments in order to develop the best model of diffuser plate degradation and the associated uncertainties. Once sufficient improvement has been made, the SBUV and TOMS data sets should be reprocessed using the new model of the degradation of the diffuser plate and the data archived for additional scientific studies required by the 1989 international assessment. SAGE II data should be used as an independent measurement of changes in the vertical distribution of ozone to compare with and support this reanalysis.

The re-evaluation and interpretation of both ground-based and satellite ozone data must, in the near future be given higher priority, and involve a broader cross section of the scientific community than in previous years.

C-1.7. References

1. Callis, L.B. and M. Natarajan, "Ozone and Nitrogen Dioxide Changes in the Stratosphere During 1979-1984," Nature, 323, 772, 1986.

2. Heath, D. F., (a) Testimony on Ozone Layer Depletion before the Subcommittee on Health and the Environment, House of Representatives, March 9 1987; (b) "Non-Seasonal Changes in Total Column Ozone from Satellite Observations: 1970-1985," Nature, March 17 issue, 1988.

3. Bowman, K.P., "Global Trends in Total Ozone," Science, 239, 48, 1988.

Chapter 2: Spacecraft Instrument Calibration and Stability

C-2.1. Introduction

It is difficult to design any instrument or system to measure ozone changes to 1% or less per year over a period of a few years. This is especially true if one requires that the instrument operate unattended, a condition that severely constrains the amount of recalibration, testing and adjustment that can be carried out, and usually limits the length of the measurement series to a few years. The difficulties become truly formidable if one further demands that the instrument operate under the harsh conditions in space.

Among the problems in space are the vacuum that allows contaminant molecules to outgas from instruments and spacecraft, and the strong solar ultraviolet radiation. When the contaminants deposit on optical surfaces and are dissociated by the radiation, the optical characteristics change, and the throughput decreases by unpredictable amounts.

Nonetheless, satellite instruments are indispensable for the determination of trends of ozone on a global basis. In spite of the difficulties and the relatively early stages of development of most of the methods and measurement technologies, they have already made enormous contributions to our knowledge of the global distribution of ozone, including its spatial and temporal variations. In the period since 1978, seven instruments have collected large amounts of data that have been reduced and are clearly relevant to the problem of ozone trends.

However, none of these was specifically designed for trend measurements. Only two of the experiment descriptions mentioned long term trends as a goal, but even these instruments did not take measures to ensure that reliable data for trend detection were obtained. Some were designed under cost constraints that precluded planning for extended operations. The operational SBUV/2 instrument was launched for trend measurements in 1984, but data are only now becoming available in sufficient amounts for careful evaluation. Thus, at this time reliance must be placed on instruments for which trend detection is an afterthought. In this situation it is necessary to make the best use of available data. In most cases, under the impetus of this study, the data were extensively reanalyzed. All available information has been critically evaluated in order to establish the accuracy and long term stability of these instruments. In some cases, the uncertainties in trend determining capabilities resulting from the present analysis are different from those reported by the experimenters.

It should be pointed out that to compare the ability of each instrument to determine trends, it is necessary to compare derived ozone amounts. Part of the differences in reported trends may result from effects introduced by the retrieval algorithms.

C-2.2. Instruments and Techniques

The complete chapter contains descriptions of the different instruments and their coverage, with detailed discussions of their measurement characteristics and potential sources of drift. In general, all techniques for measuring ozone are affected to some extent by changes in instrument sensitivity. Some techniques rely to first order on relative measurements or radiance ratios obtained over a short period of time. From an instrument point of view these are less susceptible to drift than those that require an absolute radiance measurement. In

either case, greater confidence is obtained by monitoring the in-flight sensitivity of the instrument, generally through measuring the response of the instrument to a known calibration signal. It is easier to be sure of the output of an in-flight calibration source in the infrared than in the visible, where in turn more stable sources are available than in the UV. In addition, the effects of instrument degradation are generally more pronounced in the UV than in the visible and infrared.

C-2.3. Trend Measurement Capabilities

The findings may be summarized and compared to show the altitude ranges and capabilities of the data now available. Two related quantities are compared; the minimum detectable ozone change over the life of the experiment, and the minimum detectable ozone trend, which is usually the minimum detectable change divided by the life of the experiment.

(1) Measurements of the vertical distribution

SAGE I and II

Of the error sources discussed in Chapter 2, it is apparent that for either instrument the ozone and Rayleigh cross-sections will remain constant. Taking the root sum square of the other error sources leads to the conclusion that SAGE I can discern an ozone change of 2.5% above 25 km, and 4.5% below. Similarly, for SAGE II the values are 1.5% and 4%, respectively. However, because of the difficulties of sampling the same latitudes at the same seasons and under the same atmospheric conditions, in general it is not possible to detect changes of this size unambiguously. On the other hand, the instrumental uncertainty in the differences between SAGE I and SAGE II (for situations carefully matched in latitude and season) is ± 1.5-2% between 25 and 45 km. This value is plotted in Figure C-2.1. This does not include the effects of errors resulting from systematic geophysical variations between the matched pairs of situations that are sampled. At present these have not been quantified.

In order to make a rough estimate of the annual rates of ozone decrease that can be determined, it is necessary to consider the time period over which a change might be sought. Although SAGE I operated for 34 months, because of the sampling problems, only the two complete years of operation are used. The same length of SAGE II data record is now available. Dividing the detectable changes mentioned above by their 2 years of operation indicates that above 25 km trends of the order of 0.75-1.25% per year are detectable in principle. Again, the interaction of measurement sampling with natural variability requires that these numbers be regarded as no more than suggestive. It should be pointed out that as the SAGE II mission extends to three and more years, in principle it will be able to detect correspondingly smaller trends.

There are roughly 6 years between the mid-points of the SAGE I and SAGE II data. Dividing this into the ± 1.5-2% minimum detectable total change based on instrumental factors suggests a minimum detectable trend of ± 0.3-0.4%/year, which is shown in Figure C-2.2.

SBUV

The major instrumental uncertainty in the SBUV results is due to lack of knowledge of the way the diffuser plate has degraded with time. There are no measurements from the instrument that provide this information unambiguously. A family of diffuser plate

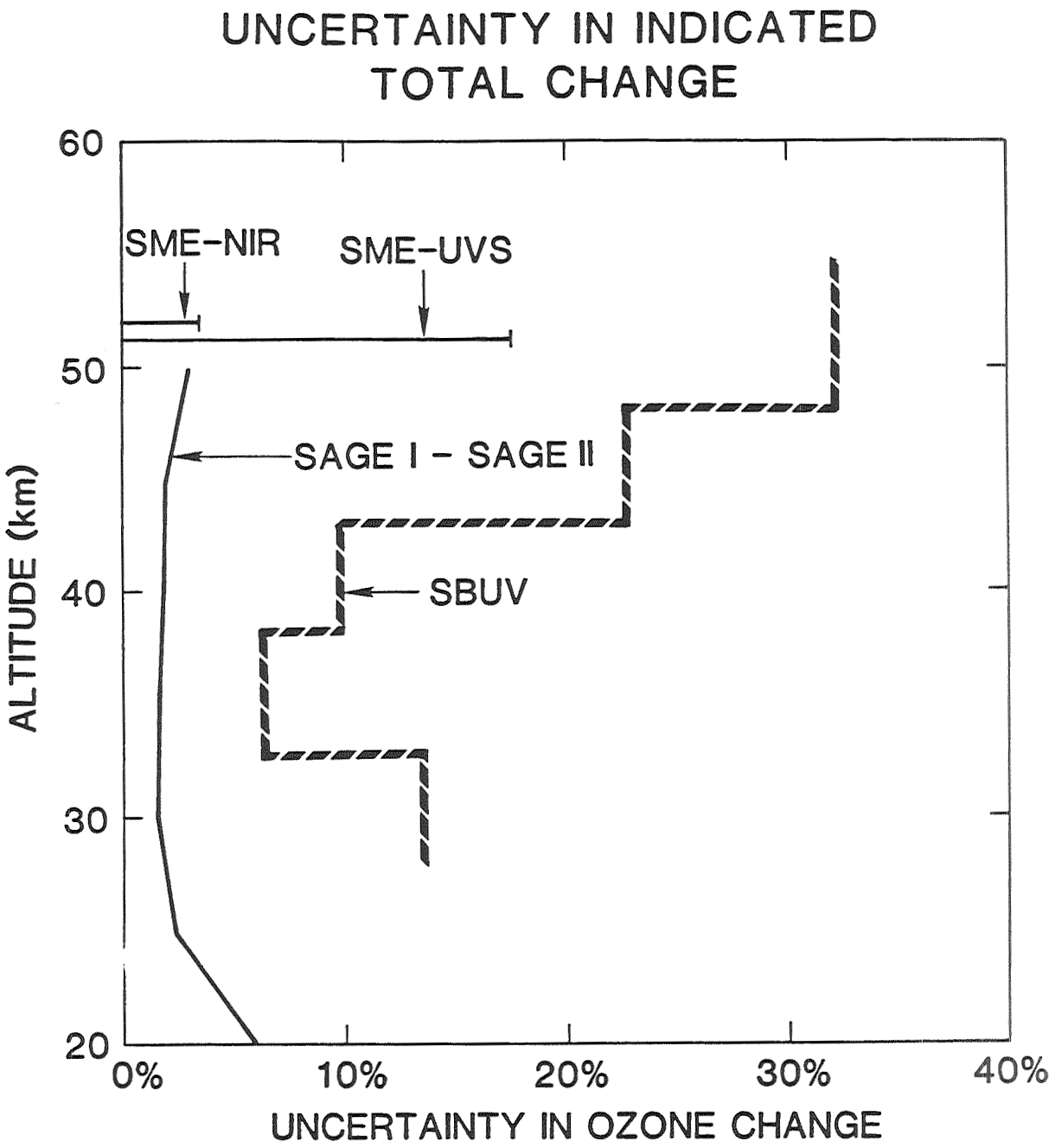

Figure C-2.1. Uncertainty in total change determined by the various experiments over their lifetimes, as functions of altitude. For SBUV, the uncertainty is half of range between models of high and low diffuser degradation.

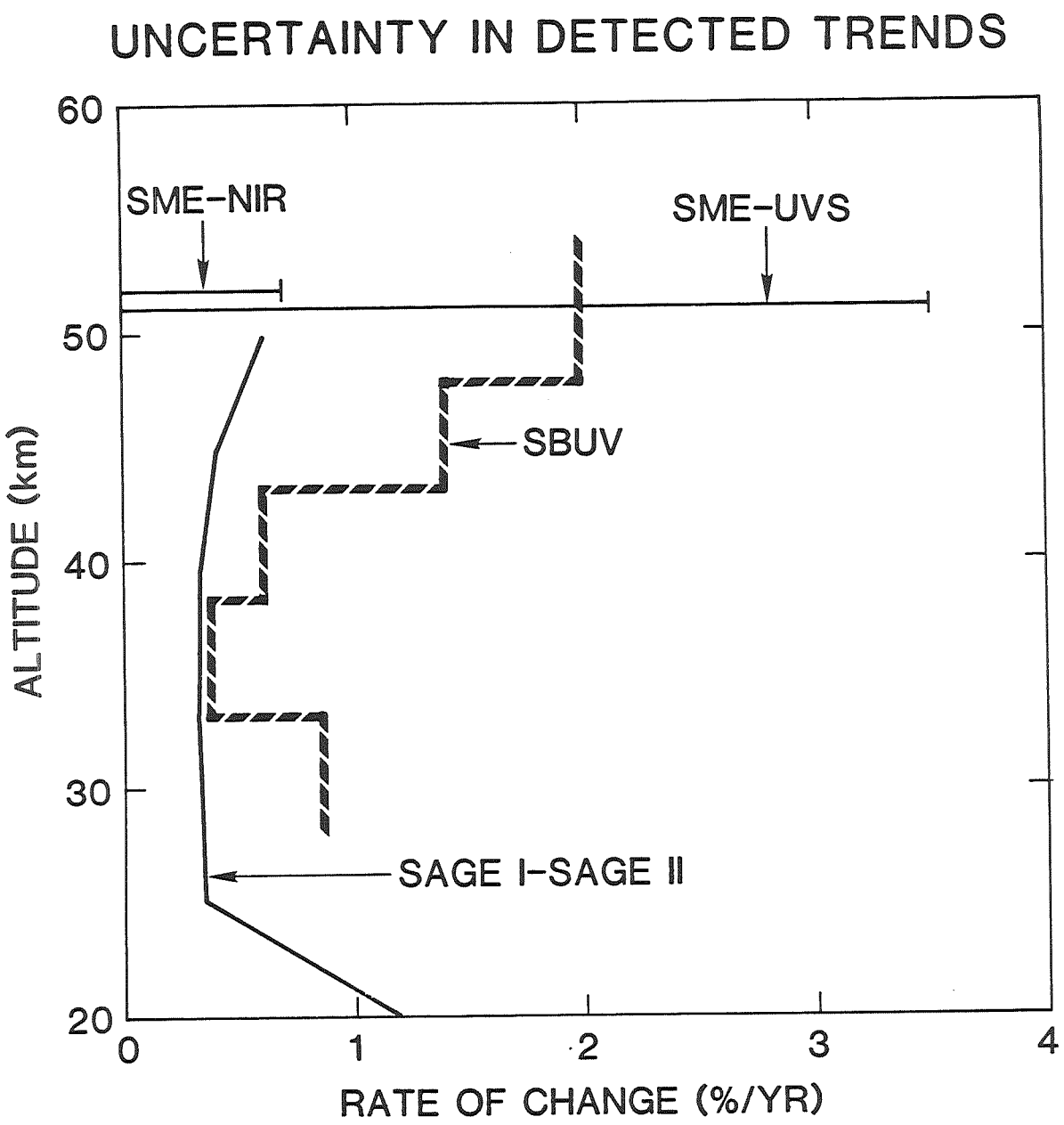

Figure C-2.2. Uncertainties of trends determined by various experiments over their lifetimes, as functions of altitude. For SBUV, the uncertainty is half of range between models of high and low diffuser degradation.

degradation models was introduced to provide a plausible range of values for the degradation. Based on differences in the model values after 8 years, the range of ozone content was calculated. One half of this range is plotted for Umkehr layers 6-10 in Figure C-2.1. Thus, in layer 10, the range is 64%, or ± 32% around the central value. Clearly the range of ozone content based on these models is very large at all levels. It must be emphasized that the bounding values are rather arbitrary, and the actual values could even be outside this range, although this is felt to be unlikely for reasons mentioned below.

The range of detectable trends is presented in Figure C-2.2 in the same way -- i.e., in layer 10 the trend range of the models is 4%/year, or ± 2%/year around the mid point of the model results.

These models assume that the coefficients relating the degradation to the exposure time and the elapsed time are constant over the 8 years, which is not necessarily true, adding another degree of uncertainty.

The change in vertical ozone distribution (in Umkehr layers) from November 1978 to November 1986 is shown in Figure C-2.3 for several different diffuser degradation models. The curve labeled SBUV is based on the data in the archives in 1987. They show a large decrease near 50 km. The curve labeled L shows the same measurements, interpreted by means of a diffuser model with low degradation, while M1 and M2 indicate results obtained using two models with more degradation than the one used to create the archived data. These illustrate the non-uniqueness of the results, their strong dependence on the diffuser model, and the position of the archived values close to the low extreme of this family of models. M1 and M2 indicate small changes, or a slight increase in ozone near 50 km, with a small decrease near 40 km, similar to that indicated by the SAGE I-SAGE II differences. As noted below, total ozone derived using M1 or M2 agree better with Dobson total ozone than the archived models. The wavelengths that provide information on the vertical distribution at 30-50 km altitude are shorter than those that determine the total ozone, so the shape of the stratospheric profile depends only on the assumptions in the diffuser degradation model. The present results give weak support to the decrease at 40 km. It is possible to construct a reasonable model of the diffuser degradation that causes the vertical distribution of the SBUV rate of ozone decrease to agree with the SAGE I-SAGE II rate, and the SBUV change in total ozone to agree with the change in Dobson total ozone, but this provides no additional independent information.

These results indicate that the uncertainties in the diffuser degradation model, and the resulting uncertainties in ozone column amounts and vertical distributions, are much greater than has been stated previously. The weight of evidence also suggests that the diffuser degradation model used in producing the archived data has underestimated the diffuser degradation, and thereby systematically underestimated the vertical ozone distribution, resulting in a false large negative trend.

SME-UVS

The arguments presented in the report indicate that the SME-UVS instrument can determine an ozone trend at 0.75 mb to ± 3.5%/year, or detect a ± 17.5% change over the 5 year lifetime of the SME spacecraft.

SME-NIR

From the considerations in the report, the trends at 0.75 mb can apparently be determined to ± 0.7%/year, or ± 3.5% over the SME lifetime. However, this technique is very different from those that have been used before, and relies on understanding a complex set

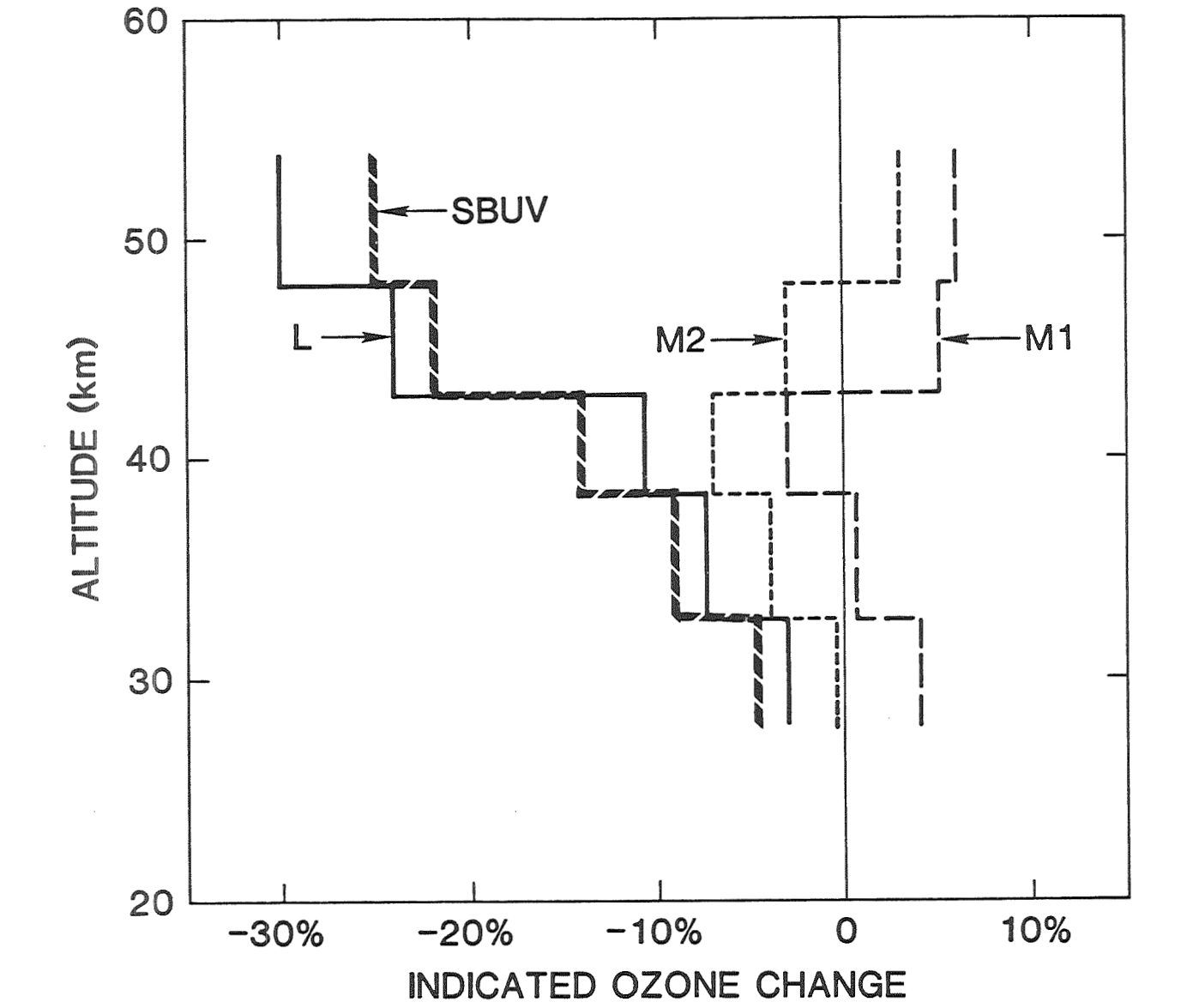

Figure C-2.3. Mid-latitude vertical distributions of ozone change from 1978 to 1986 determined from SBUV data, for several models of diffuser degradation. Curve marked SBUV used the model employed in producing the data archived as of 1987. Curve L was calculated using a model with less diffuser degradation, M1 and M2 were derived using models with more diffuser degradation than the SBUV archive model.

of photochemical reactions. Until the underlying chemistry is understood more completely, the possibility exists that additional reactions are involved, or that there are unrecognized sensitivities to other factors. Thus, the instrumental error bars shown here may be unrepresentative of the true variation.

LIMS

Because of its short lifetime, no attempt has been made to evaluate the LIMS capability to measure long term trends. In this study, LIMS has served as a useful check and source of comparisons with measurements by other techniques.

As infrared limb scanning uses a stable on-board black body for calibration, this technique should be a good candidate for long term trend measurements. The major difficulty is the requirement that detectors with sufficient sensitivity operate over a period of a few years. This will probably require cooling the detectors well below spacecraft ambient temperatures.

(2) Comparison of trend detection capabilities for the vertical distribution

Figure C-2.1 shows that at the present time the SAGE I-SAGE II difference sets the most sensitive limits on the detection of a change in the stratosphere, followed by the SME-NIR (in the lower mesosphere).

Similarly, Figure C-2.2 compares trend detection capabilities. The SAGE I-SAGE II difference is capable of detecting trends less than 0.5%/year in the stratosphere above 25 km. As noted above, as the SAGE II record becomes longer, it should be able to detect smaller trends, but this must be evaluated in the light of its sparse coverage, and the problems of obtaining comparisons under similar seasonal, latitudinal and atmospheric conditions.

In the future, if the SBUV/2 results can be proven to be highly accurate, it should be possible to use them with the SBUV measurements to determine long term changes to better than 1%/year. Determining the time history of the changes will be a more difficult task.

(3) Total ozone determinations from SBUV and TOMS

Because SBUV and TOMS employ the same wavelengths and share the same diffuser plate, they show the same trends, and have the same sensitivity to diffuser degradation. The uncertainties in total ozone were calculated, using a range of diffuser degradation models for wavelengths of 312.5 nm and longer, This leads to a range of about 4% in total ozone change over 8 years, and a consequent range of total ozone trends of 0.3-0.5%/year.

In this case, the diffuser model used to obtain the archived data results in ozone amounts near the minimum of the range. The true total ozone values could be 4% higher than those suggested by the archived TOMS data, and the downward trend could be smaller than that of the archived data by $\approx$ 0.4%/year. Diffuser models M1 and M2 thus give total ozone changes that are in good agreement with the changes observed by the Dobson network.

(4) A final observation on SBUV and TOMS results

The evidence indicates that the uncertainties in the total ozone changes and in the changes in the vertical distributions are considerably larger than has been stated previously. The preponderance of evidence suggests that the model adopted in producing the archived data has underestimated the diffuser degradation, and thereby underestimated total column ozone and ozone profile amounts in recent years. Within the uncertainties, the total amounts could have changed by the amounts indicated by the Dobson network, while the vertical profiles could have remained nearly unchanged, or had a small decrease near 40 km with a small increase near 50 km.

C-2.4. Ongoing Work

A large number of studies were carried out as part of this investigation. Two in particular that were not completed at the time of this writing should be brought to completion:

(1) A comparison of SBUV and SBUV/2 results during the period of overlap;

(2) A comparison of the SBUV, SME, and other solar measurements.

C-2.5. Future Satellite Measurements of Ozone Trends

The analyses discussed here have shown that the measurement of long term ozone trends from satellites is a difficult but viable task. Results to date, with data that were not taken for this purpose, have proven to be very instructive, and such a measurement program should continue. The measurement system should be based on a careful scientific analysis of the capabilities of the techniques with a view to optimizing them. Of necessity this will need to be tightly linked with studies on the best methods of implementation to define the instruments employed by such a system. The methods of demonstrating the stability of the systems results will also need to be addressed. This study suggests that a measurement program should include the following features:

(1) The instruments should be designed for long life and stable operation.

(2) Attempts should be made to reduce the amount of contamination to which the instruments are subject.

(3) Ideally the program should consist of more than one satellite instrument, employing different experimental techniques.

(4) The system should also include a continuous long term set of ground-based measurements, carefully maintained at a high level of accuracy.

Chapter 3: Information Content of Ozone Retrieval Algorithms

C-3.1. Introduction

We have found no serious deficiencies in the algorithms used in generating the major ozone data sets that are available. As the measurements are all indirect in some way, and the retrieved profiles have different characteristics, data from different instruments are not directly comparable. Thus the primary aim of this chapter has been to characterize the algorithms to show quantitatively:

(a) How the retrieved vertical profile is related to the actual profile. This characterizes the vertical resolution and altitude range of the data.

(b) How trends in the real ozone are reflected in trends in the retrieved ozone profile.

(c) How trends in other quantities, both instrumental and atmospheric, might appear as trends in the ozone profile.

C-3.2. Error Analysis Concepts

Error analyses for the ozone data sets that we have considered have, in general, been published in open literature, but not in a uniform and comparable way. We have therefore defined a uniform error analysis approach, and applied it to all of the data sources. The formal error analysis shows that the retrieved vertical profile $\hat{x}(z)$ can be expressed as an explicit function of the true profile $x(z)$, plus error terms due to instrument noise and systematic errors. This function can be thought of as a smoothing of the true profile, with a smoothing function we call the *averaging kernel* $A(z,z')$:

$$\hat{x}(z) = \bar{x}(z) + \int A(z,z')(x(z') - \bar{x}(z'))dz' + \textit{error terms}$$

The range of height z over which the averaging kernel has a well defined peak determines the height range of validity of the retrieved profile, while the width of the peak defines the vertical resolution of the profile. The error terms due to various sources can be examined independently. Those which lead to constant offsets or purely random errors are of minor importance when studying trends, as random errors will average out in the long run, and constant offsets make no difference to trend estimates. The most important sources of error are those that have trends themselves, which might appear as false trends in ozone.

The range of validity and vertical resolution of the ozone data sets that have been available to the Ozone Trends Panel are given in Table C-3.1. Also listed are the primary sources of systematic error which may introduce incorrect trends into the retrieved data.

C-3.3. Individual Data Sources

Dobson Total Ozone: The only algorithmic source of trend error is the omission of the effects of SO_2, which itself has a trend. Stratospheric aerosol, which has variability on a long time scale, is also omitted. This is discussed elsewhere.

TABLE C-3.1

Summary of Retrieval Characteristics

INSTRUMENT	PRESSURE RANGE[a] (mb)	ALTITUDE RANGE[a] (km)	VERTICAL RESOLUTION (km)	SOURCES OF TREND ERROR
SBUV	16 - 1	(28 - 50)	8 - 10	Diffuser plate reflectivity, aerosol
Umkehr	64 - 2	(19 - 43)	11 - 14	aerosol,sampling
SAGE I	(250 - 1)	10 - 50	1	aerosol below 25km, sampling
SAGE II	(250 - 1)	10 - 50	1	aerosol below 25km, sampling
	(1 - 0.1)	50 - 65	5	sampling
SAGE II-I	(250 - 1)	10 - 50	1	Altitude reference, filter placement
SME-UVS[b]	(1 - 0.05)	48 - 68	4	UVS and Solar Flux instrument calibration, pressure at 68 km, mesospheric aerosol.
SME-NIR	0.3 - 0.003	(55 - 85)	4 - 10[c]	Altitude reference, calibration, atmospheric temperature
LIMS	100 - 0.1	(15 - 64)	2.5	(short record)

[a]Bracketed figures are approximate equivalents.
[b]Experimenters assessment.
[c]Varying with time.

TOMS and SBUV Total Ozone: The primary source of error here is the spectral variation of the drift in diffuser plate reflectivity. The range of reasonable models of this drift presented in the Calibration Chapter leads to a possible overestimate of around 3-4% in the ozone depletion over the 8-year data period. A minor source of trend error is an under-assessment of tropospheric ozone by a factor of around two.

SBUV: Even though the archival data covers Umkehr layers 1 to 12, (altitude range approximately 0-64 km) we find that only layers 6 to 9 or 10 (28-50 km) are suitable for trend analysis. The sensitivity of the retrieval to diffuser plate reflectivity errors has a similar vertical profile to the global trend seen in SBUV version 5 data. Uncertainty in this trend due to errors in the diffuser plate reflectivity within experimental error are comparable with the trend itself.

Umkehr: The archival data covers an altitude range of layers 1 to 9 (0-48 km). We find that only layers 4 to 8 (19-43 km) are suitable for trend analysis. There are many sources of systematic error that affect an individual instrument in a way which varies with time, such as recalibration, and competence of operators. The network is not large enough to rely on these effects averaging out in the long term. We note also that aerosol effects and temperature dependence are not allowed for in the retrieval.

SAGE: SAGE has an excellent vertical resolution, but a poor sampling frequency. This means that care must be taken in deriving statistically valid trends. We have found no problems that might lead to trend errors when using data from one instrument, other than its sensitivity to aerosols below about 25 km. When comparing SAGE I with SAGE II, it must be remembered that the systematic errors in the two data sets are likely to be different. Specifically, the different treatment of the reference altitude, and differences in filter placement between the two instruments can lead to systematic differences in retrieved ozone. It should also be noted that as SAGE measures on a height scale, while SBUV measures on a pressure scale, temperature trends must be correctly modeled when comparing trends from these two instruments.

SME: The vertical resolution of the retrieval from both the UV and the NIR spectrometers degraded with time, as the attitude of the spacecraft changed. The primary source of trend errors for both instruments is the altitude reference. The NIR retrieval relies on a complete understanding of the relevant photochemistry, including its temperature dependence. We have found no errors, but it is quite possible that there is some chemistry omitted or misunderstood.

LIMS: We have found no significant sensitivities which might impact on trend assessment. However, the measurement period is rather short, so that LIMS has little to say about trends. Its main value here is to validate other data sources.

C-3.4. Discussion

In view of the above characterization of the various sources of data, it is clear that comparisons should only be made over the range of validity of the individual data sets, and at comparable vertical resolutions, degrading the higher resolution data as necessary. It would be helpful for future exercises of this kind if data suppliers could present a standard set of observing system characteristics, perhaps based on those developed for this report.

Retrieval methods appropriate to trend estimation are not necessarily the same as methods appropriate to estimation of single profiles, because it may be possible to largely eliminate random error in the long term averages required for trends. However, the retrieval methods used for the data now available are designed for single profiles. Further research is needed to design trend profile retrieval methods.

An alternative approach to trend detection is to look for changes in the quantity actually measured, without retrieving a profile. Modeled changes in the ozone distribution can be used with the forward model for a particular instrument, to determine whether the resulting perturbation in the quantity measured is detectable.

Chapter 4: Trends in Total Column Ozone Measurements

C-4.1 Introduction

Total column ozone measurements with the ground-based Dobson ultraviolet spectrophotometer began in the 1920s, and were extended toward global coverage during the International Geophysical Year in 1957-1958. Additional programs were also begun then with ground-based filter ozonometers, whose basic principle of ozone measurement through differential comparison of the absorption of two or more wavelengths of ultraviolet light is similar to that used in the Dobson instruments. As a consequence, time series of ozone measurements are now available covering various segments of the past 30 years from more than 100 ground stations, with continual data over the past 24 years from almost half of them. These data sets are the only ozone data available which extend for time periods longer than the 11-year solar sunspot cycle, and are therefore the only data which can be used for assessing any long-term changes or trends in total ozone concentrations over a period of two decades or more. The ground-based data from the stations with longer Dobson records have been carefully assessed and reanalyzed to account especially for instrument calibration changes over this extended time period. Various consistency tests were also applied to the data, leading to the rejection for present use of some data sets because of questionable quality. The filter ozonometers were improved 17 years ago, and the data recorded with them since 1972 has been utilized in some parts of this assessment.

The quantity of reliable ground-based observations from stations in the tropics and the Southern Hemisphere is sparse by comparison with those north of 30°N latitude. Estimates of possible trends in ozone concentration in regions south of 30°N latitude -- with the exception of Antarctica -- are therefore far less precise than for latitudes between 30°N and 64°N. The reanalyzed Dobson data are not adequate for determinations of changes in the total ozone column during the past three decades over latitude bands for the tropics, sub-tropics or the Southern Hemisphere.

Since 1978, total ozone measurements have been made both with upward pointing ground-based instruments and by downward-looking instruments on satellites. The existence of two systems for measurement of the concentrations of ozone provides the opportunity for intercomparisons and calibration of their results. The major questions concerning data taken with instruments not accessible to periodic checking and recalibration during more than nine years on a satellite are whether the sensitivity of the instrument for the detection of ozone has remained unchanged over that period, and whether corrections can be made for such changes if they have occurred. On the other hand, the major problems with the ground-based data are concerned with the relative sensitivities and stability of different instruments operated and calibrated by various national agencies in locations all over the world. The intercomparison of ozone data taken by satellite instruments with measurements taken by ground-based instruments during overpasses which are nearly simultaneous in time and coincident in geography has provided very valuable checks on both types of data. Taken together, the combination of satellite instruments for daily global coverage and ground-based instruments for regular long-term calibration of the satellite systems has provided detailed global ozone coverage over the time period since 1978. Because the chief problem of ozone measurement from a satellite is one of long-term degradation in its sensitivity over a decade, its values recorded on any given day are quite consistent with one another, and furnish an excellent check on ground stations through

comparison of the daily overpass results with the data reported from the latter instruments. In this manner, the satellite instruments can serve as a transfer standard for judging the degree of consistency in the results reported from all of the ground-based stations on a daily basis. Over a longer period of one to ten years, the satellite data recorded while passing over ground instruments accessible for regular checking and recalibration permit evaluation of the magnitude of any year-to-year change in the sensitivity of the satellite instrument toward total column ozone measurement.

C-4.2 Total Column Ozone Changes Since 1960 Derived from Ground-Based Data

The potential long-term precision (at ± 2 sigma) of the Dobson ozone spectrophotometer is estimated to be ±1% in the annual means, based on standard deviations from the mean analysis of individual stations. Its accuracy is strongly dependent on the quality of the calibration and operation of the instrument, as well as on the ability to assess environmental changes (e.g. an increase in tropospheric ozone). The ozone data can only be retroactively reevaluated through the availability of systematic calibrations. The precision of the reevaluated data from a "good" station is estimated to be better than 0.7% per decade. The World Primary Standard Dobson Instrument is periodically recalibrated under favorable conditions at Mauna Loa, Hawaii, and has exhibited a precision of ±0.5% over the time interval from June, 1972, to July, 1987, and can be further connected to calibrations performed in 1962 with a precision of ±1%. The precision and accuracy of another individual instrument is dependent upon their particular history and frequency of recalibration.

The total concentration of ozone in a vertical column through the entire atmosphere has long been known to vary in coincidence with several natural cycles. In addition, theoretical reasons exist for believing that total ozone may also vary in response to the activities of man, especially from the stratospheric injection of nitrogen oxides during the nuclear bomb tests of the late 1950's and early 1960's and from the release to the atmosphere of long-lived gases such as the chlorofluorocarbons (CFCs), methane, carbon dioxide and nitrous oxide. The largest natural cycle is the seasonal variation each year which produces late winter or early spring maxima in total ozone in temperate locations, and ozone minima in late summer or early autumn. The second well-established natural cycle is the variation in total ozone in concert with the quasi-biennial oscillation (QBO) in equatorial stratospheric winds, which reverse their direction approximately every 26 months. A third natural source of variability is the change in total ozone with the 11-year solar sunspot cycle. There might possibly also be variations in ozone concentrations in response to other irregular cyclic phenomena such as the El Nino Southern Oscillation (ENSO) or sporadic events such as volcanic eruptions. The rates of the ozone-removing chemical reactions involved in the NO_X and ClO_X catalytic chains are well-determined from laboratory experiments. However, stratospheric chemical reactions are complex enough to make highly desirable verification through observation of any actual effects of modifications of these catalytic chains upon ozone concentrations in the atmosphere.

C-4.3 Comparison of Ozone Data over Two Consecutive 11-Year Solar Cycles

The ozone data from the ground-based Dobson stations have been analyzed by a direct approach through comparison of the average total column ozone measurements over two

consecutive 11-year solar cycles, i.e. 1965-1975 and 1976-1986, inclusive. Averaging over successive 11-year periods effectively eliminates ozone variations attributable to the natural cycles because each period includes one solar cycle, five QBO cycles, and 11 yearly cycles. The measured ozone changes between these two periods do not represent any test of the structure for the time dependence of any variations, and could be the result of increases in the abundance of trace gases, primarily the CFCs, or in part to long-term fluctuations in natural phenomena. Because there are theoretical indications that man's activities might produce winter/summer differences in ozone trends, and because earlier examination of the long records from several north temperate Dobson stations had indicated apparent winter/summer differences in the magnitude of observed ozone changes over time, the data have been considered both in terms of yearly averages and in seasonal averages during the winter-spring ozone "season" of strong westerly circulation (December through March) in the lower stratosphere, and the "summer" (May through August) easterly regime. Because the theoretical calculations in this assessment were performed for only three summer months (June through August), the observational data have also been averaged for this three-month period. The measured ozone changes recorded in these averages over these successive 11-year periods are given in Table C-4.1 for 24 Northern Hemisphere Dobson stations. These ground-based measurements of total column ozone show an average change of -1.4±0.7% for 1976-1986 in comparison to 1965-1975 in the latitude zone between 30°N-60°N. This decrease was not uniform throughout the year, but was larger in winter, -2.5±1.0%, and smaller in summer, -0.5±0.6%. The winter-time decreases were also largest at the higher latitudes.

Model calculations of the expected changes in total column ozone from an increase in the abundances of the trace gases between these two time periods do predict greater depletions at mid and high latitudes during the winter than in summer. For the summer months, the calculated changes in ozone (-0.2% to -0.6%) from the models are similar to those indicated by the ground-based observations, but calculated decreases are less than half as large as those observed during the winter period in the middle and high latitudes. The range of calculated changes in total column ozone found with these different atmospheric models over these winter months varied between -0.4% to -0.6% at 30°N and -0.9% to -1.1% at 60°N latitude.

C-4.4 Statistical Analysis of Ground-Based Data

A statistical analysis of the ground-based ozone data from the Dobson stations has been made to assess the quantitative importance of the individual natural cycles and of the atmospheric nuclear tests, and to determine the magnitude of any remaining variations which exist in the measured ozone values after 1970. Analyses seeking any such non-cyclic trends have been made in previous statistical evaluations, as well as in this assessment, to determine whether the accumulation in the atmosphere of trace gases, especially the CFCs, has been accompanied by any non-cyclic changes in total ozone concentrations. In the multiple regression statistical analysis performed here, the potential ozone changes have been described by individual monthly trend coefficients rather than by uniform trend coefficients equally applicable for all twelve months. The one-dimensional atmospheric models used for more than a decade provide global average values for ozone concentrations at each altitude, and provide estimates only of smooth yearly trends in any changes in these values. These 1-D models do not provide, for example, any estimate of variations in trends in ozone concentrations with latitude or season. The use of monthly trend coefficients, adopted because of the apparent winter/summer differences in the magnitudes of observed ozone changes, has the effect of testing hypotheses of possible

Table C-4.1

Changes in Average Total Ozone Concentrations, as Measured at Individual Dobson Stations over the 22 Year Period, 1965-1986, Inclusive.

(Percentage Differences for 1976-1986 Compared to 1965-1975.)

North Latitude	Station	Winter[1]	Summer[2]	Annual
74.7	Resolute (Canada)	- 1.4±1.8[3]	- 0.8±0.9	- 1.6±1.0
64.1	Reykjavik (Iceland)	- 2.5±2.2	+1.7±1.3	+0.1±2.4
60.2	Lerwick (Scotland)	- 3.8±2.0	- 0.9±0.9	- 1.6±1.0
58.8	Churchill (Canada)	- 4.2±0.9	- 1.4±0.8	- 2.5±0.7
53.6	Edmonton (Canada)	- 4.7±1.3	+0.8±0.9	- 1.8±0.8
53.3	Goose Bay (Canada)	- 2.4±1.3	- 0.1±1.1	- 0.8±0.9
51.8	Belsk (Poland)	- 3.2±0.8	+1.2±1.0	- 1.2±0.9
50.2	Hradec Kralove (Czech.)	- 4.7±2.0	+1.1±0.9	- 1.8±1.1
47.8	Hohenpeissenberg (FRG)	- 1.8±1.7	+0.2±0.9	- 1.0±0.9
46.9	Caribou (Maine, US)	- 2.8±1.5	- 0.6±0.8	- 1.8±0.9
46.8	Arosa (Switzerland)	- 3.0±1.3	- 1.1±1.0	- 2.0±0.9
46.8	Bismarck (N. Dak., US)	- 3.0±1.2	- 1.4±1.0	- 2.0±0.7
43.8	Toronto (Canada)	- 1.3±1.2	- 1.3±0.8	- 1.2±0.7
43.1	Sapporo (Japan)	- 0.6±1.4	- 0.1±0.9	- 0.3±0.6
42.1	Vigna di Valle (Italy)	- 2.9±1.2	+0.7±0.9	- 0.9±0.9
40.0	Boulder (Colorado, US)	- 3.9±1.3	- 3.1±0.7	- 3.3±0.8
39.3	Cagliari (Italy)	- 2.5±1.7	- 0.7±1.1	- 1.1±1.2
36.3	Nashville (Tennessee, US)	- 1.8±1.4	- 3.3±0.7	- 2.4±0.8
36.1	Tateno (Japan)	- 0.7±1.6	- 0.5±0.8	- 0.4±0.7
31.6	Kagoshima (Japan)	+0.9±1.7	+0.5±1.0	+0.9±0.8
30.4	Tallahassee (Florida, US)	- 1.7±1.9	- 0.2±1.1	- 1.3±1.4
30.2	Quetta (Pakistan)	- 1.1±1.6	+0.1±0.8	- 0.7±0.8
25.5	Varanasi (India)	- 0.3±1.4	+0.4±0.9	- 0.2±0.9
19.5	Mauna Loa (Hawaii, US)	- 1.5±1.7	0.0±0.6	- 0.9±0.6
	30°N to 60°N	- 2.5±1.0	- 0.5±0.6	- 1.4±0.7
	40°N to 60°N	- 3.0±0.9	- 0.4±0.5	- 1.6±0.6
	30°N to 39°N	- 1.2±1.5	- 0.7±1.0	- 0.8±1.1

[1] Winter = Dec., Jan., Feb., March

[2] Summer = May, June, July, August

[3] Resolute is above the Arctic Circle, so that only less accurate moonlight measurements are available during actual winter. These "winter" data are the averages for the months of March & April.

ozone variations other than the simple assumption that any remaining trend must be equally applicable throughout the year.

These statistical analyses of the ground-based ozone data can be carried out through the examination of the individual results on a station-by-station basis, or by averaging the data over broad latitudinal bands. Both procedures have been applied in this study. Results have been obtained from three separate latitude bands covering the range from 30°N to 64°N. The scarcity of ground stations with long verified records makes latitudinal band averages south of 30°N less reliable. The data for these three latitude bands are shown in Figures C-4.1 and C-4.2 for the time period 1963 through 1986. Figure C-4.1 shows the variations in ozone concentrations for the latitude bands during the winter-spring (December through March) ozone season, while Figure C-4.2 displays the variations for the May through August period.

The magnitudes of the monthly linear trends corresponding to changes in total ozone since 1970 are shown in Table C-4.2 for three northern latitude zones with data from December 1964 through November 1986. Much less abundant data from time periods before 1965 have also been treated in a similar manner. Less reliable data have also been examined for the latitude band from 20°N to 29°N. A separate evaluation has also been made for the far-north band from 60°N to 80°N, using again some of the same stations included in the 53°N-64°N latitude band.

The magnitudes of the QBO and solar cycle effects in each latitude band are given in Table C-4.2. The well-known seasonal cycles are clearly present in the basic data and are not separately evaluated in the Table. The nuclear bomb test effects on stratospheric ozone were also evaluated in pre-1963 data, but have been calculated to be minimal by 1965, and were not included in the statistical evaluation of the data from 1965-1986. All of the statistical errors given in Table C-4.2 are at the one sigma level of significance.

The statistical estimates in Table C-4.2 of the magnitude and phase of the correlation of ozone change with the QBO, both of which vary significantly with latitude, are quite consistent with separate estimates obtained from satellite data. The measured response of total ozone to the solar cycle varies from small to about 2% peak-to-peak in the latitude bands, with the largest column ozone values found at the sunspot maximum in the winter of 1979-1980. The residual linear trends for individual months in Table C-4.2 have been averaged and give measurable changes in the annual average total column ozone of -1.7% to -3.0% in all latitude bands from 30°N to 64°N over the period from 1969 to 1986. The decreases are largest during the winter months (-2.3% to -6.2%, averaged for the four months from December to March), and smallest in the summer months (-0.2% to -1.9%, May through August, or +0.4% to -2.1%; June-August).

The trend coefficients for individual months were also tested for possible changes with the successive addition to the total data set of single years of data from 1980 through 1986, in effect a test of the appropriateness of the assumption of a linear trend since 1969. Most of the trend coefficients for the three latitude bands in Table C-4.2 show no important change with the addition of one to six additional years of data, although the overall tendency is toward more negative trend coefficients in 1986 than in 1980. However, the four months from April through July in the 40°-52° latitude band all show progressively more negative coefficients from 1980 through 1986. The measured ozone decreases for these months are not adequately described by an assumed linear variation with time since 1969, but have instead primarily occurred recently rather than gradually over the 17-year period, 1969-1986. An alternate statistical treatment with a non-linear function whose slope is approximately twice as large in 1986 as in 1965 provides a set of trend coefficients which

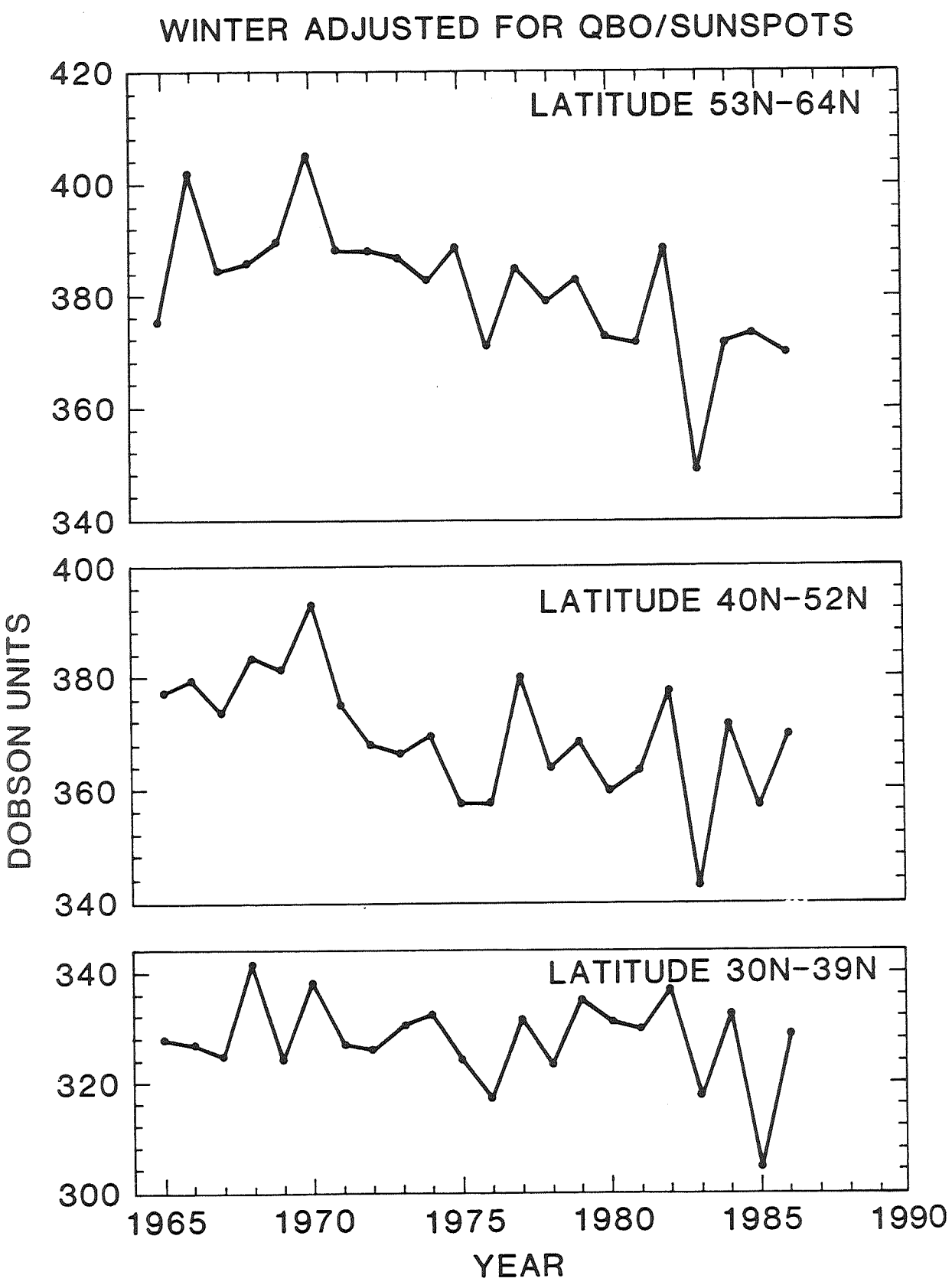

Figure C-4.1. Winter-Spring ozone concentrations (in Dobson Units) for three latitude bands in the Northern Hemisphere. (December, January, February, March; Data begin with December 1964, and end with November, 1986.) The calculated statistical contribution from the QBO and the solar sunspot cycle have been removed from the data.

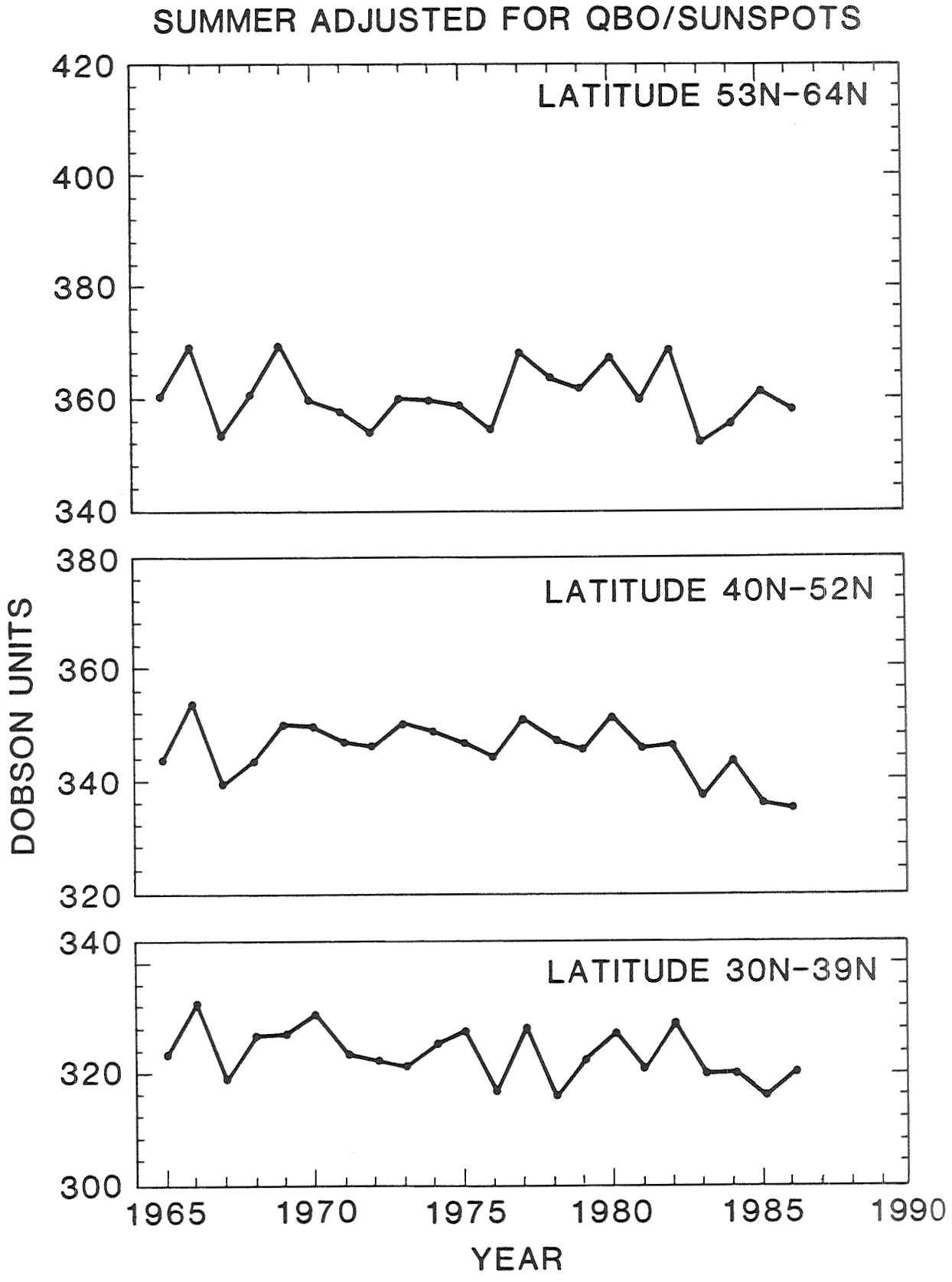

Figure C-4.2. Summer (May-August) ozone concentrations (in Dobson Units) for three latitude bands in the Northern Hemisphere. The calculated statistical contribution from the QBO and the solar sunspot cycle have been removed from the data.

Table C-4.2

Coefficients of Multiple Regression Statistical Analysis of Re-analyzed Dobson Measurements of Total Ozone Concentrations Collected into Latitudinal Band Averages. (Data are expressed in total percent changes for the period 1969-1986.)

	Latitude Band		
Month	53-64°N	40-52°N	30-39°N
January	- 8.3±2.2	- 2.6±2.1	- 2.2±1.5
February	- 6.7±2.8	- 5.0±2.2	- 1.2±1.9
March	- 4.0±1.4	- 5.6±2.3	- 3.5±1.9
April	- 2.0±1.4	- 2.5±1.7	- 1.7±1.3
May	- 2.1±1.2	- 1.3±1.1	- 1.7±0.9
June	+1.1±0.9	- 1.8±1.0	- 3.3±1.0
July	+0.0±1.1	- 2.2±1.0	- 1.3±1.0
August	+0.2±1.2	- 2.4±1.0	- 1.0±1.0
September	+0.2±1.1	- 2.9±1.0	- 1.0±0.9
October	- 1.1±1.2	- 1.5±1.5	- 0.9±0.8
November	+1.5±1.8	- 2.4±1.3	- 0.1±0.8
December	- 5.8±2.3	- 5.5±1.7	- 2.1±1.1
Annual Average	- 2.3±0.7	- 3.0±0.8	- 1.7±0.7
Winter Average	- 6.2±1.5	- 4.7±1.5	- 2.3±1.3
Summer Average (a) JJA	+0.4±0.8	- 2.1±0.7	- 1.9±0.8
(b) MJJA	- 0.2±0.8	- 1.9±0.7	- 1.9±0.8
QBO*	- 2.0±0.6	- 1.3±0.6	+1.9±0.6
Solar*	+1.8±0.6	+0.8±0.7	+0.1±0.6

* Percent changes per cycle, minimum-to-maximum. All uncertainties are expressed with one sigma statistical significance.

Average of Monthly Ozone Trends in Dobson Units per year and Percent change in 17 years (See Table C-4.2 above - annual average):

DU/yr:	- 0.52±0.16	- 0.63±0.17	- 0.32±0.14
%/17 yrs:	- 2.3±0.7	- 3.0±0.8	- 1.7±0.7

Uniform Trend in Ozone Change Assumed throughout the year, in Dobson Units per year and in Percent Change in 17 years:

DU/yr:	-0.14±0.13	-0.47±0.13	-0.17±0.11
%/17 yrs:	-0.7±0.6	-2.3±0.7	-0.9±0.6

is marginally superior to the standard simple assumption of linearity in such trend estimates.

The trend coefficients found for multiple regression analysis with the usual assumption of a single trend applicable throughout the year in comparison with the results from 1-D atmospheric models are given at the bottom of Table C-4.2 in parentheses in percent change over the 17 years from 1969 to 1986. Differences exist: (a) among the indicated trends for different seasons, and between (b) a yearly ozone change obtained as the average of the monthly trends and (c) the yearly ozone change found with the assumption of a uniform trend throughout the year. The value in Table C-4.2 from (b) is always more negative than from (c). Because the trends found in winter and summer months are usually significantly different from one another, the basic assumption underlying (c) is not a satisfactory model for northern latitude ozone data, and the regression coefficients in parentheses should be replaced by the regression coefficients for individual seasons. The underestimate of the average ozone loss in (c) relative to (b) is the consequence of the greater statistical weight given to the more precise summer data in calculating a uniform trend to the data for all of the months simultaneously. The calculation of a yearly average absolute change in ozone concentration or in percentage loss is itself somewhat artificial to the extent that the differences between winter and summer trends may reflect different underlying physical or chemical mechanisms leading to ozone variability.

The changes calculated in total column ozone with current atmospheric models as the consequence of variations in the output of ultraviolet radiation over the 11-year solar cycle are broadly consistent with the changes indicated by the multiple regression analysis. However, while the predicted decreases in total column ozone caused by the increased abundances of trace gases (including the CFCs, methane, nitrous oxide and carbon dioxide) are consistent with the observed decreases during the summer period, the mean values of observed winter-time decreases are larger than calculated in the atmospheric models.

In assessing the overall changes in total ozone concentrations, it should be kept in mind that observational balloon-sonde data suggest that tropospheric ozone concentrations may have increased in mid-latitudes in the Northern Hemisphere by as much as 1% per year over the past 20 years. Such changes in the lower atmosphere are equivalent to an increase in total column ozone of about 2%, and would appear in total ozone observations in combination with any changes in stratospheric ozone.

C-4.5 Total Column Ozone Changes from Satellite Data

The total ozone data measured by the SBUV and TOMS instruments on the Nimbus 7 satellite require independent calibration because of the slow degradation with accumulated exposure to direct solar radiation of the diffuser plate common to the operation of both. The quantitative influence of this degradation in the diffuser plate on total column ozone observations can be checked by comparison of the total ozone found during satellite overpasses of ground stations. Three separate, not totally independent procedures have been used in these satellite/ground intercomparisons. The first used a set of data from 41 Dobson stations, with no selection of the ground-based data for overall quality of the data from these stations. A second procedure has utilized the overpass data for a total of 92 Dobson and filter ozonometer stations from 1978 on, with selection of the ground-based data such that records from individual stations were eliminated when the ground data for any particular month showed excessive scatter in the overpass differences. A third method involved satellite overpasses of Mauna Loa, Hawaii, on those days during which the World

Primary Standard Dobson instrument was undergoing its regular periodic recalibration at that location. An overpass of an individual Dobson station is illustrated in Figure C-4.3 with the TOMS ozone readings for June 29, 1979, in the vicinity of the Hawaiian Islands. The circled measurement was recorded at Mauna Loa on that day by the World Primary Standard instrument. (Ozonesonde data were used to correct for the ozone amounts between the altitude of the Mauna Loa Observatory and the mostly oceanic surface sensed by TOMS.)

All three satellite/ground tests gave consistent results indicating that the ozone measurements with the satellite instruments drifted over time by -3.5±0.5% during the nine years following satellite launch in October 1978. The overpass data versus 41 stations are shown by the small dots in Figure C-4.3, while the crosses represent average values for the comparisons with the World Primary Standard at Mauna Loa during the indicated summers. Further, an independently derived algorithm for treatment of the satellite data has shown close agreement with this ground-based calibration of the satellite instruments, confirming that a drift of this magnitude was quite consistent with the known instrument properties. The choice among the various algorithms consistent with the satellite operational data has been made by accepting the ground-based comparisons as a valid recalibration of the satellite instruments.

The total ozone data accumulated with the TOMS instrument have therefore been provisionally recalculated with the assumption that the algorithm used to convert measured instrumental radiances into ozone concentrations has been systematically drifting by a total of -3.5% over the nine-year period from 1978-1987. Detailed analysis of the auxiliary satellite data is still continuing to determine whether more precise calibration data can be recovered. The drift has not been uniform as shown by the line in Figure C-4.4, and the data have been modified on the basis of specific correction factors for each month mirroring the uneven degradation over time. This normalization procedure assumes that no significant latitudinal bias exists in the drifting of the conversion algorithm with time. When calculated in this way, the normalized TOMS satellite data show a decrease of total column ozone between October 1978 and October 1985 in all latitude zones in both the Northern (-1.1% to -3.7%) and Southern (-1.1% to -9.0%) Hemispheres, as shown in Table C-4.3. The time period from late 1978 to late 1985 corresponds generally to the decline from solar maximum (December 1979) to solar minimum (summer 1986), and these changes therefore represent a combination of ozone variability attributable to inceases in trace gases and to declining solar activity. Because the satellite data do not yet include even one full 11-year solar sunspot cycle, no attempt has been made to separate these trends in the satellite data set taken alone, or to evaluate the magnitudes of the variations accompanying the solar sunspot and QBO cycles.

Data from the latitudes poleward of 53° latitude in each hemisphere are not included in the global or hemispheric calculations of Table C-4.3, but are given separately for the bands between 53°-65° in both hemispheres. No band analysis poleward of 65° has been given because of the absence of any measurements from the polar night. The differences in the zonal average ozone concentrations indicated by TOMS, after calibration to the ground-based instruments, are shown in Figure C-4.5 by month and latitude, with contour lines for every 2% difference in ozone. The data have been averaged over the years 1986 plus 1987, and 1979 plus 1980 to smooth out most of the fluctuations associated with the QBO. The large losses of ozone associated with the Antarctic spring appear in the lower right of Figure C-4.5. However, ozone decreases as large as 5% are indicated year-round as far north as 60°S, for most months to 50°S, and in mid-summer to 40°S.

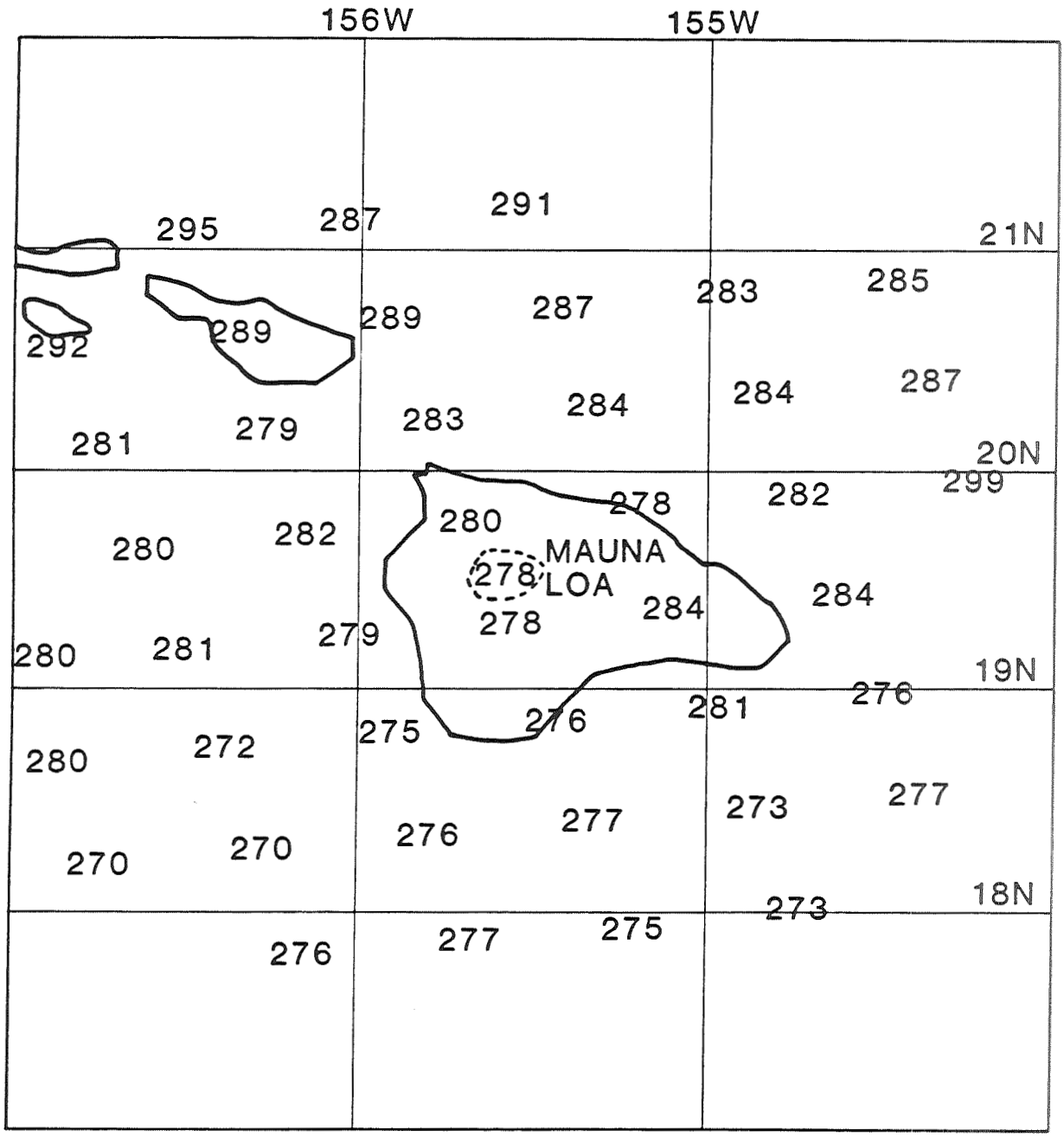

Figure C-4.3. Intercomparison of TOMS overpass measurements of total ozone with World Primary Standard Dobson ozone measurements at Mauna Loa Observatory, Hawaii, June 29, 1979. The Mauna Loa measurement is enclosed in the broken circle.

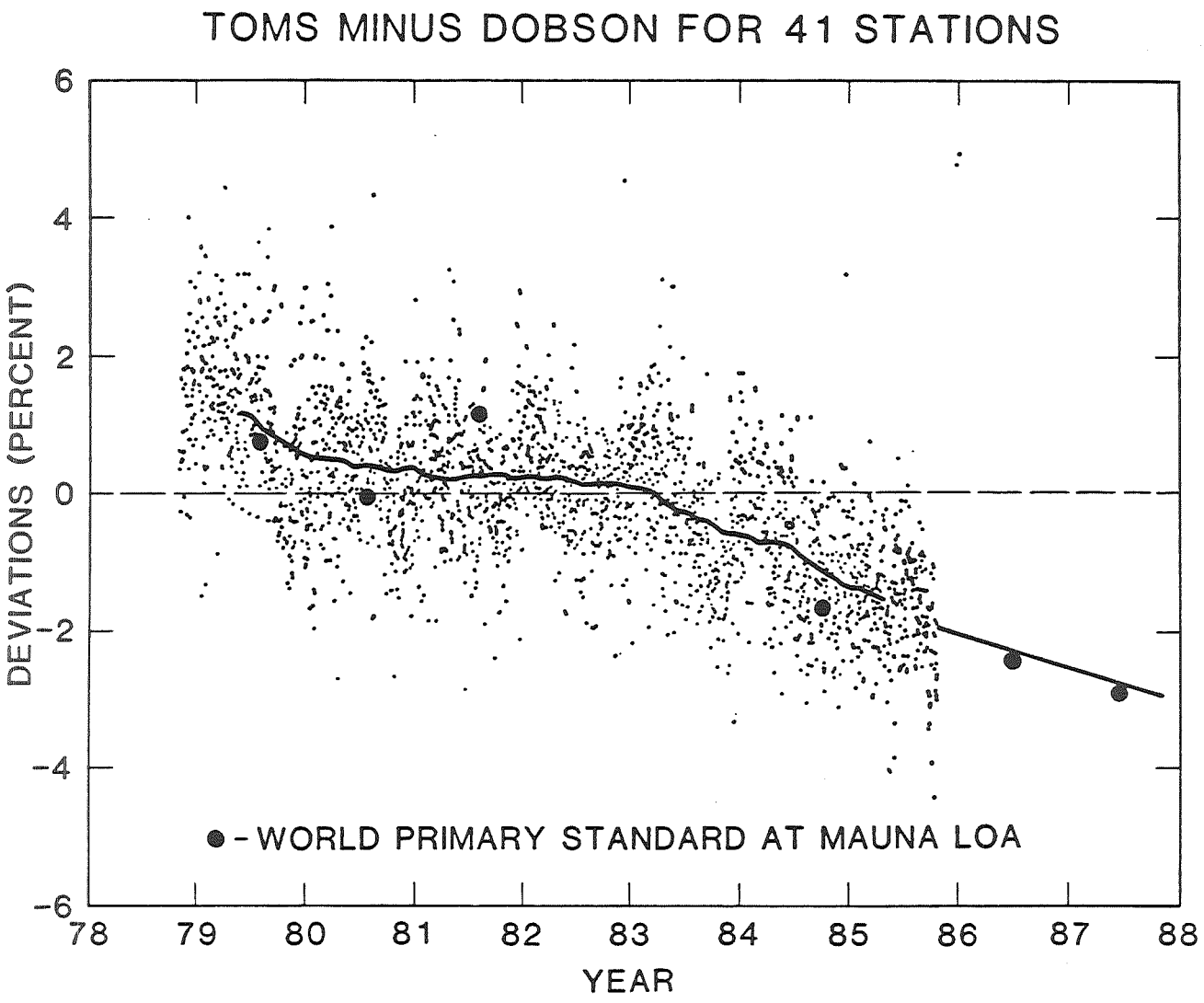

Figure C-4.4. Intercomparisons of TOMS overpass measurements of total ozone with ground-based ozone data from 41 stations (small dots) and with the World Primary Standard Dobson during summer measurements at Mauna Loa, Hawaii.

Table C-4.3

Percentage Changes in Total Column Ozone

(Measured by TOMS on Nimbus 7, Calibrated by Comparison with Ground-Based Measurements)

Latitude Band	Total Change from 11/1978 to 10/1985	From Table C-4.2 (1969-1986)	Total Change from 11/1978 to 11/1987
Global, except high latitudes			
53°S - 53°N	- 2.6±0.5		- 2.5±0.6
Hemispheric			
0 - 53°S	- 2.6±0.9		- 2.9±0.9
0 - 53°N	- 2.1±1.5		- 1.8±1.4
Bands			
53°S - 65°S	- 9.0±1.8		-10.6±1.6
39°S - 53°S	- 5.0±1.8		- 4.9±1.8
29°S - 39°S	- 3.2±2.4		- 2.7±2.1
19°S - 29°S	- 2.5±1.9		- 2.6±1.5
0 - 19°S	- 1.1±0.8		- 2.1±0.8
0 - 19°N	- 1.1±1.5		- 1.6±1.3
19°N - 29°N	- 3.5±2.2		- 3.1±1.9
29°N - 39°N	- 3.7±2.0	-1.7±0.7	- 2.5±1.7
39°N - 53°N	- 2.7±1.7	-3.0±0.8	- 1.2±1.5
53°N - 65°N	- 2.4±1.6	-2.3±0.7	- 1.4±1.4

(Linear trends with an autoregressive model through TOMS data, with uncertainties at the one sigma level of significance.)

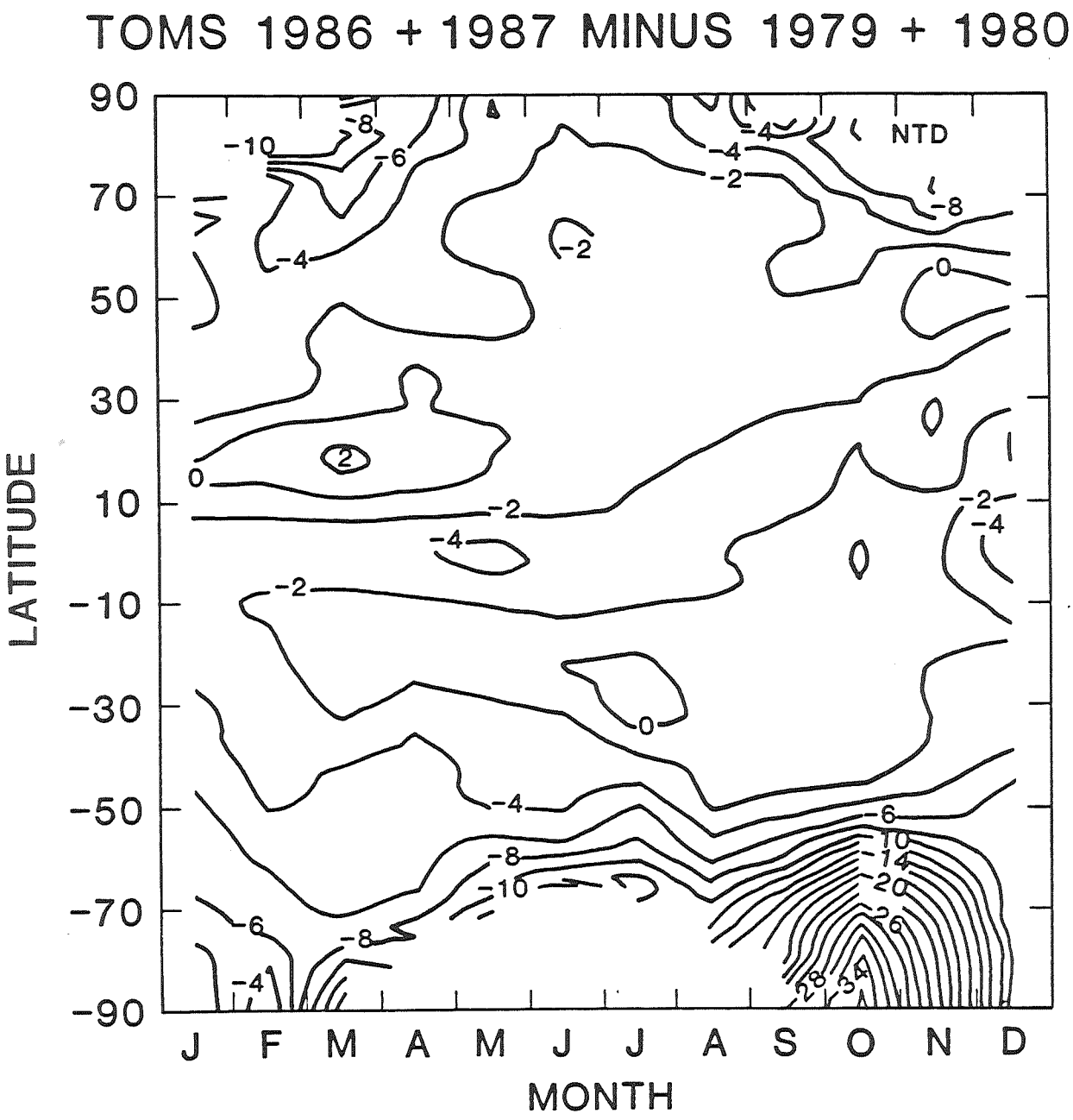

Figure C-4.5. Changes by month and latitude in total ozone between 1979/1980 and 1986/1987 as measured with TOMS on the Nimbus 7 satellite. (Two year averages are used to minimize differences originating with the QBO.) Contour plots are given for intervals of 2 percent change. The TOMS data have been normalized to the Dobson (NTD) ground-based data as shown in Figure C-4.4. The TOMS instrument operates with sunlight scattered from the atmosphere and therefore provides no data from the areas in the polar night.

Atmospheric model calculations of changes in total column ozone from 1979 to 1985 predict a decrease representing the sum of a loss because of the increased abundance of CFCs and other trace gases, and an additional loss because of the declining phase of the solar sunspot cycle. The model calculations show a greater change in total column ozone at mid to high latitudes in winter (-0.5% to -1.5%) than in summer (-0.2% to -0.6%), while the contribution to ozone decrease from the lessening solar activity is found to be relatively the same in the models for all seasons and latitudes. The magnitude of the solar cycle variation is uncertain because of lack of precise knowledge of the variations in short wavelength solar ultraviolet emission over the complete solar cycle, and is estimated to lie between -0.7% and -2.0% from the maximum to the minimum of the cycle.

The change in total column ozone in the Northern Hemisphere predicted in the models is generally consistent with the observations over the period 1979 to 1985, although the measurements suggest that the largest changes may have occurred in the mid-latitudes while the models predict the largest changes at high latitudes. Because the models used in these calculations do not have the capability of predicting the loss of ozone associated with the Antarctic ozone hole phenomenon, comparisons of model calculations with Southern Hemispheric observations must be made only with substantial reservations about the significance of the results.

Examination of the normalized TOMS satellite data given in Table C-4.3 suggests that total column ozone in the Northern Hemisphere has increased since passing the combination of the intensive QBO of 1985 and the solar minimum in 1986. On the other hand, the decrease of total column ozone averaged over the Southern Hemisphere appears to have continued through 1987 at approximately the same rate as for 1978 to 1985. Such an observation could be the consequence of sufficient losses in ozone through the special conditions of Antarctic springtime to cancel out any projected increase in total ozone from the increasing phase of the solar cycle. The current solar cycle should peak about 1991, after which the cyclical change in ozone concentration in response to solar variability is expected again to trend downward.

C-4.6 Recommendation

The ground-based Dobson measurement system and, to a lesser extent, the filter ozonometers, play important roles in the global ozone monitoring system. They do this both through direct determinations of ozone concentrations over specific geographic locations over a long period of time, and by ground-truth calibrations of the satellite systems. While much of the data from these systems has been reanalyzed in this assessment, more accurate re-evaluations can be made by examination of the day-to-day measurements at each individual ground-based station by the various national meteorological services. With vigorous efforts to carry out such re-evaluation of data, the existing 25 to 30 year records of the ground-based stations can be made even more useful for determination of trends in ozone concentrations over the past three decades. Vigorous efforts in upgrading past data can be especially useful now and in the next few years. Such re-evaluation and interpretation of data on total ozone concentrations should involve broader participation of the scientific community than it has in previous years. Finally, the measurement of ozone on a global basis requires a truly international effort supported strongly by the various national organizations.

Chapter 5: Trends in Ozone Profile Measurements

C-5.1 Introduction

Atmospheric modelers predicted (in 1984, for example) that within about a century release of chlorofluorocarbons at the 1980 rate (along with a doubling of carbon dioxide and methane and a 20 % increase of nitrous oxide) would change the global average ozone column between +0.2 and -5.2 % , and the change in local ozone at 40 km would be -35 to -55 % [WMO, Chapter 13, 1985]. The great sensitivity of local ozone in the upper stratosphere to chlorine has led to an emphasis on this region as possibly supplying an early warning with respect to global ozone change. The Solar Backscattered Ultra-Violet (SBUV) satellite instrument has four channels that are used to measure total ozone and other channels that are used to measure the vertical profile of ozone in the upper stratosphere. The ground based Dobson stations measure the total ozone vertical column, and some Dobson instruments are used in the Umkehr mode to measure the vertical profile of ozone. Chapter 4 is concerned with trends that have occurred in the ozone vertical column, and Chapter 5 is concerned with trends that have occurred in the vertical profiles of ozone in the upper stratosphere, where ozone is especially sensitive to chlorine. This region is variously given as 30 to 50 km, 16 to 1 mb, or Umkehr layers 6 through 9.

The Solar Backscattered UltraViolet (SBUV) instrument was launched on the Nimbus 7 satellite in October 1978. For the period 1979 to 1985, the newly (1986) interpreted data showed (among many other things): (1) The maximum local ozone reduction occurred at an altitude of 50 km, instead of at the theoretically predicted 40 km [WMO 1985, Chapter 13]. (2) Between ± 30 degrees latitude the maximum local ozone reduction was 20 to 25 % instead of the theoretically predicted 10 to 15 % [WMO, 1985, page 761]. The job of this chapter is the relatively narrow one of confirming, disproving, or modifying the SBUV reported ozone changes in the middle and upper stratosphere. Eight other systems were found that give information about the ozone vertical profile between 1979 and 1987 that are judged to be applicable to this study (Table C-5.1). To the extent that the SBUV trends are not supported, the question becomes: What changes in ozone are given by the other observations?

C-5.2 Solar Backscattered Ultraviolet Instrument, SBUV

According to the archived SBUV data for the time interval 1979-1986, the ozone changes are not subtle effects buried in noisy data and requiring a detailed analysis to see if they are statistically significant. They are large effects clearly visible to the naked eye, for example, Figures C-5.1 and C-5.2. The plots in the left column of Figure C-5.1 show the original data in Dobson units, and those on the right column show data that have been de-seasonalized by removing the annual and semi-annual seasonal components. The plots show a definite downward non- linear trend in the SBUV ozone data. They show seasonal variations that are comparable to the seven-year change, which places serious requirements on sampling of the data in the search for trends. The graphs of ozone in Umkehr layer 6 show a sharp dip beginning in mid 1982, which is ascribed to the volcanic eruption of El Chichon in April 1982. A more extensive set of SBUV data is given as contour plots of percentage ozone mixing ratio change (1979-1986) as a function of altitude and latitude, Figure C-5.2. The solid lines show the ozone changes within the zone where SBUV has primary information content (Chapter 3); and the points outside this region, derived from a

TABLE C-5.1. Ozone Measuring Systems and Periods of Available Data

Type	Description	Time Period
Satellite	Solar Backscattered Ultraviolet (SBUV)	Oct 1978 - Feb 1987
Satellite	Stratospheric Aerosol and Gas Experiment (SAGE)	Feb 1979 - Nov 1981
Satellite	SAGE II	Oct 1984 - present
Satellite	SBUV/2	Dec 1984 - present
Ground-based	Umkehr stations using Dobson spectrophotometer	1950's - present
Satellite	Solar and Mesospheric Explorer (SME)	Jan 1982 - Dec 1986
Satellite	Solar Maximum Mission (SMM or UVSP)	1985 - present
Satellite	Limb Infrared Monitor of the Stratosphere (LIMS)	Oct 1978 - May 1979

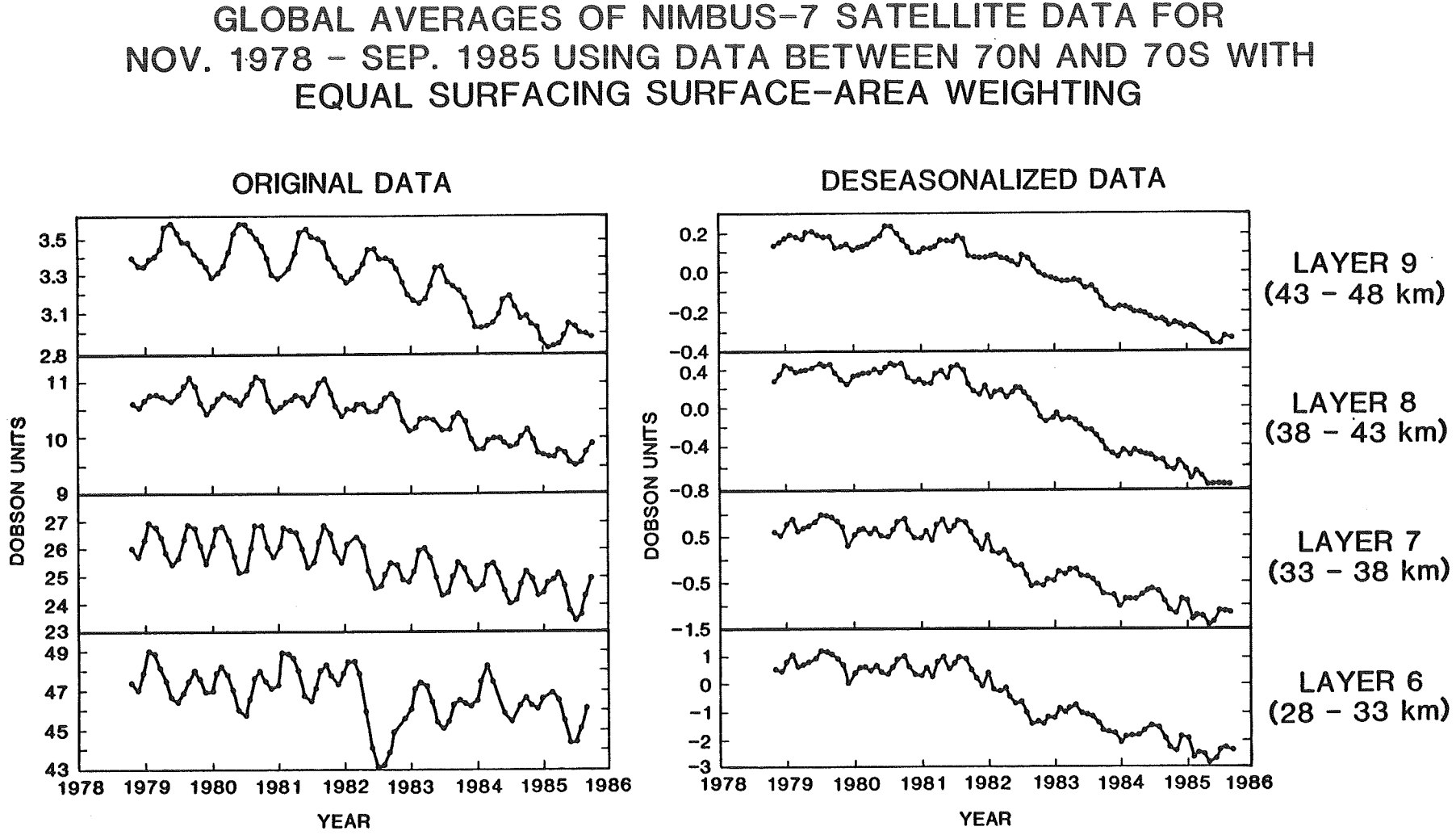

Figure C-5.1. Zonal averages of SBUV ozone data for November 1978 to September 1985, averaged between 70°S and 70°N with equal surface weighting, including Umkehr layers 6-9.

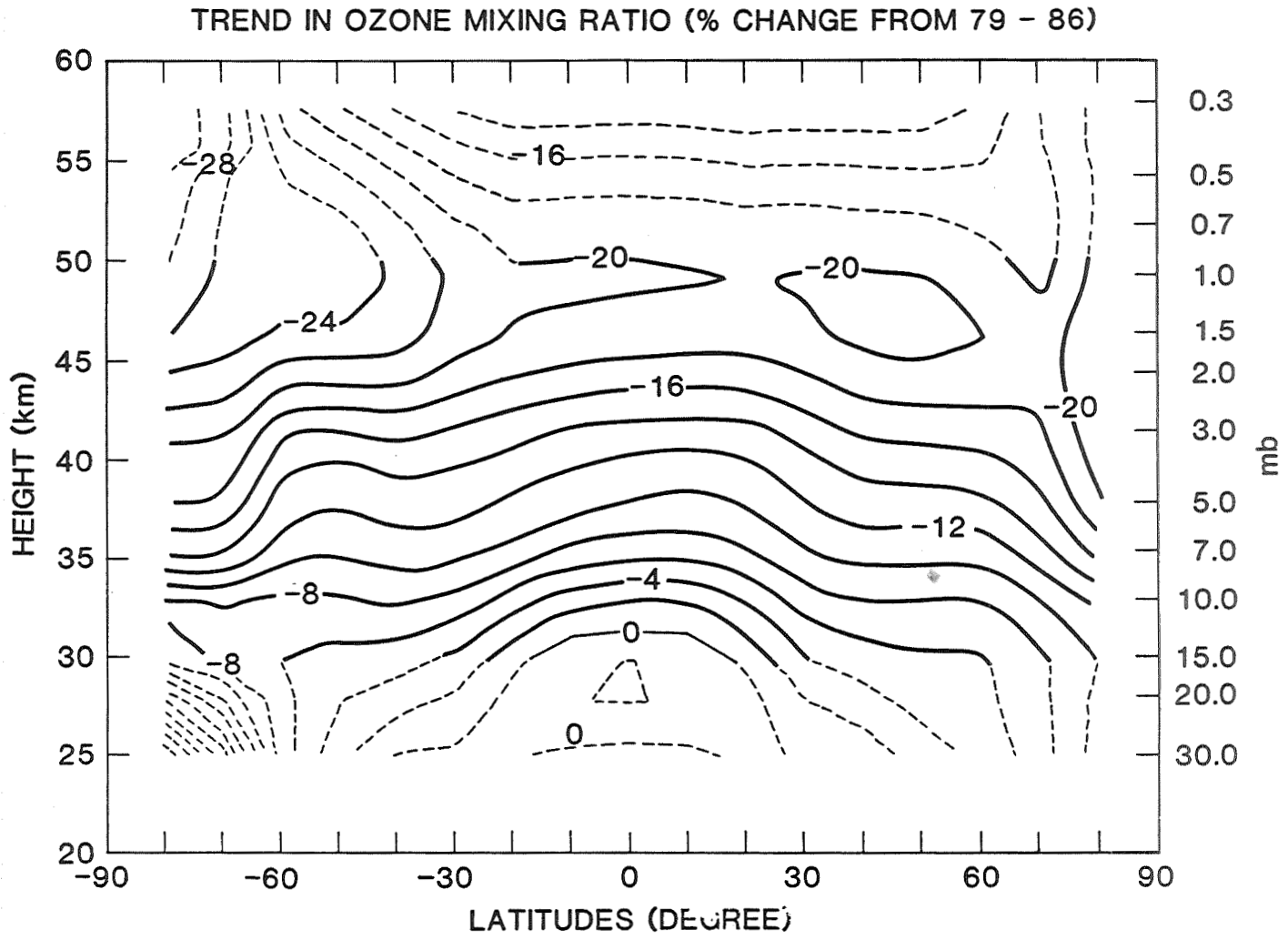

Figure C-5.2. The percentage change in SBUV ozone mixing ratio as a function of altitude and latitude from 1979 to 1986. The percentage change is computed for each pressure and latitude. The solid lines are within the region where SBUV has primary information content (Chapter 3). The dashed lines are extrapolations based on a climatological model.

climatological model, are shown as dashed lines. This figure shows local ozone reductions at 50 km to be 20 percent or more at all latitudes.

The approach of this chapter is first to compare the SBUV results against other satellite and ground based systems in terms of conspicuous aspects of the primary data, such as Figures C-5.1 and C-5.2, and later to examine derived statistical quantities.

C-5.3 Ozone Changes From Comparison of SAGE I and SAGE II

(1) Conspicuously visible results:

A comparison of SAGE I and SBUV ozone measurements is presented for the periods February 1979 through November 1981, and a comparison of SAGE II and SBUV is made for the period October 1984 through December 1986. The SBUV data were searched for those events nearly coincident in time and space to the SAGE I/II events. The working data for such coincidences are analyzed as time series in several latitude bands, for example, see Figure C-5.3 for Umkehr layers 8 and 9 at 40 south. SAGE I ozone layer amounts are consistently lower than SBUV in 1979-1981 by 4 or 5 % in layers 7-9 and higher than SBUV by 4% in layer 6 while SAGE II ozone layer amounts are consistently higher than SBUV in 1984-1986 by 10 ± 3 %, a change of up to 15 %. For Umkehr layers 6 through 9, the 1980-1985 offset between SAGE and SBUV increases monotonically with altitude by between 4 % and 15 %. The magnitude and sign of this conspicuous offset is a large fraction of the entire change in ozone given by SBUV between 1979 and 1986, Figure C-5.2. The large decrease in ozone that SBUV reports in layers 7-9 over this same period, 8 to 17 %, is not supported by SAGE I and SAGE II data comparisons. On the basis of conclusions reached in Chapters 2 and 3, this difference is ascribed to an insufficiently corrected degradation of the SBUV diffuser plate.

(2) Small ozone changes requiring careful statistical analysis:

SAGE I and SAGE II satellite data are used to estimate the change in the upper stratospheric ozone profile between 1980-81 and 1985-87. The previous comparisons between SAGE I and SAGE II involved the Umkehr-layer amounts and were designed to compare SAGE I and II with SBUV observations. The fundamental SAGE measurements are concentration profiles as a function of geometric altitude from 25 km to 50 km. On the basis of spatial intersections between SAGE I and SAGE II over corresponding three-year periods that are six years apart, comparisons are performed between SAGE I and SAGE II ozone concentration measurements. (Because of differences of sampling pattern, the number of spatial intersections between SAGE I and SAGE II is much smaller than the number of coincidences between SAGE and SBUV, causing the SAGE I/II comparisons to be noisy, relative to Figure C-5.2 for example). The percentage differences are averaged in time within 10 degree latitude bands and plotted versus altitude in Figure C-5.4. Except at 60°S, the magnitude of the differences is only on the order of 5 %. For the 13 ozone change profiles, the altitudes of maximum percentage ozone reduction are between 40 and 45 km, and the magnitudes of these maximum ozone reductions vary between 2 and 8 %. With some exceptions, the pattern is an ozone decrease in the upper stratosphere and another decrease near 25 km between 1980 and 1986.

An analysis of all SAGE I/II spatial intersections between 20 to 50°N and 20 to 50°S gives the ozone-change profiles of Figure C-5.5. The average ozone-change profiles show: (i) an ozone decrease between 35 and 45 km with the maximum ozone reduction of 3 % occurring at 40 km, (ii) another region of similar percentage ozone decrease occurring at

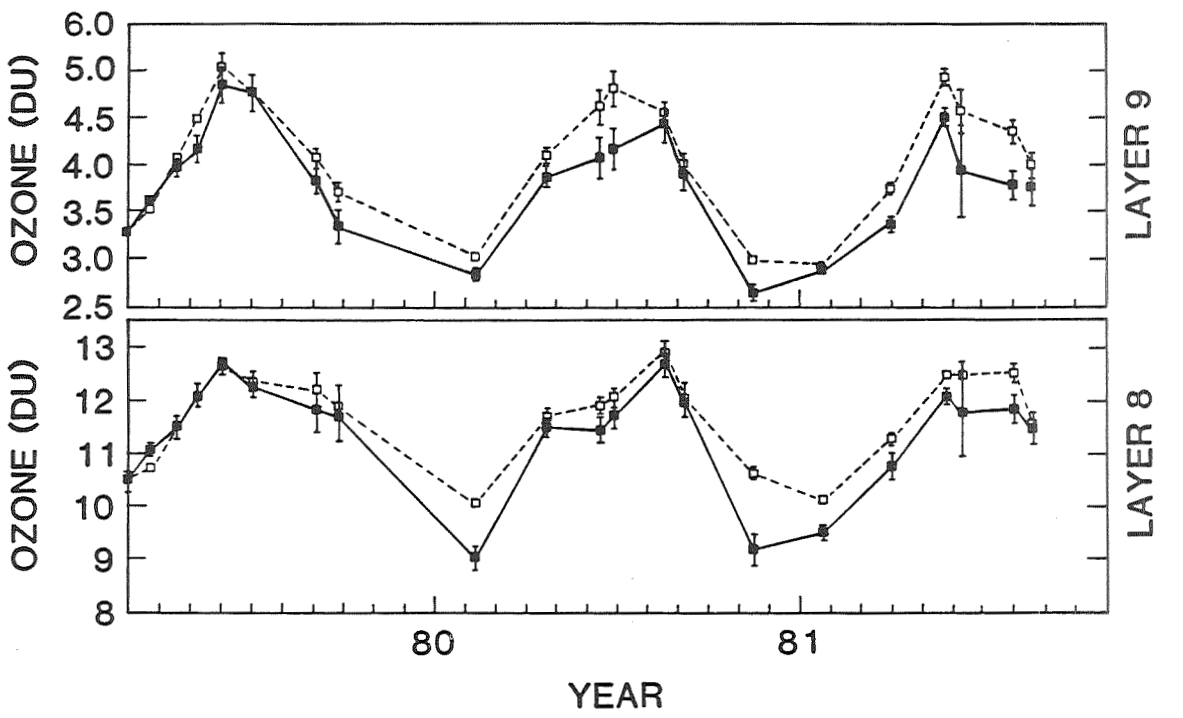

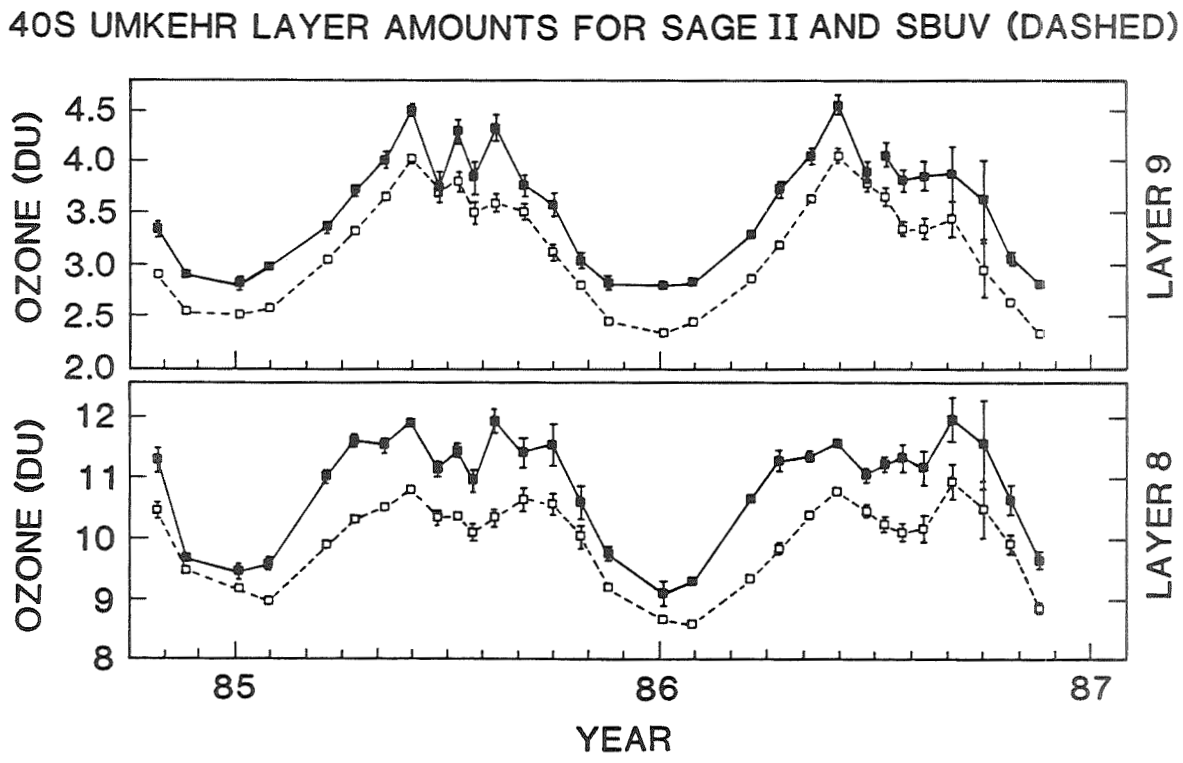

Figure C-5.3. Zonal average ozone over Umkehr layers 8 and 9 at 40°S. Upper panels: time series of SAGE I and SBUV coincident measurements for 1979-81. Lower panels: time series of SAGE II and SBUV coincident measurements for 1985-87. The error bar represents the 95% confidence interval on the zonal mean. Lines connecting means are intended only as a visual aid.

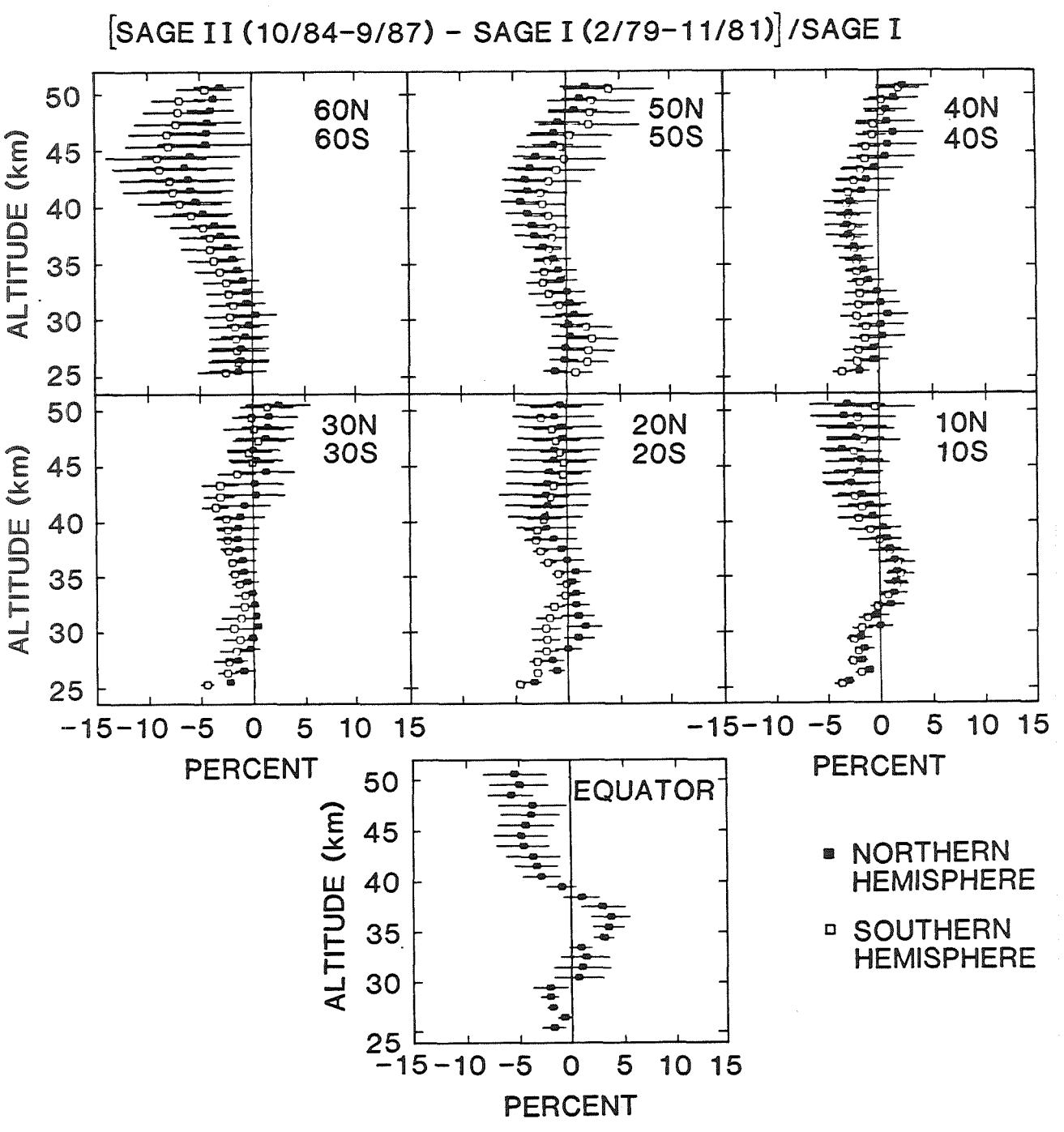

Figure C-5.4. Mean percentage difference between SAGE II and SAGE I versus geometric altitude (SAGE I is the reference). For each latitude band approximately 8 intersections (corresponding altitudes and latitudes, six years apart) were available from which to compute percentage differences. The average percentage difference along with its standard error are plotted. The standard error reflects only the variations between the 8 percentage differences in a given latitude band.

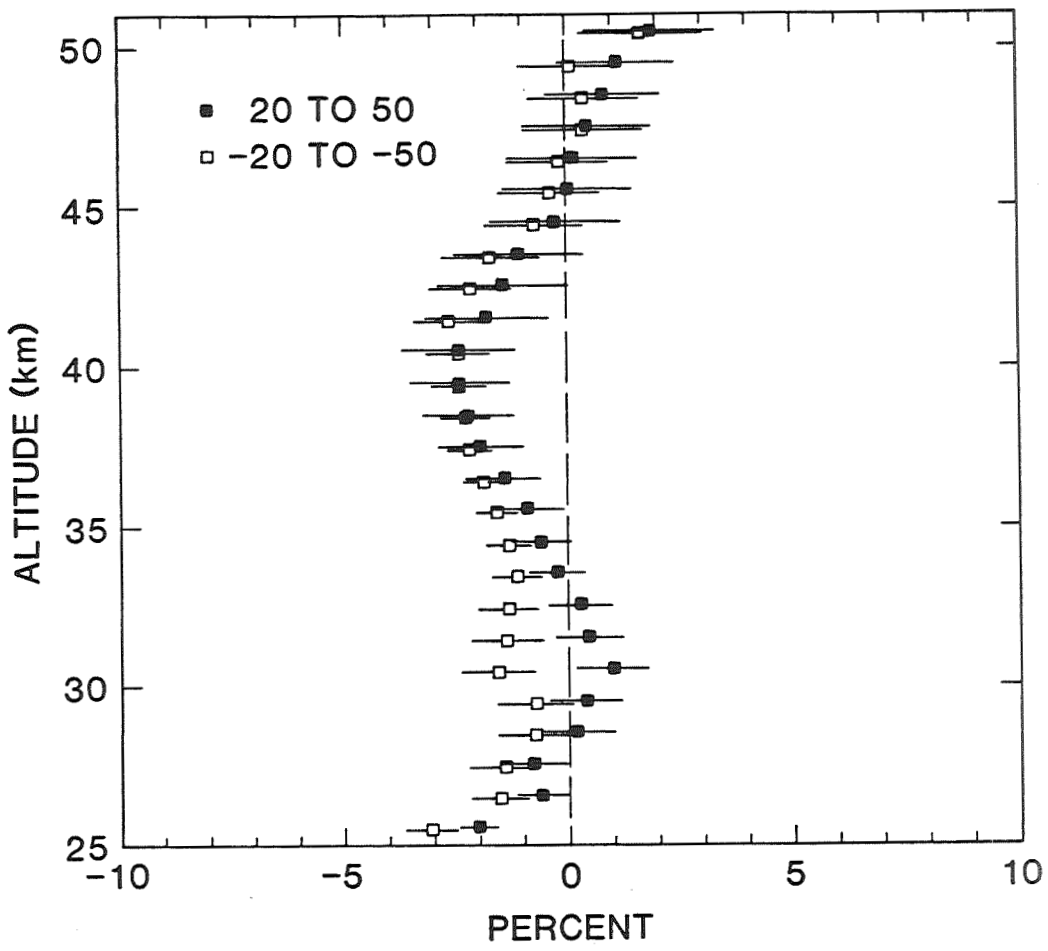

Figure C-5.5. Mean percentage difference between SAGE II and SAGE I versus geometric altitude (SAGE I is the reference). All intersections occurring between 20°N and 50°N (or 20°S to 50°S) were combined into one sample. The horizontal bars are the standard errors of the sample of percentage differences. Within each hemisphere approximately 2500 SAGE I profiles and 6000 SAGE II profiles were used in computing the statistics.

about 25 km, and (iii) essentially zero ozone change at 30 km and at 50 km (Note that Figure C-5.4 shows some ozone decrease at 50 km for 0 and ± 60 degree latitude). The 95 % confidence level for the average ozone reduction in the upper stratosphere indicated by SAGE over the five year period is ± 3 %. The estimated relative systematic error is ± 4 % between the SAGE I and SAGE II instruments. The unexpected, indicated 3 % ozone reduction at 25 km, near the ozone concentration maximum, should be given careful consideration in the future.

C-5.4 Solar Backscattered Ultraviolet II (SBUV - 2)

The National Plan for ozone monitoring is to launch another SBUV instrument about every two years, to obtain overlapping periods of ozone satellite data, and to use this matching procedure along with the Dobson instruments to correct for instrumental degradation. The first example of this plan was the SBUV/2 system that was launched in December 1984, and it has been returning data suitable for deriving total ozone and the ozone profiles since early 1985. A potentially powerful method to verify, modify, or disprove the SBUV reported trends would be to compare SBUV with validated SBUV/2 data in at least these two ways: (i) Compare the ozone magnitudes reported by the two twin instruments immediately after launch. (ii) Look for a change using the first two years of SBUV and the corresponding two years of SBUV/2 five years later (as was done with SAGE I/II). Members of the team responsible for SBUV/2 data told the Ozone Trends Panel in January 1988 that the reinterpreted data were so preliminary and so incompletely examined (even after three years since launch) that they should not be used in this report.

C-5.5 Umkehr Measurements of Upper Stratospheric Ozone

Direct examination of the Umkehr data for layers 6, 7, and 8 shows that ozone decreased noticeably between 1979 and 1986, but this simple method of inspection is complicated by the large effect of aerosols from El Chichon volcano in the middle of this period (Figure C-5.6, upper panel). In terms of the injected quantity of stratospheric sulfate aerosols, El Chichon was one of the most powerful volcanoes of the century. An objective method for correcting the effect of aerosols on Umkehr observations uses stratospheric aerosol profiles observed by LIDAR, a particle size distribution based on stratospheric (but not site coincident) measurements, ozone-sonde profiles, and radiative transfer theory similar to that for the Umkehr inversion algorithm. This method was applied to five northern mid-latitude Umkehr stations (between 36°N and 52°N) to estimate changes in the ozone profile from 1978 through 1987. Combining statistical errors and estimated errors due to aerosols, Umkehr data for five stations show ozone changes: -3 ± 3 % in layer 6; -8 % ± 4 % in layer 7; and -9 % ± 5 % in layer 8, between 1979 and 1986. At layer 8, for example, the ozone change given by archived SBUV is about -15 %, (Figure C-5.2) and that given by SAGE I/II is -3 ± 3 % (Figure C-5.5). The SAGE and Umkehr error estimates are for a 95 % confidence level but do not include possible systematic errors.

C-5.6 SBUV-SAGE-LIMS Ozone Intercomparison (Spring 1979)

These data show that three totally different, newly launched satellite systems agree with each other to about 4 or 5 % in measuring zonal mean ozone amounts over a one month period in Umkehr layers 6 to 9, Figure C-5.7.

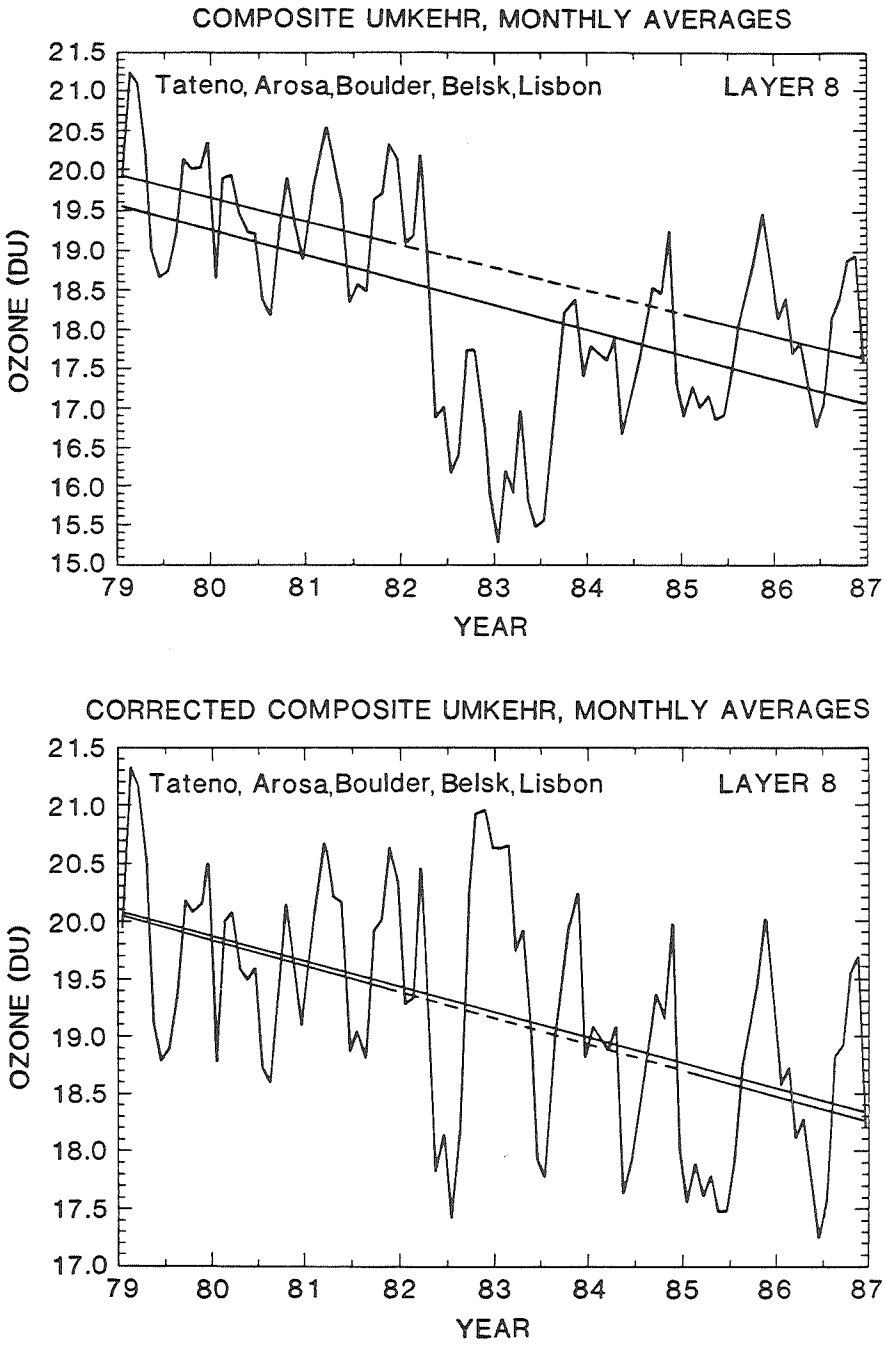

Figure C-5.6. Plots of monthly average ozone concentration vs time in Umkehr layer 8 for five Umkehr stations for precisely eight years including 1979 through 1986. Data are used as supplied by the World Ozone Data Center at Toronto. The data in the upper panel have not been corrected for stratospheric aerosol error. Note the effect of El Chichon during the winter of 1982-83. The data in the lower panel have been corrected for aerosols by DeLuisi et al.[1]. The least squares lines are: (i) Solid line includes all seven years of data. (ii) Solid-dashed-solid line omits precisely the three years 1982, 1983, and 1984.

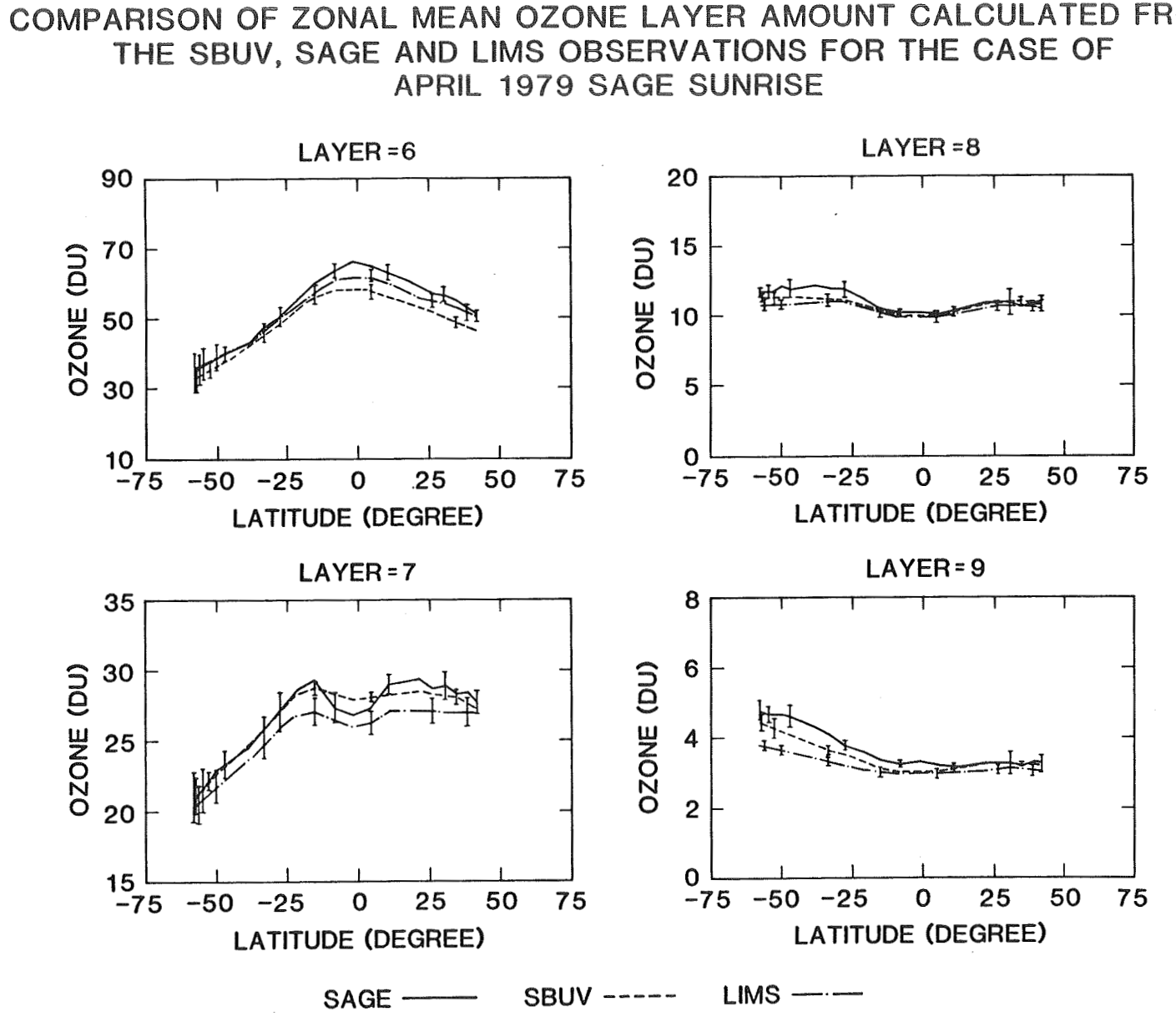

Figure C-5.7. Comparison of zonal mean ozone layer amount calculated from the SBUV, SAGE and LIMS observations for the case of April 1979 SAGE sunrise.

C-5.7 Trends at Upper Boundary of Stratosphere (SBUV, SME, SMM)

At 1 mb, the upper altitude limit of SBUV measurements and the lower altitude limit of SME measurements, five years of SME data (1982-1986) and three years of SMM data (1985-1987) at 55 km show no conspicuous ozone decrease. This absence of trend at 55 km is evidence against a 20 % decrease at 50 km, which is given by SBUV (Figure C-5.2). The body of ozone data taken by SME and SMM between 53 and 57 km supports the conclusion by SAGE that no large ozone decrease occurred at 50 km between 1979 and 1987.

C-5.8 Rocket Ozonesonde (ROCOZ-A)

In March-April 1979 and 1985, two series of rocket ozone soundings were conducted at Natal, Brazil. Above 22 km, stratospheric ozone variability was two percent or less during the three weeks of the 1985 measurement campaign, with stratospheric temperature and pressure variabilities half that amount. For Umkehr layers 6, 7, 8, and 9, two triplets of instruments (in 1979: SBUV, LIMS, SAGE I; in 1985: SBUV, SAGE II, ROCOZ-A) gave instrument-to-instrument variability, relative to the average of the three, averaging 4 %.

Figure C-5.8 shows a tropical ozone profile from 2 to 50 km as measured by ROCOZ-A and by electrochemical (ECC) analyses on balloons. The figure includes comparisons between SAGE II and ROCOZ-A, and comparisons between SBUV and ROCOZ-A. Between 20 and 1.5 mb the difference, SBUV minus ROCOZ-A, is always negative, -5 to -19 %. Between 20 and 50 km the difference, SAGE minus ROCOZ-A, is sometimes positive and sometimes negative, never exceeds 5 percent, and averages about - 1 %. The significance of such comparisons depends on the calibration of the reference instrument against an absolute standard.

ROCOZ-A measurements are reported to be systematically high by 5 or 10 % when checked against a laboratory-calibrated in situ instrument (Hilsenrath et al.[2]). ROCOZ-A ozone measurements have been compared in a single flight against an in situ ozone photometer and a mass spectrometer. In this comparison ROCOZ-A gave ozone values that were 8 % higher than the photometer and 4 % lower than the mass spectrometer. The 12 % difference between the in situ photometer and the mass spectrometer is cause for concern, since both instruments are laboratory-calibrated and considered to be absolute standards.

In Section C-5.2 it is stated that this chapter looks first for conspicuous trends in the data, readily seen by the eye. In this section this viewpoint is extended to obtain an overall judgment about credibility of ozone profile trends as measured by satellites. From an examination of the agreements and differences shown by direct comparisons, such as Figures C-5.3, C-5.4, C-5.7, and C-5.8, it is difficult to believe that existing satellite instruments determine upper stratospheric ozone much better than 4 percent, and by extension it probably would require at least a 4 percent change to be reliably detected as a change.

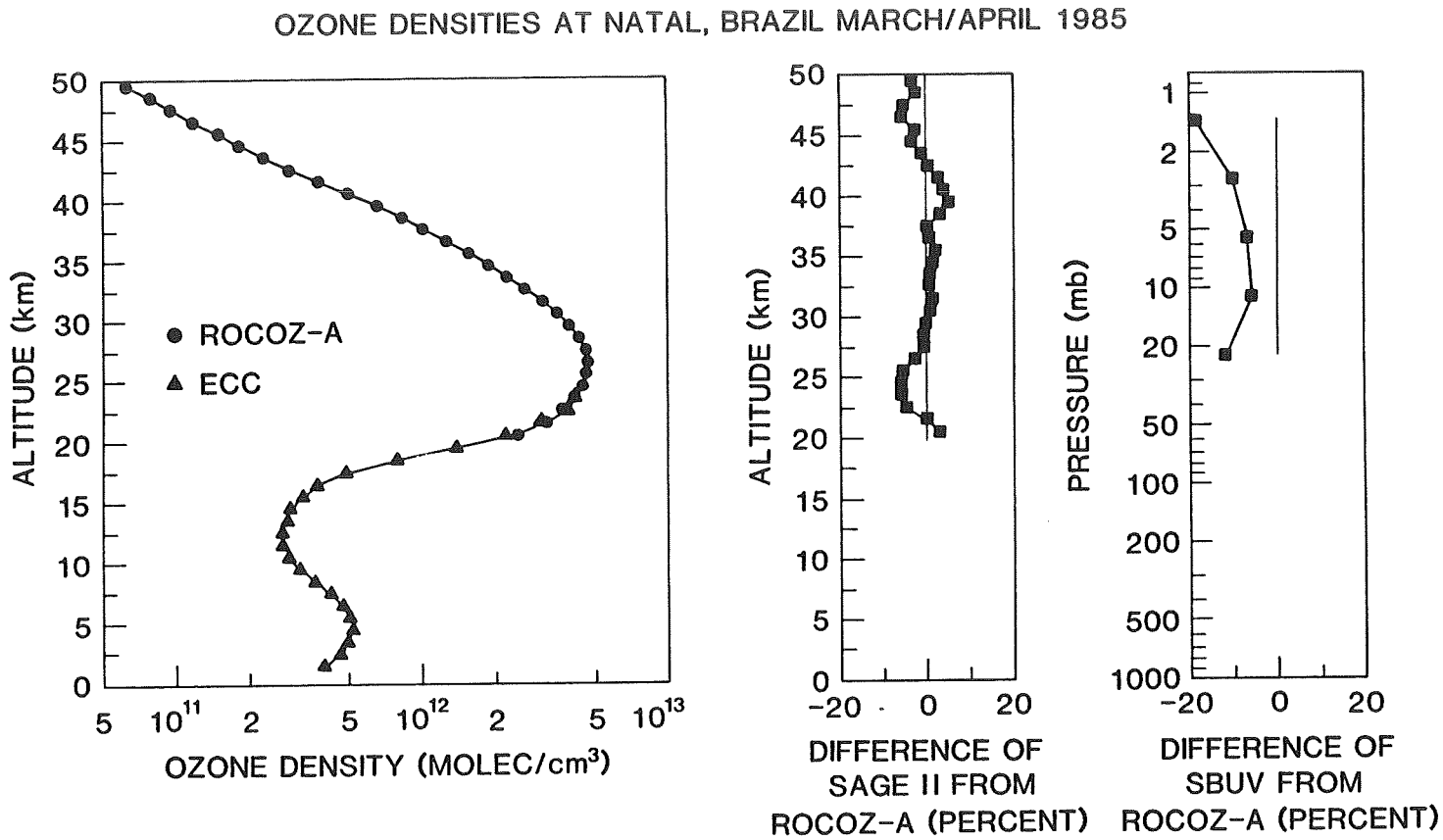

Figure C-5.8. Average ozone vertical profile based on ROCOZ-A and chemical ozonesondes at Natal, Brazil in March and April 1985. Middle panel: SAGE II minus ROCOZ-A, vertical profile of ozone percentage difference at Natal in 1985 as a function of geometrical altitude. Right panel: SBUV minus ROCOZ-A, vertical profile of ozone percentage difference at Natal in 1985 at Umkehr layers and as a function of pressure.

C-5.9 Conclusions

(1) The best estimates of the vertical profiles of ozone change in the upper stratosphere between 1979 and 1986 are judged to be those given by the two SAGE satellite instruments.

(A) SAGE II minus SAGE I gives a much lower ozone reduction than that given by the archived SBUV data; for example at temperate latitudes and at 40 km, SBUV gives 15 % and SAGE gives 3 % . With added considerations from Chapters 2 and 3, the difference is largely ascribed to systematic error in the treatment of the SBUV diffuser plate.

(B) The average SAGE profiles of ozone changes between 20 and 50 degrees north and between 20 and 50 degrees south are given by Figure C-5.5. The altitude of maximum ozone reduction is 40 km, in agreement with atmospheric models. The magnitude of maximum ozone reduction is 3 ± 3 % (95 % confidence level) at 40 km. The central value of this ozone reduction is less than the consensus of current theoretical models; a set of different models gives ozone reductions that range from 5 to 12 % at an altitude near 40 km (Chapter 7). The relative systematic error between SAGE I and II is estimated to be 4 % ; an error estimate for the models is not available.

(C) There is an unexpected 3 % ozone reduction at 25 km, near the ozone concentration maximum, which should be given careful consideration in the future.

(2) Five ground based Umkehr stations between 36 and 52 degrees north, corrected for the effects of volcanic aerosols, report an ozone reduction between 1979 and 1987 at Umkehr layer 8 of 9 ± 5 % (95 % confidence level including a term for uncertainty in the aerosol correction, but not including possible systematic errors). The central estimate of upper stratospheric ozone reduction given by SAGE at 40 km is less than the central value estimated by the Umkehr method at layer 8.

(3) In the future, the best way to improve knowledge of ozone profile changes between 1979 and 1987 will be to compare the first two years of validated SBUV/2 data against seasonally matched two years of the early SBUV data, similar to the procedure used by SAGE I/II.

(4) To measure upper stratospheric ozone changes as small as 5 % in 10 years, the instrument operators and data interpreters must have an extremely high level of ability, sophistication, dedication, and financial support. Such a measurement is a formidable scientific and engineering challenge. It requires continual attention to instrument performance, calibration, and verification; and there needs to be a large amount of duplicate, overlapping measurements. This task will not be achieved if it is regarded as a routine monitoring operation.

C-5.10 References

[1]DeLuisi, J.J., D.U. Longenecker, and C.L. Mateer. An analysis of northern midlatitude Umkehr measurements corrected for stratospheric aerosols for the years 1979-1986. Personal communication, January 1988.

[2]Hilsenrath, E., W. Attmannspacher, A. Bass, W. Evans, R. Hagemeyer, R. A. Barnes, W. Komhyr, K. Mauersberger, J. Mentall, M. Proffitt, D. Robbins, S. Taylor, A. Torres,

and E. Weinstock, Results from the balloon ozone inter-comparison campaign (BOIC), J. Geophys. Res. 91, 13,137-13, 152, 1986.

Chapter 6: Trends in Stratospheric Temperatures

C-6.1. Findings

A sufficiently large ozone loss in the stratosphere will have a significant and detectable impact on the stratospheric radiative balance and therefore temperatures. We have examined and intercompared satellite, radiosonde, and rocketsonde observed temperatures over the period 1979 to 1986 to estimate trends in temperature from 100 to 0.5 mb. These data sets are summarized in Table C-6.1. The intercomparisons are shown in Figure C-6.1 for the layers 100-50, 100-30, 30-10, 10-5, 5-1, and 0.5 mb for global and 30°N to 30°S average temperature. With some exceptions the data sets generally agree in magnitude and direction of the changes from 1979 to 1986.

Radiosonde analyses from 1970 to the present show no significant trends in temperature below 30 mb except perhaps in the equatorial and Antarctic regions. Trends earlier than 1979 above 30 mb could not be computed because adequately calibrated satellite measurements are not available, and the rocket data have insufficient spatial coverage to establish global trends.

A warming of the lowest stratospheric layers is evident in the 1982-1983 period which we attribute to the El Chichon aerosol. This warming has a significant impact on trend estimation over the 1979-1986 period; hence we report temperature differences between the beginning and end of the period by averaging 1979 with 1980 and 1985 with 1986 observations and then taking the difference between the two averages. Figure C-6.2 shows the 30°N to 30°S difference verses altitude determined from the radiosonde, rocketsonde, and satellite data sets. The error bars are the uncertainty estimates given by the investigators. The rocket data are shown for tropical sites.

In order to estimate the temperature changes which would result if the SBUV reported ozone changes were correct, radiative equilibrium computations were performed. To minimize the uncertainty in temperature changes due to dynamical heating, equinoctial tropical conditions were used. The results using three separate models (Table C-6.2) are shown in Figure C-6.3. The figure indicates that a decrease of 5.5°K would be expected at the stratopause in the tropics for the ozone perturbation shown. An additional decrease of 1°K is expected due to the decreasing solar flux from 1979 to 1986. When these temperature changes are convolved with the NOAA satellite SSU channel 47X weighting function, centered at 0.5 mb, a change of -4.6°K in brightness temperature results. In contrast, Figure C-6.2 shows a -1.3 ± 1°K change in the SSU 47X observations. Thus the upper stratospheric ozone change indicated by SBUV appears inconsistent with the temperature observations subject to a slight uncertainty in the year to year changes in dynamical heating. The same computations were also performed using SAGE ozone profiles. When the SAGE ozone is used the temperature change predicted to be observed by SSU 47X is about 1°K, consistent with the temperature observations, but inconsistent with the predicted result using SBUV ozone.

C-6.2. Conclusions

(1) The stratospheric radiosonde and satellite temperature data sets (Table C-6.1) intercompare reasonably well over the period 1979-1986 although points of disagreement exist (Figure C-6.1).

Table C-6.1

Temperature Data Sets

Data Set	Dates	Altitudes	Comments
Angell & Korshover	1958-Present	100-30 mb	Global radiosonde from 63 stations mostly in Northern Hemisphere. No Russian data before 1970, Angell & Korshover (1983).
Berlin	1962-Present	100-30 mb	Northern Hemisphere, radiosonde, digitized, map analysis. Labitizke et al. (1985).
Rocketsonde	1969-Present	30-55 km	Six sites, edited and corrected Datasonde profiles, Schmidlin (private communication).
NOAA Satellite	1979-Present	100-0.4 mb	Intercalibrated zonal mean measurements of brightness temperatures, Nash & Forrester (1986).
NMC	1979-Present	100-0.4 mb	NOAA Satellite retrieved mapped temperatures which includes rocketsonde correction, Gelman et al. (1986).

Table C-6.2

Radiative Transfer Models

Model	Organization	Reference
1	NASA/GSFC	Rosenfield et al. (1987)
2	NOAA/GFDL	Schwarzkopf and Fels (1985), Fels and Schwarzkopf (1975), Lacis and Hansen (1974)
3.	University of Oxford	Shine (1987)

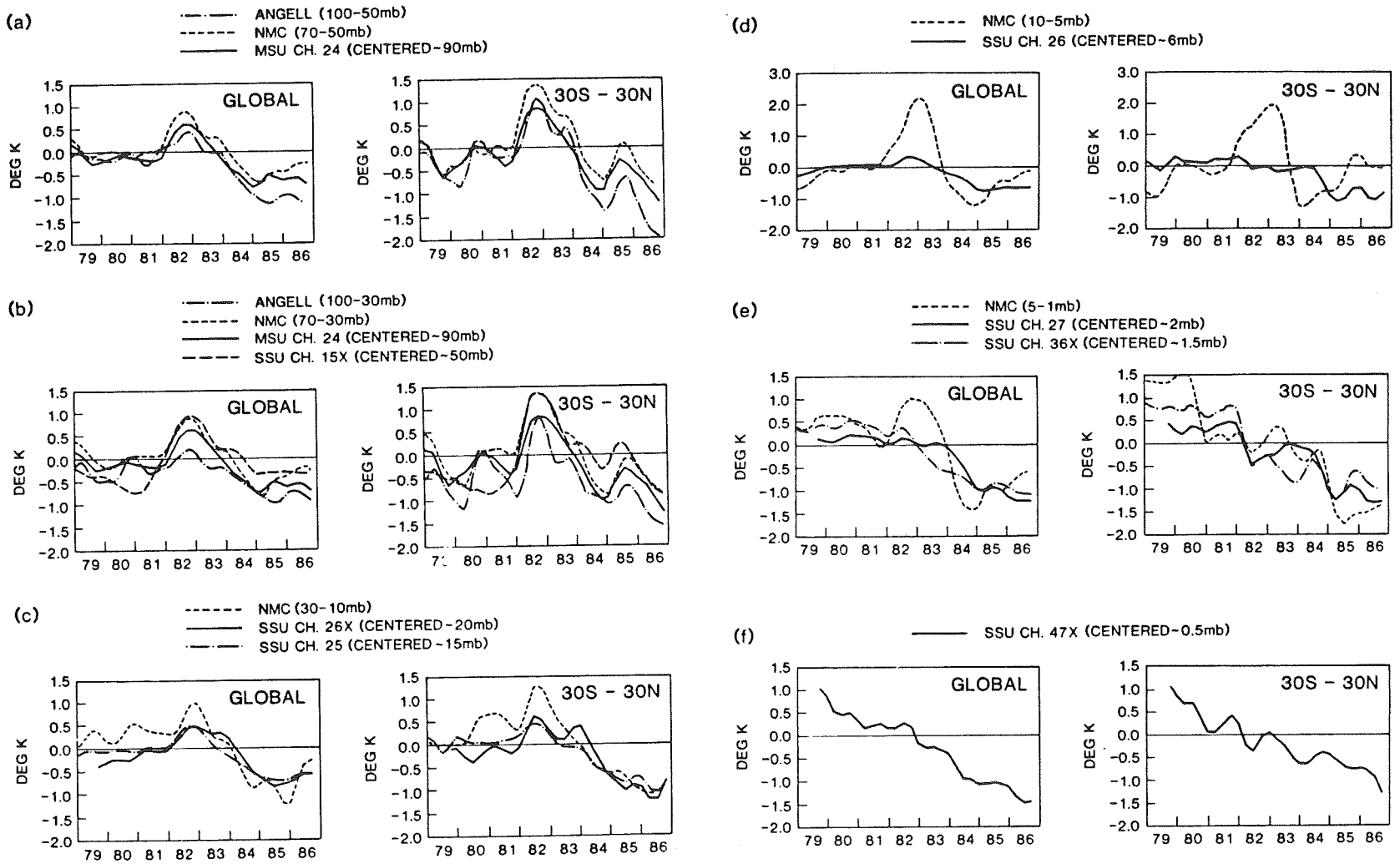

Figure C-6.1. Intercomparison of temperature trends at different levels in the stratosphere from 1979-1986. Data sets used are described in Table C-6.1.

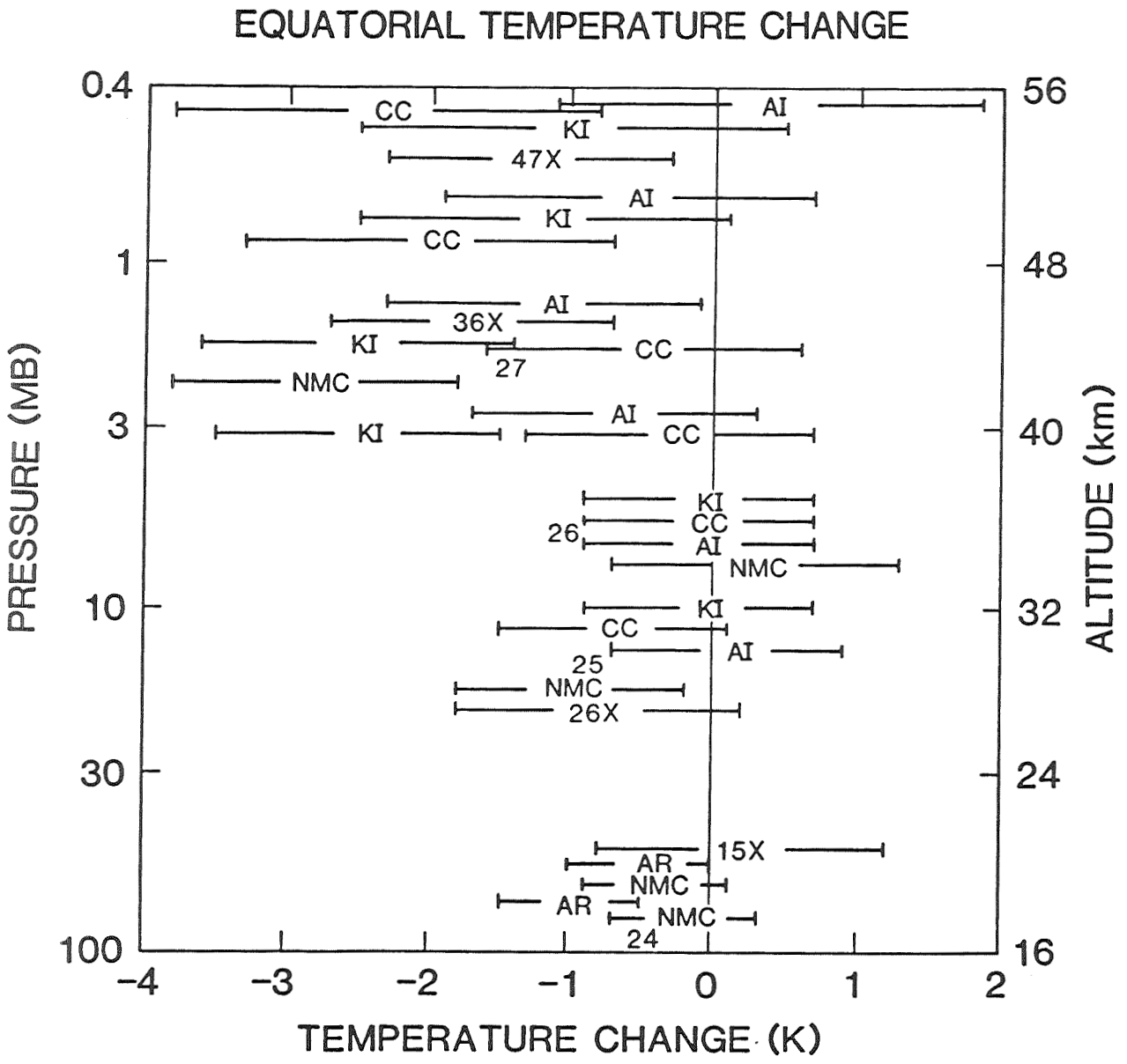

Figure C-6.2. Temperature differences from 1979/80-1985/86 from 30°N to 30°S as well as rocket data. NMC indicates National Meteorological Center data while AR is Angell and Korshover's radiosonde analysis. AI is Ascension Island rocket data; CC is Cape Canaveral and KI is Kwajelein. Satellite data denoted by channel number. Error bars indicate measurement uncertainty as indicated by the investigators (see Chapter 6, for details).

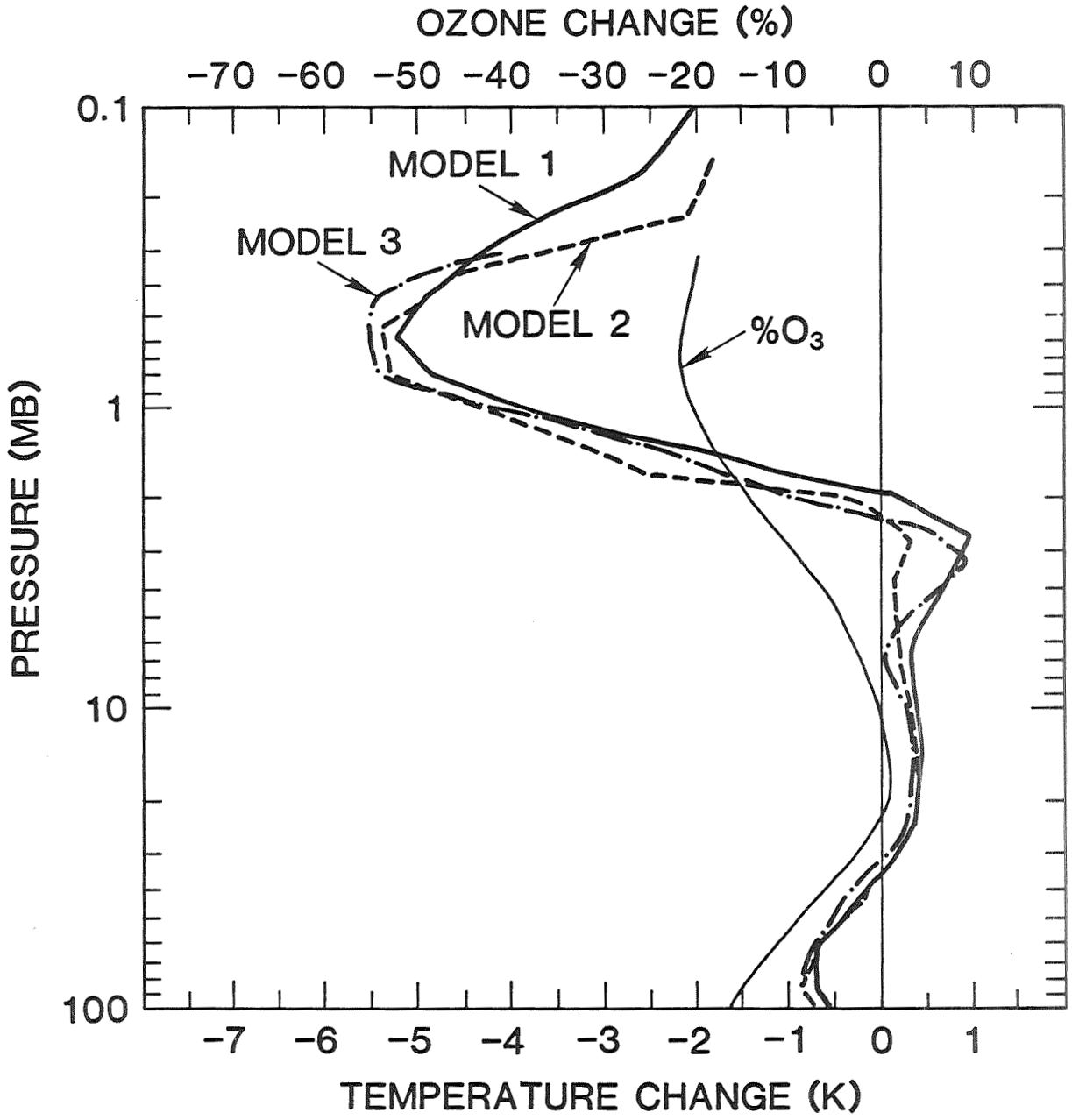

Figure C-6.3. Differences in radiative equilibrium temperatures using SBUV observed ozone for the years 1979 and 1986. The models used are indicated in Table 6-2.

(2) The six year difference in global temperatures between 1979 to 1980 and 1986 to 1985 averages shows a global decline between -1.75°K at 0.5 mb to -1°K and less below 5 mb. The uncertainty in these changes ranges from ±1.5°K at 1 mb to ±0.5°K below 1 mb. This method of estimating trends is adopted to minimize the effect of the El Chichon aerosol cloud.

(3) Radiosonde observations below 30 mb from 1970 to the present show no significant trends in temperature except in the equatorial and Antarctic regions. Global trends above 30 mb prior to 1979 cannot be determined due to inadequate stratospheric satellite temperature data.

(4) Using the reported SBUV ozone changes from 1979 to 1986, we compute a radiative equilibrium tropical temperature decline of 5.5°K. An additional 0.8 °K decline is expected due to the decrease in solar flux over that phase of the solar cycle. When this change is convolved with the SSU 47X weighting function centered at 0.5 mb, the detectable temperature change is -4.6°K. This compares to the observed -1.3°K ± 1°K tropical change (Figure C-6.2). Thus the reported SBUV ozone changes in the upper stratosphere appear to be inconsistent with the observed temperature changes. However, the smaller SAGE reported ozone changes are generally consistent with the observed temperature change.

Chapter 7: Theory and Observations

C-7.1. Goals and Model Scenarios

The main objective of the theoretical studies outlined here and presented in greater detail in Chapter 7 of the Ozone Trends Report is to apply models of stratospheric chemistry and dynamics to understand the forces that control stratospheric ozone and that are responsible for the observed variations. The model calculations are intended to simulate the observed behavior of atmospheric ozone over the past three decades (1955-1985) for which there exists a substantial record of both ground-based and (more recently) satellite measurements.

Two-dimensional stratospheric models from four different research groups were used to simulate changes in ozone with latitude, season and height. The increase of trace gas abundances, the 11-year variations in solar radiation, and the input of nitrogen oxides from atmospheric nuclear tests around 1960 were all taken into account by the model scenarios. Nevertheless, other geophysical phenomena, such as the quasi-biennial oscillation (QBO), the El Nino-Southern Oscillation (ENSO), and the 1982 volcanic eruption of El Chichon, cannot be readily modelled and were not included. The time line of the calculated globally averaged column ozone from 1960 to 1985 is shown for three of the models in Figure C-7.1.

An important element of globally averaged ozone change is the large decrease in column ozone observed over Antarctica in the spring over the last 8-10 years. The models used in this study did not include the unusual chemistry associated with the Antarctic ozone hole, and hence will not represent the decline in column ozone south of 50°S that has occurred since the mid-1970's.

Through comparisons of the modelled history of atmospheric ozone with the recently re-evaluated data on ozone trends we hope to:

(a) simulate the observed temporal and spatial variations of ozone;

(b) identify the roles of human activity, solar cycle variations and other undetermined natural variability in altering stratospheric ozone;

(c) focus on the specific patterns, or "fingerprints", of ozone change that can be uniquely associated with a specific cause;

(d) gain confidence in our models for stratospheric ozone and their ability to predict future change.

C-7.2. Calibration of Models Against Atmospheric Observations

An important test for stratospheric models is their ability to simulate the mean concentrations of chemical species in the atmosphere over the past decade for which we have the detailed measurements. All models show the main features of the global ozone distribution as observed by satellites and Dobson stations. A pronounced seasonal and latitudinal variation in total ozone column is calculated with maximum values occurring at high latitudes during late winter or spring. In one of the models, however, the maximum is delayed until early summer. Comparison with altitude profiles indicate that the models

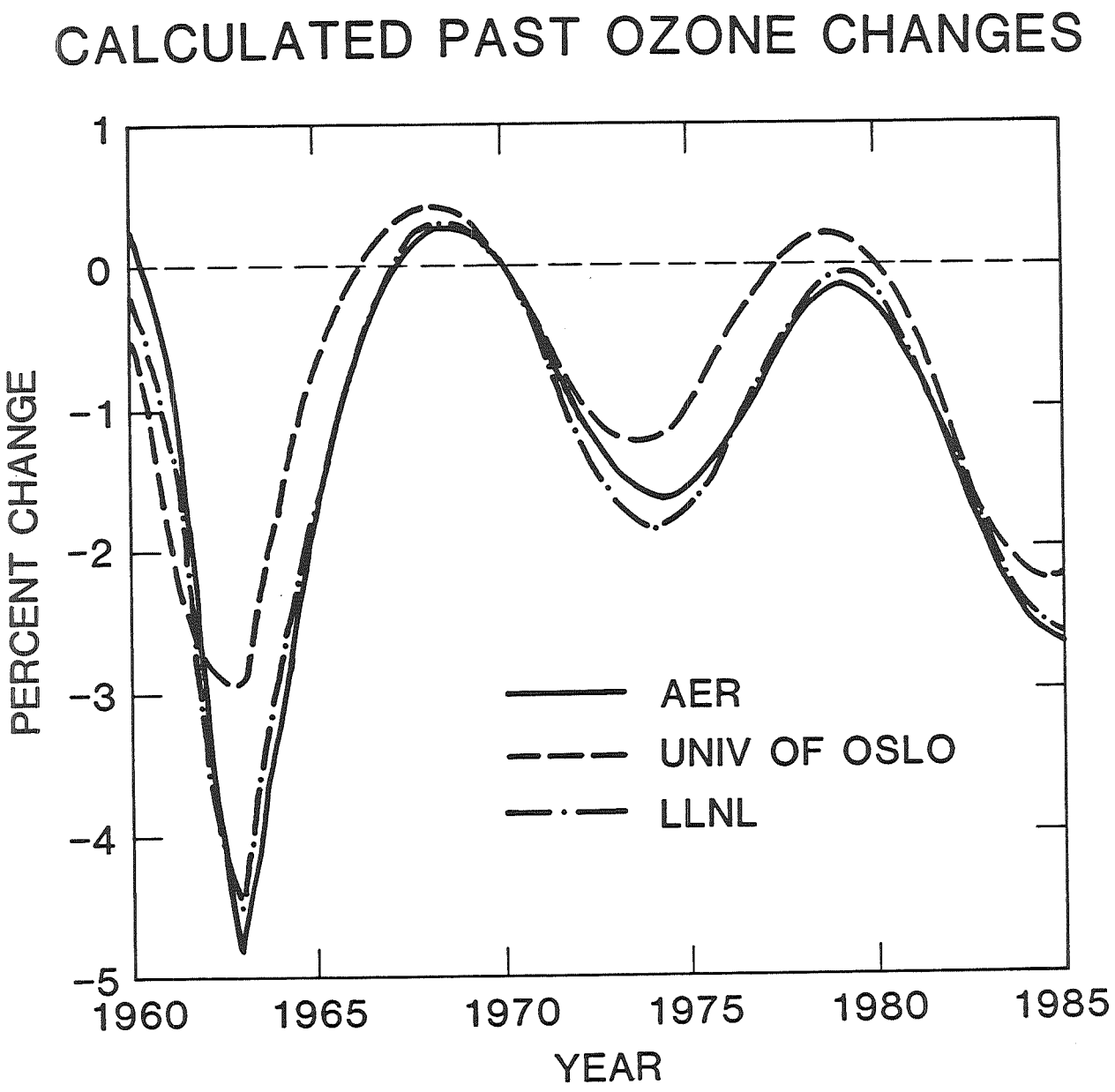

Figure C-7.1. Time line of global column ozone change (%) predicted for the period 1960-1985. The complete scenario was used for all models, including trace gases, solar cycle and nuclear tests. The percent change was normalized for each simulation at 1970 (Models: AER, LLNL, and Oslo).

underpredict ozone concentrations in the upper stratosphere where photochemical processes are dominant. Observations of key constituents in stratospheric chemistry, such as NO_x and ClO, are in general agreement with the calculated distributions, although some clear differences exist.

C-7.3. Fingerprints of the Three Major Stratospheric Perturbations

The injection of nitrogen oxides from the nuclear bomb tests during the late 50's and early 60's are predicted to have had a pronounced effect on the total ozone column during the first half of the 1960's, but a negligible impact from 1970 and afterwards. The impact of the nuclear tests is estimated to have been particularly large at high northern latitudes immediately after the 1962 tests. Although observations indicate low values of ozone in the early 60's, the comparison is inconclusive.

The solar output of ultraviolet light (UV) varies over the 11-year solar cycle and induces variations in stratospheric ozone. Changes in column ozone are predicted to be rather uniform with latitude and season. There is uncertainty, however, in the magnitude of the solar cycle in the UV. Results from two differing interpretations of measured UV variations over the solar cycle yield global column ozone changes of -0.7 and -2.0 % from maximum (1979) to minimum (1985) of the solar cycle.

Increased levels of trace gases (CFCs, N_2O, CH_4 and CO_2) lead to calculated decreases in column ozone showing a distinct pattern with latitude and season. The models predict that column ozone changes should have become noticeable during the 1970's and are largest over the last decade. From 1979 to 1985 column ozone is predicted to have changed about -0.3 to -0.6 % on a global, annual average due to trace gases alone. The largest ozone decline is expected to have taken place at high latitudes during winter and early spring. Three models (AER, LLNL, and Oslo) predict column ozone decreases during high-latitude winter that are 2 to 3 times larger than corresponding declines at high latitudes during summer and at low latitudes throughout the year. A particular exception is one model (Cambridge) that predicts a summer increase in ozone over the time period 1979 to 1985. The effect of the solar cycle is thus predicted to have been dominant over this period except for high-latitude winter.

All models predict that changes in the vertical distribution of ozone from 1979 to 1985 are dominated by increases in trace gases. Reductions in ozone concentrations resulting from reduced output of solar ultraviolet radiation show a broad maximum throughout the stratosphere with largest values of order 1-3 % in the upper stratosphere. Increases in trace gases reduce calculated ozone concentrations by 5-9 %, centered around 40 km altitude with largest depletions at high latitudes. The ranges given here reflect both seasonal and model-to-model variations. At 50 km the ozone depletions are less pronounced, but still noticeable. In the lower stratosphere and troposphere ozone is predicted to have increased as a result of trace gas increases; however, there are substantial differences between the models.

C-7.4. Comparison with Observed Changes in Ozone Columns

Ozone changes calculated from the complete scenario including trace gases, solar cycles and nuclear tests have been compared with observed changes over the last two decades, a period for which there exist substantial ground-based observations in the northern mid-

latitudes. More detailed global comparisons have been made for the period beginning 1979, which begins the era of satellite monitoring of ozone.

One comparison of calculated and observed trends in column ozone has been made by differencing the average over two consecutive solar cycles, 1965-1975 and 1976-1986, and is shown in Figure C-7.2. In this way solar cycle effects are minimized, making the impact of trace gases more apparent over the time period 1970-1981. Ozone changes calculated for the northern summer are small but in agreement with the uncertainty limits of the observations and the differences between models. During the winter months the models underestimate the mean observed ozone depletion by about a factor of two, especially at high latitudes.

Observed trends in column ozone from the Dobson network for 1969 through 1986 show statistically significant declines in ozone for several latitude bands in the Northern Hemisphere, after the effects of solar cycle, nuclear tests and QBO have been removed. Comparison of these results with predictions for the impact of trace gases alone indicates that the models underestimate decreases in ozone column over this period during winter by as much as a factor of three. The statistical significance of this discrepancy, as well as its cause, is not resolved.

Between 1979 and 1985 global maps of column ozone based on the reanalyzed TOMS and SBUV datasets (see Chapter 4) are available for comparison with model calculations. Predicted changes in column ozone are somewhat less than the observed changes. Due to the dominant effect of the waning solar activity over this period, however, it is difficult to identify uniquely the trace gas effects from the observations of this period. Calculated changes in column ozone as a function of latitude and season due to trace gas increases and solar cycle variations are given in Figure C-7.3 for each of the models.

C-7.5. Comparison with Observed Changes in Vertical Structure

Calculated changes in the vertical distribution of ozone have been compared with observations over the last eight years for which we have satellite data from SAGE and SBUV, as well as ground-based Umkehr measurements. Results are shown in Figure C-7.4. Calculated decreases peak at about -8 % near 40 km altitude. Model simulations are in general agreement with the SAGE I-II record and the recently corrected Umkehr data; reanalyzed SBUV profiles are still uncertain at this time and have not been used for comparison. Calculations predict substantially less ozone depletion near 50 km, about -2.5 %, than is shown in the SBUV data archived as of 1987, about -20 %. The models do, however, predict substantially larger decreases between 45 and 50 km altitude than is deduced from the SAGE I-II data.

Temperature reductions over the same time period, due mainly to ozone reductions in the upper stratosphere, are calculated to be about 1.8°K in the 45-50 km region and are in good agreement with the observed changes.

C-7.6. Future Change: Expectations Through 1991

After the solar cycle passed through its minimum in 1985, the impact of solar cycle and trace gases should act in opposite directions on column ozone. Model calculations were extended through the next anticipated solar maximum and are shown in Figure C-7.5.

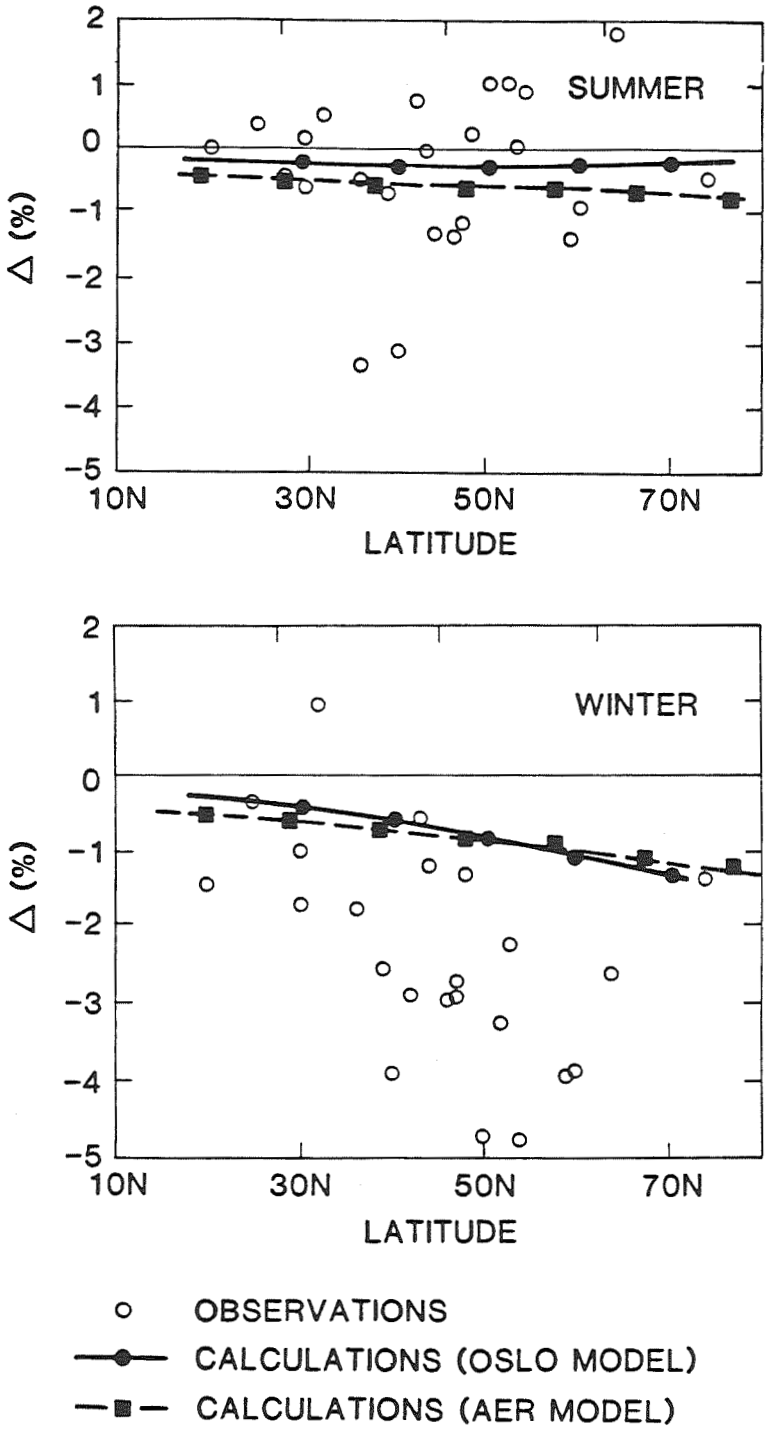

Figure C-7.2. Differences between 11-year averages, 1965-1975 and 1976-1986, of column ozone as a function of latitude. The upper panel refers to northern summer (May-August) and the lower panel to northern winter (December-March). Points represent individual Dobson stations and the lines refer to model simulations (solid=Oslo, dashed=AER).

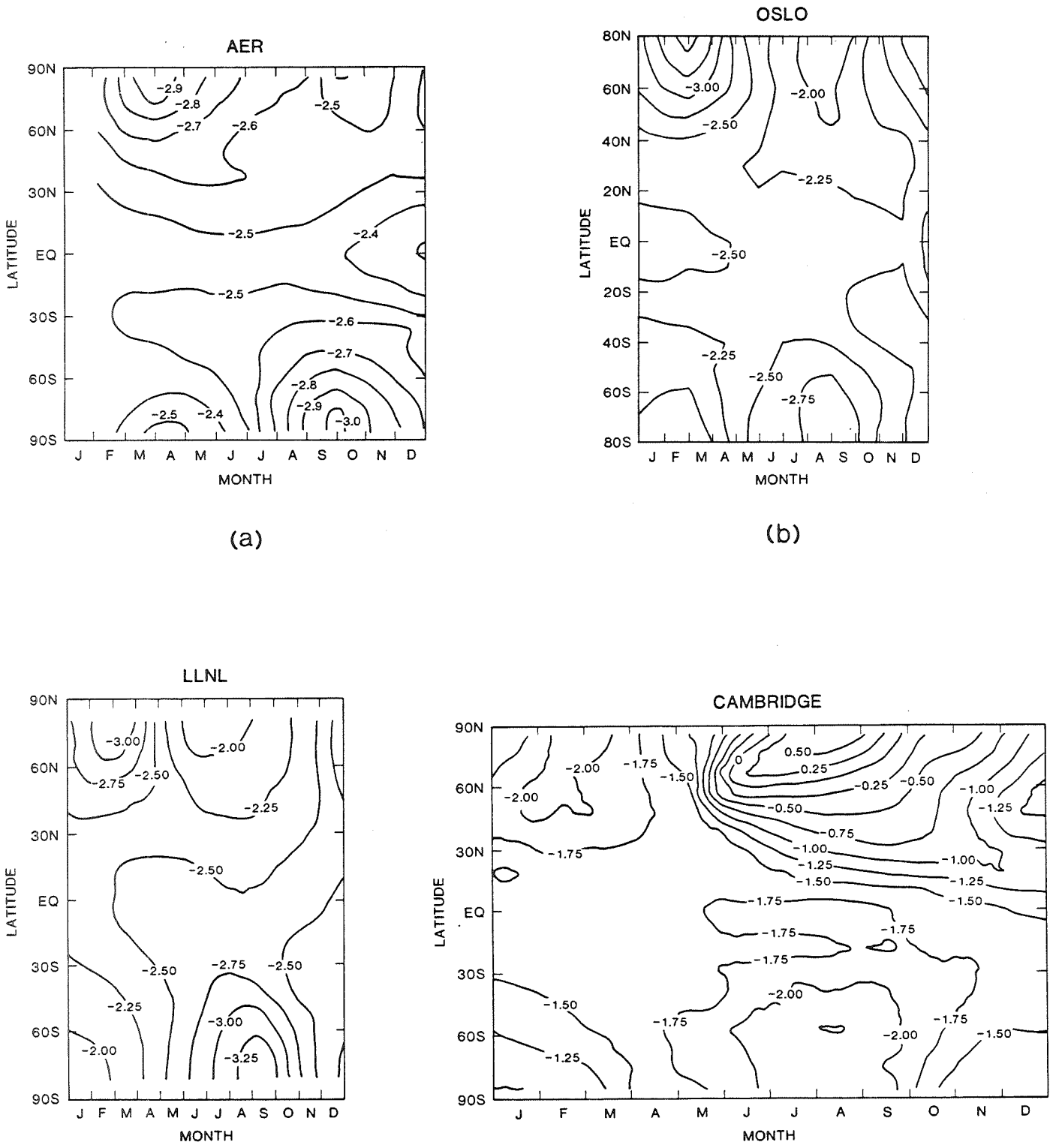

Figure C-7.3. Changes in column ozone between 1979 and 1985 as a function of season and latitude as calculated by the four 2-D models. Trace gas increases and solar cycle effects (reference case) are included (Models: a = AER, b = Oslo, c = LLNL, d = Cambridge.)

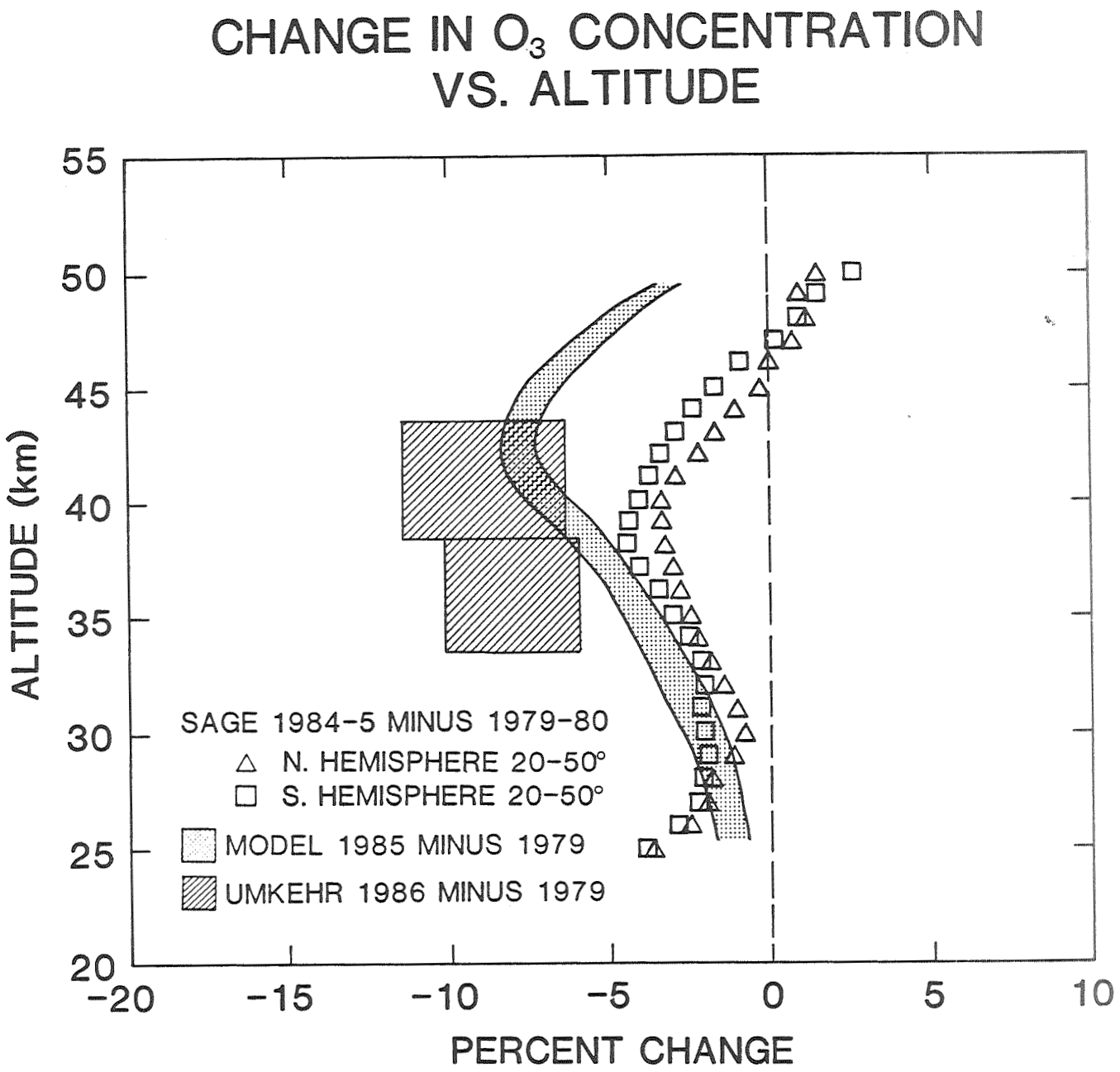

Figure C-7.4. Changes (%) in mid-latitude ozone profiles from 1979 to 1987. Differences based on SAGE I-II (1979-80 vs. 1984-85) averaged over 20x-50x latitude are shown by squares; averaged Umkehr data for the northern mid-latitudes (1979 vs 1986) are denoted by the hatched areas; and model predictions (1979 vs 1985) are given by a band.

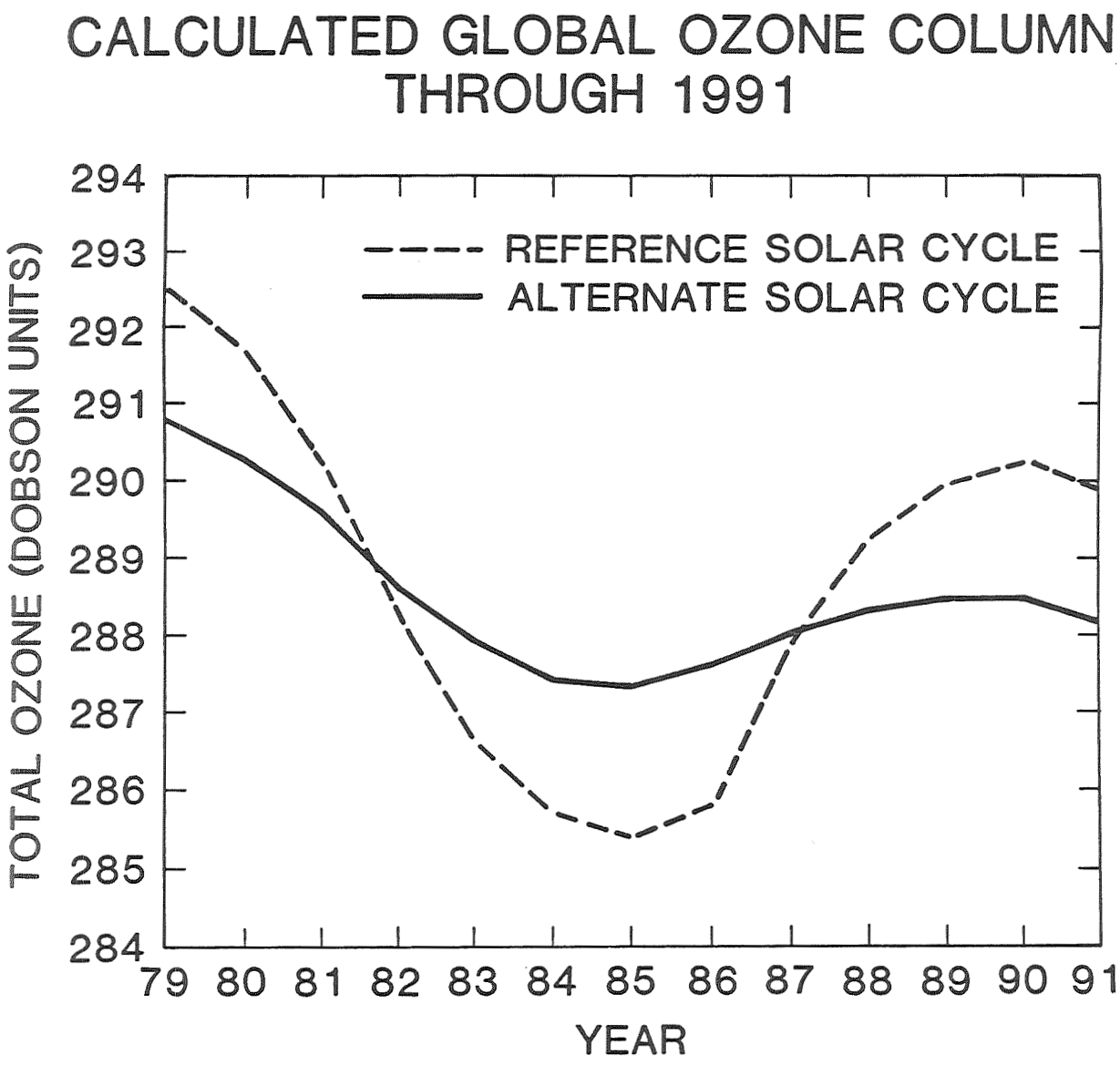

Figure C-7.5. Time line of global column ozone (Dobson units) from 1979 to 1992 calculated by the Oslo model for two different models of the solar cycle variability (dashed line = Heath & Schlesinger, solid line = SME).

Toward 1991 the stratospheric response to the increase in solar ultraviolet radiation may offset or even reverse the predicted decrease in total column ozone that would be caused by the increasing abundances of trace gases alone. Column ozone is predicted to undergo small or negligible increases until 1991, with the possible exception of high latitudes in winter where there might be slight decreases. There is some indication from the reanalyzed TOMS data that little or no decrease in column ozone in the Northern Hemisphere has occurred since solar minimum (1985-86).

After 1991 when the solar ultraviolet output declines, the total ozone column is again expected to decrease markedly as both effects combine to reduce ozone.

C-7.7. Conclusions

The comparisons we have made support the conclusion that in the upper stratosphere there has been a decrease in northern hemispheric ozone which is due in part to increases in trace gases. The calculations agree with observations, or slightly overestimate this effect. Predicted changes in column ozone over the last two decades (through 1986) are broadly consistent with observed ozone at mid and high latitudes in the Northern Hemisphere, but during the winter months the 2-D models underestimate ozone decreases. This indicates that there might be some important process, possibly in the lower stratosphere, not yet accounted for in the current 2-D stratospheric chemical models.

Chapter 8: Trends in Source Gases

C-8.1. Introduction

"Source Gases" are defined as those species that introduce halogen (mostly chlorine), hydrogen and nitrogen compounds into the stratosphere. These gases are emitted at the Earth's surface, either naturally or anthropogenically, are long-lived in the troposphere and many show significant and well documented increases in their tropospheric concentrations. Table C-8.1 summarizes the current concentrations of source gases and their rates of increase along with estimates of their tropospheric lifetimes.

C-8.2. Findings

It is noted that the absolute accuracies of the concentration measurements are still unsatisfactory for several of these source gases, e.g., CCl_4, CH_3Br, $CBrClF_2$, $CBrF_3$, CCl_2FCClF_2 and CO, mainly because calibration standards of suitable concentrations and integrity are not available. In addition, the global rates of increase for several of these gases, $CHClF_2$, $CBrClF_2$ and $CBrF_3$, are also uncertain because their increases have been monitored at a few stations only. Nevertheless, for the latter gases, the lifetimes are sufficiently long, such that a local increase is indicative of a global trend. The existence of a global increase in CO remains uncertain.

Most of the other concentrations and increase rates listed in Table C-8.1 are well established globally. Available evidence indicates that increases in the levels of CH_4, CO_2 and N_2O have been sustained for long periods and that the increases derive from large scale human activities, mainly food and energy production. From this viewpoint, it would be expected that possible trends in CO may also have been sustained for a long time. It also seems improbable that the present trends of these gases will be arrested or reversed in the near future.

The highest relative rates of increase are observed for the exclusively man-made source gases (all gases in Table C-8.1 except CH_3Cl, CH_3Br, N_2O, CH_4, CO and CO_2), because their lifetimes are long compared to the time since the beginning of release and they have not reached steady state. The two exceptions are CCl_4 and CH_3CCl_3 which are approaching steady state. The chlorinated source gases have been identified as possible agents of stratospheric ozone change. Their combined increase expressed as total chlorine is given in Figure C-8.1.

Evidence for increasing concentrations of $CBrClF_2$ and $CBrF_3$, often referred to as halons, is only just beginning to become available, but already significant trends are observed. The status of a possible trend in CH_3Br remains uncertain. However, it is likely that the total concentration of bromine is increasing with time in the troposphere.

Emission estimates of CCl_2F_2 and CCl_3F had been released up to 1986 by CMA and production figures for these gases in western countries are available. However, estimates of global emissions of these and other man-made halogenated source gases are no longer made. The measurement of their global increase in concentration, together with independent estimates of their lifetimes provides a means of estimating these emissions. Measurements of trace gas concentrations and trends at specific locations have been used to estimate regional emissions.

Table C-8.1

Updated Global Trends and Tropospheric Concentrations of Source Gases for 1986
(Where appropriate and available, lifetimes are also tabulated.)

Source Gas	Concentration 1986 pptv	Rate of increase 1986 pptv/yr	%/yr	Lifetime[a] yr
CCl_2F_2[(a)]	392	16.7	4.3	111^{+222}_{-44}
CCl_3F[(a)]	226	9.0	4.0	74^{+31}_{-17}
CH_3CCl_3[(a)]	139	6.2	4.5	7±1
CCl_4[(a,b)]	129	1.8	1.4	≈ 40
CCl_2FCClF_2[(b)]	32	3.6	11.3	≈ 90
$CHClF_2$[(b)]	92	6.5[(c)]	7.1	≈ 20
CH_3Cl	≈600	-	-	≈ 1.5
$CBrF_3$[(b)]	2.0	0.3	15	≈110
$CBrClF_2$[(b)]	1.7	0.2	12	≈ 25
CH_3Br[(b)]	10-15	?		≈ 2
N_2O	$(306\text{-}309)\times10^3$	$(0.65\text{-}0.8)\times10^3$	0.2-0.3	≈150
CH_4[(d)]	1638×10^3	$(13\text{-}16)\times10^3$	0.8-1.0	≈ 10
CO[(b)]	103×10^3	(see 8.7)		0.1-0.2
CO_2[(d)]	345×10^6	1.2×10^6	0.4	
Total Cl[(e)]	3185	104	3.3	
Total F[(e)]	1300	67.5	5.2	
Total Br[(e)]	14-19	0.5	3-4	

[(a)] The lifetimes of the first four species has been derived from observations (see Chapter 8.2), the others are adopted from WMO (1986).

[(b)] Calibration uncertain.

[(c)] Southern Hemisphere.

[(d)] 1985 data.

[(e)] The total amounts include all the appropriate compounds listed in this Table, which are thought to be the major species of global importance. Because of its exceedingly long lifetime CF_4 is not included in total F.

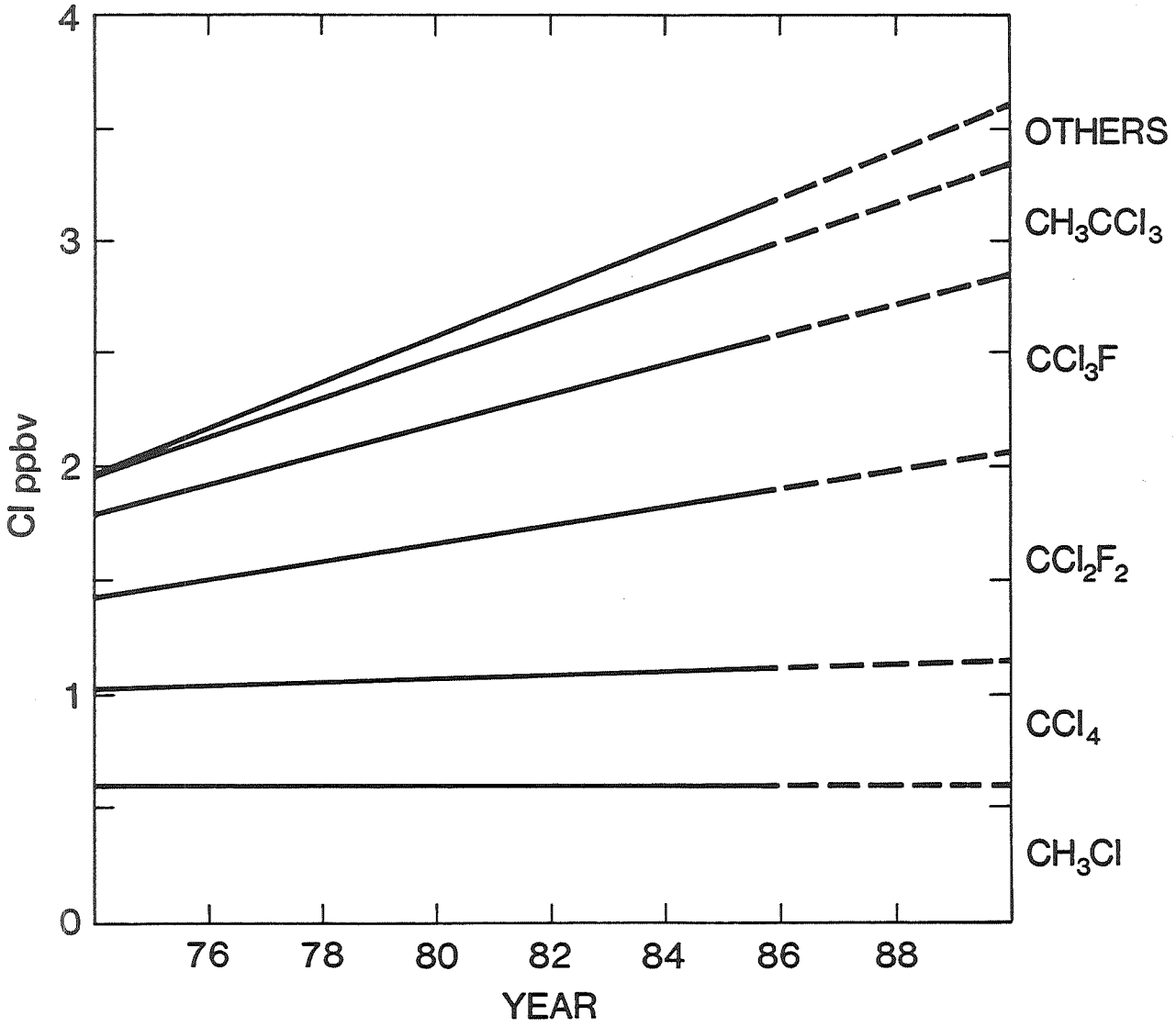

Figure C-8.1. Measured and predicted cumulative increases of chlorinated source gases in the troposphere over the past decade and up to 1990. Concentrations are in chlorine atom equivalents. Future increases are indicated by dashed lines, based on constant emission rates at current levels.

Chapter 9: Trends in Stratospheric Minor Constituents

C-9.1. Introduction

Ozone is predicted to change in response to changes in the concentrations of stratospheric minor constituents containing chlorine, bromine, hydrogen, and nitrogen. Observations discussed in Chapter 8 confirm that the atmospheric concentrations of the sources of these trace constituents are increasing. Our current understanding of stratospheric chemistry suggests that these source trends should be reflected in the concentrations of the stratospheric minor constituents. This chapter reviews the experimental evidence for concentration changes in trace stratospheric species.

C-9.2. Halogens

An unambiguous long-term increase in the total column amount of atmospheric HF of between 5 and 10 percent per year has been observed over the last decade in measurements from the ground and from aircraft. This is consistent, within error bars, with predictions based on the measured increase of organic fluorine in the troposphere. An increase of the column amount of atmospheric HCl has also been observed. Aircraft data which measure the column amount in the stratosphere show a large increase (5 percent per year). Ground-based data from the observatory at Jungfraujoch measure the total column above the station which includes both tropospheric and stratospheric components, indicate a smaller change (about 2 percent per year). These data now extend into 1987 and have been reanalyzed to account for seasonal variations in the trend estimates. Trend measurements of HCl are especially difficult to make because a large and variable contribution of tropospheric HCl to the total column, a large seasonal variation, and a possible interference from volcanically injected HCl, are superimposed on the small annual increase expected. It should be noted that any differences between the absolute values and/or trends determined from ground-based and aircraft measurements should, in general, be attributable to a tropospheric column contribution in the former. In the present case, this comparison leads to a tropospheric HCl column above Jungfraujoch which is somewhat larger than reported in a limited set of independently measured tropospheric HCl concentrations, but the differences are within the uncertainties of the measurements plus meteorological variability.

There is not yet a clear indication of an increase in the column amount of upper stratospheric ClO (expected to be increasing at the same rate as HCl). There are insufficient data to study the long-term trends of stratospheric bromine compounds.

C-9.3. Nitrogen Compounds

Satellite-based measurements of NO_2 have been interpreted as showing large (60-70 percent) increases over the time period from 1979 to 1984, but such increases are not supported by ground-based and aircraft measurements over that time. Subsequent analysis of SAGE data also do not support the large increases originally suggested, but do not rule out the possibility of smaller changes (10-20 percent) during the 1979-1984 period, especially in the Southern Hemisphere. Such increases, if real, must be due to changing

inputs of odd nitrogen from either the mesosphere (NO produced from ionic processes in the thermosphere) or troposphere (NO produced in lightning discharges), as they are much larger than the very small (~1 percent) increases expected over that time period due to the increasing concentrations of stratospheric N_2O. SBUV data of NO at and above the stratopause region seem to imply some long-term decrease in the tropics over the time period 1979 to 1986, but no clear trends were seen at high latitudes. No definitive changes in the total amount of stratospheric odd nitrogen, which includes NO, NO_2, HNO_3, N_2O_5, $ClONO_2$, and HNO_4, can be deduced at this time.

C-9.4. H_2O / HO_X

Balloon-borne frost-point hygrometer measurements of water vapor made over Boulder, Colorado since 1980 show no evidence of a trend in the middle and lower stratosphere (20-120 mb). Analysis of data obtained previously over Washington, D. C. appeared to show some unexplained cyclical variation over the time period 1963 to 1980, but these data are complicated by substantial short-term variability and a quasi-biennial oscillation. There is also no evidence of a trend in the total OH column over Fritz Peak, Colorado over the period from 1980 to 1987, although some unexplained variation prior to 1980 was obtained. Neither of these unexplained variations is related to the expected increase in stratospheric hydrogen species associated with the oxidation of the increasing amounts of stratospheric methane.

C-9.5. Conclusions

In order to determine unambiguously the long-term trends of these species, a campaign of frequent measurements of these constituents must be carried out. In the long term, the Network for the Detection of Stratospheric Change (NDSC) will be highly useful for trend determination. Plans have already begun for setting up stations in both the United States and Europe. This network must evolve into a set of worldwide stations which measure the concentrations of key atmospheric molecules on a continuing basis. In the short term, measurements need to be continued using existing instruments at their current locations (e.g. HCl and HF from Jungfraujoch, ClO from Hawaii, OH from Fritz Peak, H_2O from balloon measurements in Boulder, etc.). In addition, the SAGE I and SAGE II NO_2 and H_2O data should be fully exploited after release by its science team. Periodic measurements of trace constituent concentrations by aircraft instruments and the shuttle-borne ATMOS instrument could also play an important role in determination of their long-term trends. When the UARS satellite is launched additional information concerning trends should be available from several instruments on that satellite.

Chapter 10: Trends in Aerosol Abundances and Distribution

C-10.1. Introduction

Stratospheric aerosols have been implicated in remote sensing errors that affect the analysis of long-term ozone trends, and have been connected with the formation of the Antarctic ozone 'hole.' Within the guidelines established for this assessment of ozone trends, the following broad objectives concerning aerosols were sought:

(i) To define the fundamental characteristics of stratospheric aerosols, particularly their morphological, radiative and chemical properties;

(ii) To analyze long-term aerosol databases for possible trends that might influence the identification or interpretation of long-term ozone trends;

(iii) To assess the transient impacts of volcanically-generated aerosols on remote sensing observations (for example, Umkehr and SBUV) over the last one to two decades, and to consider possible schemes for correcting aerosol errors in these baseline ozone data records;

(iv) To describe polar stratospheric clouds (PSC's) in terms of their frequency, spatial extent, duration and physico-chemical properties, on the basis of observational and theoretical studies.

C-10.2. Findings

After consideration of the extensive scientific information available on stratospheric aerosols, we have reached the following conclusions:

(1) On the basis of recorded data, no significant trends can be detected in the properties of the global background stratospheric aerosol layer. Likewise, polar stratospheric clouds do not appear to have changed substantially over the early period of their observation (1979-1984). However, in 1987 the Antarctic PSC's persisted several weeks longer than usual--well into October--with more sightings of very dense clouds than in previous years. The aerosol (and PSC) data records are of a short enough duration that small trends over longer time spans cannot be precluded.

(2) The stratospheric aerosol loading is occasionally greatly enhanced as a result of a major volcanic eruption. Such eruptions (for example, El Chichon in 1982), even in remote locations, can perturb the stratosphere worldwide, including the polar regions in both hemispheres, for periods of several years or more. During these (volcanic) periods, the atmospheric radiant fields are anomalous, complicating the interpretation of remote sensing data.

(3) New intercomparisons between SAGE and SME satellite observations show that significant aerosol loadings (with respect to remote ozone sounding measurements) rarely occur above about 35 kilometers--that is, within the altitude region where the accuracy and information content of the SBUV ozone-profiling system is greatest. Hence, background aerosols are not likely to be responsible for ozone errors of more than a few percent in SBUV layers 6 to 9 (25 to 50 km), nor can aerosols explain any long-term ozone trend in the SBUV data. Even so, volcanic aerosols may cause sizeable errors in SBUV ozone

profile measurements during relatively short periods following major eruptions. There is also little evidence to support the idea of persistent widespread mesospheric aerosol layers (except at the summer mesopause) that might significantly interfere with remote ozone observations.

(4) The impact of volcanic aerosols on ground-based Umkehr measurements is gretest in the upper Umkehr layers (7-9, above about 30 km) and the lower layers (1-3, below about 20 km). Although the Umkehr data may be roughly corrected for aerosol effects using lidar and satellite data on the vertical and horizontal distributions of particles, the residual ozone errors in post-volcanic years may exceed several percent at the most sensitive altitude levels. Accordingly, for ozone trend analysis, very careful handling, or neglect, of Umkehr data collected during volcanically-disturbed periods is recommended.

(5) Direct observations of polar statospheric cloud properties, together with independent measurements of related physical and chemical parameters, strongly imply that PSC's are initimately involved in the formation of the Antarctic ozone hole. This conclusion is based on the following facts:

i) PSC's appear in the proper temporal sequence and spatial configuration to be closely associated with the development of the ozone hole;

ii) Thermodynamic data suggest that PSC's may be formed through co-condensation of H_2O, HNO_3 and HCl vapors; cloud particle sedimentation is also consistent with the observed dehydration and denitrification of the winter polar vortex;

iii) Measured PSC optical and morphological properties are compatible with the PSC composition and microphysics inferred above.

PSC's are also known to occur in the northern polar winter stratosphere. Accordingly, effects of PSC formation on ozone concentration could be investigated in the Northern Hemisphere as well as in the Southern Hemisphere. Although much has been learned in the last few years about PSC's and their relation to the ozone hole, considerable uncertainty remains concerning the basic phenomena at work.

C-10.3. Discussion

The advent of satellite-based sensors has led to a global description of stratospheric aerosols. The recorded morphology and climatology of these trace atmospheric constituents have become more comprehensive and precise. Through satellite observations, a clearer global picture of the distribution of stratospheric particles, as well as the evolution of volcanic eruption clouds like that of El Chichon, has been gained. The negative impact of aerosols on the remote sensing of ozone (and other species) is now well established. This report confirms previously expressed doubts on the use of certain data sets such as Umkehr for accurate ozone trend analysis during periods which are influenced by volcanic eruptions. Nevertheless, the overall accuracy of Umkehr data for studying ozone climatology and cyclic variations should not be compromised by occasional volcanic eruptions, if proper account is taken of anomalous aerosol effects. The SBUV ozone sensors are in general less susceptible to aerosol degradation than Umkehr sensors; studies of global ozone morphology with the SBUV system should not be greatly affected by aerosol-generated errors. Even so, in times and in regions of volcanic disturbance, the SBUV data must be interpreted with great care.

The recent linkage of polar stratospheric clouds to the evolution of the Antarctic ozone hole is a major exciting advance. Careful analysis has indicated that nitric acid and water vapors can condense in the winter polar stratosphere to form nitric acid ice clouds. The resulting denitrification of stratospheric air is in all likelihood crucially related to the chemical processes that uniquely lead to the ozone hole. Furthermore, current laboratory studies on heterogeneous chemistry support the idea that certain key reactions may be greatly accelerated in the presence of ice clouds. The formation of PSC's, and the concomitant processing of stratospheric trace constituents, are logically related to the global structure of the stratospheric aerosol layer and the presence of background particles upon which PSC's may form.

Chapter 11: Observations and Theories related to Antarctic Ozone Changes

C-11.1. Introduction

During 1985 there was a report of a large, sudden, and unanticipated decrease in the abundance of spring-time Antarctic ozone over the last decade. By 1987, ozone decreases of more than 50% in the total column, and 95% locally between 15 and 20 km had been observed. A change of this magnitude was not predicted by any of the photochemical models. The scientific community quickly rose to the challenge of explaining this remarkable discovery. Theoreticians soon developed a series of chemical and dynamical hypotheses to explain the ozone loss. Unfortunately, there was inadequate observational data to differentiate between the different theories. Consequently, field measurement campaigns were organized rapidly to determine the chemical composition and physical structure of the stratosphere over Antarctica in spring-time in order to test the different theories that had been proposed. Three different theories were proposed to explain the spring-time ozone hole:

(1) The ozone hole is caused by the increasing atmospheric loading of man-made chlorine (chlorofluorocarbons (CFCs)) and bromine (halons) containing chemicals. These chemicals efficiently destroy ozone in the lower stratosphere in the Antarctic because of the special geophysical conditions, of an isolated air mass (polar vortex) with very cold temperatures, that exist there:

(2) The circulation of the atmosphere in spring-time has changed from being predominantly downward over Antarctica to now being upward. This would mean that ozone-poor air from the troposphere would be transported into the lower Antarctic stratosphere instead of ozone-rich air from the upper stratosphere:

(3) The abundance of the oxides of nitrogen in the lower Antarctic stratosphere are periodically enhanced by solar activity. The oxides of nitrogen are produced in the upper mesosphere and thermosphere and then transported downward into the lower stratosphere in Antarctica resulting in ozone being chemically destroyed.

Therefore, the key questions facing the scientific community are whether the observed changes in Antarctic ozone are due to natural variability or to human activities, and whether the behavior of ozone above the Antarctic is an early warning of future changes in global ozone or whether it will always be confined to the Antarctic because of the special geophysical conditions that exist there.

C-11.2. Ozone Observations

Changes in total column ozone over high southern latitudes in spring-time have been measured by several different techniques from the ground and from satellites. These corroborate one another providing a clear picture of the changes which have taken place. A significant change in the springtime total ozone content over the Antarctic was first reported by the British Antarctic Survey using the Dobson station data at Halley Bay (76°S) with a smaller change seen at Argentine Islands (65°S). The satellite data not only confirm the decrease reported from ground station data but demonstrate that the phenomenon is of large regional scale, at least the size of the Antarctic continent. The key aspects of the Antarctic ozone hole are:

(1) There is compelling evidence from both ground based data (Figure C-11.1) and satellite data (Figure C-11.2) that the springtime abundance of ozone dropped rapidly after the late 1970's. However, given the high level of interannual variability in Antarctic ozone it is difficult to draw strong quantitative conclusions about the magnitude of ozone decreases during the 1970's.

(2) The rapid decline in Antarctic total column ozone occurs mainly during the month of September, and low values of ozone persist until the breakdown of the polar vortex in late October or November (see #4).

(3) The rate of decline of ozone during September appears to be increasing.

(4) The region of low ozone over Antarctica persisted until late November in 1987, which is the latest since measurements began (Figure C-11.3).

(5) The total column of ozone was lower in 1987 at all latitudes south of 60°S than any previous year since measurements began. The October monthly zonal mean total ozone amounts at 50, 60, 70, and 80 degrees south were about 8%, 20%, 40%, and 50% lower, respectively, than in 1979. Figure C-11.4 shows data for the latitude band from 79°S - 81°S.

(6) Although the ozone depletion is largest in the Antarctic spring-time, ozone appears to have decreased since 1979 by 5% or more at all latitudes south of 60°S throughout the year (Figure C-11.5).

(7) In some instances, total column ozone as measured by the Nimbus 7 Total Ozone Mapping Spectrometer (TOMS) instrument changed dramatically (25-50 Dobson Units (DU)) over areas as large as several million square kilometers within a matter of a day or two and these reductions persisted for up to a few days.

(8) The altitude profiling by balloon-borne ozonesondes show significant ozone layer depletions at a number of stations and are consistent with Stratospheric Aerosol and Gas Experiment (SAGE) satellite ozone profile results.

(9) Balloon ozonesonde and SAGE satellite data indicate that the ozone decrease over Antarctica is confined to an altitude region between about 12 and 24 km. There is no evidence from the SAGE data of the depletion extending above about 25 km altitude.

(10) In October of 1987, the ozone concentrations between 15 and 20 km had decreased by more than 95% from their values two months earlier (Figure C-11.6).

C-11.3. Polar Stratospheric Cloud Observations

Polar stratospheric clouds (PSCs) form during the winter as the stratospheric air over Antarctica becomes very cold with the long absence of sunlight. The vertical extent of PSCs correlate with cold temperatures. The atmospheric temperatures increase during spring-time starting at higher altitudes, so that in the maximum altitude at which PSCs can exist decreases with time. Satellite observations of PSCs began in late 1978. The persistence of PSCs which are thought to play a key role in the formation of the "Antarctic ozone hole" has increased since 1984. The 1985 observations show for the first time the occurrence of PSCs at 16 km throughout the month of September and into October. Further, PSCs lasted into October in 1987 at altitudes as high as 18 km.

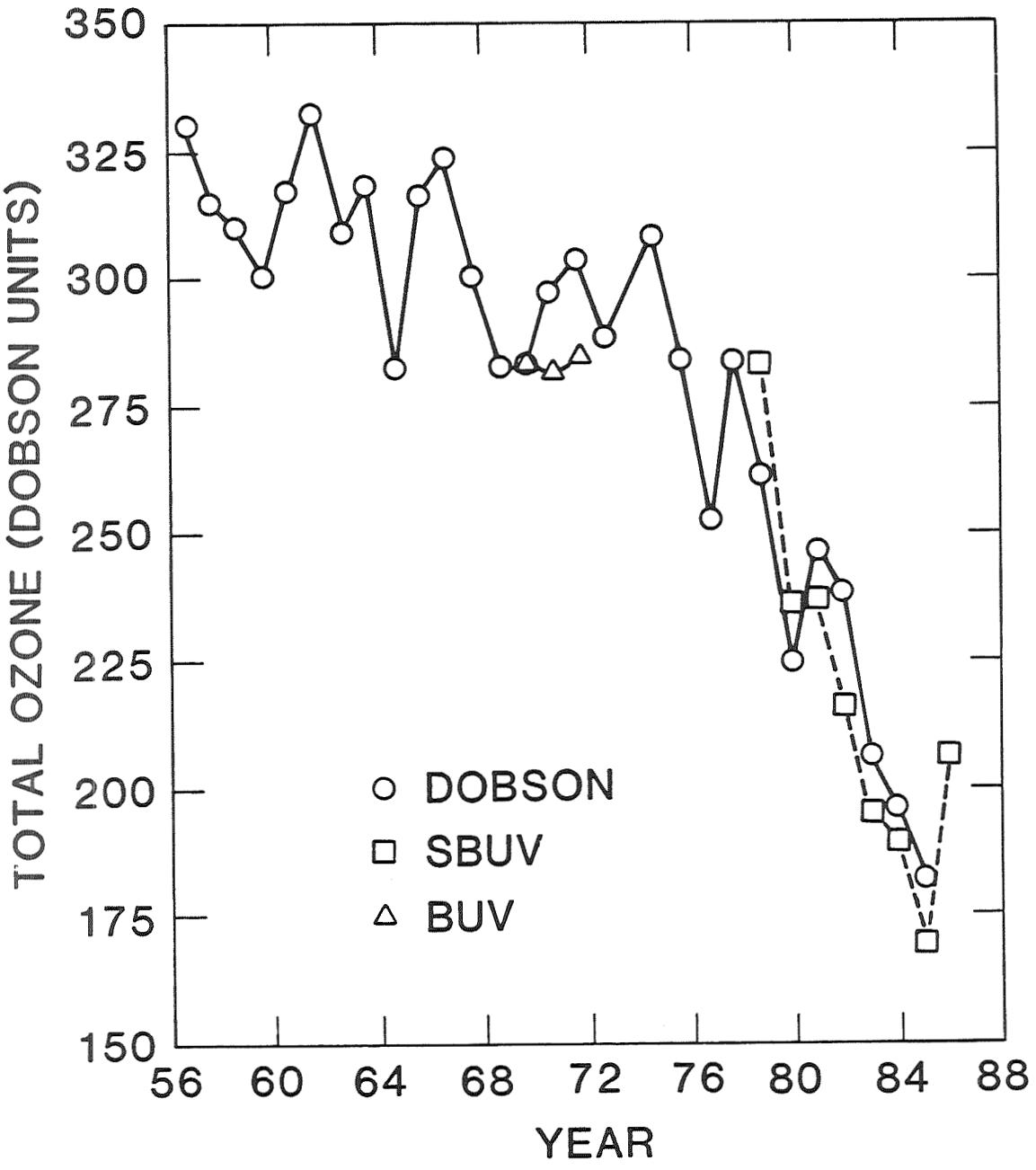

C-11.1. October monthly mean total ozone measured over Halley Bay Station, Antarctica.

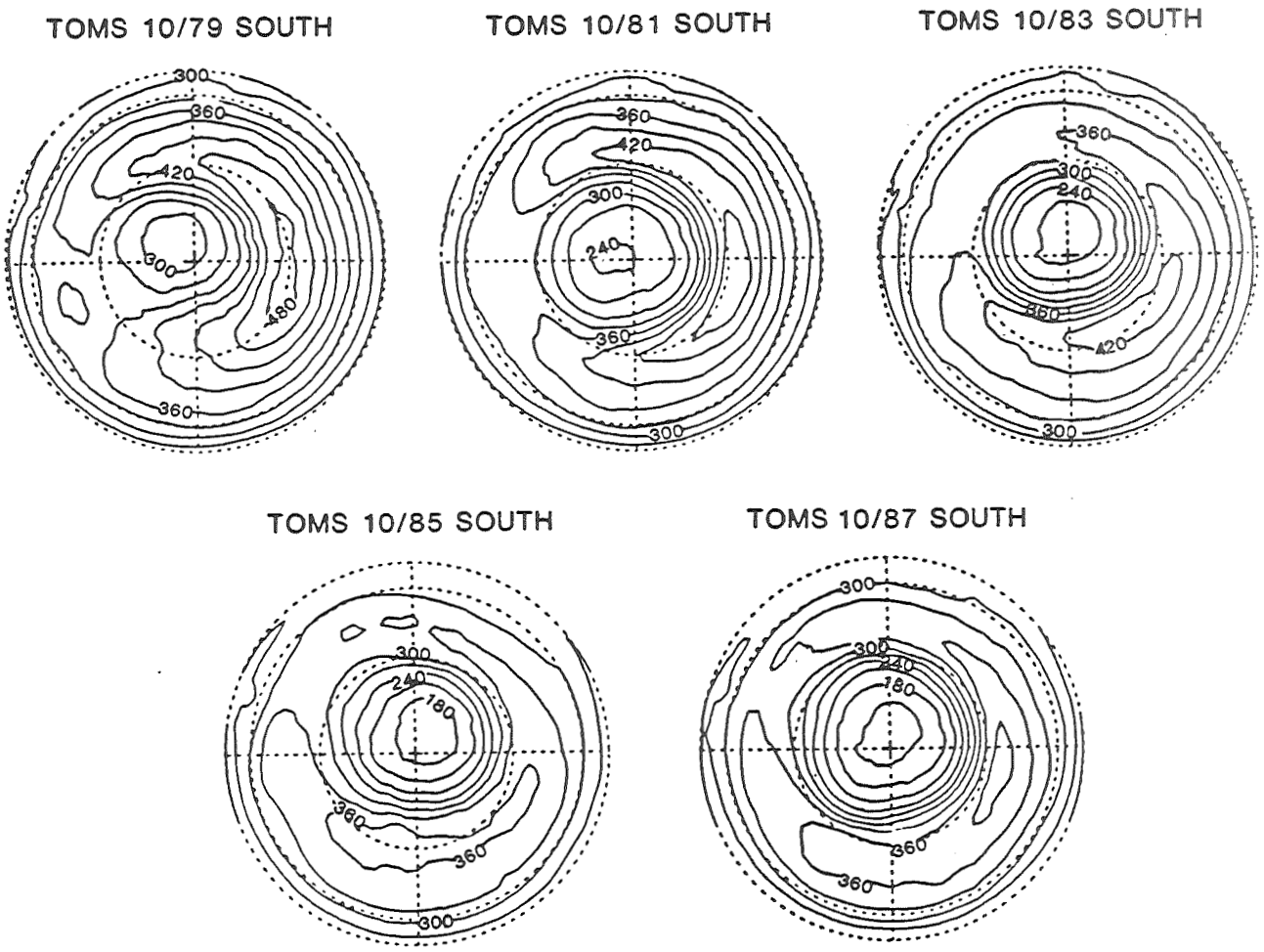

C-11.2. Southern Hemisphere maps (polar orthographic projection) of October monthly mean total ozone in odd years since 1979. Greenwich meridian is toward the top of each map. The equator is the outside edge.

TOMS OZONE (SOUTH POLE)

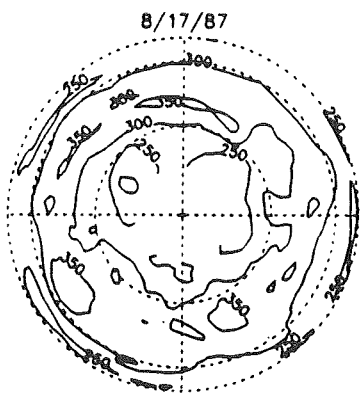

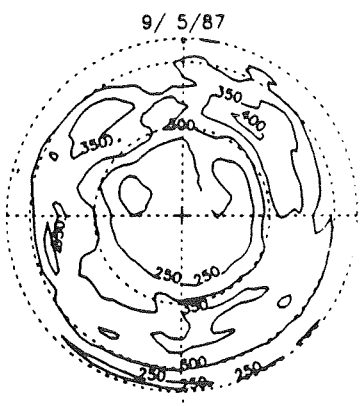

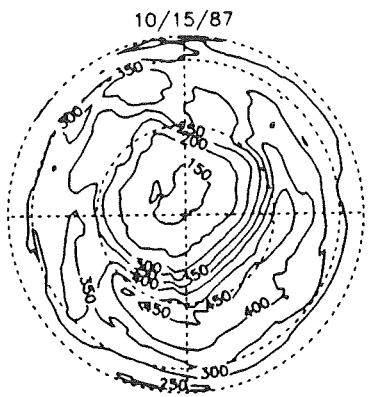

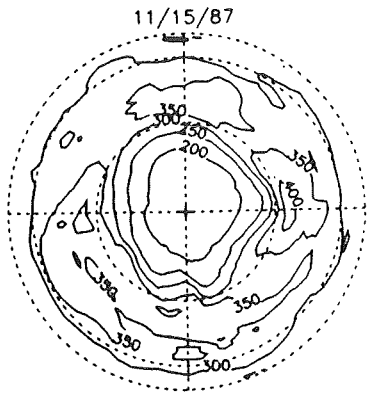

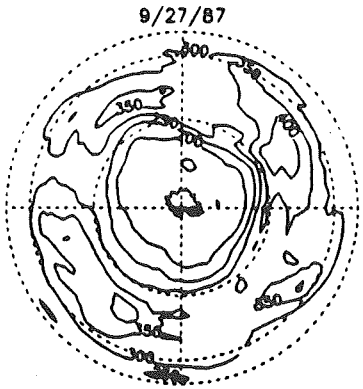

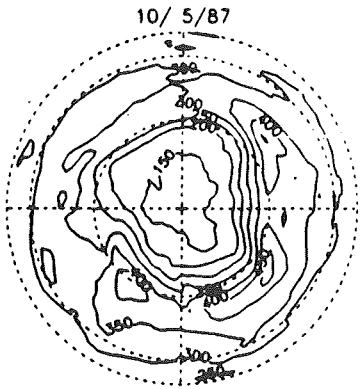

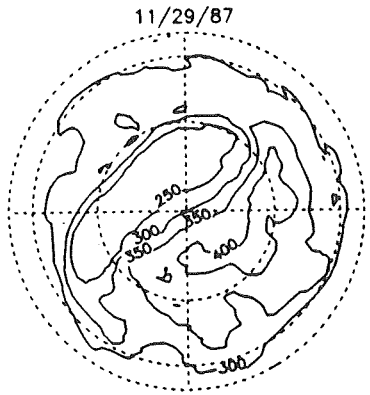

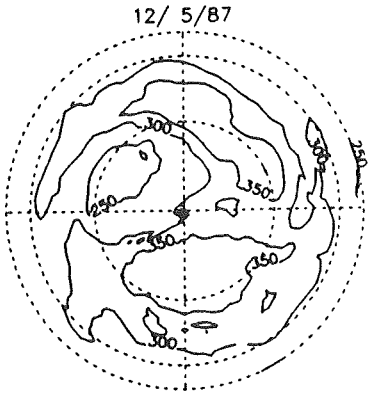

C-11.3 (1). Daily Southern Hemisphere maps of total ozone measured by TOMS (polar orthographic projection). Period shown includes the formation of the ozone minimum in 1987.

C-11.3 (2). Daily Southern Hemisphere maps of total ozone measured by TOMS (polar orthographic projection). Period shown includes the breakup of the ozone minimum in 1987.

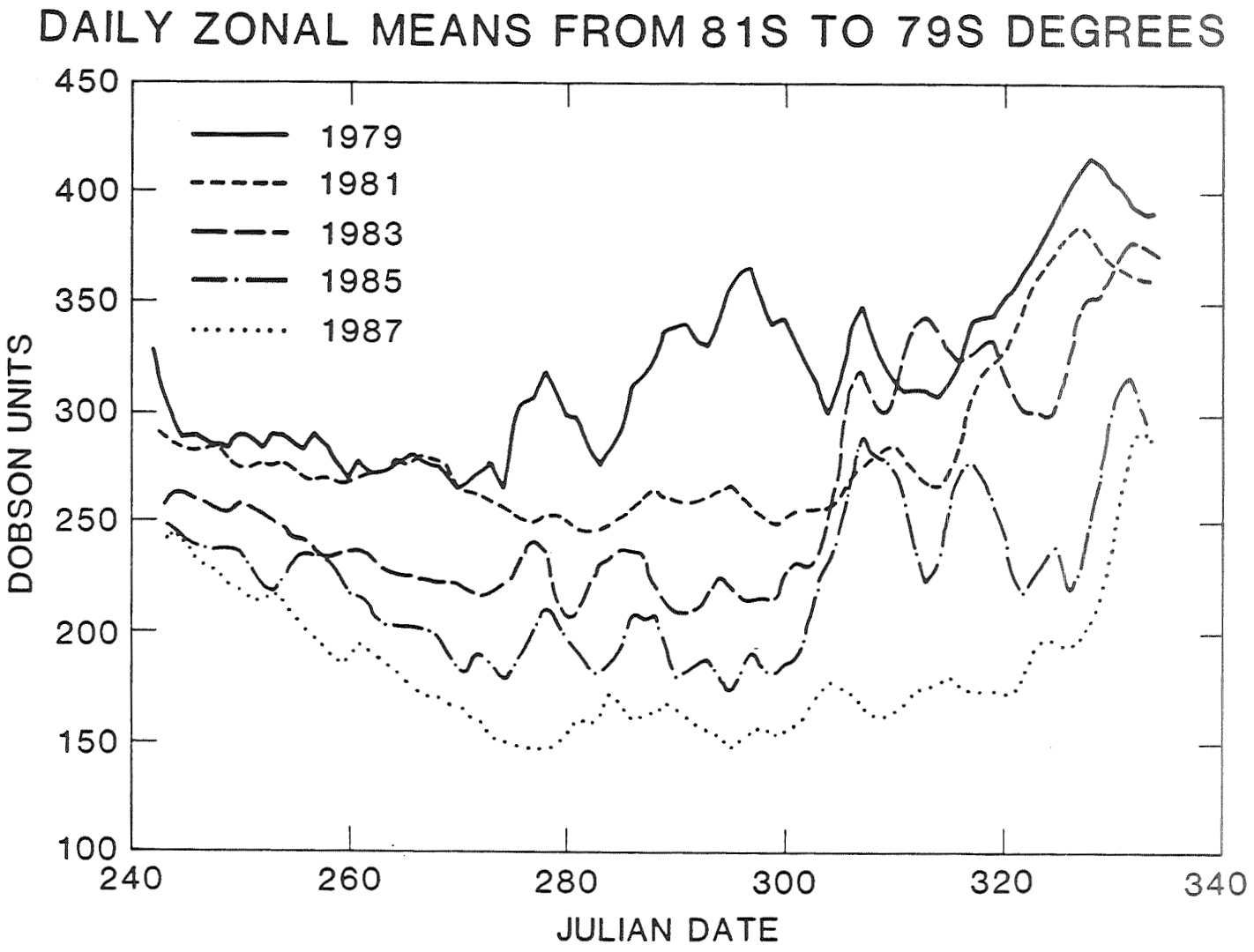

C-11.4. Zonally averaged TOMS ozone from 81°S to 79°S for odd years from 1979-1987 during the months of September, October, and November.

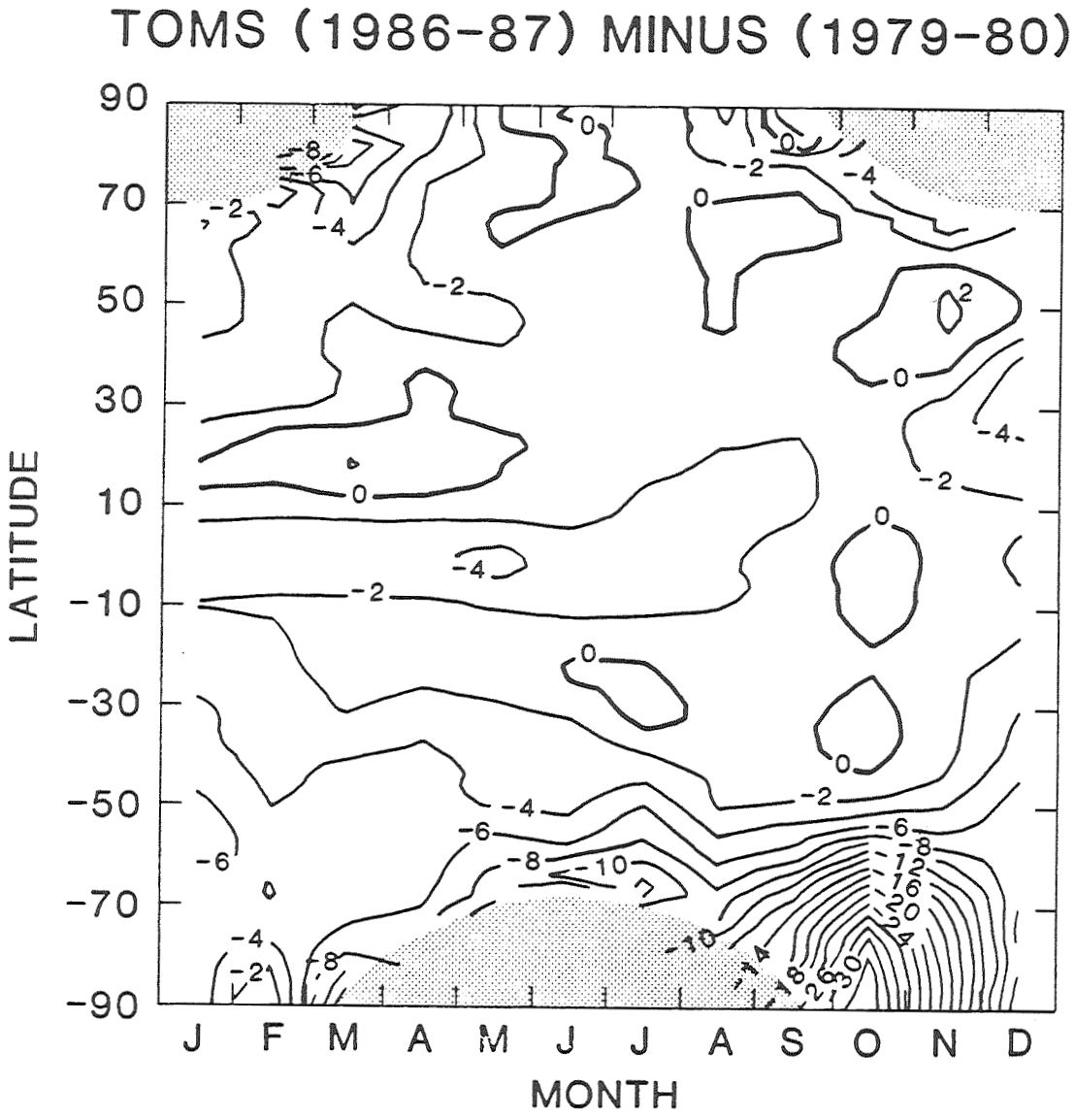

C-11.5. Percentage total column ozone changes from the TOMS instrument over a seven year period as a function of latitude and season. Shaded areas represent regions of no data during the polar night.

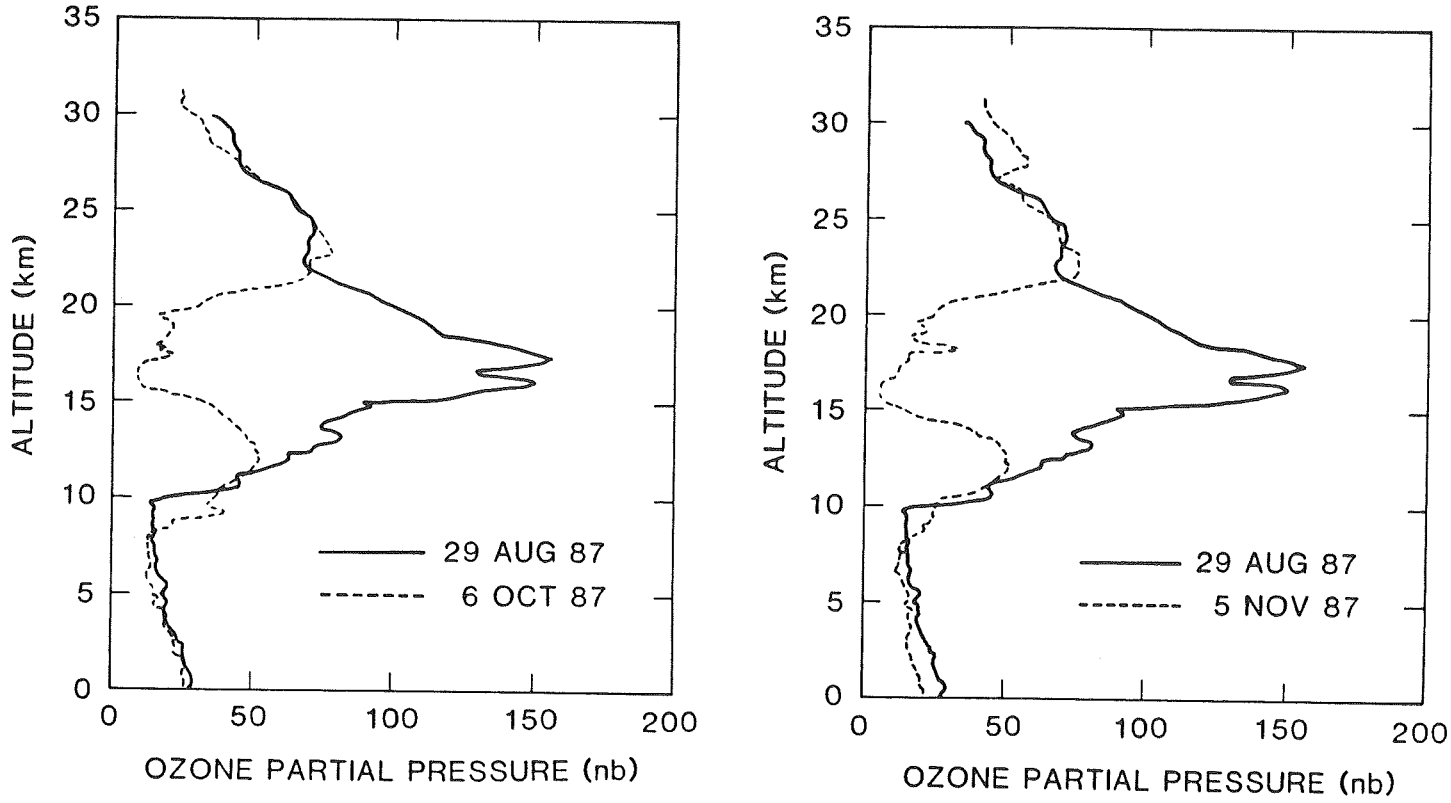

Figure C-11.6. Vertical profiles of ozone using ECC sondes from McMurdo.

C-11.4. Temperature Observations

Substantial evidence has been presented for a decline in the temperature of the lower stratosphere over Antarctica since 1979 in October and November. The downward trends appear most strongly in the month of October when a substantial decline is observed in the middle as well as the lower stratosphere. During the month of November the trend is confined to the lower stratosphere with maximum negative trend of about 1°K/year centered at about the 100 mb (16 km) level. August and September temperatures show little or no trend over the 1979-1985 period. The October decline appears in both rawinsonde station data and NMC gridded data that include satellite information. This suggests that the ozone depletion has a significant impact on the normal spring radiative warming of the Antarctic stratosphere.

C-11.5. Transport Theories for the Antarctic Ozone Hole

The polar lower stratosphere of the Southern Hemisphere is very different from that of the Northern Hemisphere. Strong zonal symmetry of surface conditions in the Southern Hemisphere produces a circulation that is much more symmetric and undisturbed by planetary wave activity than that of the Northern Hemisphere. This leads to conditions in the lower stratosphere in which the lower stratospheric polar vortex is relatively intense, maintaining its integrity throughout the winter season and well into spring. Dynamical modeling suggests that relatively little mixing with air at other latitudes occurs, at least at altitudes where the vortex is sufficiently intense. The air within the polar vortex thus remains very cold and dynamically isolated. When the Sun returns to the South Pole in springtime, temperatures may be near radiative equilibrium. Solar heating might therefore play a more important role in driving the seasonal change there than it does in the Northern Hemisphere, where temperatures are kept well above radiative equilibrium by stronger wave forcing.

The observed Antarctic ozone decline occurs in the lower stratosphere where transport by atmospheric motions has a major influence on the ozone mixing ratio. It is reasonable to suggest that a relatively small climate shift in the Southern Hemisphere could produce a significant change in the total ozone over Antarctica, since the transport of ozone into that region during winter and spring is limited by dynamical constraints associated with the symmetry of the circulation and is very weak in comparison to the almost complete mixing that occurs in the Northern Hemisphere. It is also conceivable that colder temperatures at the beginning of spring produced by weaker wave forcing, or enhanced solar heating in springtime associated with increased aerosols, could lead to transient upwelling during the spring season that would contribute to the springtime ozone decline. But it is very unlikely that diabatic heating rates would be both sufficiently large and suitably distributed to produce the ozone column reduction observed in 1987.

Evidence from NMC analyses suggests that temperatures in the lower stratosphere over Antarctica have declined over the period 1979-1985 for the months of October and November, and a corresponding decline in the wave driving for September is observed in the same data. Calculations of the radiative temperature change associated with the observed ozone decline suggest that the radiative effect of the ozone decline is comparable in magnitude to the observed trend. The radiative temperature change is largest at the 100 mb level and its vertical structure in the lower stratosphere is very similar to that of the NMC trend for November. During October, a middle stratospheric temperature decline is observed in addition to the lower stratospheric decline. This temperature decline in the

middle stratosphere is not expected on the basis of radiation alone, but appears more likely to be associated with decreased wave driving during the previous month. Some combination of altered wave driving and radiative response to ozone changes seems necessary to explain the trend observed in NMC data over the 1979-85 period.

Published attempts to model the springtime Antarctic ozone decline purely as a response to changed transport processes require that low-ozone air be moved into the lower stratosphere from below. Such a movement of air would also require local increases of long-lived trace species of tropospheric origin such as N_2O, CCl_3F (CFC-11) and CCl_2F_2 (CFC-12). Data from the instruments aboard the ER-2 aircraft show that these trace species remain relatively constant at and above the 400°K potential temperature surface (about 15 - 16 km) during September as ozone declines significantly, so that transport of ozone-poor air is unlikely to contribute significantly to the overall decline above this altitude. At lower potential temperatures (i.e. lower altitudes) the ozone decline may be caused by a combination of chemical and meteorological processes. These data support the hypothesis that a chemical sink for ozone is required within the polar vortex. However, the role of radiative and dynamical processes in establishing the conditions necessary for the ozone depletion and in controlling the temperature, cloudiness, and precise degree of isolation of the Antarctic ozone hole must be carefully considered.

C-11.6. Chemical Theories and Observations for the Antarctic Ozone Hole

Two distinctly different classes of chemical theories have been proposed to explain the observed loss of springtime Antarctic ozone. The first proposes that the abundance of the oxides of nitrogen are periodically enhanced due to changes in solar activity, while the second proposes that the efficiency of reactions involving chlorine and bromine species are enhanced. Current theories which attempt to describe ozone loss in the Antarctic stratosphere in terms of catalytic chemical destruction involving chlorine or bromine all have the following features:

(1) conversion of a substantial fraction of the Cl_x contained in the reservoir molecules HCl and $ClONO_2$ into active forms of chlorine such as ClO either by heterogeneous reactions in PSCs or by enhanced OH abundance;

(2) cycles that effectively catalyze the recombination of O_3 with itself, involving ClO in the rate limiting step with HO_2, itself, or BrO, forming HOCl, the Cl_2O_2 dimer, or Cl and Br, respectively;

(3) drastic reduction in NO_2 abundance resulting from removal of NO_y as HNO_3 in the condensed phase of PSCs.

Recent laboratory data has shown conclusively that heterogeneous reactions of $ClONO_2$ (g)[1] and N_2O_5 (g) with H_2O (s)[2] and HCl (s) are rapid enough to play an important role in the chemistry of the Antarctic stratosphere. In particular, HCl was shown to stick efficiently to water ice particles and readily diffuse into water ice crystals at low temperatures forming solid solutions. Dissolved HCl in solid solutions was also shown to be very mobile greatly enhancing its reactivity with reactant species on the crystal surfaces. The HNO_3 formed by $ClONO_2$ reactions with ice and HCl-ice remains in the condensed phase, where-as the chlorinated products desorb into the gas phase.

---

[1] (g) refers to gas phase

[2] (s) refers to solid phase

Our understanding of the chemical composition of the spring-time Antarctic atmosphere increased dramatically during 1986 and 1987. Observations of the vertical distribution and column content of a large number of species, including ozone (O_3), water (H_2O), chlorine monoxide radical (ClO), chlorine dioxide (OClO), chlorine nitrate ($ClONO_2$), hydrochloric acid (HCl), bromine monoxide radical (BrO), hydrofluoric acid (HF), nitric oxide (NO), nitrogen dioxide (NO_2), nitric acid (HNO_3), total odd nitrogen (NO_y), nitrous oxide (N_2O), methane (CH_4), carbon tetrachloride (CCl_4), methylchloroform (CH_3CCl_3), and CFCs 11 and 12, were made by ground-based observations from McMurdo in 1986 and 1987, and by in-situ and remote sensing techniques from the ER-2 and DC-8 aircraft based in Punta Arenas, Chile in 1987. In addition, the size distribution, abundance, and composition of particles was determined by instrumentation aboard the ER-2; the vertical distribution of aerosols from 12 to 28 km by the DC-8 lidar; and the size distribution from balloon-sondes from McMurdo, in an effort to understand the role of heterogeneous processes. The data clearly demonstrated that the chemical composition of the Antarctic stratosphere in springtime was highly perturbed compared to that expected at these latitudes based on measurements at mid-latitudes and chemical models that predate these new data. The distribution of chlorine species is significantly different from that observed at mid-latitudes, as is the abundance and distribution of nitrogen species. At present it is not clear whether the abundance of total inorganic chlorine (the summed abundance of chlorine in all inoorganic chemical forms) is perturbed relative to that expected, or just the partitioning. In addition, it was observed that the amount of total water within the chemically perturbed region of the vortex was significantly lower than that at the same potential temperatures immediately outside it.

Based on the observations made at McMurdo and from the aircraft campaign the weight of observational evidence strongly suggests that chemical mechanisms involving man-made chlorine are primarily responsible for the observed decrease in ozone within the polar vortex at potential temperatures greater than 400°K. It is clear that meteorology sets up the special conditions of an isolated air mass (polar vortex) with very cold temperatures required for the perturbed chemistry. It is also clear from the 1987 ER-2 flights that the region of dehydrated and denitrified air maintained a sharply defined latitude gradient throughout most of the campaign. The meteorological flow must therefore have been such as to maintain a kind of "restrainment vessel", in which the perturbed chemistry could proceed without being influenced by mixing in more normal stratospheric air from outside or below. The concept of mixing at the region of sharp latitudinal gradient is important, since mixing has the potential to supply nitrogen oxides which would tend to decelerate the chlorine chemistry. The meteorology is thus important in the termination phase as well as in the initiation phase.

As stated earlier there is strong evidence that the chemical composition of the springtime Antarctic stratosphere is highly perturbed compared both to midlatitudes and to the summer / fall Antarctic stratosphere. The data show that while the abundance of total chlorine (the summed abundance of chlorine in all organic and inorganic chemical forms) is probably consistent with that expected, the partitioning of Cl_x was highly perturbed compared with that observed at mid-latitudes and normally expected at high latitudes. The concentrations of HCl were low, whereas the concentrations of OClO and ClO were significantly elevated. Somewhat elevated concentrations of $ClONO_2$ were also observed. This is clear evidence that the balance was dramatically shifted from inactive forms of chlorine towards reactive species that can catalytically destroy ozone. In-situ ER-2 and ground based measurements of ClO showed that its abundance within the chemically perturbed region of the Antarctic atmosphere is a factor of 100 to 500 greater than that measured at comparable altitudes at midlatitudes, reaching a maximum value of about 1 ppbv near local noon at approximately 18.5 km altitude. The in-situ aircraft data demonstrated that within the chemically

perturbed region of the vortex near 18.5 km the abundance of ClO during September of 1987 was sufficient to account for the destruction of ozone if our current understanding of the chlorine-ozone ClO dimer catalytic cycle is correct. The rate of decrease in ozone during the month of September at the highest altitudes at which the ER-2 was operated was consistent with simultaneously observed concentrations of ClO. During the month of August, there was no strong positive, large-scale correlation between ClO and O_3 observed, whereas by the middle of September, as the ozone concentration was dropping at ER-2 altitudes, a strong anti-correlation developed on the larger spatial scales. This observational evidence is consistent with chlorine catalysis of ozone destruction.

The bromine monoxide radical was observed at abundances of a few pptv within the chemically perturbed region of the vortex at the flight levels of the ER-2. The abundance of BrO decreased at lower altitudes. Total column measurements of BrO from the DC-8 and from McMurdo in 1987 are currently being analyzed. The low measured abundances of BrO mean that the catalytic cycle involving the $BrO + ClO \rightarrow Br + Cl + O_2$ reaction is not the dominant catalytic mechanism for ozone destruction, but nevertheless probably accounts for about 10% of the ozone destruction at the ER-2 flight levels.

The in-situ ER-2 observations of the abundance of odd nitrogen, which is the sum of all nitrogen-containing reservoir and radical species, show, like total water, very low values within the chemically perturbed region of the vortex, indicating that the atmosphere has been denitrified, as well as dehydrated. Abundances of gas phase NO_y of 8-12 ppbv were observed outside the chemically perturbed region, while abundances of 0.5 to 4 ppbv were observed inside the chemically perturbed region. In addition, some of the NO_y observations suggest that NO_y component species are incorporated into polar stratospheric cloud (PSC) particles, and nitrate was observed in the particle phase on some of the filter samples and on some of the wire impactor samples taken in the chemically perturbed region of the vortex. The ground-based and aircraft column measurements of nitric oxide, nitrogen dioxide, and nitric acid exhibit a strong decrease in the abundance of these species towards the center of the vortex. These low values of nitrogen species are contrary to all theories requiring elevated levels of nitrogen oxides, such as the the proposed solar cycle theory .

Observational data that air within the chemically perturbed region of the vortex is dehydrated and that the NO_y abundances are very low are consistent with theories that have been invoked whereby the chlorine reservoir species, $ClONO_2$ and HCl, can react on the surfaces of polar stratospheric clouds to enhance the abundance of active chlorine species, i.e. ClO. The observations also support the picture that the abundance of NO_y is low because odd nitrogen can be removed from the atmosphere tied up in ice crystals which can then gravitationally settle to much lower altitudes. Low abundances of NO_y are needed to prevent the rapid reconversion of ClO to $ClONO_2$.

C-11.7. Global Implications

Besides its dramatic character and its sudden appearance, the major reason for concern about the "ozone hole" is that the processes, which appear to play a decisive role in the polar environment and which are not fully understood or included in atmospheric models, might be important at other latitudes and contribute to a global ozone depletion. There are two observations discussed in this Ozone Trends Report that suggest that there is an urgent need for additional research:

(a) there is evidence of ozone depletions in winter at mid and high latitudes in the Northern Hemisphere that are larger than calculated using photochemical models, and

(b) while the column ozone depletion is largest in the Antarctic spring-time, ozone appears to have decreased since 1979 by more than 5% at all latitudes south of 60°S throughout the year.

There are two processes currently not included in photochemical models that might provide explanations for these two observations:

(1) The observation of winter-time ozone decreases in the Northern Hemisphere might be explained by heterogeneous chemical processes:

Since aerosols (primarily composed of liquid sulfuric acid) are present in the stratosphere at all latitudes, it is important to understand if heterogeneous processes similar to those that are important in Antarctica could occur at other latitudes and possibly lead to ozone destruction in other regions of the atmosphere. At present the importance of heterogeneous processes at other latitudes is unknown.

It should be noted that both the abundance and catalytic efficiency of the liquid sulfuric acid aerosol particles in the global Junge layer are lower than the PSCs over Antarctica. However, some heterogeneous processes might periodically become important and lead to ozone destruction after large volcanic eruptions, when the amount of particles in the stratosphere is enhanced by several orders of magnitude. If heterogeneous processes are important at mid-latitudes then the concentrations of ClO should be elevated in the Junge layer as they were over Antarctica. Measurements of the vertical distribution of the ClO radical at mid-latitudes in summer in the Northern Hemisphere from balloon (24-40 km) and aircraft platforms (15-20 km) show that the abundance of ClO in the peak region of the aerosol layer, i.e. 16-20 km, is not significantly elevated as in the chemically perturbed region of the Antarctic ozone hole. This indicates that conversion of inactive reservoir forms of inorganic chlorine, i.e. HCl and ClNO3, to the active form, i.e. ClO, does not appear to be detectably enhanced (less than a factor of 3 to 5) in this region of the stratosphere in summer.

Although there are significant differences in the meteorology of the Arctic and Antarctic, PSC's are formed in the Arctic and might play an important role in controlling ozone. Arctic temperatures at 70 mb reached -87°C in early February 1984, probably sufficient to cause dehydration. An intensive field measurement campaign similar to that used to investigate the Antarctic ozone hole is required.

(2) The observation of year-round decreases in ozone outside of the polar vortex in the Southern Hemisphere might be explained by a "dilution effect" from the spring-time Antarctic ozone hole:

The possibility of a "dilution effect" of the polar anomaly observed in spring over Antarctica must be considered as another possible global (or least Southern Hemisphere) implication of the Antarctic ozone hole. Since the chemical lifetime of ozone in the lower stratosphere is of the order of a year, air masses, with depleted ozone amounts, move toward the equator as soon as the winter vortex ceases to exist (November and December). As volumes of air with extremely low ozone are transported toward lower latitudes every year, the effects might partly accumulate and a limited change in the total hemispheric ozone content might become noticeable. At present this issue is being addressed using both multi-dimensional theoretical models and the TOMS satellite data by examining changes in total column ozone in both hemispheres. While the ozone depletion is largest in the

Antarctic spring-time, normalized TOMS data indicate that total column ozone has decreased since 1979 by more than 5% at all latitudes south of 60°S throughout the year. At this time it is premature to judge if this is caused by a dilution of the air from the region of very low ozone, a changed meteorology, or some other unidentified phenomenon. However, at least some of the decrease is likely due to dilution.

Appendix 1: Statistical Approaches to Ozone Trend Detection

Ready, widespread acceptance of the results of a scientific investigation depends critically on the credibility of the study, and in the case of a data-oriented study this in turn depends largely on two factors: the quality of the data on which the study is based, and the quality of the subsequent analysis of those data. Data quality for each of the measuring systems is discussed in the relevant chapters, and here we offer only broad comments. The prime focus of this Appendix has been on data analysis techniques, and on these we offer more specific suggestions.

Trend estimates:

There are many ways to quantify the trend in a set of data including fitting a straight line, fitting a ramp (or hockey stick) function, or comparing averages over different time windows. In each case, the resulting quantity should be accompanied by an appropriate standard error.

Standard errors:

A standard error has meaning only in the context of a model for the way in which the data were sampled, and if the data show evidence of spatial or temporal correlation, the sampling model must reflect this. Computer software for building the required sampling models and calculating the corresponding trend estimates and standard errors is widely available, and should be used more extensively.

Current results:

Trend estimates based on fitting ramp functions reported in Chapter 4 and those of Reinsel, Tiao and their co-workers adequately account for serial correlation and its seasonal structure, and represent the state of the art. Estimates of trends from TOMS data also reported in Chapter 4 allow for serial correlation, but not for its seasonal structure. Although not state of the art, the results should be close. Standard errors of other trend estimates obtained by least squares fitting without allowance for serial correlation may be incorrect by factors of more than 3.

Ground-based total ozone column data:

It has been demonstrated that the quality of Dobson total ozone column data can be improved substantially by retroactive application of corrections based on calibration changes. This is best carried out by complete recalculation of each day's data on the basis of corrected algorithms, but useful improvements can be made by corrections made to monthly averages. Stations should be urged to give a higher priority to such adjustments to historical data, and to ensuring publication of the adjusted data by the World Ozone Center.

Ground-based ozone profile data:

The largest remaining question about the quality of the ozone profile data obtained by the Umkehr technique is the impact of aerosols. This question will have to be resolved before the Umkehr network can fulfill its dual roles of providing ground-based information about trends in ozone profiles, and providing ground truth for the validation of satellite-borne instruments.

Satellite ozone measurements:

The realization that the effect of diffuser plate degradation on Nimbus 7 cannot be uniquely separated from other instrument changes underscores the difficulty of maintaining measurement stability with satellite-based systems. This illustrates the continuing need for cross-checking of all types of measurements, a need about which there has been a tendency to become complacent.

SECTION D

MODEL PREDICTIONS OF FUTURE OZONE CHANGE

D.1. Introduction

The concern over changes to the global environment, in particular to stratospheric ozone, has spurred the development of stratospheric models. Atmospheric chemistry and transport are combined in current models and used to make predictions of the changes in ozone that may be expected over the next century. Modelling the global ozone distribution requires chemical transport models for tropospheric as well as stratospheric ozone and other trace gases, but emphasis on model development has been placed on stratospheric chemistry and circulation. These models take into account the increasing concentrations of source gases, such as CH_4, N_2O and chlorofluorocarbons (CFCs), and calculate the chemical changes in the stratosphere. All models predict the direct photochemical effects, and a few models now examine perturbations to stratospheric temperatures and circulation and their feedback on ozone. The models used in these assessment studies do NOT include the chemistry associated with polar stratospheric clouds that is now believed to be part of the Antarctic ozone "hole" (see Section C of this report). Therefore, neither predictions of the hole, past and future, nor the global or hemispheric significance of Antarctic chemistry, are included in this assessment.

The conclusions from the Ozone Trends Report (see summaries in section C of this report) indicate that depletions in column ozone since 1969 at northern mid-latitudes appear to be as much as two to three times greater than predicted. Those predictions involved some of the same 2-D models that are used in this assessment. If the discrepancy between models and observations over the past 20 years is significant, then a major question arises as to what uncertainties should be placed on our current predictions for the next 100 years. Potential causes of the larger than predicted decrease in column ozone center on the lower stratosphere since calculated changes to ozone concentrations in the upper stratosphere are consistent with observations. Of the many possible sources of error in the Ozone Trends Report simulations, three may be singled out: (1) errors in the standard gas-phase chemistry involving chlorine in the lower stratosphere; (2) failure to include a heterogeneous chemistry in the Northern Hemisphere that is similar to, but different from, that occurring over Antarctica; (3) a small long-term trend in lower stratospheric circulation and temperatures. Points (1) and (2) can be addressed directly by a vigorous research program involving theoretical modelling, laboratory studies and, especially, aircraft expeditions to measure the photochemistry of the lower Arctic stratosphere. Such a measurement campaign would be similar to the Antarctic campaign of September 1987, which was led by NASA, involving NOAA, CMA, universities and international cooperation. If the unexplained part of the recent decline is associated with point (3), climate change, then it would have been difficult to detect over the last 20 years. Hence, we must pursue our current research on the feedback of climate change on ozone perturbations.

This section D presents an update of the previous assessment (WMO, 1986, Chapter 13; NASA Ref. Pub. 1162, 1986). It is a limited study of predicted ozone perturbations and considers only a few of the scenarios examined previously. The focus here is on (1) a time-dependent scenario into the next century that is a continuation of the period 1955-1985 which was simulated for the Ozone Trends Assessment, (2) a steady-state scenario

including a first look at the new generation of 2-D models in which the ozone perturbations feed back upon the circulation, and (3) the impact of the most recent re-evaluation of the chemical kinetics and photochemical input data.

Results are presented from both 2-D (latitude-by-altitude) and 1-D (altitude) models. The continued development of 2-D models and computing capability has led to their application as the standard assessment tool for modeling stratospheric ozone. The 2-D models have a much greater advantage over 1-D models than is apparent by the number of dimensions, in that they are able to describe the perturbations to ozone as a function of latitude and season. The 1-D models cannot adequately simulate seasonal changes in column ozone; they are used primarily for investigatory purposes; and 1-D model results are included here in section D.3 mainly for historical perspective in comparing to previous assessments over the past decade.

The scenarios for the future composition of the atmosphere are discussed in Section D.2. Implications of the recent re-evaluation of the chemical model, denoted here as JPL-87, are described in section D.3. Predictions of ozone for the steady-state scenario, representative of trace gas abundances expected by the middle of the next century, are presented in section D.4. The predicted evolution of the stratosphere for the immediate future is given in section D.5, using a time-dependent scenario for the period 1985 to 2015 which assumes a continuation of the currently observed growth rate for the source gases. Some calculations extended beyond 2015. Plans for a major intercomparison in order to understand the differences among current models are presented in section D.6. Our confidence in predicting stratospheric change is discussed in section D.7 along with expected developments in theoretical modeling.

D.2. Scenarios for Future Atmospheric Composition

For the time-dependent scenario (TD) used in these predictions, the 2-D models produce a history of ozone concentrations by explicitly integrating over each year using fluxes or tropospheric concentrations of the source gases (CFCs, N_2O, CH_4, CO_2, and other halocarbons) that are prescribed for each year from Table D-1. The assumed scenario is a simple extrapolation of the recent history of the atmosphere: emissions of CFCs remain unchanged at estimated 1985 levels, and the observed trends in other trace gases continue. The TD scenario should be sufficiently accurate for the near future, but prediction of atmospheric composition becomes more uncertain for long-term scenarios. The continued, but slowing growth of stratospheric chlorine is similar to that anticipated if the Montreal Protocol were adopted. Our ability to project growth in other trace gases with more diversified sources is more limited, however, and this uncertainty is particularly acute for CH_4 which plays a direct chemical role in counteracting the impact of chlorine increases.

The steady-state scenario (SS) in these assessments compares a contemporary atmosphere "1980", described by trace gas concentrations at the beginning of this decade, with a highly perturbed atmosphere "20xx" that we expect to be reached on a time scale of 50 to 100 years, sometime well into the next century. The "1980" atmosphere is based on measured tropospheric concentrations of the trace gases. The "20xx" atmosphere contains the following assumptions:

N_2O increases at the currently observed rate, 0.25 %/yr, for about 70 years, equivalent to a 20 % increase.

Table D-1

Model Scenarios

(A) TIME-DEPENDENT SIMULATION (TD)

Trace Gas	1985-2015
N_2O	0.25% per yr
CH_4	1.0 % per yr
CO_2	0.5 % per yr
$CFCl_3$ (CFC-11)	265 Gg per yr
CF_2Cl_2 (CFC-12)	412 Gg per yr
CH_3CCl_3	454 Gg per yr
CCl_4	131 Gg per yr
CH_3Br	20 ppt unchanged
CH_3Cl	700 ppt unchanged

This calculation is a continuation of the simulations for the period 1955-1985 which are discussed in the Ozone Trends Assessment. The total stratospheric chlorine abundance in 1985 was approximately 3 ppb. Gg = 10^9 g.

(B) STEADY-STATE PERTURBATION (SS)

Atmosphere:	"1980"	"20xx"
N_2O	300 ppb	360 ppb
CH_4	1.6 ppm	3.2 ppm
$CFCl_3$ (CFC-11)	170 ppt	800 ppt
CF_2Cl_2 (CFC-12)	285 ppt	2200 ppt
CH_3Br *	20 ppt	40 ppt
CO_2 *	340 ppm	680 ppm
CH_3Cl	700 ppt	unchanged
CH_3CCl_3	100 ppt	unchanged
CCl_4	100 ppt	unchanged
H_2O (tropopause)	3.0 ppm	unchanged
CO	100 ppb	unchanged

The pair of calculations is based on Table 13-1 of WMO (1986): a 1980 standard with 2.48 ppb Clx and a mid-21st century simulation with 8.2 ppb Clx. Mixing ratios are used as lower (tropospheric) boundary conditions.

(*) The changes in CH_3Br (only source of Brx) and CO_2 were not able to be included in all models.

CH_4 increases at the currently observed rate, 1 %/yr, for about 70 years, equivalent to a 100 % increase.

CFC-11 and CFC-12 are used in the models as surrogates for increases in the total organic chlorine abundance of the atmosphere. Stratospheric chlorine also includes contributions from other CFCs such as CFC-113, from the hydrochlorofluorocarbons (HCFCs) such as HCFC-22, and from other chlorocarbons such as CCl_4 and CH_3CCl_3. All of these species contribute chlorine to today's stratosphere, but concentrations of HCFCs and CH_3CCl_3 are not expected to build up as large as those of CFCs because they are destroyed predominantly in the troposphere by reaction with hydroxyl radicals (OH). The concentrations chosen for "20xx" represent a steady-state abundance for the current 1985 emissions of CFC-11 and CFC-12. These levels of stratospheric chlorine, 8.2 ppbv, are expected on time scales of 100 years if CFC emissions do not change substantially.

CH_3Br is used in the models as a surrogate for all brominated gases that contribute to stratospheric bromine. An increase of 20 pptv approximates the possible build up during the next century of the halons (CF_3Br(1301) and CF_2ClBr(1211)) and other brominated species.

CO_2 increases, about 0.5 %/yr, may possibly lead to a doubling near the end of the 21st century.

The concentrations of trace gases prescribed for these two atmospheres are given in Table D-1 and are based on a similar scenario from the previous assessment (WMO, 1986, Chapter 13). The 2-D models are integrated for several years with these fixed boundary conditions until a steady state is achieved (i.e., the annual cycle of ozone repeats).

D.3. Revised Chemical Kinetics and Photochemical Data: JPL 87-41

Since the last NASA assessment of the stratosphere, the single most important event in terms of modeling stratospheric chemistry has been, without a doubt, the recognition of the Antarctic ozone "hole". Its impact on the chemical models and laboratory kinetics has been to generate a whole new chemistry involving the interaction of chlorine species with stratospheric aerosols in order to explain the rapid depletion of ozone from the low-to-middle stratosphere over Antarctica in the spring.

With the exception of this heterogeneous chemistry, changes in the chemical models have been modest since the assessment of two years ago. In so far as they impact the calculated distribution of ozone, a synopsis of the major changes from JPL-85 (WMO, 1986) to JPL-87 (Section E) is as follows:

$OH + HO_2 \rightarrow H_2O + O_2$: rate increased by about 20 % at the stratopause. The levels of HO_x decreased. In the region 50-60 km altitude where HO_x chemistry is the dominant loss of ozone, the O_3 concentrations increased by about 10 %.

$NO_2 + O \rightarrow NO + O_2$: rate increased by about 15 % in the middle stratosphere. Concentrations of NO_2 changed little; the loss of ozone by NO_x chemistry increased; and O_3 concentrations in the region 25-30 km altitude declined by 5 %.

$NO_2 + h\nu \rightarrow NO + O$: quantum yield increased by about 20 %. The major effect was to change the NO/NO_2 ratios in the stratosphere by a similar amount, about 20 %. In the region 25-30 km altitude, NO_2 concentrations remained nearly constant while NO increased.

$O_3 + h\nu \rightarrow O_2 + O$: revised cross-sections 185-225 nm. The photolysis of O_2 in the middle and lower stratosphere is very sensitive to the absorption by O_3 at wavelengths between 205 and 225 nm. In this wavelength region the overhead column of ozone above 30 km altitude has optical depth of order 1, and the production of odd-oxygen calculated below 30 km altitude responds strongly to changes in the value of the cross-section as well as the overhead ozone (e.g., the "self-healing" effect when large ozone depletions occur above 30 km altitude). The sensitivity of ozone to the assumed value for these cross-sections is one of the largest in the models, with 5 % changes translating into equivalent changes in the ozone concentrations.

The ozone changes for the contemporary atmosphere noted above refer to calculations made with a 1-D model (GISS); results from a 2-D model (AER) are qualitatively similar, but have smaller magnitudes: see changes in the ozone profiles shown in Figure D-1a. A notable change in the 2-D models with JPL- 87 is the large region of the lower stratosphere over the tropics with increased levels of ozone, leading to higher ozone columns over most of the globe. Dobson maps showing the total ozone column calculated with JPL-87 and the percent difference in ozone columns calculated with JPL-87 minus those with JPL-85 are given for the AER model in Figures D-1b&c. The newer chemical model has resulted in lower ozone columns only at highest latitudes. Other changes in JPL-87 resulted in modest changes to the abundances of individual species not described here.

The impact of JPL-87 on ozone perturbations predicted for the trace gas scenario SS is small. For the 1-D models shown in Table D-2, the typical decrease predicted in column O_3 for the steady-state scenario (without bromine) is now -2 % versus -3 % in 1985. [Bromine increases were not included in the overall trace gas scenario in WMO (1986); the current scenario incorporates these. However, most results from the 2-D models quoted here do not include bromine chemistry.] Adding bromine to the trace gas scenario results in a larger decrease, about -3 %, for most 1-D models. For 2-D models, the impact of JPL-87 upon the steady-state scenario (SS) is also modest. Results from the AER model show depletions that are more negative by about -0.5 % over most latitudes and seasons as seen in Figures D-2 and D-3 and discussed further in section D.4.

The definition of a globally averaged ozone depletion for 2-D models is mathematically straightforward, but not meaningful when trying to interpret the effects of a predicted decrease in ozone. For example, the pattern of ozone decreases predicted with the AER 2-D model using JPL-87 (Figure D-3) varies from -1 % to -6 % over latitude and season. The impact of this decrease on solar ultraviolet at the surface of the Earth depends on the total column (Figure D-1b) and the solar zenith angle (a function of latitude, season and time of day). The globally averaged number, -2.9 %, is larger than the depletion predicted from the chemically equivalent 1-D model, -1.9 %. This difference is typical for most models. The 2-D models more accurately represent the circulation of the stratosphere through a combination of advection (winds) and diffusion (mixing). The 1-D models include only vertical diffusion and cannot simulate the net upward transport of gases in the tropical stratosphere and the balancing downward flow at high latitudes. In addition to simulating the seasonal cycle of ozone over all latitudes, the 2-D models more accurately reflect the true global average for ozone and its perturbations when comparing with globally integrated satellite measurements.

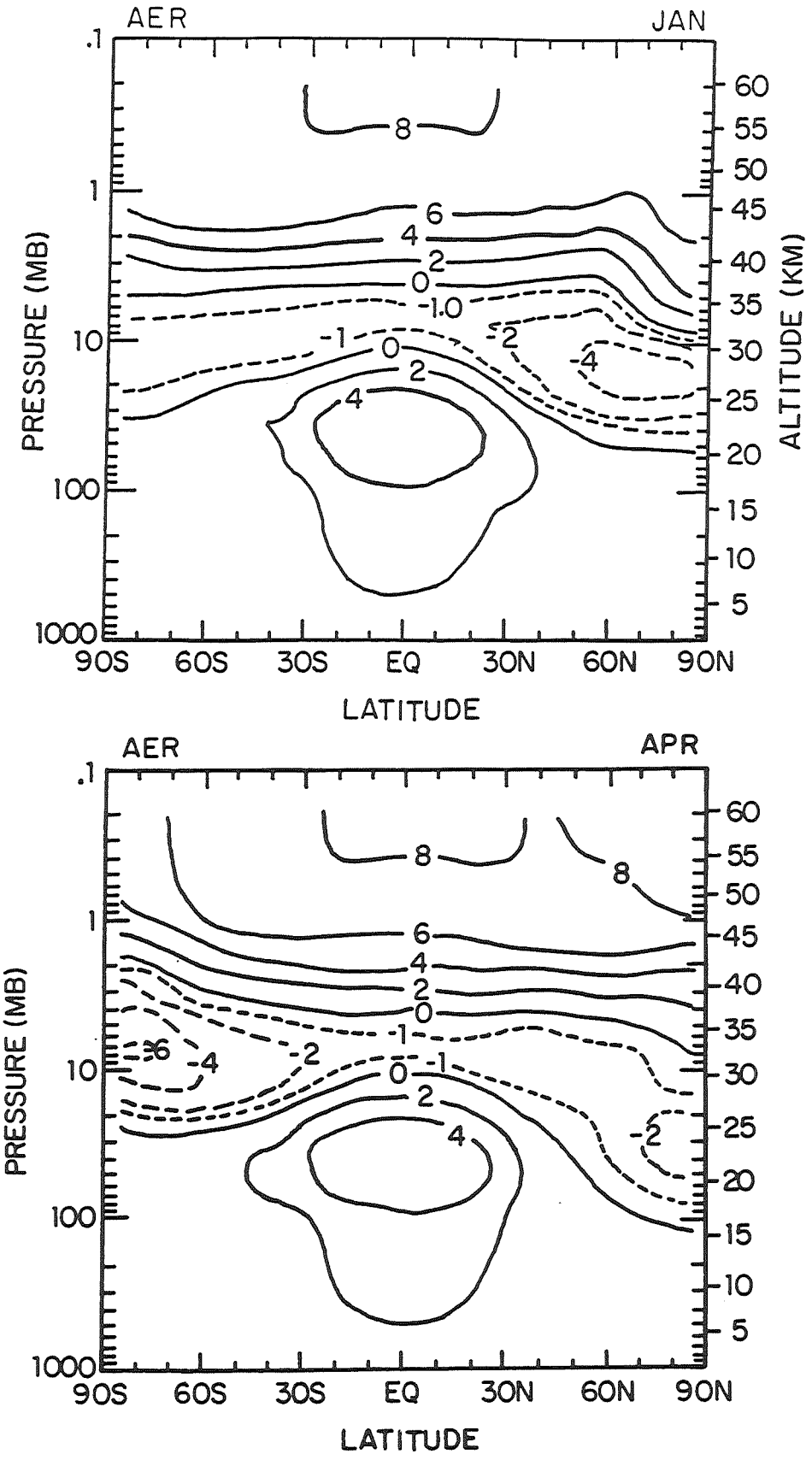

D-1a. Ozone profile changes (%) from JPL-85 to JPL-87 chemical models with the AER model for the months of January and April.

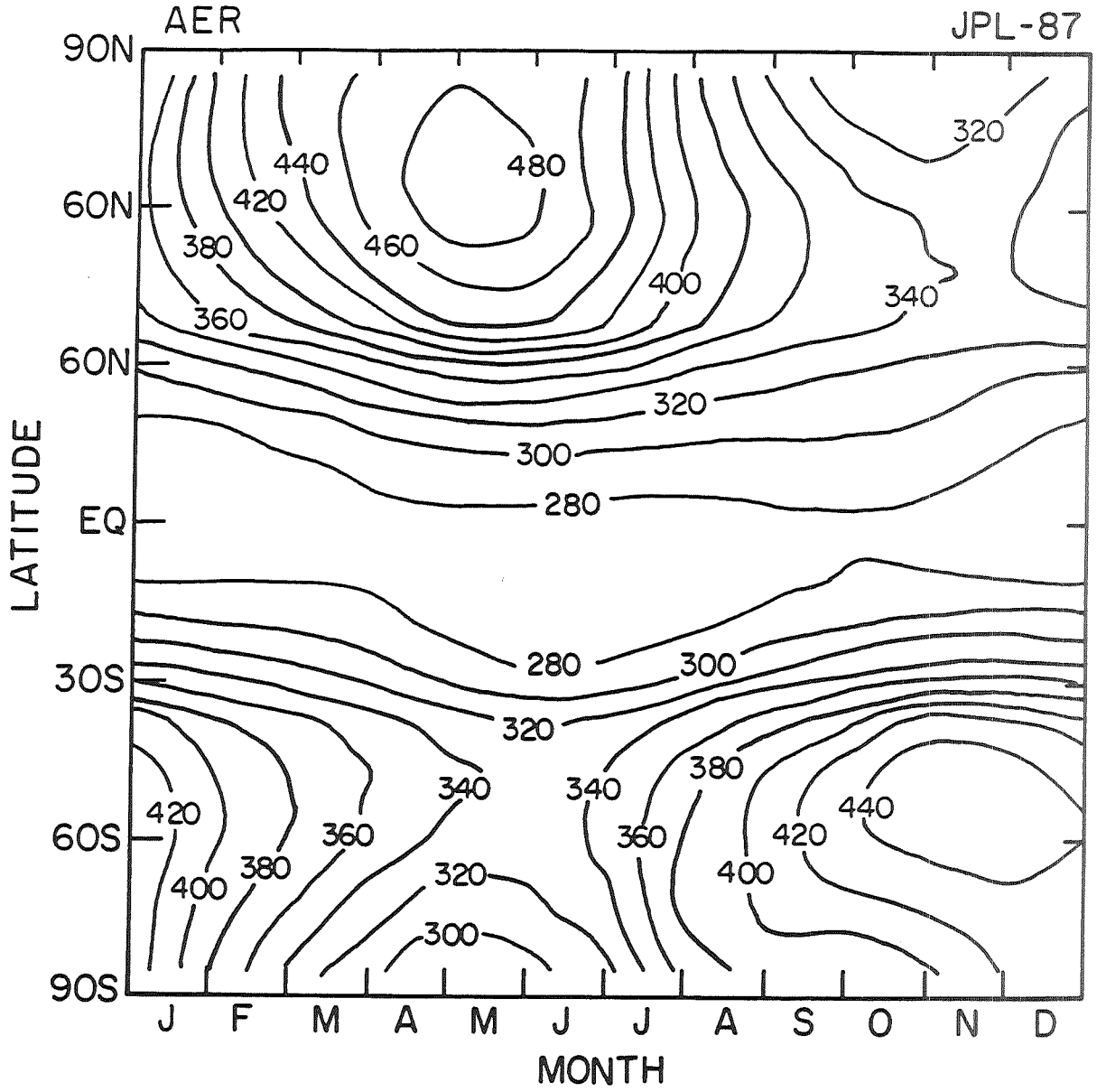

D-1b. Dobson map of ozone columns (Dobson Units) as a function of latitude and month from the AER model using JPL-87 chemical model.

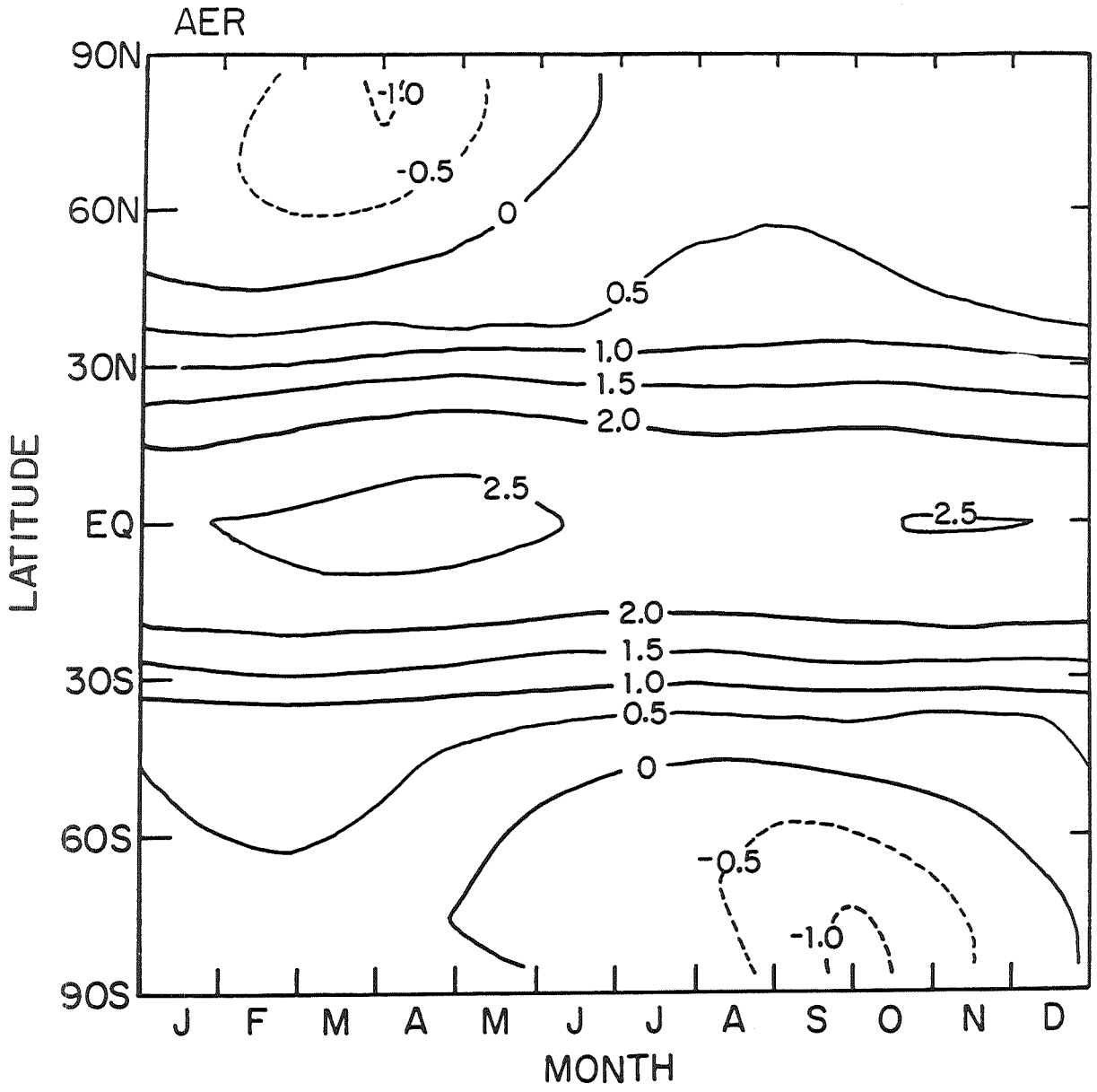

D-1c. Dobson map of ozone column changes (%) with the AER model from JPL-85 to JPL-87 chemical models.

Table D-2.

1-D Model Results: Change in Column Ozone from 1980 to "20xx"

MODEL (contributor)	AER (Ko)	Cal.Tech (Yung)*	DuPont (Fisher)	GISS (Prather)	LLNL (Wuebbles)
JPL-87 chemistry					
TG=Clx+CH_4+N_2O	-1.9	-2.1	-2.5	-2.0	-----
TG+CO_2+T	------	------	-1.0	------	+1.0
TG+Brx	-3.2	-2.5 .	------	-3.0	-3.1
JPL-85 chemistry (WMO, 1986)					
TG=Clx+CH_4+N_2O	-3.3 .	-----	-3.1	-3.0	-3.4
TG+CO_2+T	----	----	-1.4	------	+0.2

---

* stratospheric column only
TG = Trace gas scenario for chemically active tracers
CO_2 + T = Temperature feedback due to changes in CO_2 and O_3.

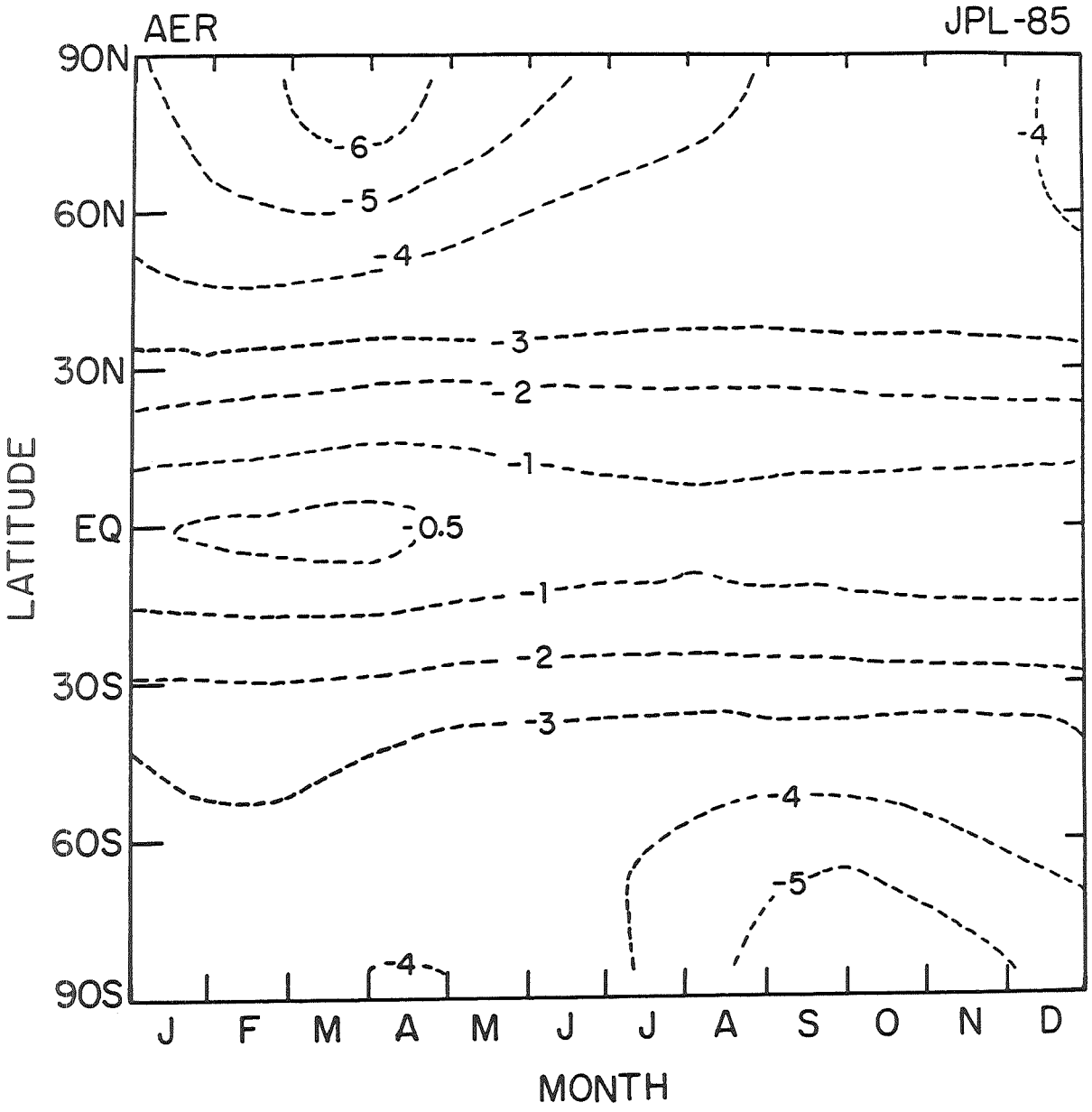

D-2a. Dobson map of ozone column changes (%) for the SS scenario from the AER model using JPL-85.

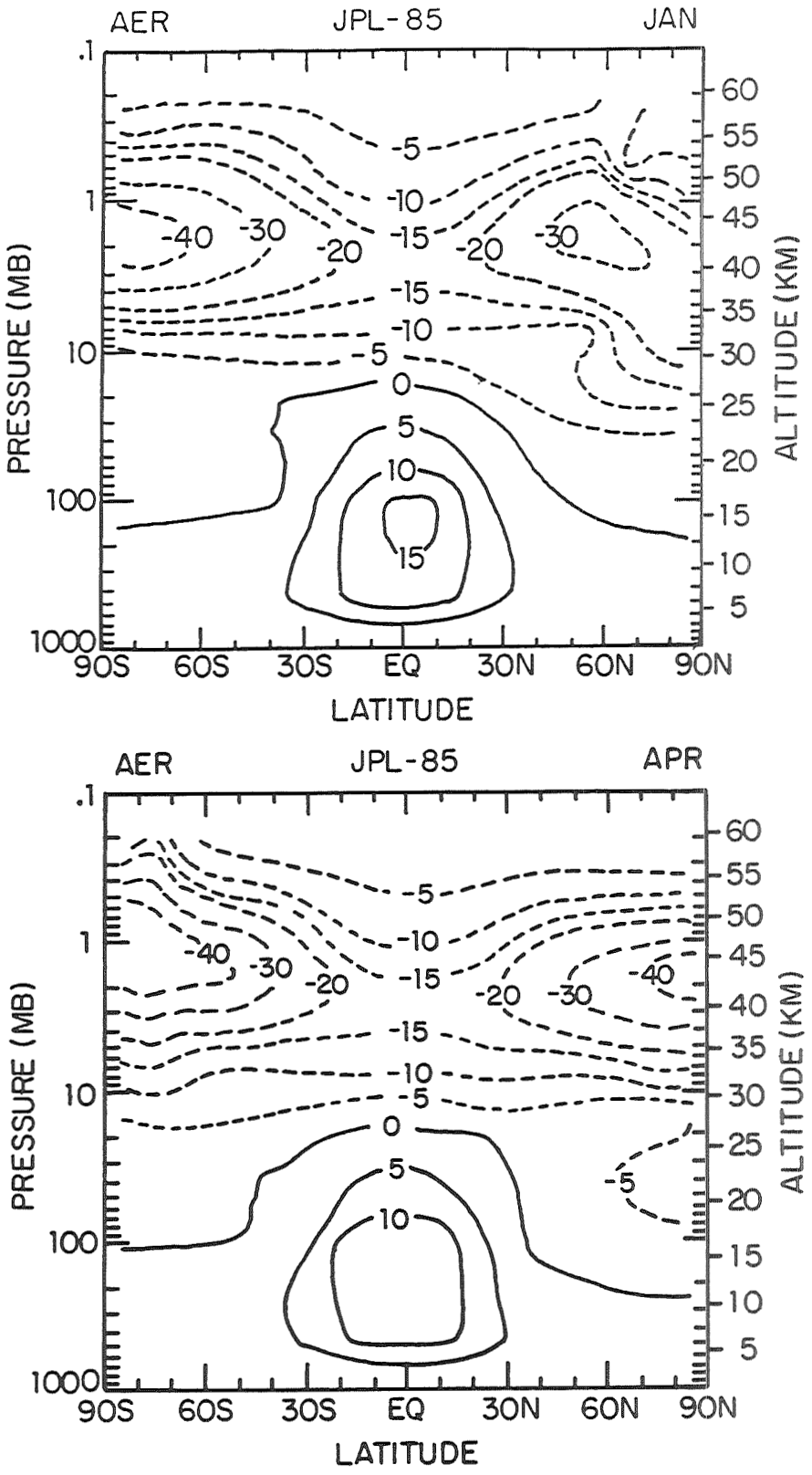

D-2b. Ozone profile changes (%) for the SS scenario from the AER model using JPL-85 for the months of January and April.

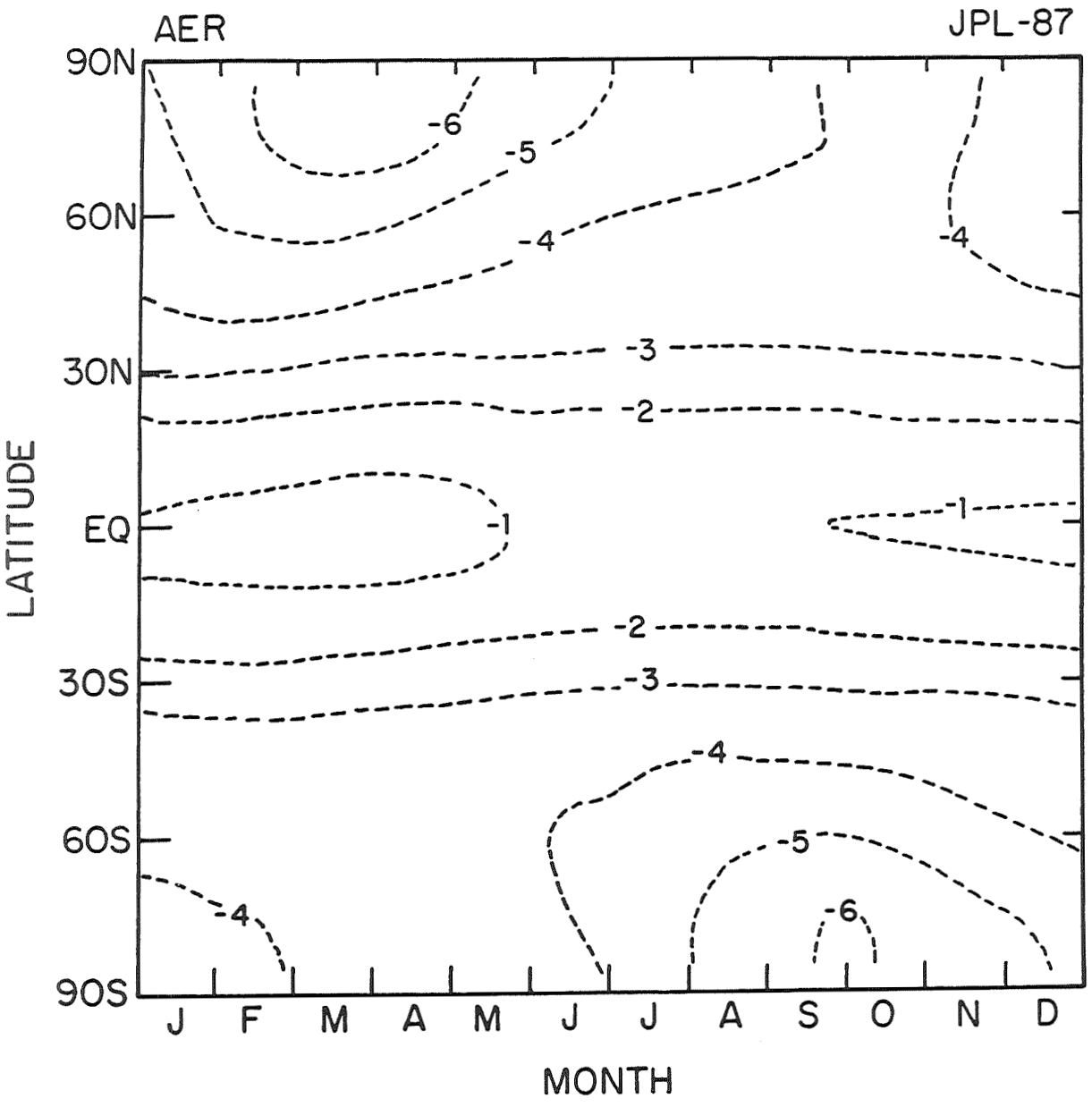

D-3a. Dobson map of ozone column changes (%) for the SS scenario from the AER model using JPL-87.

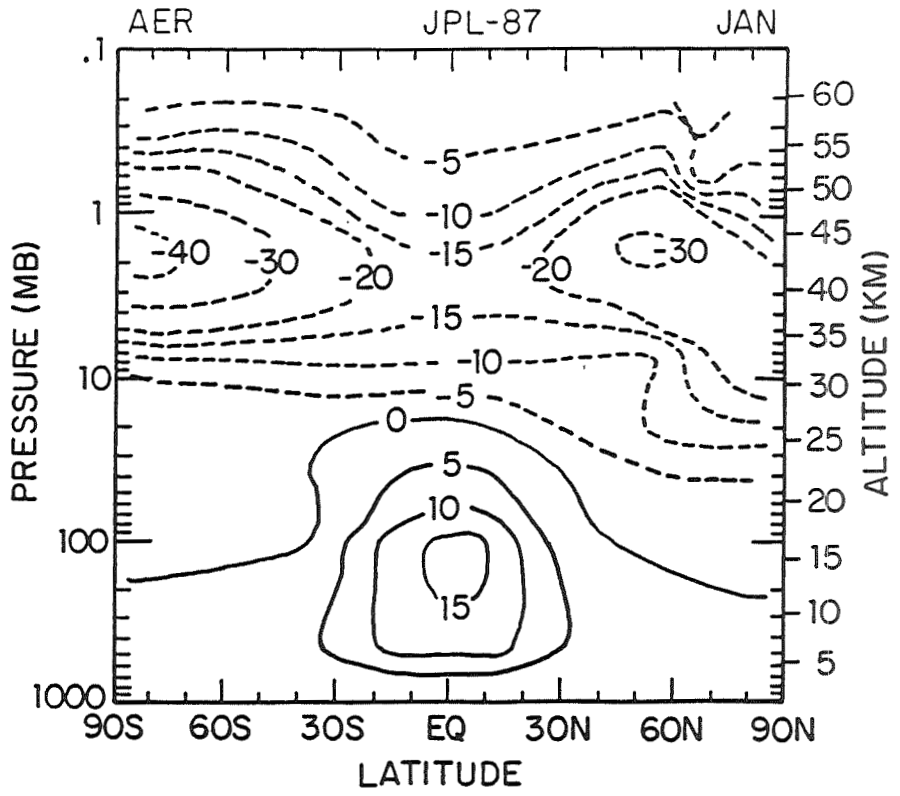

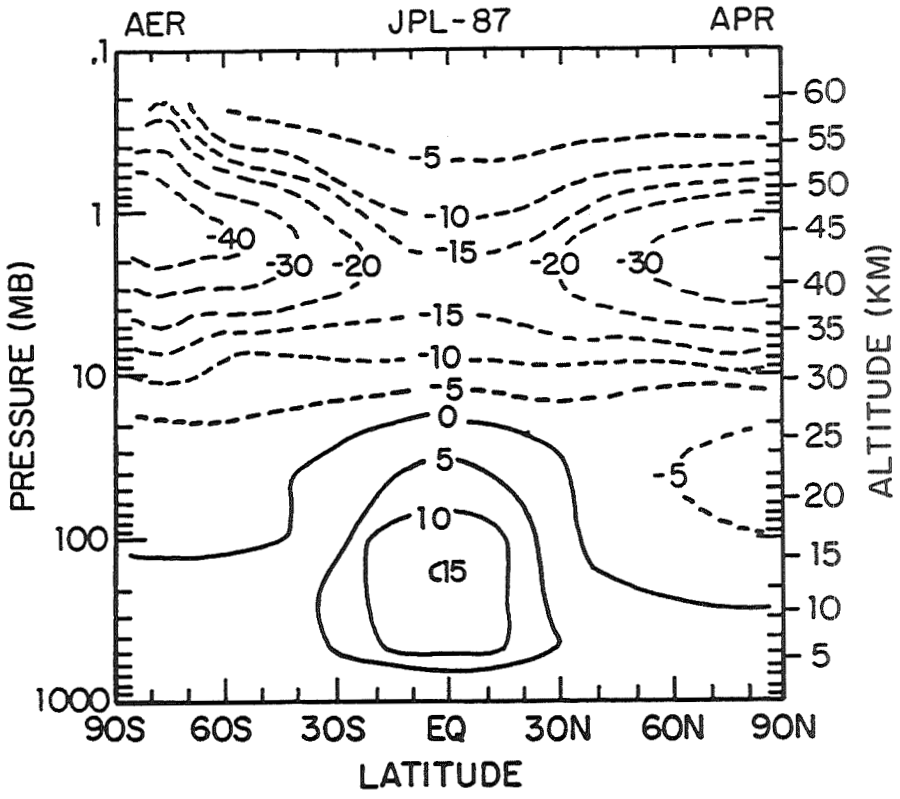

D-3b. Ozone profile changes (%) for the SS scenario from the AER model using JPL-87 for the months of January and April.

D.4. Steady-State Changes: 1980 vs. 20xx

The steady-state scenario (SS) in these assessments compares a contemporary atmosphere "1980" with a highly perturbed atmosphere that is expected sometime in the next century "20xx". In these simulations the models are integrated for a sufficient number of years with repeating, fixed boundary conditions until a steady state is achieved and the annual chemical cycle of the atmosphere repeats. The 2-D models contributing to this scenario are listed in Table D-3 with their salient characteristics. Results are presented first for what has been designated the "standard" 2-D models in which the stratospheric circulation and temperatures are seasonally and latitudinally varying, but do not respond to changes in ozone and CO_2. A second type of 2-D model uses predicted changes in ozone and CO_2 to recalculate stratospheric temperatures without deriving new transport parameters. Changes in temperature affect the chemical rates and feed back upon the ozone distribution. These models have been used in previous assessments (WMO, 1986) and this assessment focuses on results from these two types. Results from a third type of 2-D model are new to these assessments: one that uses ozone and CO_2 changes to derive perturbations to the stratospheric circulation which in turn feeds back on the predicted ozone. As discussed below, these full feedback models have been developed recently and we are just beginning to understand them and gain confidence in their predictions.

Standard 2-D Models with Fixed Temperature & Transport

These 2-D models have formed the basis of previous assessments. Most employ a residual circulation which is a combination of the direct motion of stratospheric winds and the net transport by eddies. In contrast the "Eulerian" models calculate transport from the zonal mean winds alone and require horizontal diffusion to account for eddy transport (e.g., the Cambridge model). For a more detailed description of 2-D models see Chapter 12 of the previous assessment (WMO, 1986). All of these circulations are based on the observed properties of the present stratosphere. These models have been developed and refined in terms of accurately simulating the chemical cycles in the stratosphere; they have been tested against available observations of stratospheric species; their results are published extensively.

The AER model results are shown in Figures D-2 for JPL-85 chemistry and Figures D-3 for JPL-87. Depletions of column ozone in the tropics are -0.5 to -1.5 % with little seasonal dependence. Poleward of 45 degrees, ozone decreases exceed -3 % in all seasons with changes greater than -5 % poleward of 60 degrees during spring. The percentage decreases in column ozone seem to scale with the total ozone (see Dobson map, Figure D-1b). The JPL-87 revisions have had little impact on the ozone perturbations associated with the SS scenario. Local concentrations of O_3 are depleted most near 40-45 km altitude: equatorial losses are about -15 to -20 %, whereas high latitude losses may exceed -40 %. A region of modest increase in ozone occurs predominantly in the troposphere and in the lower tropical stratosphere, in part due to increases in CH_4.

Results from the standard Oslo model are shown in Figures D-4. Global changes in column ozone are about -1 % in the tropics, but depletions increase rapidly with latitude, reaching -11 % in Arctic spring and -7 % in Antarctic spring. The pattern is similar to the AER model except that it shows much higher maximum depletions in the polar spring with a correspondingly sharper seasonal variation in loss at high latitudes. Ozone profiles show depletions in excess of -40 % outside of tropics in region 40-45 km altitude, and increases, mainly in the troposphere, restricted to below 22 km altitude in tropics and 16 km altitude elsewhere.

Table D-3

Descriptions of 2-D Models

MODEL	contributor	circulation	chemistry	scenario
GSFC	Guthrie	standard[o]	JPL-83	SS (Clx+CH_4+N_2O)
		feedback[1]	JPL-83	SS (Clx only)
LLNL	Wuebbles	feedback[2]	JPL-85	SS & TD (Clx+CH_4+N_2O)
AER	Ko	standard[o]	JPL-85	SS & TD (Clx+CH_4+N_2O)
			JPL-87	SS (Clx+CH_4+N_2O)
NCAR	Hitchman	feedback[3]	JPL-85	SS (non-standard)
NOCAR	Garcia	feedback[4]	JPL-87	SS (Clx+CH_4+N_2O+CO_2)
				SS (Clx only)
Oslo	Isaksen	standard[o]	JPL-85	SS (Clx+CH_4+N_2O)
		feedback[5]	JPL-85	SS & (Clx+CH_4+N_2O+CO_2) TD
Cambridge	Pyle	standard[6]	JPL-87	TD (Clx+CH_4+N_2O+CO_2)

[o] residual circulation assuming fixed transport (dQ=0) and temperature (dT=0).

[1] residual circulation with feedback: the closure equation used to calculate dQ assumes that the rate of change of the zonal momentum equation occurs evenly to both sides of the equation; eddy momentum forcing balances the other terms.

[2] residual circulation with feedback: assume dT=0; thus changes in the UV heating (via ozone) drive a circulation (dQ) to maintain temperature.

[3] residual circulation with feedback: calculate dQ and dT; fixed source of gravity and Rossby waves drive the circulation; waves interact with the zonal mean flow.

[4] residual circulation with feedback: calculate dQ and dT; fixed source of gravity waves drives the circulation; waves interact with the zonal mean flow.

[5] residual circulation with T feedback: circulation fixed (dQ=0); temperature changes (dT) calculated from Newtonian approximations for CO_2 cooling and O_3 heating.

[6] Eulerian circulation: eddy transports are fixed based on observed temperatures; T and winds respond to changes in heating.

a

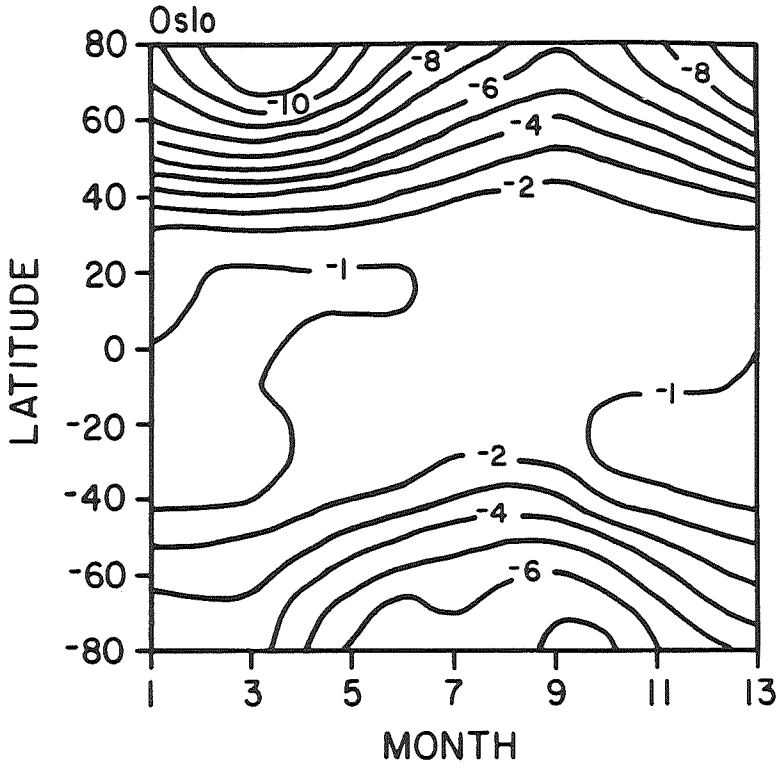

b

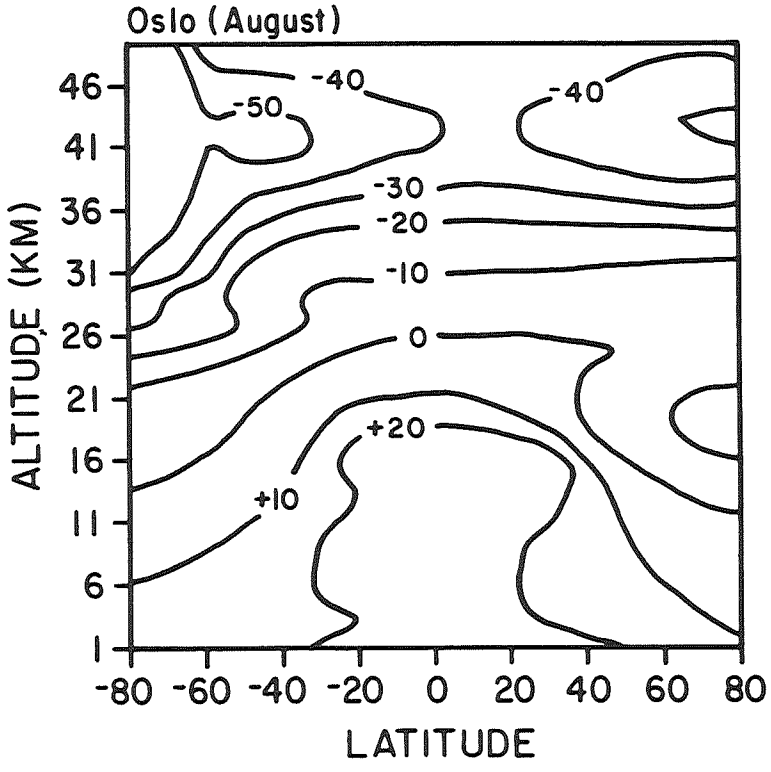

D-4a. Dobson map of ozone column changes (%) for the SS scenario from the Oslo model.

D-4b. Ozone profile changes (%) for the SS scenario from the Oslo model for the month of August.

Results from the standard GSFC model are shown in Figures D-5. The predicted depletions of column ozone are similar to the previous results in the tropics and mid-latitudes, increasing from -1 % near the equator to -3 % by 50 degrees. At high latitudes, however, the pattern is quite different from the other models, showing peak Arctic depletions of -7 % in the summer and a very noisy pattern in the Antarctic. Profile changes in the upper stratosphere are typical of other models, except in the Antarctic and in the lower stratosphere. These differences are consistent with the unusual pattern of column perturbations.

2-D Models with Temperature Feedbacks but Fixed Transport

The first efforts to account for non-chemical changes in the stratosphere due to ozone perturbations focussed on temperature. The decreases in O_3 near 45 km altitude that are predicted at high levels of chlorine would lead to a substantial reduction in the heating of the stratopause region by sunlight and should, therefore, reduce the temperature of that region. In parallel, increases in CO_2, while warming the lower atmosphere, lead to more efficient cooling of the stratosphere and, hence, to further temperature reductions. The impact of lowered temperatures throughout most of the stratosphere is to reduce the efficiency of chemical reactions that destroy ozone and, thus, to increase ozone concentrations part way back to their unperturbed values.

The Oslo model reported results for the SS scenario shown in Figures D-6 that included estimated temperature changes caused by both CO_2 and O_3 perturbations, but temperatures are not adjusted in the lower stratosphere and troposphere. When compared with their standard model as shown in Figures D-4, column depletions at high latitudes are reduced by almost a factor of two, changing from about -1 % to 0 % in the tropics year-round and about -7 % to -4 % at mid-latitudes during winter. Similarly, changes to the vertical profile of ozone are lessened, with maximum ozone changes about -30 %, instead of more than -40 % with the standard model.

The Cambridge model is essentially different from others reported here in that stratospheric transport is calculated in an Eulerian framework. Temperature and zonal mean winds are allowed to respond to alterations in the heating and cooling, but the eddy mixing is kept constant. The response of this model to ozone and CO_2 perturbations is thought to be similar to a residual circulation model in which the net transport is fixed, but further intercomparisons between models are needed to understand the feedbacks in the Cambridge, model. The Cambridge model has recently published (ref. 1) calculations for a steady- state scenario similar to SS predicting maximum depletions in column ozone at the equator and smaller losses at high latitudes. The gradient of column ozone depletions is opposite that of the assessment calculations described here and is believed to be caused mainly by the large drop in stratospheric temperatures below 25 km altitude, about -8°K, that was driven by the doubling of CO_2. If the temperature of the lower stratosphere were reduced by this much, then indeed the chemical response would lead to substantially increased ozone columns at high latitudes, as confirmed in separate calculations by the AER group (not shown). The real question raised by this paper is what magnitude of temperature change should be associated with large increases in CO_2. The most recent version of the Cambridge model has continued to develop the radiation scheme and now shows CO_2 sensitivities similar to their earlier work, predicting only modest declines in stratospheric temperatures with a doubling of CO_2, about -2°K below 25 km altitude. Their new results for the SS scenario were not available for this assessment, but are expected now to be similar to the other results described above. Trends in stratospheric temperature would have a significant influence on ozone, especially later in the 21st century when larger changes are expected.

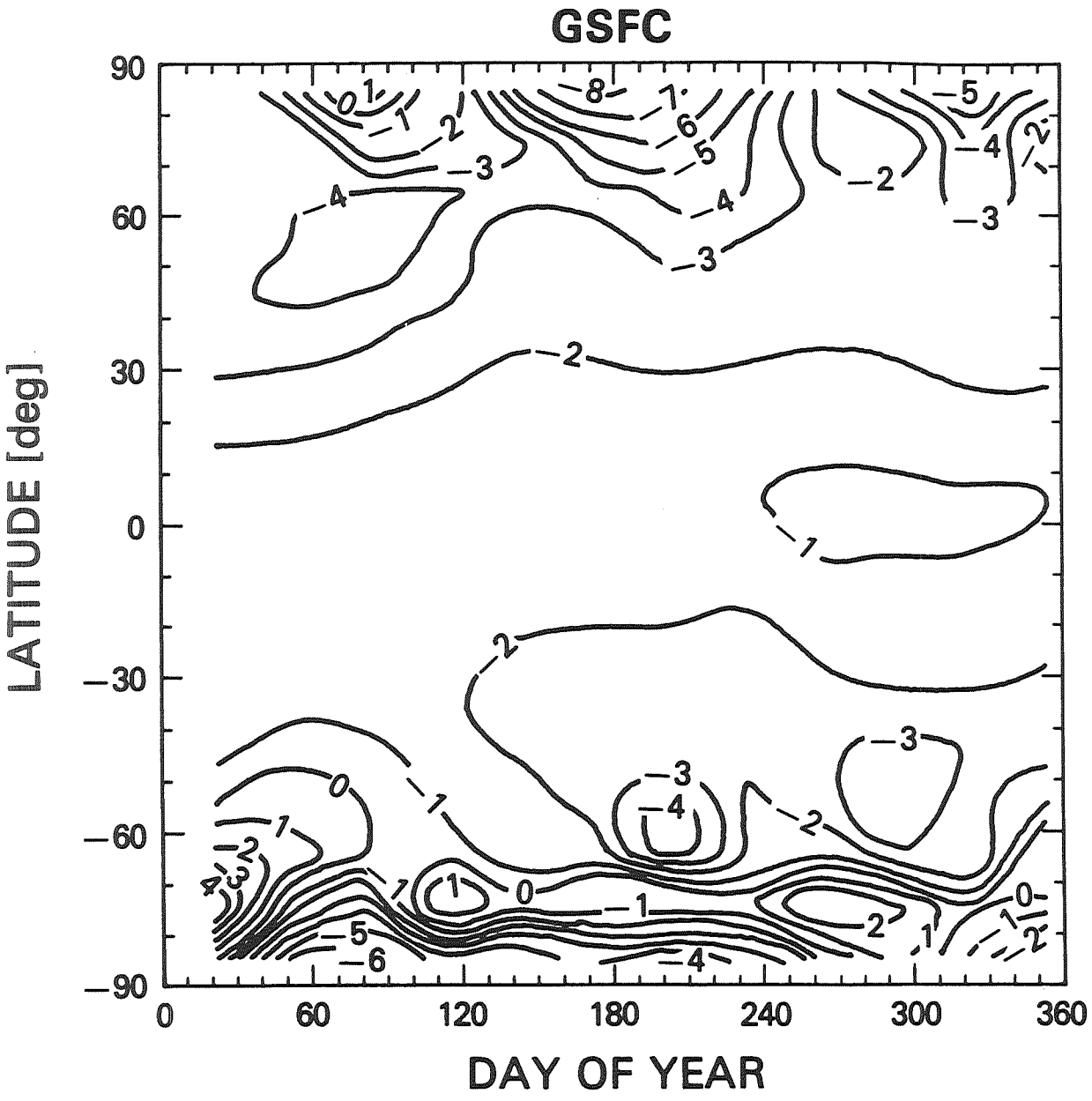

D-5a. Dobson map of ozone column changes (%) for the SS scenario from the GSFC standard model.

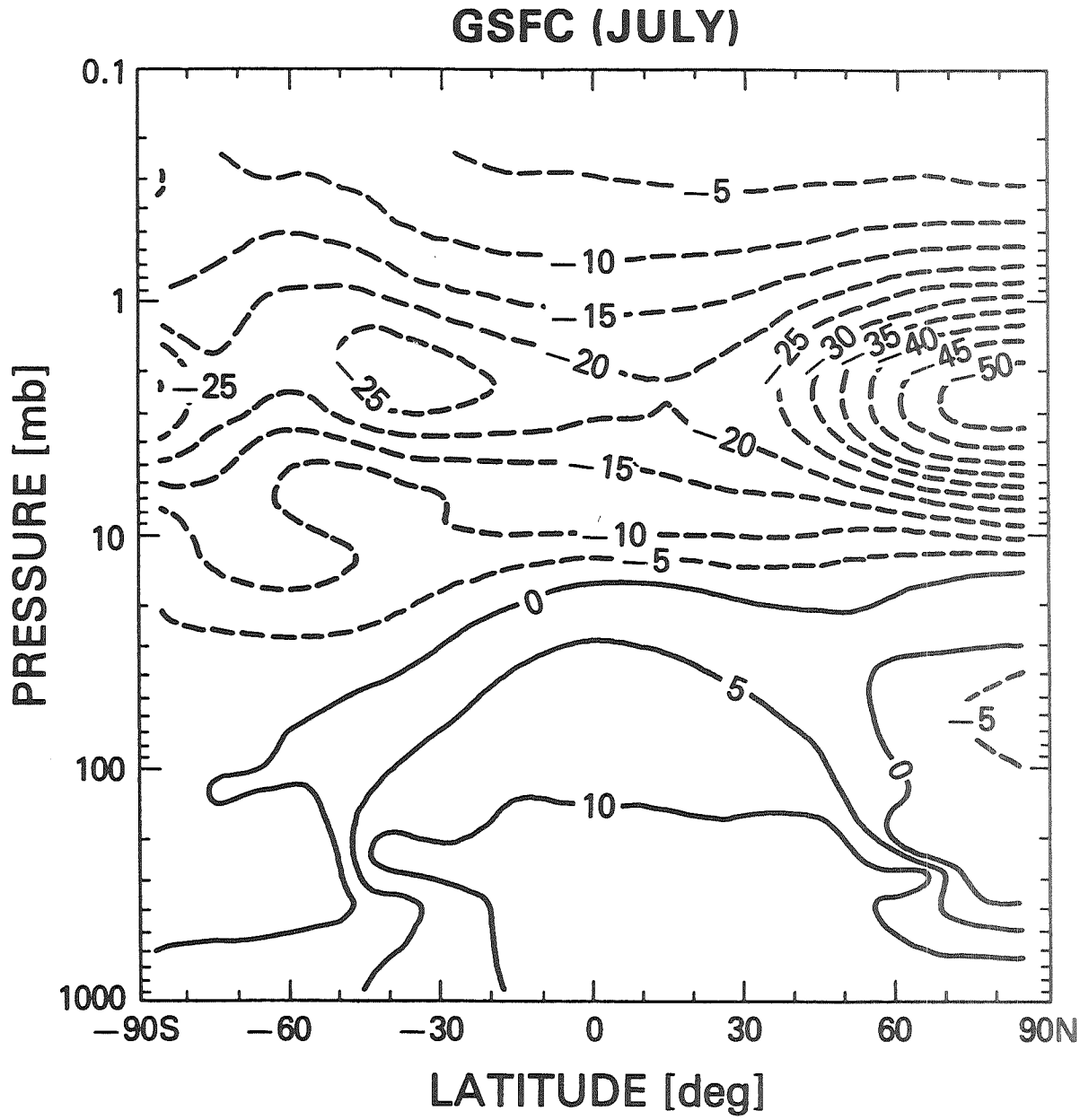

D-5b. Ozone profile changes (%) for the SS scenario from the GSFC standard model for the month of July.

a

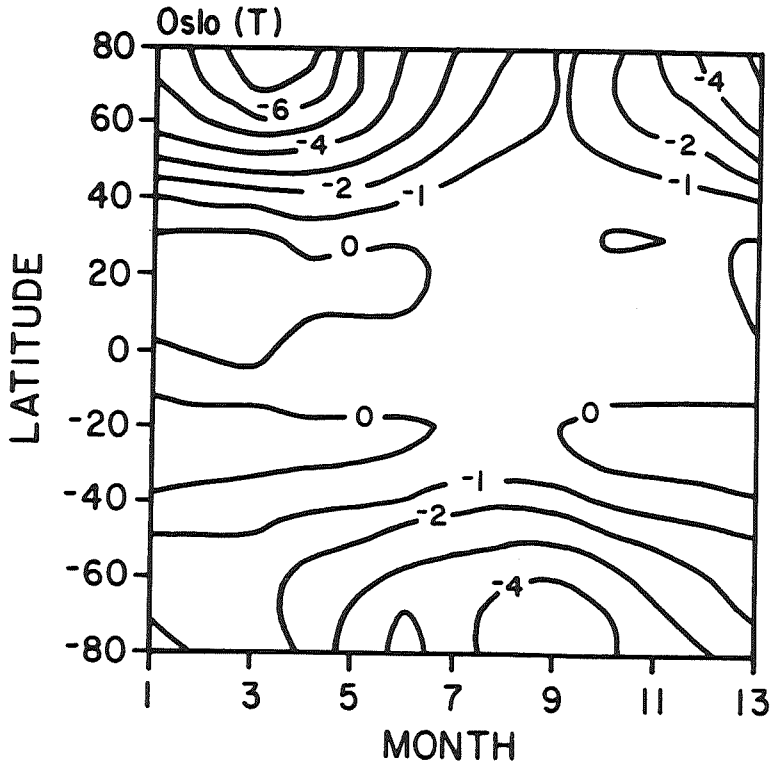

b

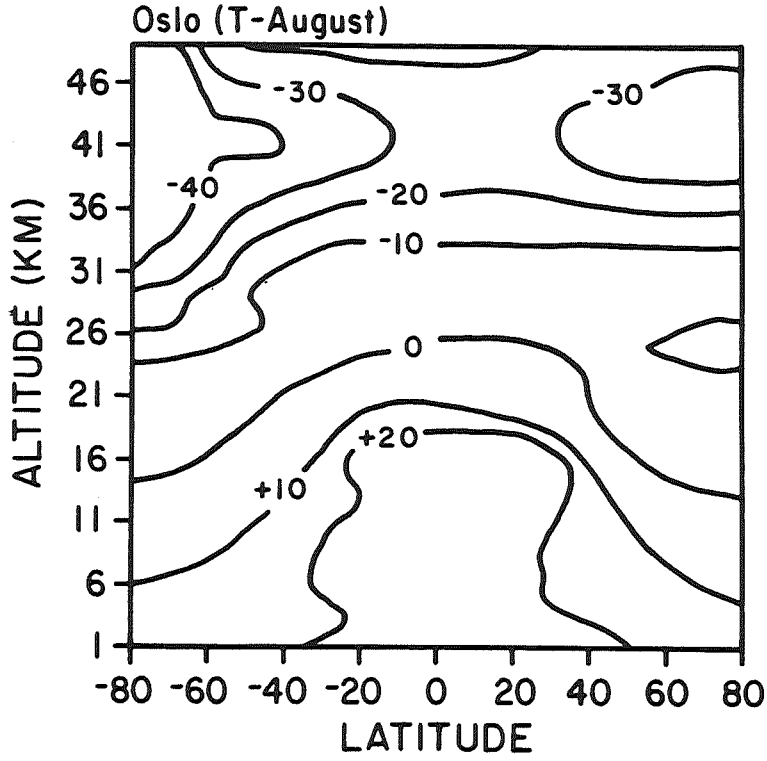

D-6a. Dobson map of ozone column changes (%) for the SS scenario from the Oslo model with T feedback.

D-6b. Ozone profile changes (%) for the SS scenario from the Oslo model with T feedback for the month of August.

2-D Models with Variable Stratospheric Circulation

The most ambitious research in these assessments involves a new class of 2-D chemical models: those that attempt to predict the impacts of O_3 and CO_2 perturbations on the stratospheric circulation and its feedback again on O_3. The new feedback mechanisms need to parameterize the forces that drive stratospheric transport in terms of stratospheric O_3 (heating) and CO_2 (cooling). Some of the model formulations make ad hoc assumptions about the response to a change in the net heating; others are based on parameterizations of 3-D physical processes believed to be responsible for driving the residual 2-D circulation. They are not completely evaluated, and the results must be regarded with significant uncertainty at the present time. Model validations and intercomparisons are planned to assess the different approaches.

The LLNL model (Figures D-7) assumes that as CO_2 and O_3 change the temperature will remain unchanged and thus the circulation must respond to maintain the initial temperature. Therefore this model shows none of the ameliorating effects on the ozone depletion due to reductions in stratopause temperatures. When compared to the standard models above, the LLNL model has larger depletions in the tropics, -2 % to -3 %, but similar peak losses at the end of polar winters, as large as -6 % (similar to Oslo), and large winter- to-summer difference at high latitudes. The ozone profiles show large losses in the region 40-45 km altitude ranging from -30 % in the tropics to -50 % at high latitudes, and small increases of order +5 % to +10 % in lower stratosphere and troposphere. In order to interpret which effects are associated with the circulation feedback, however, we must compare this calculation with a parallel simulation that holds the circulation fixed (currently in progress; not available for this assessment).

The GSFC model with feedback (Figures D-8) has reported results using JPL-83 kinetics that include only the high chlorine part of the "20xx" atmosphere in the SS scenario and not the other trace gases (CH_4, N_2O and CO_2). (Thus, it does not include the countering influence of CH_4 increases on chlorine increases between "1980" and "20xx".) Largest depletions of column ozone occur in the tropics, as large as -9 %, with smaller average depletions at mid- latitudes ranging from -3 % to -6 %. The seasonal pattern of ozone loss at high latitudes is quite different from other models with largest depletions occurring in mid-summer rather than early spring. The magnitude of ozone depletion in the tropics is consistent with earlier model calculations for a chlorine-only scenario (see AER results in Chapter 13, WMO, 1986). The much smaller decreases calculated at high latitudes may be due to compensating effects from changes in circulation or a reduction in stratospheric temperatures. As with the LLNL model, we are not yet able to assess the impacts of the circulation feedback at this time.

The NOCAR model has a lower boundary of 100 mbar, missing part of the lower stratosphere and all of the troposphere, and thus it cannot calculate total column ozone. Results from the NOCAR model are for profiles only and include two SS scenarios: one with chlorine increases only (Figure D-10), and the other with the full SS scenario including CO_2 (Figure D-9). The profile pattern in both cases is typical of the other models with largest decreases in the region 40-45 km altitude and at high latitudes. The Cl_x alone scenario predicts extremely high ozone losses at 45 km altitude for mid and high latitudes, exceeding -50 %. Including the other trace gases plus the decrease in stratopause temperatures greatly reduces this loss to about -30 %. The corresponding changes predicted in temperature are shown in Figure D-11. At the equinox, temperature decreases of -10°K at 45 km altitude are typical of the Cl_x alone scenario, while the complete SS scenario results in decreases of about -16°K. Ozone losses during March at the tropical

stratopause near 45 km altitude are -35 % for Clx alone and only -15 % for the full SS scenario including CO_2 and temperature feedback.

The NCAR model is a fully coupled model that includes the effects of doubling CO_2. The calculations contributed by the NCAR used a different steady-state scenario than specified for this assessment. In particular, the chlorine content of the stratosphere changed from 2.0 to 6.6 ppb instead of 2.5 to 8.2 ppb as in SS. We include some of their results with the warning that they may not be compared directly with the other calculations in this section. Perturbations to the ozone profiles for December are shown in Figure D-12. Substantial increases of order +10 % occur in the region 50-60 km altitude, are consistent with results from the NOCAR model, and may be caused by the reduction in temperature associated with CO_2. Results from the NCAR model also support the Cambridge and AER calculations in that the cooling of the stratosphere due to doubling of CO_2 alone should lead to an increase in column ozone: in the NCAR scenario for CO_2 only, by +1 % between 40°S and 40°N, but by as much as + 4 % poleward of 70 degrees.

Application of feedback mechanisms in the stratospheric models shown here demonstrates the current scientific diversity of this topic. Caution must be applied therefore when using any of these results in an assessment such as this. We must recognize, however, that the complete atmospheric response to changing composition must be incorporated in assessments if we are to progress to better, more realistic models of the future atmosphere. The intercomparison planned for 1988-89 should lead to a better understanding of the roles of circulation and temperature, as well as of ozone, in an evolving atmosphere.

D.5. Time Dependent Model Calculations: 1985-2015 and beyond

This assessment includes, for the first time, time-dependent two-dimensional model calculations of ozone changes predicted for the next 30 years. For the time-dependent scenario (TD) the 2-D models explicitly integrate over each year using fluxes or tropospheric concentrations of the source gases (CFCs, N_2O, CH_4, CO_2, and other halocarbons) prescribed for each year from Table D-1. Some of the contributed calculations continued the TD scenario beyond 2015. Extrapolation of current growth rates for CH_4 and N_2O are questionable, even to 2015, since we are at present uncertain as to the exact causes of their increases. Nevertheless, continuation of the simple assumptions for atmospheric change in Table D-1 are probably a reasonable estimate of future composition until we are able to prepare more detailed and accurate models for atmospheric composition.

Dobson maps from three models, showing the percent change in column ozone as a function of latitude and season for the intervals 1985-2000 and 1985-2015, are shown in Figures D-13 (AER), D-14 (Oslo) and D-15 (LLNL). From 1985 to 2000, both LLNL and Oslo models predict small decreases in column ozone, less than -1 %, over most of the globe, but with larger decreases at high latitudes during late winter and early spring. By the year 2015, decreases greater than -1 % are apparent over most of the globe, and the high latitudes during early spring are expected to see ozone losses of -2 to -3 %. The AER model shows similar patterns with latitude and season for column ozone, but without such large depletions at the high latitudes in early spring. The LLNL and Oslo models show a large winter-to-summer range in depletion at high northern latitudes, perhaps indicative of a summer recovery in the column ozone.

Perturbations to ozone profiles for the intervals 1985-2000 and 1985-2015 are shown in Figures D-16 (AER) and D-17 (Oslo). Both models show substantial decreases, as large

as -10 % by the year 2000 in the region 40-45 km altitude outside of tropical latitudes. These decreases in ozone concentrations are as large as -20 % by 2015 in the Oslo model and -15 % in the AER results. Increases in ozone occur only in the troposphere and sometimes the lower stratosphere. Changes to the ozone profile for the interval 1985-2040 from the Cambridge model are shown in Figure D-18. Decreases in the region 40-45 km altitude are large, as much as -30 %, but by 2040 in this model increases occur throughout the stratosphere below 25 km altitude and are responsible for the net increase in global ozone discussed below.

A time-line of the percent change calculated for total ozone since 1985 is shown in Figures D-19 (LLNL), D-20 (AER) and D-21 (Cambridge). The change in globally averaged column ozone from 1985 to 2015 is more than -2 % for the AER simulation, about -1 % for the LLNL model (with smaller values from the corresponding 1-D model), only -0.7 % for the Oslo model (not shown), and less than -0.5 % for the Cambridge calculations. These depletions refer to global averages; losses are greater at mid and high latitudes (see Figure D-20).

In all of the models most of this decline in column ozone takes place during the first 15 years; in the later years, the increases in CH_4, as well as the reduced rate of increases in CFCs (with the fluxes held fixed as of 1985, the growth in concentration slows as they approach steady state), result in continued ozone decline in the AER and LLNL calculations, but at a slower rate. The Cambridge model predicts a reversal with increases in global ozone after 2010, which may represent a more sensitive model response to the increases in CH_4 and CO_2.

For these time-dependent calculations the AER and LLNL results did not include the effects of reduced stratospheric temperatures due to increases in CO_2 over this period, whereas the Oslo and Cambridge models did. On the basis of the steady-state calculations described above, one might expect that colder stratospheric temperatures (caused by reductions in O_3 and increases in CO_2) would reduce the chemical destruction of ozone and ameliorate the predicted depletions, particularly at high latitudes. This effect might explain partly why the ozone depletions from the Cambridge model reverse sign by the middle of the next century.

The balance of perturbing influences on column ozone will depend on the relative growth in atmospheric abundances of CO_2, CH_4 as well as CFC. Future assessments need realistic scenarios.

Overall, perturbations to column and profile ozone in these time-dependent calculations have similar patterns to those presented for the steady-state scenarios in section D.4. The changes in column ozone predicted by the year 2015 for this scenario are modest and may be masked by natural geophysical variability or by solar cycle effects (see Chapter 7, Ozone Trends Report), with the notable exception of high latitudes in early spring where depletions as large as -3 % are predicted. The vertical distribution of ozone during this period shows a clear signature of the elevated levels of chlorine with substantial reductions near the stratopause as large as -20 % at high latitudes.

D.6. Model Intercomparisons

The Upper Atmosphere Research Program of NASA is coordinating a major intercomparison of stratospheric models during 1988. The goal of this and previous intercomparisons has been an improved understanding of stratospheric chemistry and dynamics. The most recent intercomparisons sponsored by NASA and other agencies occurred in the preparation of Chapter 12 (NASA/WMO 1986) and in the 2-D workshop

chaired by Paul Guthrie in January 1987. The focus continues to be on 2-D models, which currently represent the best capability for assessing stratospheric change. Some of the numerical experiments in the intercomparison can be performed with 3-D models, and contributions are welcomed. Participating groups will be expected to contribute to the following topics and will be assigned one or more of the tasks to review for the intercomparison.

Part 1, Photochemistry & Radiation, will examine the fundamental calculations of photolysis rates and radiative heating and cooling for a prescribed atmospheric structure (i.e., temperature) and ozone. A special emphasis will be placed on the calculation of cooling rates for a doubling of CO_2. Part 2, Transport, will study differences in the 2-D and 3-D models in so far as they transport trace gases through the stratosphere. An analytic form of the wind fields and diffusion tensor will be specified, as well as a hypothetical trace gas with an analytically specified chemistry. Three different types of trace gases will be proxies for a tropospheric source gas, ozone transport into the lower stratosphere and troposphere, and the rate at which a tropospheric release reaches the upper stratosphere. Differences among models will result from grid resolution, numerical methods and approximations. Part 3, The Current Atmosphere, is a straight comparison of the "1980" atmosphere from this assessment with observations. It will include a detailed analysis of the problem of predicting O_3 at 40 km altitude, a comparison of calculated and observed Dobson maps, densities and ratios of short-lived species such as NO/NO_2 and OH/HO_2, lifetimes of N_2O and CFCs, the budget of stratospheric NO_y, and aerosol chemistry in the Antarctic. Part 4, The Assessment Runs, will examine the differences in the steady-state perturbation of this assessment: "1980" → "20xx". In studying this ozone perturbation we will focus on both the standard models and the feedback models. The impact of changes in temperature will be determined separately from changes in the stratospheric circulation.

D.7. Summary: Global Ozone versus the Antarctic Ozone Hole

This current assessment of ozone changes predicted for the future is not significantly different from the previous assessment (WMO, 1986). Changes in the chemical models and atmospheric models have not altered the basic results: the expected decline in ozone should be moderate over the tropics and largest at high latitudes during late winter and early spring (coinciding with the seasonal maximum in ozone column). The time-dependent and steady-state scenarios show the same patterns. The large depletions in ozone near 40 km are a consistent result across all the models.

There are still large differences among the models when feedback mechanisms operating on the circulation and temperature of the stratosphere are included. Two issues represent major uncertainties in our predictions and are currently important research topics with regard to modeling the stratosphere: (1) how the stratosphere will respond dynamically to ozone perturbations, (2) the evolution and global impact of the Antarctic ozone hole, and (3) the effects of polar stratospheric clouds and heterogeneous chemistry in the Arctic winter.

The application of 2-D models in predicting ozone perturbations is now standard. This assessment demonstrates the importance of predicting the patterns of global ozone change as a function of latitude and season. The models used most often in assessment studies are those with fixed circulations. Several of the models shown here have included some feedback of the ozone change on the transport of trace gases; however, predicting changes in stratospheric circulation is still a research topic. Support for model development in the Upper Atmosphere Theory and Data Program is directed towards 2-D models with

feedback mechanisms and towards 3-D models with coupling to both the chemistry and climate.

Since the current assessment models do not adequately simulate the chemistry believed to be responsible for the Antarctic ozone hole, they cannot answer the critical questions: Is the Antarctic ozone hole going to spread over the Southern Hemisphere? Over the globe? Will the unusual chemistry of the Antarctic hole appear in the Arctic? If the answer is even a partial "yes", then our current assessments as reported in this document are inadequate. On the other hand, if the Antarctic ozone hole is restricted to the region where dense stratospheric clouds form, then the global ramifications may be modest and these predictions should represent global ozone (not including Antarctica).

The Upper Atmosphere Research Program of NASA is currently supporting several independent efforts to model the recent behavior of the Antarctic ozone hole and, in particular, to study the impact of the hole on the southern mid-latitudes as it disperses in the late spring. This continued research and development involves models, laboratory kinetics and field measurements. We are thus preparing for assessments following this one to be able to include predictions of the future behavior of the Antarctic ozone hole and its possible global ramifications.

D.8 Reference

(1) Eckman, Haigh & Pyle, Nature, 329, pp.615-619, 1987. See case E.

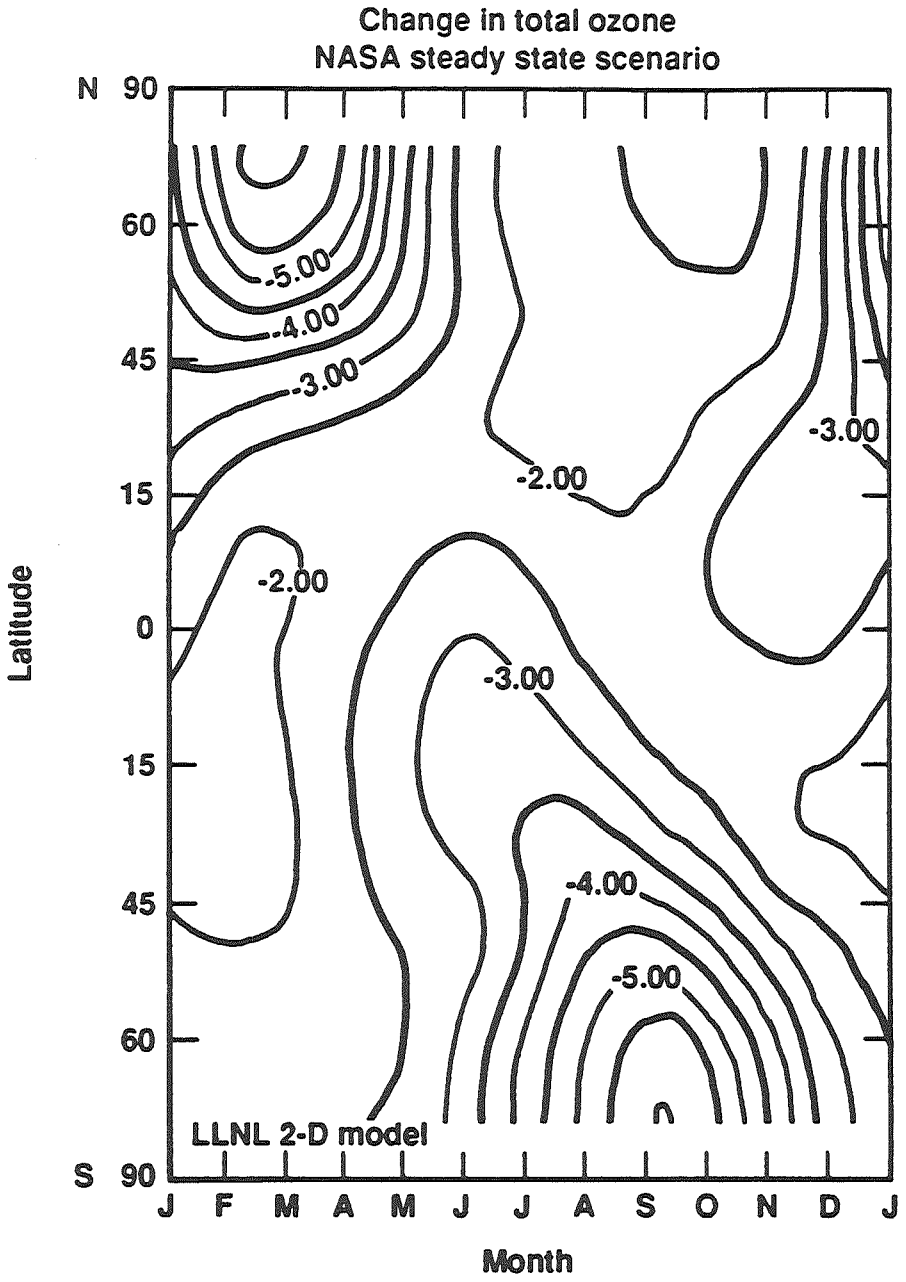

D-7a. Dobson map of ozone column changes (%) for the SS scenario from the LLNL model.

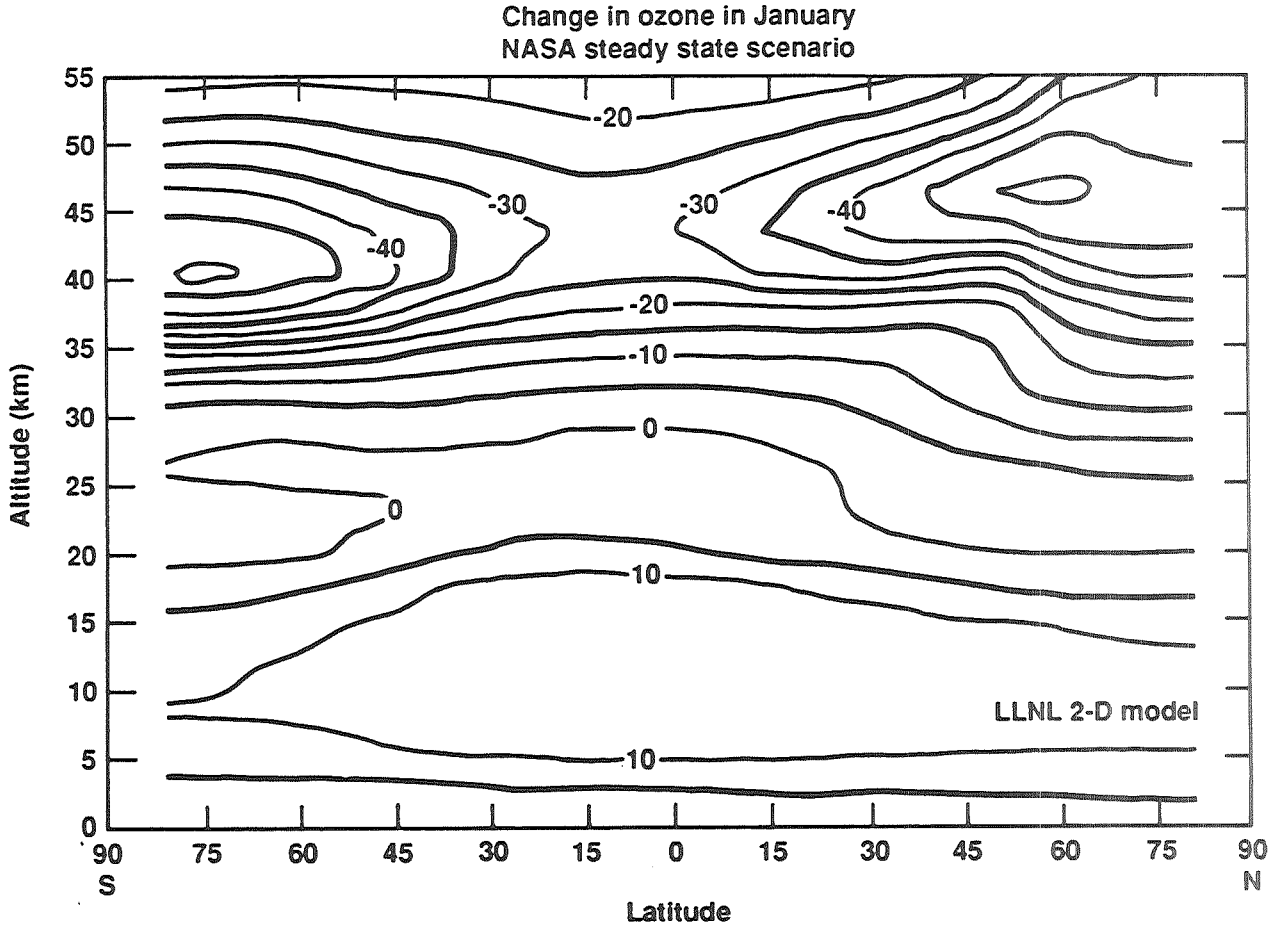

D-7b. Ozone profile changes (%) for the SS scenario from the LLNL model for the month of January.

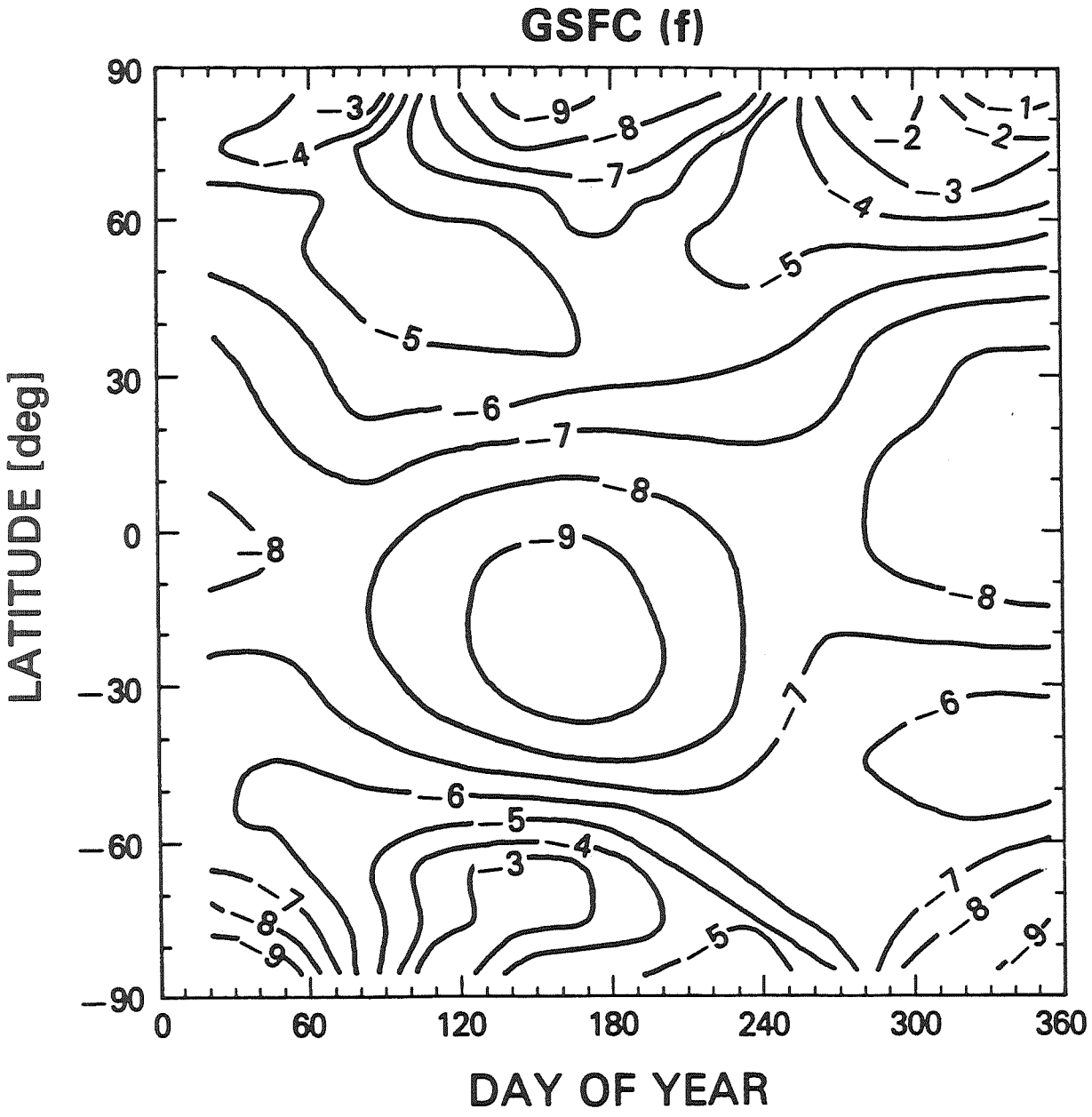

Figure D-8a. Dobson map of ozone column changes (%) for the high-chlorine only scenario from the GSFC model with feedback.

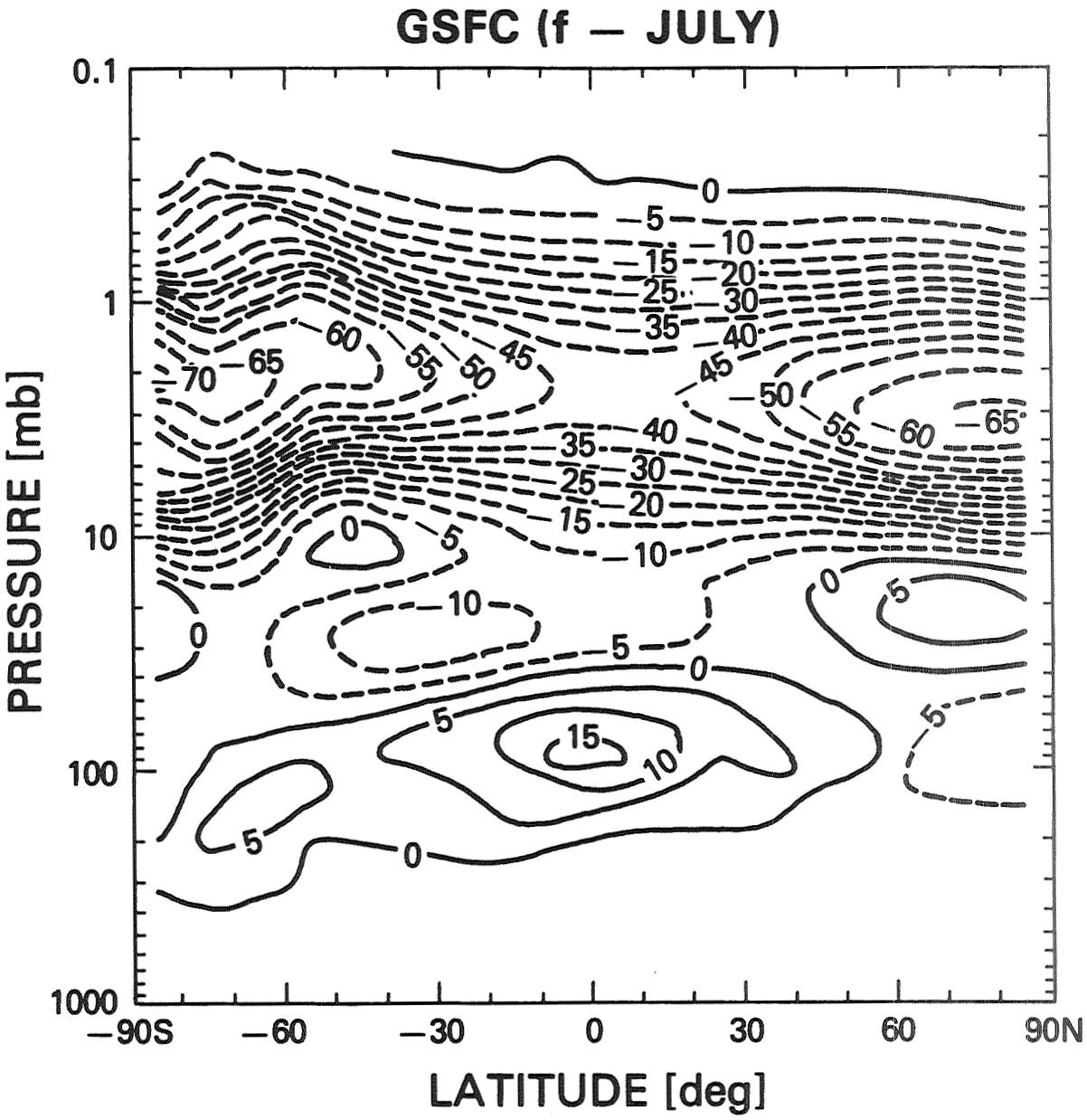

D-8b. Ozone profile changes (%) for the high-chlorine only scenario from the GSFC model with feedback for the month of July.

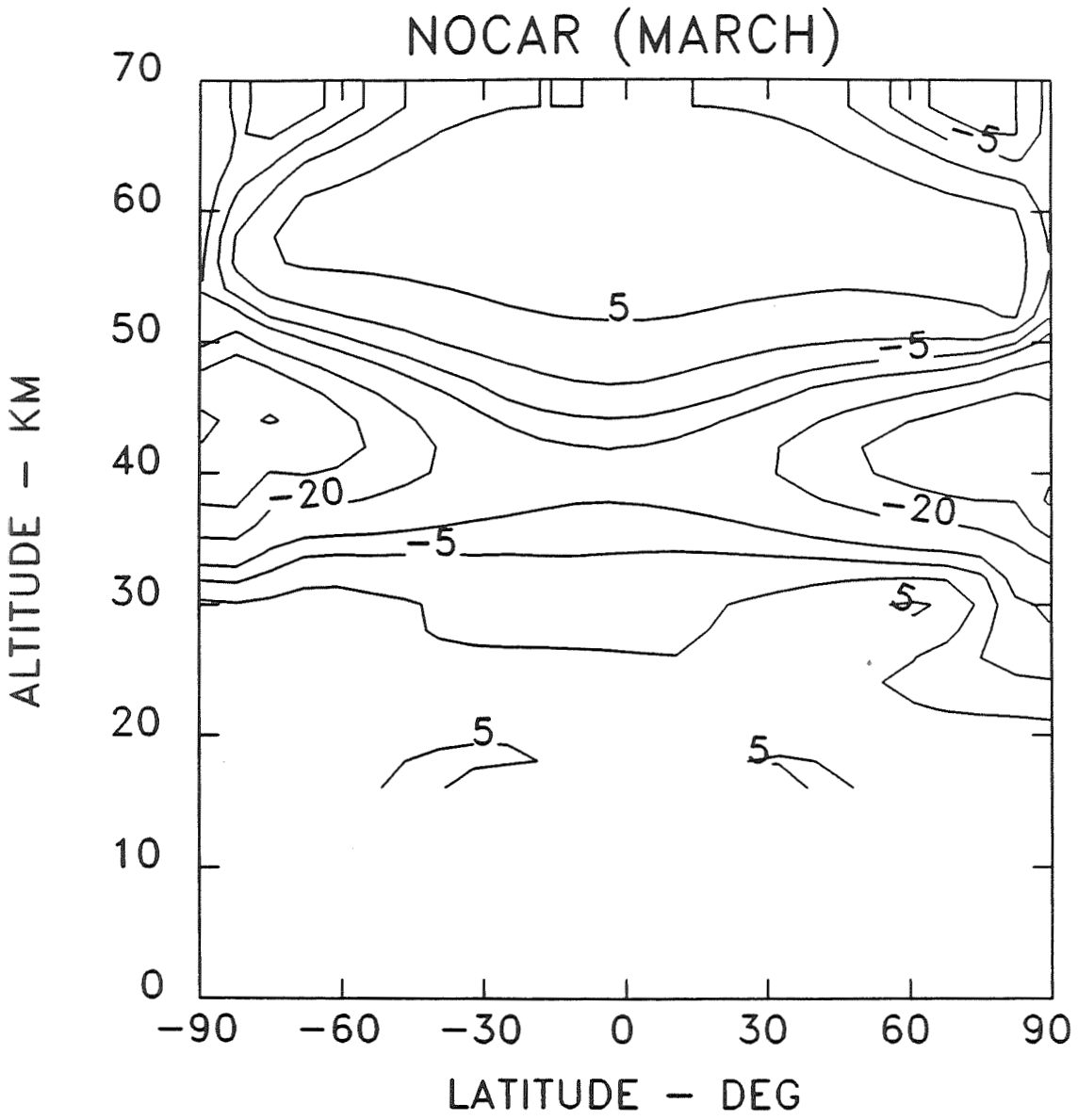

D-9 (1). Ozone profile changes (%) for the SS scenario from the NOCAR model for the month of March.

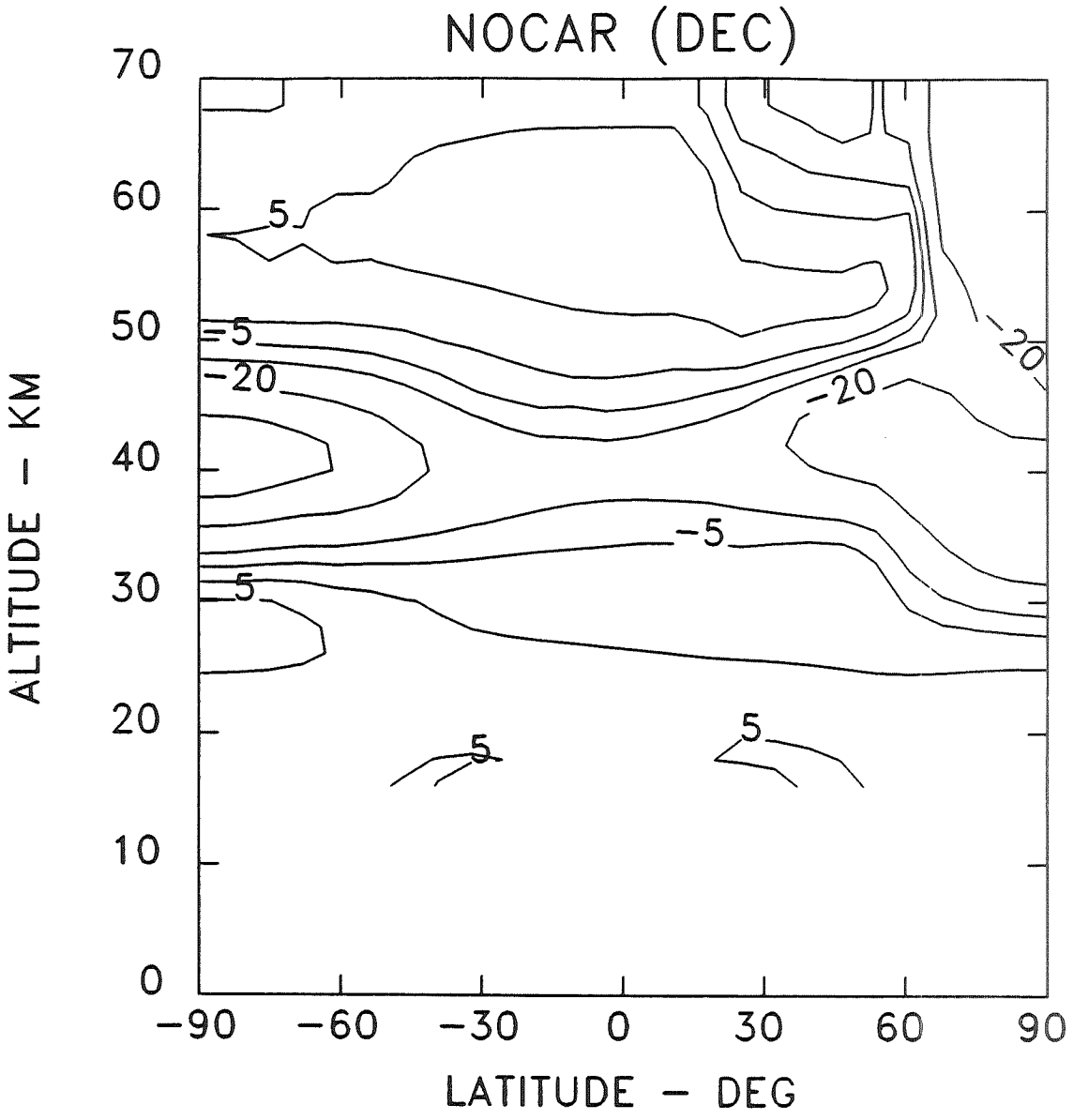

D-9 (2). Ozone profile changes (%) for the SS scenario from the NOCAR model for the month of December.

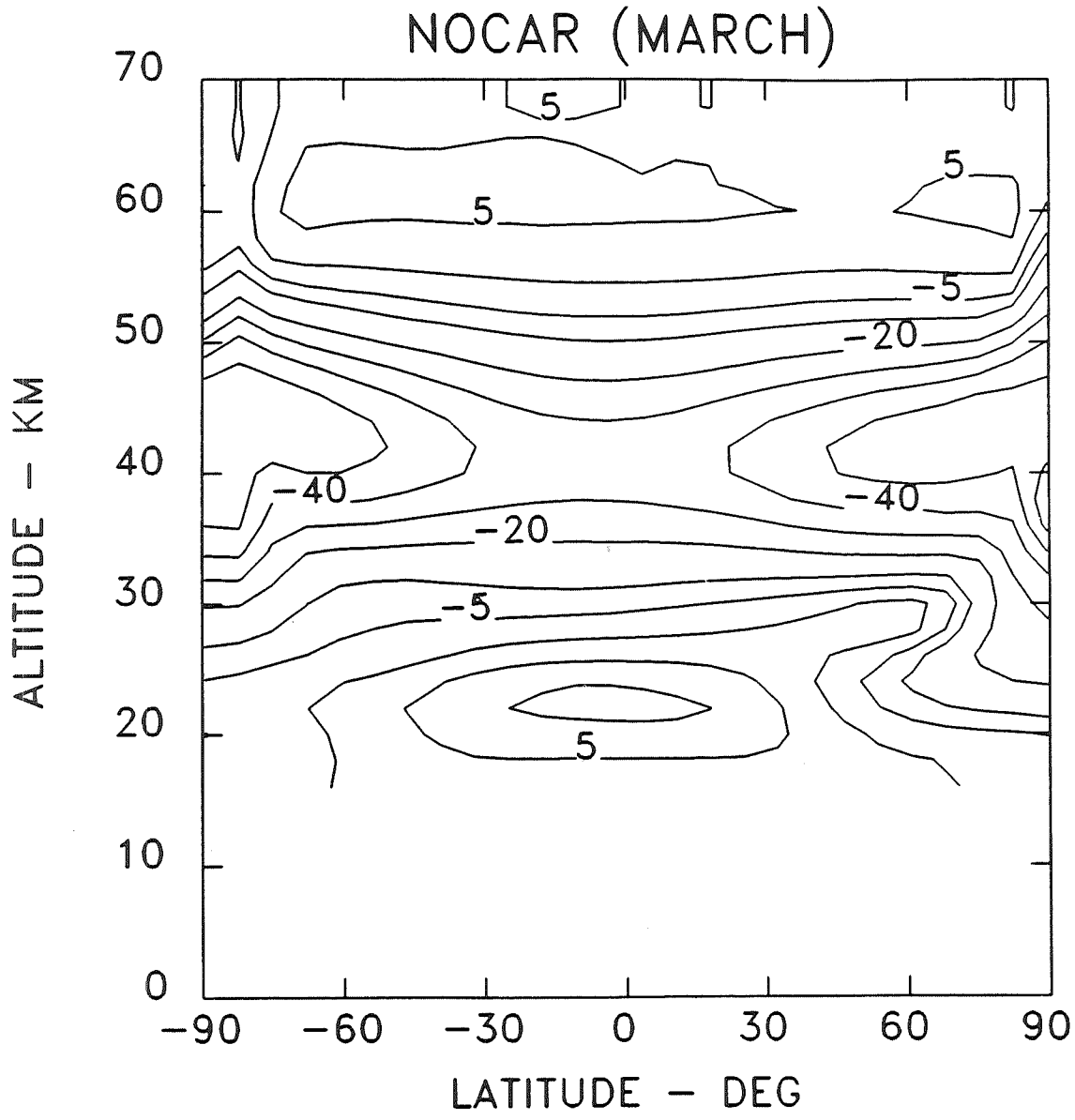

D-10 (1). Ozone profile changes (%) for the high-chlorine only scenario from the NOCAR model for the month of March.

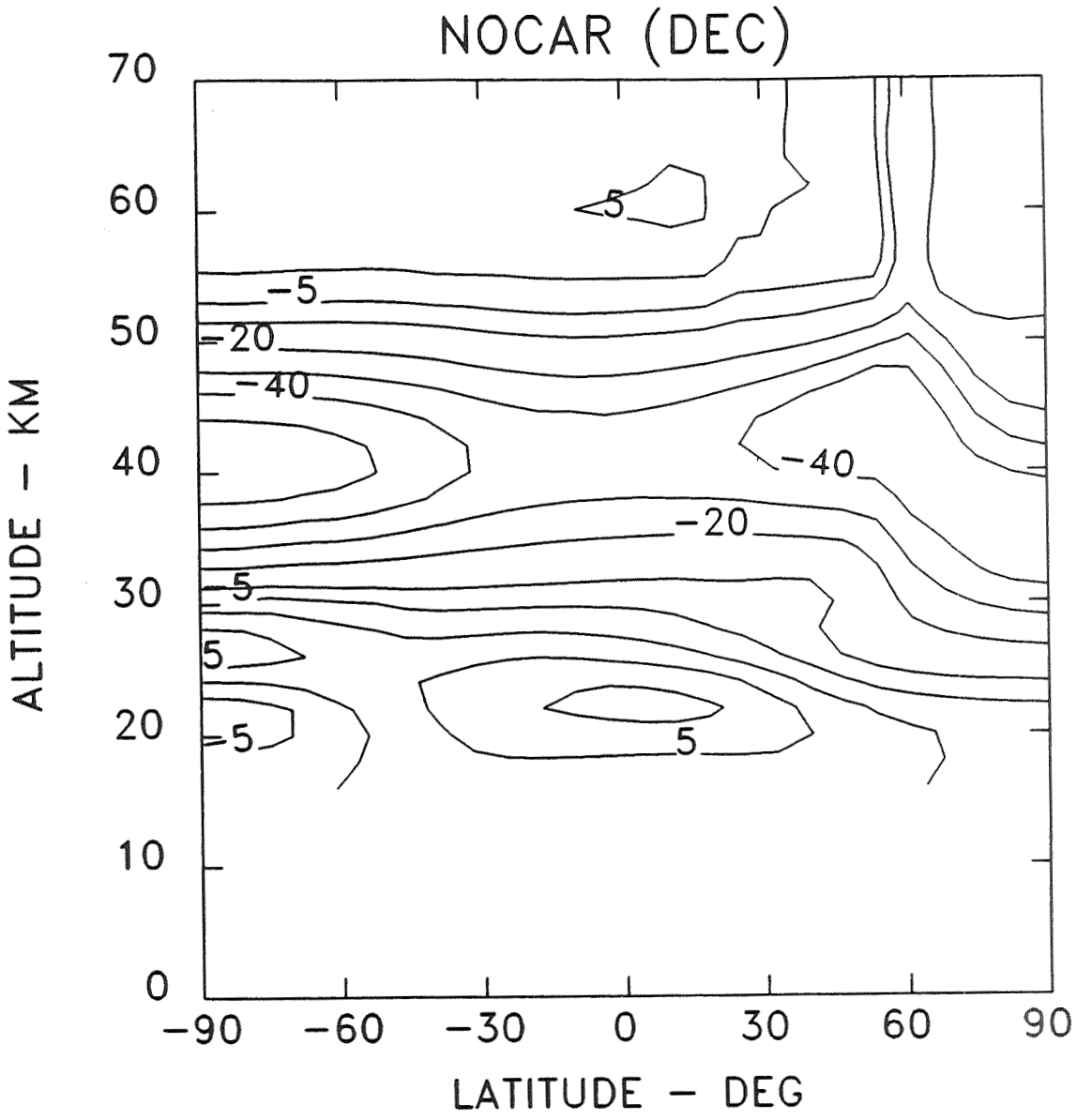

D-10 (2). Ozone profile changes (%) for the high-chlorine only scenario from the NOCAR model for the month of December.

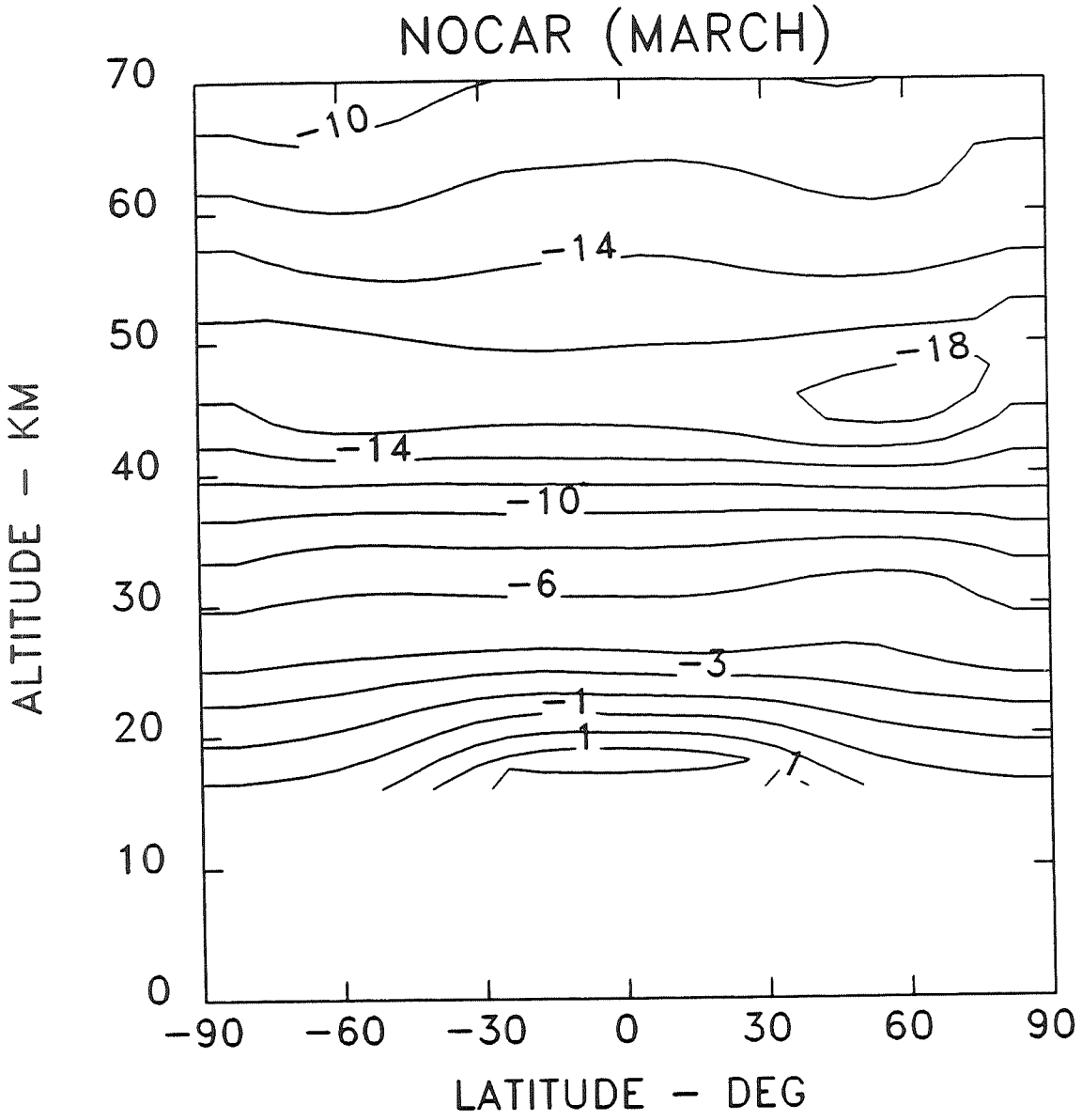

D-11a. Temperature changes for the SS scenario from the NOCAR model for the month of March.

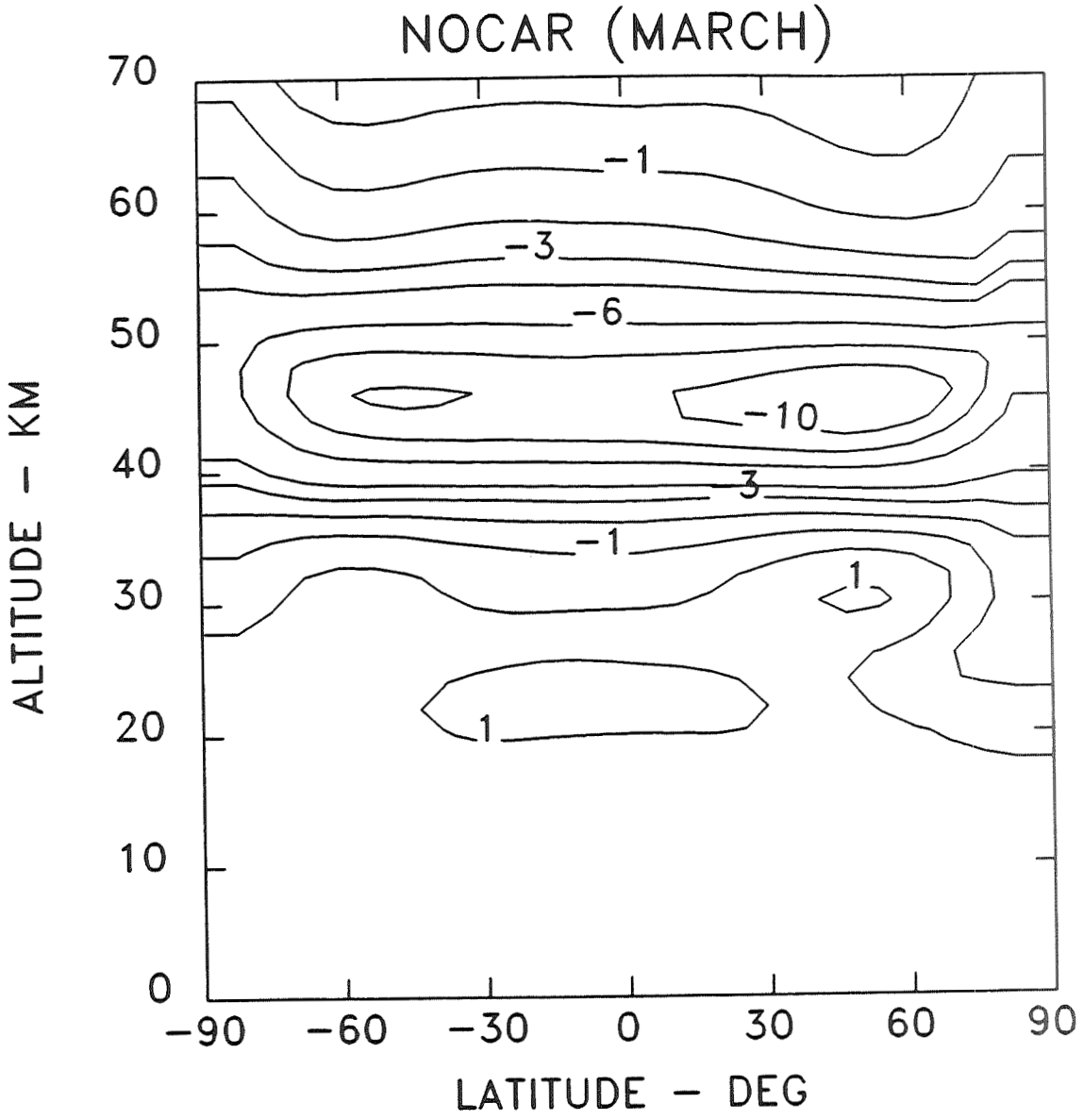

D-11b. Temperature changes for the high-chlorine only scenario from the NOCAR model for the month of March.

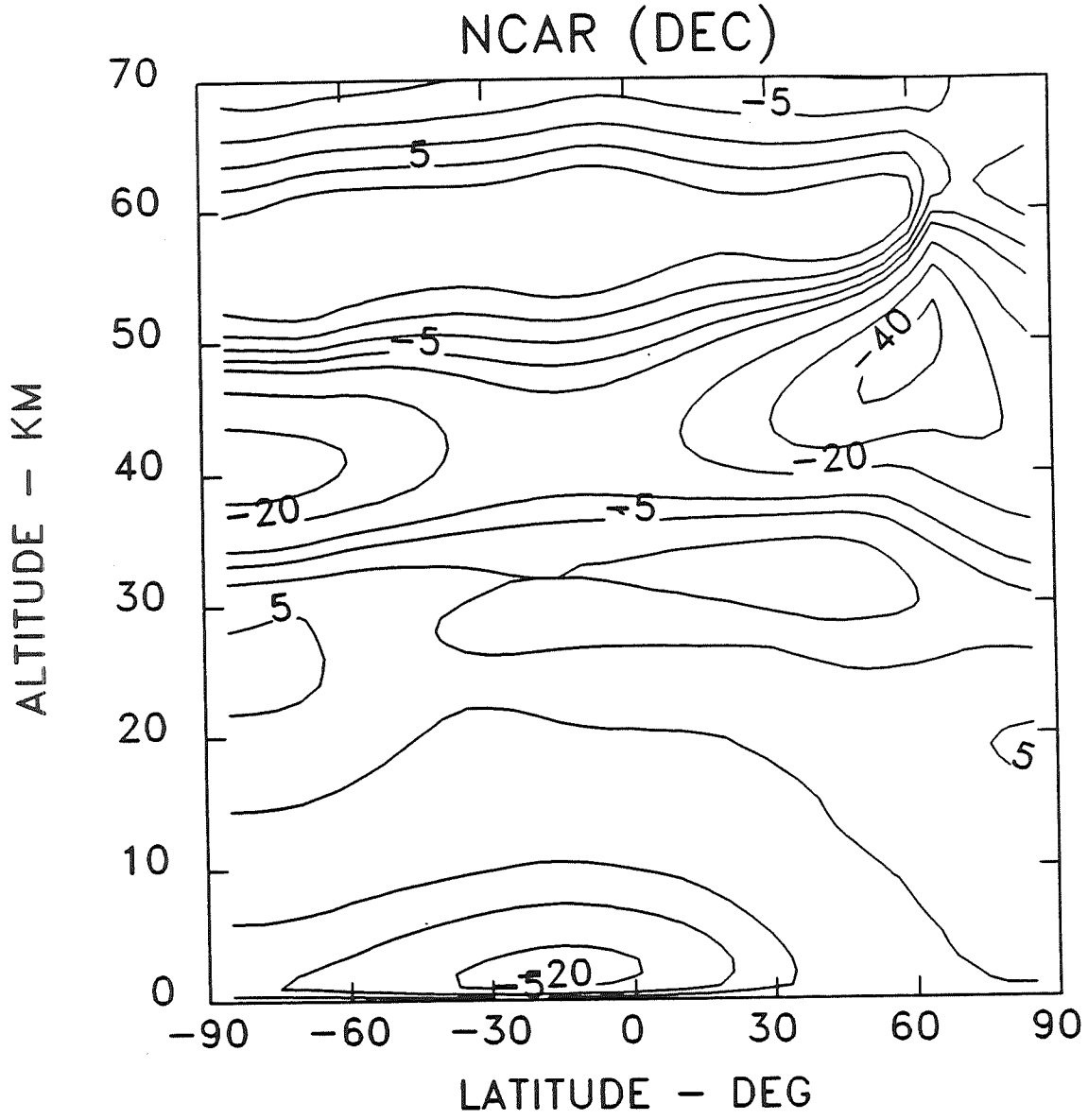

D-12. Ozone profile changes (%) for a non-standard steady-state scenario from the NCAR model for the month of December.

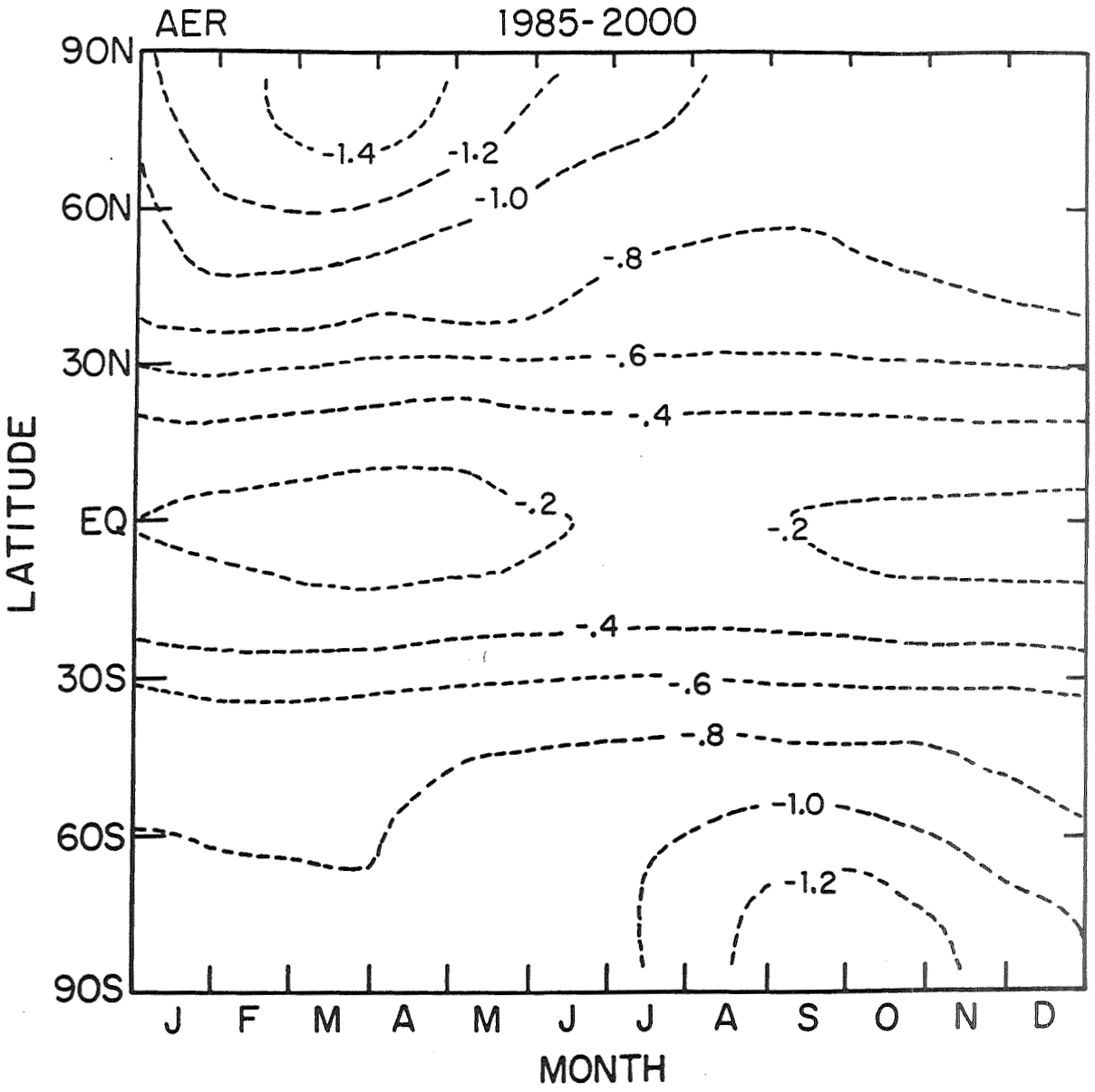

D-13 (1). Dobson map of ozone column changes (%) for the TD scenario 1985-2000 from the AER model.

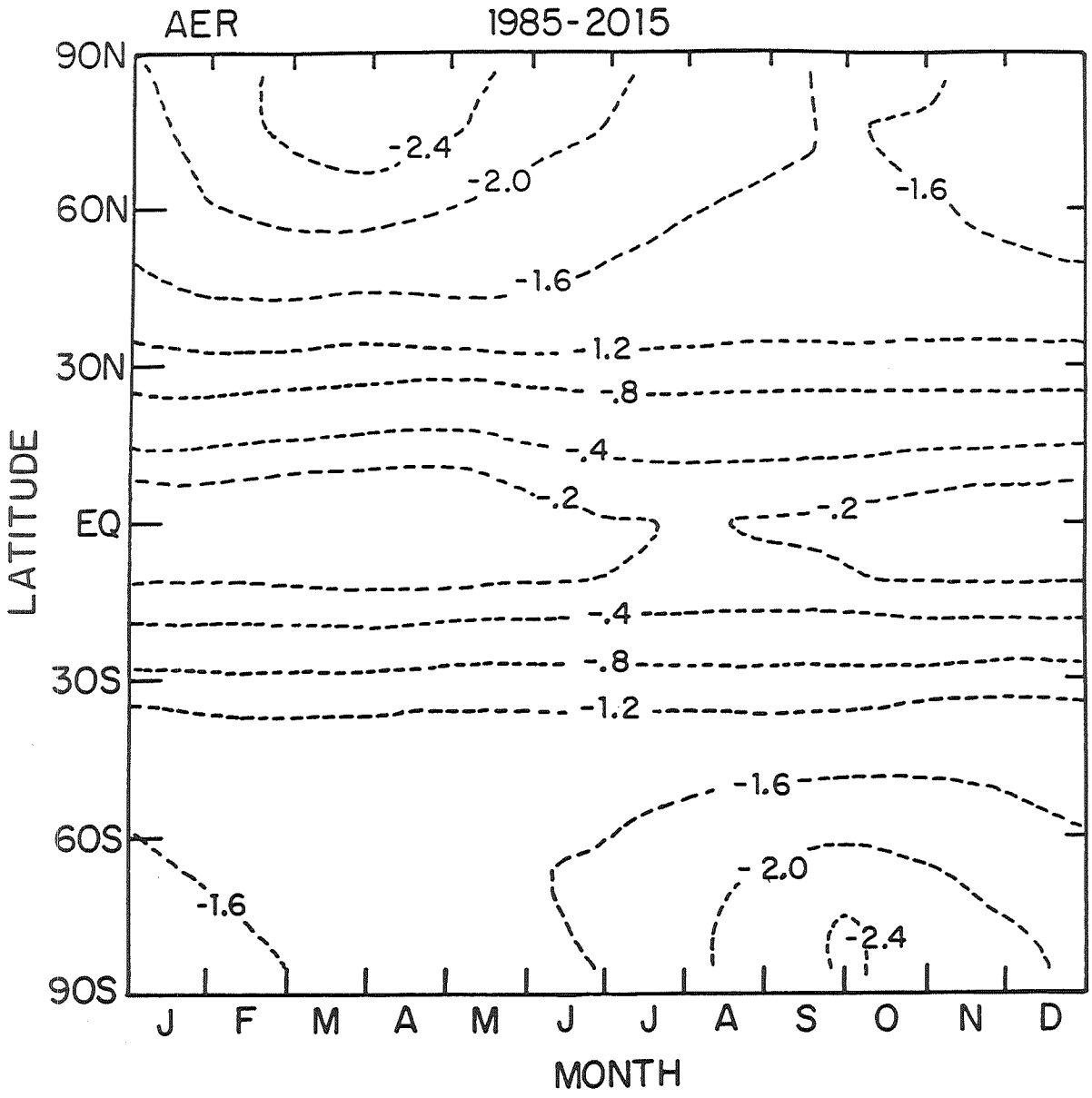

D-13 (2). Dobson map of ozone column changes (%) for the TD scenario 1985-2015 from the AER model.

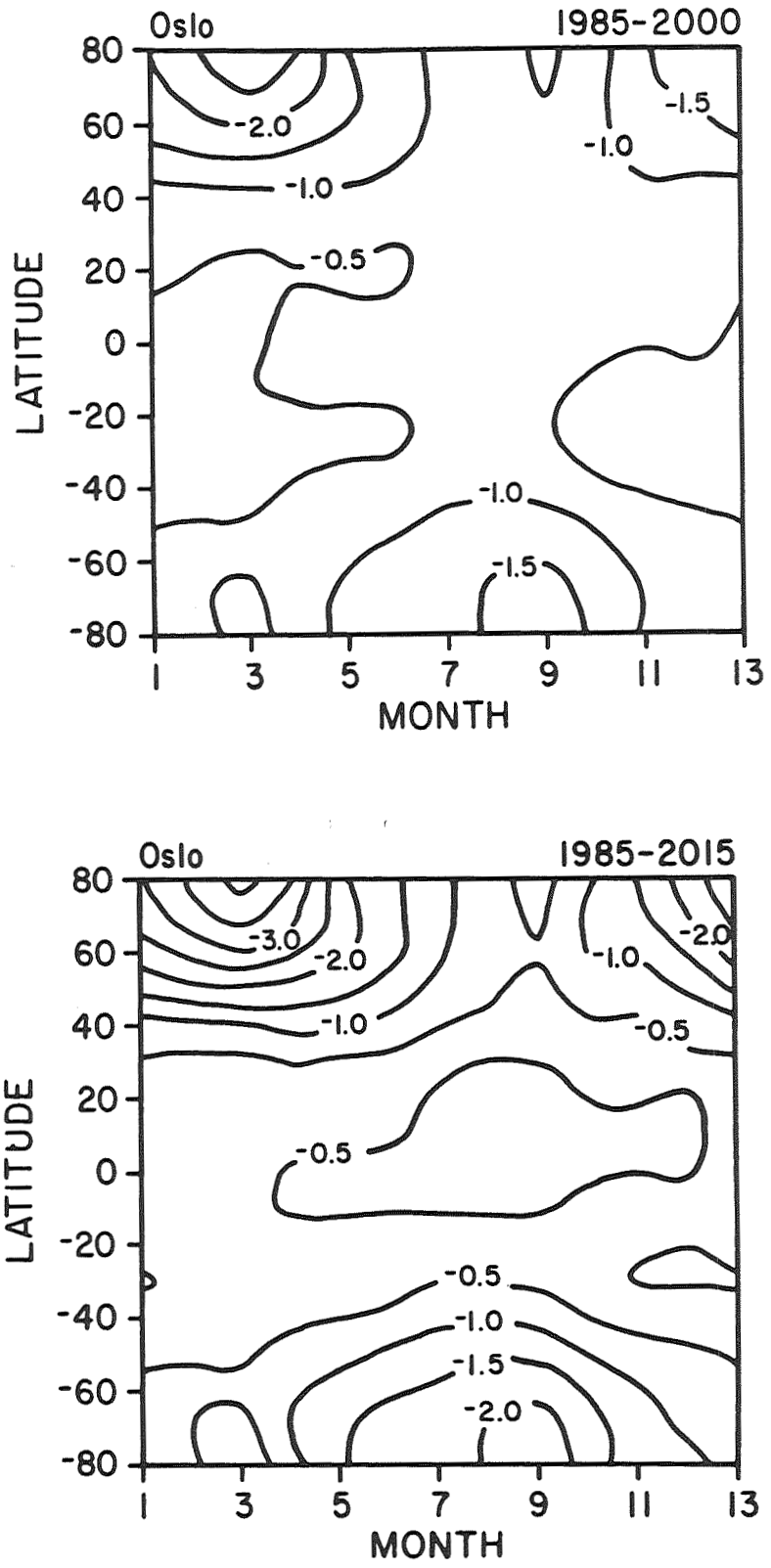

D-14. Dobson map of ozone column changes (%) for the TD scenario 1985-2000 and 1985-2015 from the Oslo model.

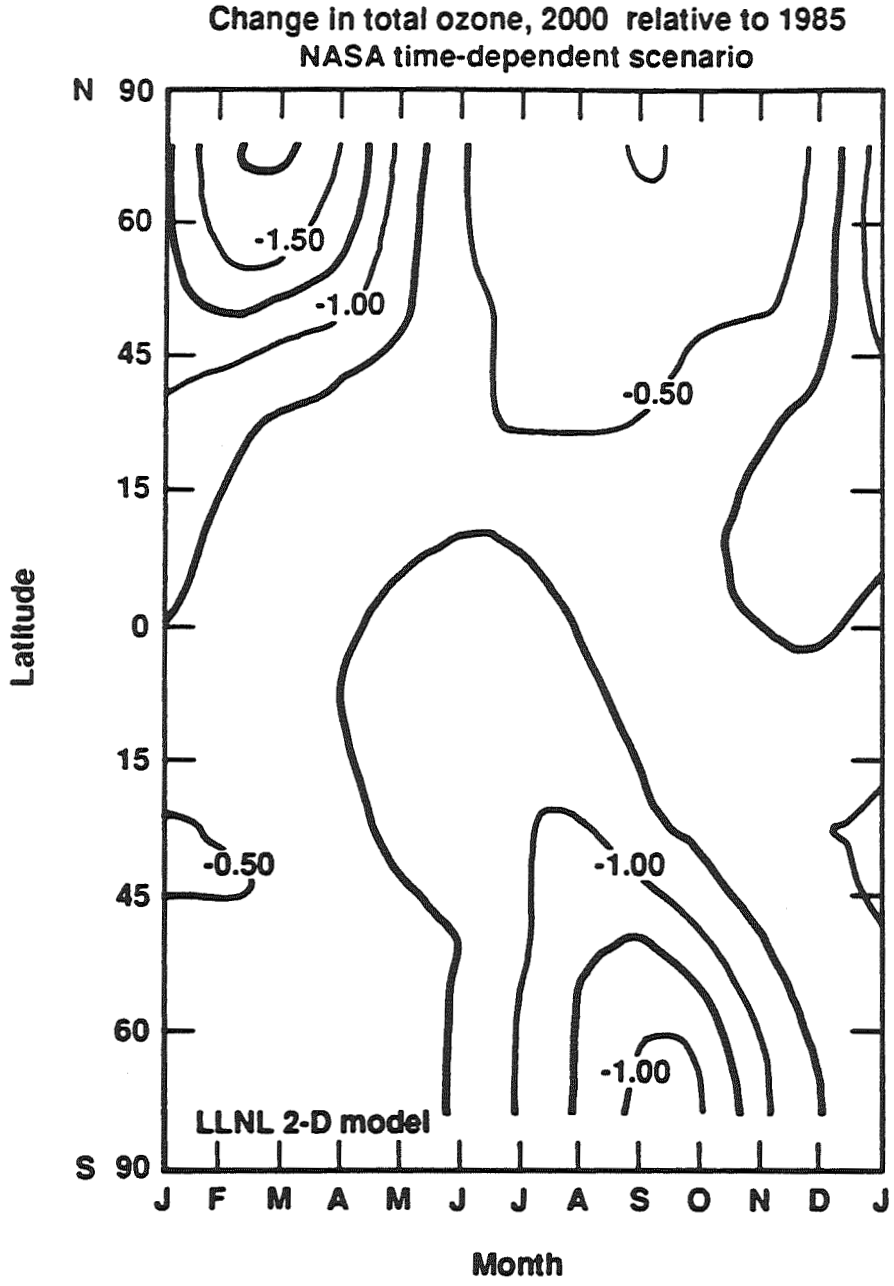

D-15 (1). Dobson map of ozone column changes (%) for the TD scenario 1985-2000 from the LLNL model.

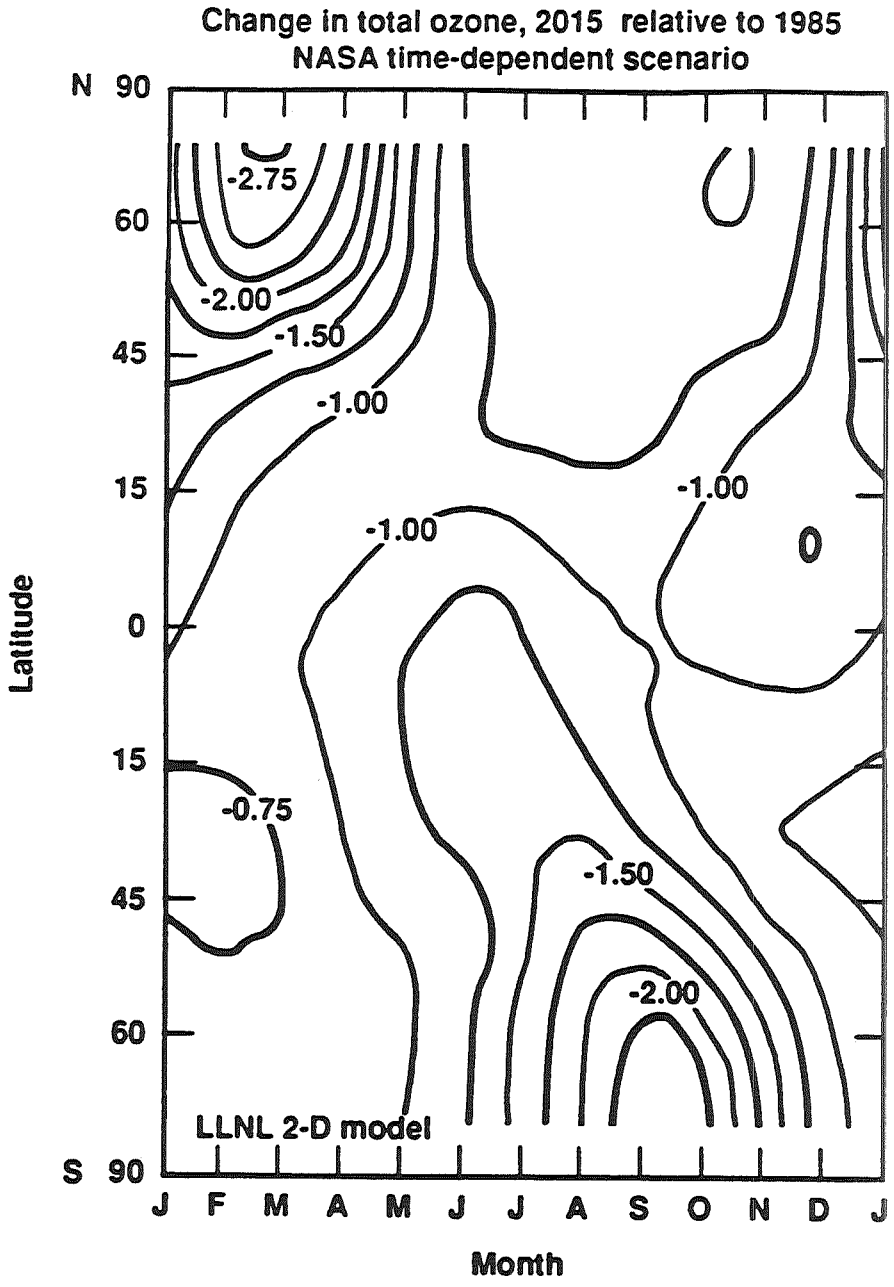

D-15 (2). Dobson map of ozone column changes (%) for the TD scenario 1985-2015 from the LLNL model.

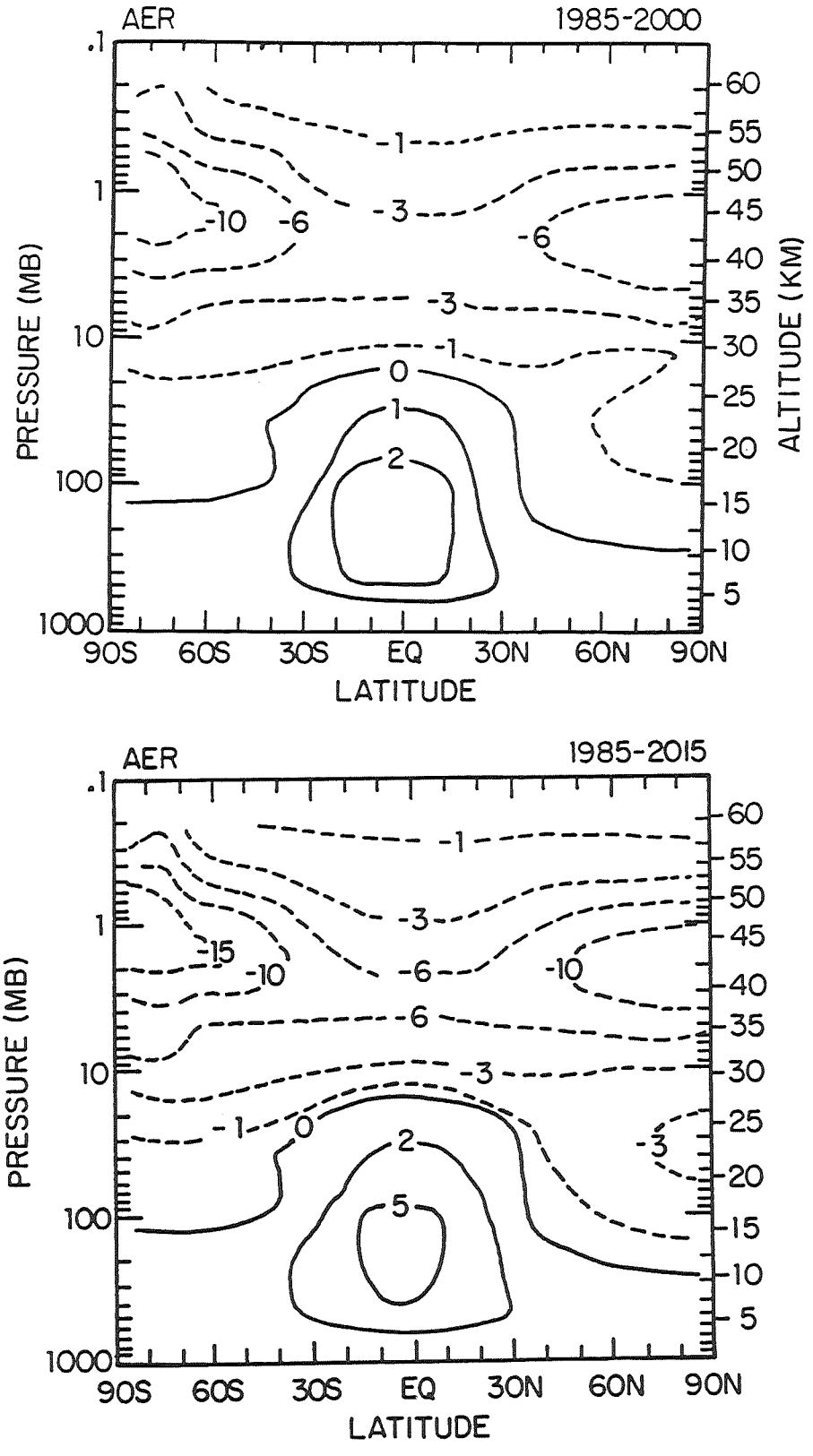

D-16. Ozone profile changes (%) for the TD scenario 1985-2000 and 1985- 2015 from the AER model for the month of April.

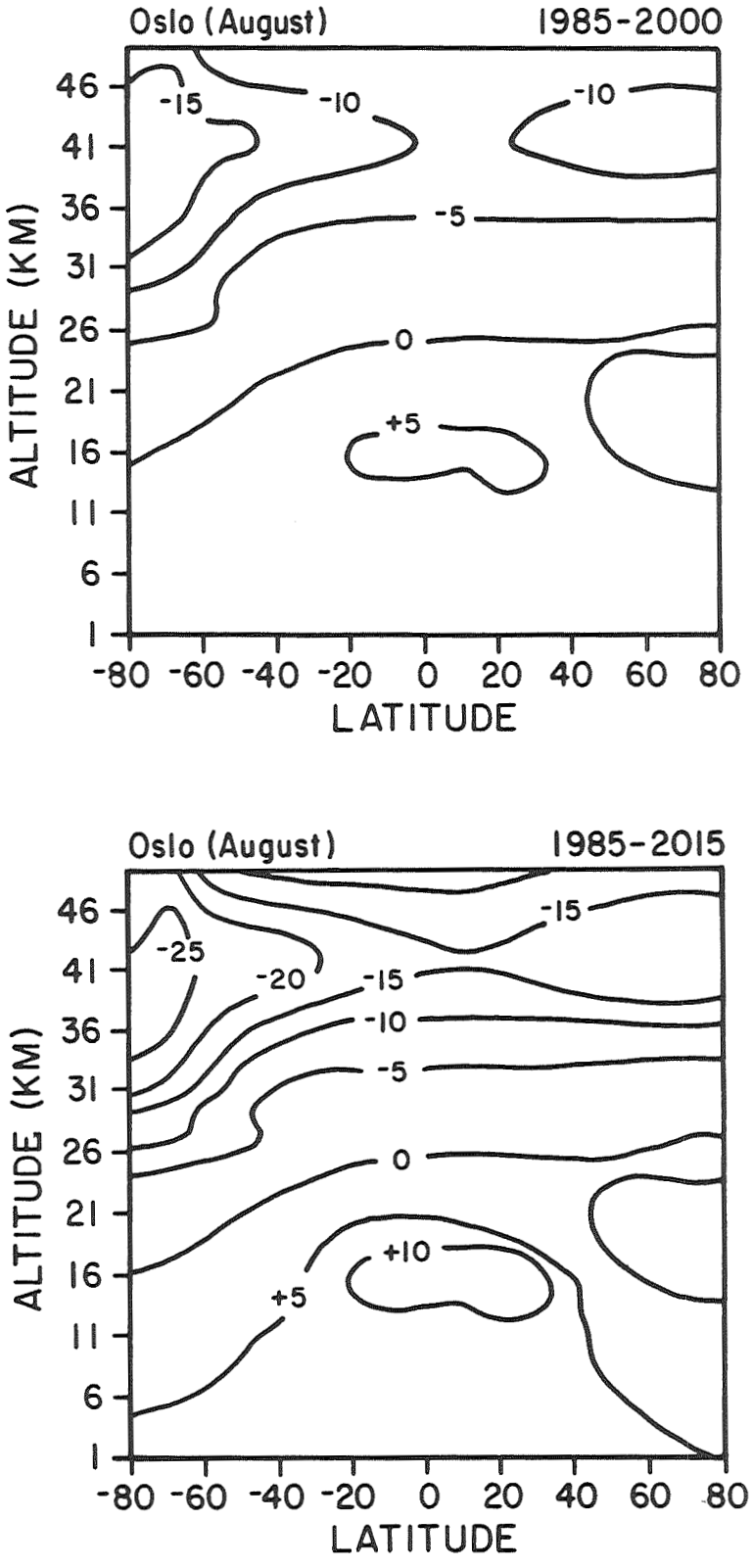

D-17. Ozone profile changes (%) for the TD scenario 1985-2000 and 1985- 2015 from the Oslo model for the month of August.

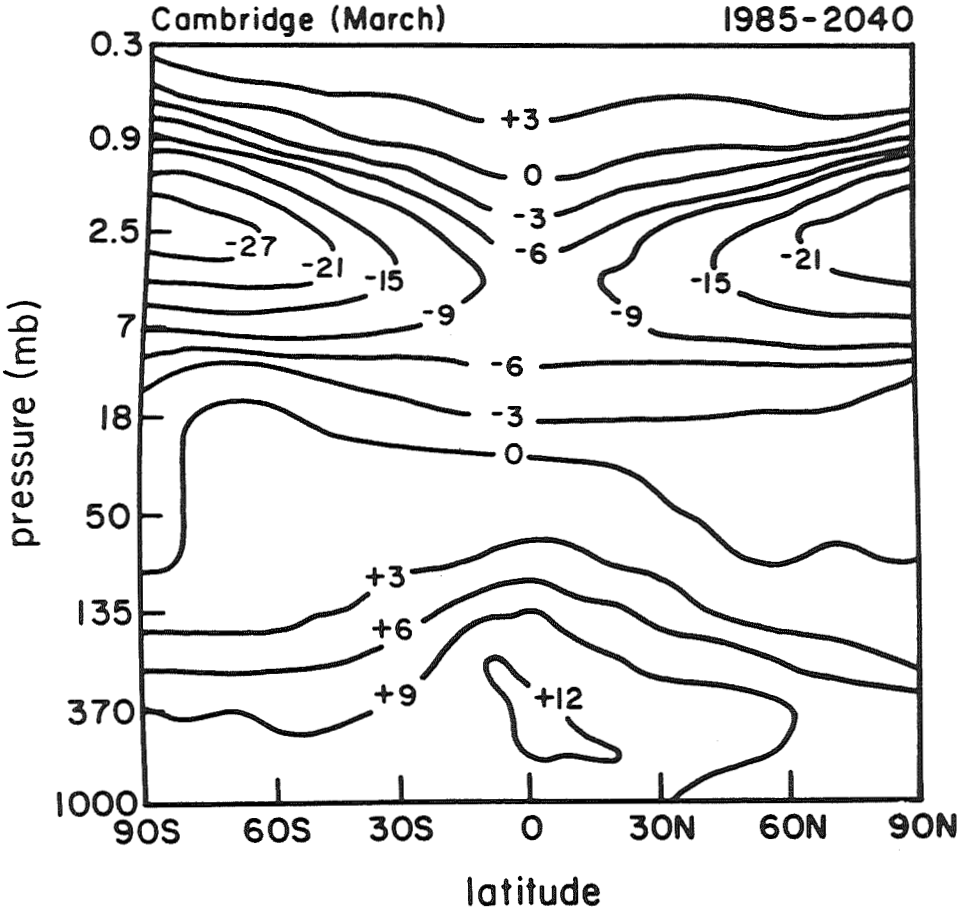

D-18. Ozone profile changes (%) for the extended TD scenario 1985-2040 from the Cambridge model for the month of March.

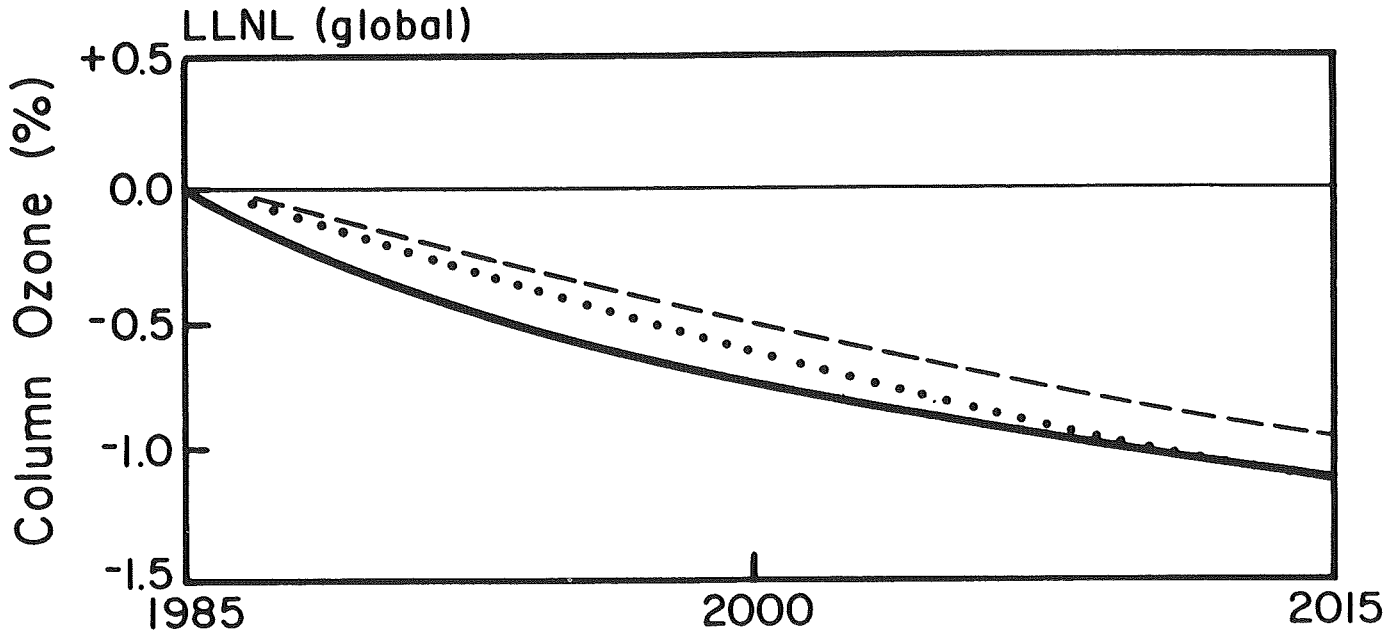

D-19. Global column ozone change (%) with time for the TD scenario from the LLNL model. The solid line shows results for the annually averaged column from the 2-D model using JPL-85; the dotted line, for the equivalent 1-D model; and the dashed line, for the 1-D model using JPL-87.

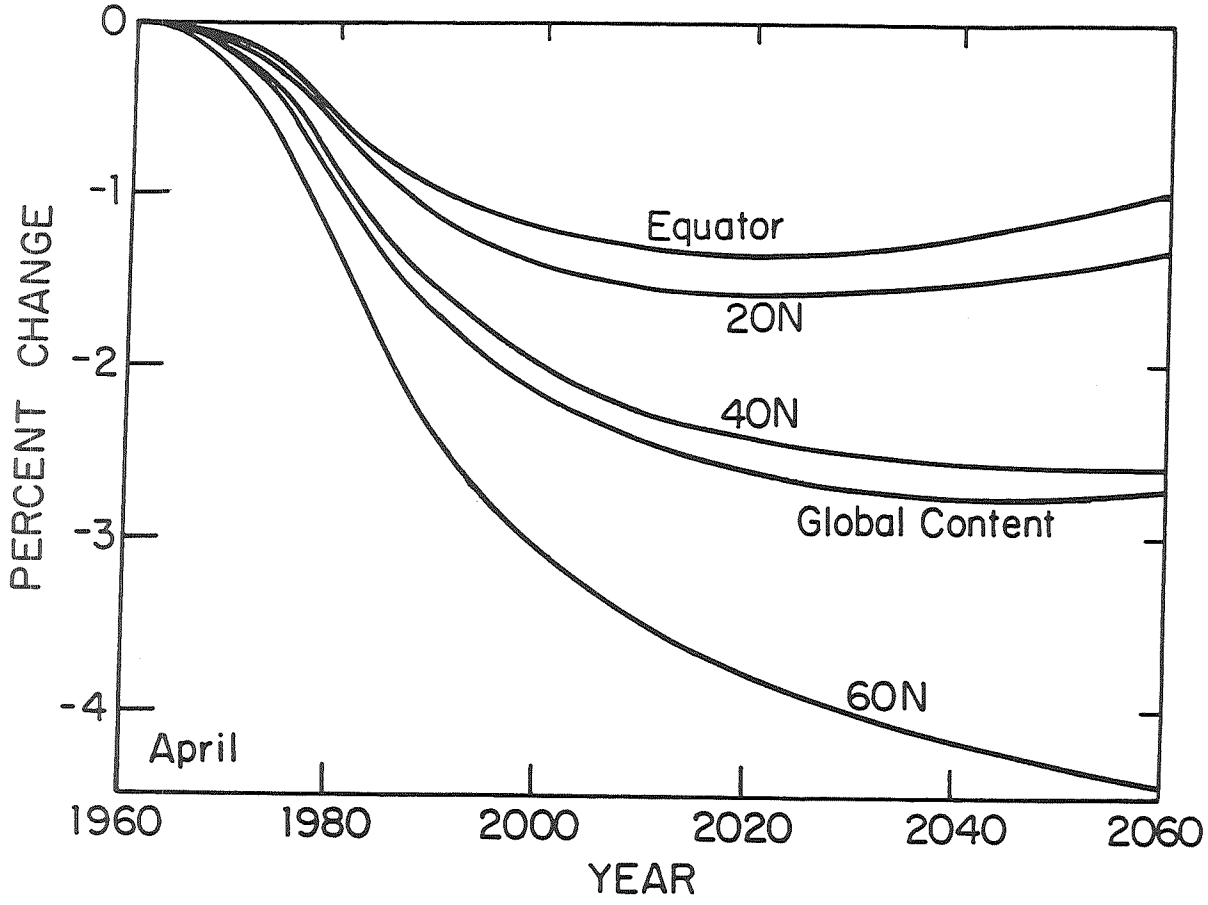

D-20. Global column ozone change (%) with time for the extended TD scenario from the AER model. Results are shown for the month of April and include latitude bands as well as the global average. The model calculations used transport parameters different from those reported for the standard TD scenario (Figures D-13 & D-16).

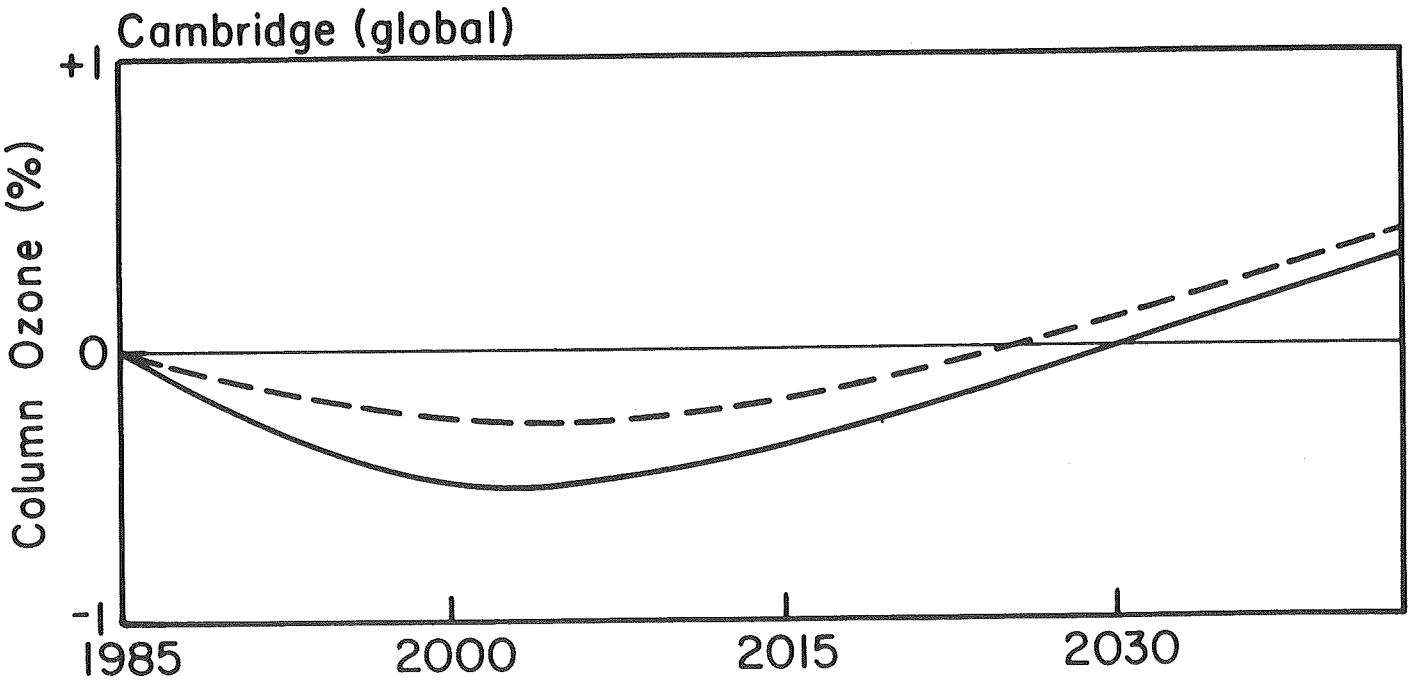

D-21. Global column ozone change (%) with time for the extended TD scenario from the Cambridge model. The solid line shows results for the TD scenario; the dashed line shows calculations using a similar scenario but with reduced chlorine emissions in accord with strict adherence to the Montreal protocol.

SECTION E

CHEMICAL KINETICS AND PHOTOCHEMICAL DATA FOR USE IN STRATOSPHERIC MODELING

E.1 Introduction

This compilation (JPL Publication 87-41) is the eighth evaluation of rate constants and photochemical cross sections prepared by the NASA Panel for Data Evaluation. The Panel was established in 1977 for the purpose of providing a critical tabulation of the latest kinetic and photochemical data for use in the modeling of stratospheric processes with particular emphasis on the ozone layer and its possible perturbation by anthropogenic and natural phenomena. Copies of the complete evaluation are available from the Jet Propulsion Laboratory, Documentation Section, 111-116B, California Institute of Technology, Pasadena, California, 91109.

E.2 Basis of the Recommendations

The recommended rate constants and cross sections are based on laboratory measurements. In order to provide recommendations that are as up to date as possible, preprints and written private communications are accepted, but only when it is expected that they will appear as published journal articles. In no cases are rate constants adjusted to fit observations of stratospheric concentrations. The Panel considers the question of consistency of data with expectations based on chemical kinetic theory, and when a discrepancy appears to exist, this fact is pointed out in the accompanying note. The major use of theoretical extrapolation of data is in connection with three-body reactions, in which the required pressure or temperature dependence is sometimes unavailable from laboratory measurements, and can be estimated by use of appropriate theoretical treatment. In the case of important rate constants for which no experimental data are available, the Panel may provide estimates of rate constant parameters based on analogy to similar reactions for which data are available.

E.3 Recent Changes and Current Needs of Laboratory Kinetics

Laboratory studies have produced no major changes in homogeneous kinetics and photochemistry used to model the normal stratosphere since the publication of our previous evaluation, JPL Publication 85-37. There are approximately thirty-seven changes in the rate constant recommendations in the present evaluation, but these are for the most part minor. Nonetheless, an important refinement has been made in the rate constant for OH + HO_2, and some significant changes in NO_x chemistry have also been made. Forty- two new reactions have been added, representing processes which play small but possibly significant roles in the stratosphere. Some reactions which are thought to be unimportant in the stratosphere are included for completeness and for possible applications to laboratory studies.

The recent emphasis on Antarctic chemistry, with its unusual characteristics of low temperature, high concentrations of active chlorine species, and the presence of polar

stratospheric clouds, has focused attention on three areas of stratospheric chemistry not previously considered very important: (1) chemistry at temperatures as low as 180 K; (2) heterogeneous reactions, especially on ice particles; and (3) certain reactions such as ClO + ClO, which are normally not competitive in the stratosphere because of the low ClO concentration.

Very few laboratory studies of stratospheric chemistry have been conducted at temperatures below 220 K, partly because of difficulties with enhanced surface reactivity, and because such work has not been considered relevant to the stratosphere. It is now apparent that increased emphasis should be placed on the temperature regime of 180-220 K, especially since the simple Arrhenius temperature coefficients of several very important reactions, e.g., $Cl + CH_4$ and $HO_2 + O_3$, are not sufficiently reliable for extrapolation to very low temperatures. Indeed, the Arrhenius equation may prove to be unacceptable for wide temperature ranges, because of the more complex dependence shown by many reactions.

An additional aspect of low temperature chemistry is the possibly enhanced role of complex formation. Examples are the formation of O_2 complexes with species such as ClO and atomic chlorine. The kinetics and thermochemistry for these processes are not well known. In this connection, we have now provided uncertainty estimates in the tabulation of equilibrium constants. The chemistry and photochemistry of complexes may also be significant in certain cases.

Heterogeneous chemistry on aerosol particles had previously been considered to be of marginal importance in the stratosphere. It has nevertheless long been recognized that certain very slow gas phase processes, such as hydrolysis of chlorine nitrate, might be significantly accelerated on particle surfaces. It is now thought that such processes on ice particles are possibly of major importance in Antarctic ozone chemistry. The effects of volcanic emissions, which temporarily increase the stratospheric particle loading by large amounts, may also be important in short term (two to three year) ozone fluctuations.

Measurements in Antarctica show that unexpectedly high concentrations of ClO are present in certain regions within the polar vortex. As a consequence, reactions such as ClO + ClO may play a major role in the chlorine chemistry of that region. Very little is known about the chemistry of the Cl_2O_2 dimer, which may exist in more than one isomeric form.

It should also be mentioned that a table of enthalpy data has now been added as an Appendix.

E.3.1 O_x Reactions

The kinetics of the O, O_2, and O_3 system appear to be well established. There remains some concern about the possible roles of excited states of O_2, especially $O_2(^1\Delta)$, but at present there is no evidence that these states have any important effects on the overall chemistry of the stratosphere.

Recent laboratory studies indicate a 60% yield of electronically excited $O_3(^3B_2)$ as an intermediate in the $O + O_2 + M$ reaction. Based on their rate constant for quenching to the ground state, the ratio of excited O_3 to ground state O_3 is at most a few parts per thousand at 60 km, and decreases sharply at lower altitudes. Thus, unless the quenching process itself results in chemical change, the process may be insignificant.

E.3.2 $O(^1D)$ Reactions

The data base for $O(^1D)$ kinetics is in fairly good condition. There is good to excellent agreement among independent measurements of the absolute rate constants for $O(^1D)$ deactivation by the major atmospheric components, N_2 and O_2, and by the critical radical-producing components, H_2O, CH_4, N_2O, and H_2. There are fewer direct studies of the products of the deactivation processes, but in most cases these details appear to be of minor importance. Some processes of interest for product studies include the reactions of $O(^1D)$ with CH_4 and halocarbons. Possible kinetic energy effects from photolytically generated $O(^1D)$ are probably not important in the atmosphere but may contribute complications in laboratory studies. The rate coefficient for the reaction of $O(^1D)$ with HCN should be measured since it may play a role in the atmospheric oxidation of this trace gas.

E.3.3 HO_x Reactions

Our knowledge of the kinetics of HO_x radicals has continued to improve. The most significant development with this report is on the $OH + HO_2$ reaction. This reaction is a key HO_x radical termination step throughout much of the atmosphere. New measurements appear to explain a discrepancy between previous low pressure and high pressure measurements as due to the presence of atomic H and O in the low pressure discharge flow experiments. The recommended rate coefficient for the $OH + HO_2$ reaction has been increased and the previous pressure dependence has been removed. The recommendation for $k(HO_2 + O_3)$ has also been revised, but the overall situation for this reaction is less satisfactory. All of the data for the temperature range 240-400 K cannot be fit satisfactorily with a single Arrhenius equation. The recommendation is weighted heavily toward the low temperature data for stratospheric applications. High quality measurements that avoid the limitations of the previous studies are still needed for both reactions.

E.3.4 NO_x Reactions

The data base for NO_x reactions is relatively well established. The rate constant for the important $O + NO_2$ reaction has been revised resulting in a 20% increase at 220 K. Our understanding of the important $OH + HNO_3$ reaction has improved due to confirmation of a small pressure dependence, which helps explain some of the earlier divergence between flash and flow studies. The equally important $OH + HO_2NO_2$ reaction is not as well characterized, particularly with regard to the temperature dependence. Additional studies of the $HO_2 + NO_2 + M$ recombination are also needed, especially on the temperature dependence of the low pressure limit. Recently, direct studies of some key NO_3 reactions have become available, greatly improving the reliability of that data base.

The data for NH_2 reactions are sparse. There are a large number of studies only for the $NH_2 + NO$ reactions and these show a factor of two discrepancy between flow and flash systems.

E.3.5 Hydrocarbon Oxidation

Our understanding of hydrocarbon oxidation in the atmosphere has improved considerably in the past few years. All hydrocarbons are released at the surface of the earth, and their degradation in the troposphere is initiated by reaction with OH (and with ozone in the case of olefins). Depending on their reactivity with OH, only a fraction of the surface flux of hydrocarbons is transported into the stratosphere, where their oxidation serves as a source of water vapor. In addition, the reaction of atomic chlorine with these hydrocarbons (mainly CH_4) constitutes one of the major sink mechanisms for active chlorine. Even

though CH_4 is the predominant hydrocarbon in the stratosphere, we have included in this evaluation certain reactions of a few heavier hydrocarbon species.

In the stratosphere, CH_4 oxidation is initiated by its reaction with either OH, Cl, or $O(^1D)$ leading to formation of CH_3 and subsequently CH_3O_2. Several details of the subsequent chemistry are unclear, primarily because two key reactions are not well characterized. These reactions are: (1) $CH_3O_2 + HO_2$, which exhibits an unusual temperature dependence analogous to that for the $HO_2 + HO_2$ reaction and (2) $CH_3OOH + OH$, which has been recently studied in a competitive system and found to be extremely rapid. Discrepancies in the absorption cross sections of CH_3O_2 and HO_2 have added to the uncertainty regarding the rate coefficient for the $CH_3O_2 + HO_2$ reaction. Even though the rate constants for the two reactions mentioned above are not very well known, the effects of these uncertainties on stratospheric O_3 perturbation calculations are negligible.

One area of hydrocarbon oxidation which has seen a great deal of improvement is that of product analysis. However, some additional work may be required to measure branching ratios for reactions such as $CH_3O_2 + CH_3O_2$ and $CH_3O_2 + HO_2$.

The oxidation scheme for higher hydrocarbons has not been fully elucidated. However, the rate of transport of these hydrocarbons into the stratosphere can be easily calculated since the rates of reactions with OH are well known. In most cases it is expected that the radicals formed from the initial OH or Cl attack will follow courses analogous to CH_3, and ultimately lead to CO.

E.3.6 Halogen Chemistry

The recommendations for the important ClO_x reactions have not changed significantly since the previous evaluation. This reflects the fact that most of the important homogeneous gas phase processes are well understood. There is a better upper limit to the rate of reaction of $ClONO_2$ with HCl and a new entry for the reaction of $ClONO_2$ with H_2O. The data indicate that these homogeneous gas phase reactions are too slow to be important in the the chemistry of the stratosphere, but it is possible that the corresponding heterogeneous reactions may be important under certain conditions such as those in the atmosphere above Antarctica.

There are still a number of questions regarding the important ClO + ClO reaction: the absolute rate as a function of T and P; the relative importance of bimolecular and termolecular reaction channels as a function of T and P; the dependence of product branching ratios on T and P; importance of the dimer and its reactions and photochemistry; possible role of complex formation with O_2.

There are new entries for the reactions of OH with seven potential alternative chlorofluorocarbons. There are only minor changes in the data base for reactions of BrO_x and FO_x species apart from changes in the recommendations for the reactions of Br atoms with HO_2 and H_2O_2. There have been several recent studies of the important BrO + ClO reaction which have improved our knowledge of the rate constant at room temperature, but further work is required to determine the temperature dependence and product ratios.

E.3.7 SO_x Reactions

The data base on homogeneous sulfur chemistry continues to change and expand as we obtain more detailed laboratory data on a number of oxidative processes. In particular, we now have information on the temperature-dependence of several SH reactions important in

the atmospheric oxidation of H_2S and first-time information on several HSO reactions. Nevertheless, our understanding of the reactivity of these radicals is still far from complete. Similar improvements have been seen in the data for the reactions of SO with several atmospheric molecules (notably ClO, BrO, and NO_2). Of particular interest are the first direct measurements of $HOSO_2$ which had been postulated as an intermediate in the oxidation of SO_2 into sulfuric acid via the sequence

$$OH + SO_2 + M \rightarrow HOSO_2 + M$$

$$HOSO_2 + O_2 \rightarrow HO_2 + SO_3$$

New data result in a direct determination of the rate constant for the second reaction and support a homogeneous gas phase SO_2 oxidation mechanism involving no net change in HO_x per H_2SO_4 formed while negating a reaction sequence involving SO_3 formation via the OH + $HOSO_2$ reaction (a mechanism which would have resulted in the loss of two OH radicals per H_2SO_4 formed). However, there is a need for still further information on the atmospheric reactivity of $HOSO_2$ and perhaps even on reactions involving its possible complexes with O_2 or H_2O. Along these latter lines, it has been demonstrated that the formation of the $HOSO_2 \cdot O_2$ adduct predominates in solution. While the acidic natures of both $HOSO_2$ and $HOSO_2 \cdot O_2$ result in their deprotonation in solution and existence as the SO_3^- and SO_5^- anions, these results suggest the possible atmospheric importance of the O_2 adduct in its hydrated form. In this and most discussions, SO_3 has been thought of as equivalent to sulfuric acid. This is supported by laboratory results which suggest the rapid isomerization of the adduct $SO_3 \cdot H_2O$ to H_2SO_4 with a barrier to this process of less than 13 kcal/mol. Further information on the reactions of SO_3 with other atmospheric species is needed to assess the competition of these reactions with SO_3 hydrolysis.

Additional progress has been made in developing an understanding of the mechanisms of OCS and CS_2 oxidation. There are now additional studies providing rate constant and primary product information for the reactions of OH with both species. In the case of CS_2 there have been direct observations of reversible adduct formation with OH as well as further confirmation of its O_2-enhanced pressure dependent oxidation by OH. Recent data for OH + OCS does not reveal a rate constant dependence on total pressure or O_2 pressure despite the observation of direct formation of SH in both the CS_2 and OCS reactions and the postulation of similar complex (adduct) mechanisms. New data indicate that the direct bimolecular reactions have markedly different Arrhenius parameters from one another, thereby suggesting significant energetic differences in the reaction surfaces describing adduct formation. Further information regarding the elementary steps in the oxidation of both species should further our understanding of complex mechanisms in general.

E.3.8 Metal Chemistry

Twelve new reactions of sodium species have been introduced in this evaluation. Sodium is deposited in the upper atmosphere by meteors along with larger amounts of silicon, magnesium, and iron; comparable amounts of aluminum, nickel, and calcium; and smaller amounts of potassium, chromium, manganese, and other elements. The interest is greatest in the alkali metals because they form the least stable oxides and thus free atoms can be regenerated through photolysis and reactions with O and O_3. The other meteoric elements are expected to form more stable oxides.

The total flux of alkali metals through the atmosphere is relatively small, e.g., one or two orders of magnitude less than CFCs. Therefore extremely efficient catalytic cycles are

required in order for Na to have a significant effect on stratospheric chemistry. There are no measurements of metals or metal compounds in the stratosphere which indicate a significant role.

It has been proposed that the highly polar metal compounds may polymerize to form clusters and that the stratospheric concentrations of free metal compounds are too small to play a significant role in the chemistry.

Some recent studies have shown that the polar species NaO and NaOH associate with abundant gases such as O_2 and CO_2 with very fast rates in the atmosphere. It has been proposed that reactions of this type will lead to the production of clusters with many molecules attached to the sodium compounds. Photolysis is expected to compete with the association reactions and to limit the cluster concentrations in daylight. If atmospheric sodium does form large clusters, it is unlikely that Na species can have a significant role in stratospheric ozone chemistry. In order to assess the importance of these processes, data are needed on the association rates and the photolysis rates involving the cluster species.

E.3.9 Photochemical Cross Sections

The absorption cross sections of O_2 around 200 nm -- that is, at the onset of the Herzberg continuum -- have been remeasured in the laboratory and are now in better agreement with the values inferred from solar irradiance measurements in the stratosphere.

The temperature dependence of the absorption cross sections of HO_2NO_2 and H_2O_2 in the 300 nm region might be significant and should be determined. The photochemistry of the ClO dimer, Cl_2O_2, must be studied in detail.

E.4 Atmospheric Chemistry

E.4.1 Overview

The ozone content of earth's atmosphere can be considered to exist in three distinct regions, the troposphere, stratosphere, and mesosphere. The unpolluted troposphere contains small amounts of ozone, which come from both downward transport from the stratosphere and from in situ photochemical production. The chemistry of the global troposphere is complex, with both homogeneous and heterogeneous (e.g., rain-out) processes playing important roles. The homogeneous chemistry is governed by coupling between the carbon, nitrogen, hydrogen, and oxygen systems and can be considered to be more complex than the chemistry of the stratosphere, due to the presence of higher hydrocarbons, long photochemical relaxation times, higher total pressures, and the high relative humidity which may affect the reactivity of certain key species such as HO_2. Significant progress is being made in understanding the coupling among the different chemical systems, especially the mechanism of methane oxidation which partially controls the odd hydrogen budget. This is an important development, as reactions of the hydroxyl radical are the primary loss mechanism for compounds containing C-H (CH_4, CH_3Cl, CHF_2Cl, etc.) or C=C (C_2Cl_4, C_2HCl_3, C_2H_4, etc.), thus limiting the fraction transported into the stratosphere.

The stratosphere is the region of the atmosphere where the bulk of the ozone resides, with the concentration reaching a maximum value of about 5×10^{12} molecule cm^{-3} at an altitude of ~25 km. Ozone in the stratosphere is removed predominantly by catalytic processes, but assignment of the relative importance of different catalytic cycles and the prediction of their future impact are dependent on a detailed understanding of chemical reactions which form,

remove and interconvert the catalytic species. A model calculation of stratospheric composition may include some 150 chemical reactions and photochemical processes, which vary greatly in their importance in controlling the density of ozone. Laboratory measurements of the rates of these reactions have progressed rapidly in recent years, and have given us a basic understanding of the processes involved, particularly in the upper stratosphere. Despite the basically sound understanding of overall stratospheric chemistry which presently exists, much remains to be done to quantify errors, to identify reaction channels positively, and to measure reaction rates both under conditions corresponding to the lower stratosphere (~210 K, ~75 torr) as well as the top of the stratosphere (~270 K, ~1 torr). As previously mentioned, Antarctic conditions require the consideration of even lower temperatures.

The chemistry of the upper stratosphere, i.e. 30-50 km, is thought to be reasonably well defined, although there appear to be some significant differences between the predicted and observed chemical composition of this region of the atmosphere which may be due to inaccurate rate data or missing chemistry. In this region the composition of the atmosphere is predominantly photochemically controlled and the photolytic lifetimes of temporary reservoir species such as HOCl, HO_2NO_2, $ClONO_2$, N_2O_5 and H_2O_2 are short and hence they play a minor role. Thus the important processes above 30 km all involve atoms and small molecules. The majority of laboratory studies of these reactions has been carried out under the conditions of pressure and temperature which are encountered in the upper stratosphere, and their overall status appears to be good. No significant changes in rate coefficients for the key reactions such as $Cl + O_3$, $NO + ClO$, $NO + O_3$, etc., have occurred in the last few years. Historically, a major area of concern in the chemistry of the upper stratosphere has involved the reaction between HO and HO_2 radicals, which has had considerable uncertainty in the rate constant. This HO_x termination reaction plays an important role in determining the absolute concentrations of HO and HO_2, and since HO plays a central role in controlling the catalytic efficiencies of both NO_x and ClO_x, it is a reaction of considerable importance. Recently the uncertainty in the rate coefficient for the reaction has decreased, now being thought to be about a factor of 1.3 to 1.8 over the range of atmospheric conditions. It should be noted that the $HO + H_2O_2$, $HO + HNO_3$ and $HO + HO_2NO_2$ reactions have little effect on controlling the HO_x concentrations above 30 km. For reactions such as $O + HO$ and $O + HO_2$, which control the HO_x radical partitioning above 40 km, the data base can be considered to be quite good.

One area in which additional studies may be needed is that of excited state chemistry, i.e., studies to determine whether electronic or vibrational states of certain atmospheric constituents may be more important than hitherto recognized. Possible examples are O_2^*, O_3^*, HO^*, or N_2^*.

The chemistry of the lower stratosphere is quite complex, with significant coupling between the HO_x, NO_x and ClO_x families. In this region of the atmosphere (15-30 km), both dynamics and photochemistry play key roles in controlling the trace gas distributions. It is also within this region that the question of the pressure and temperature dependences of the rate coefficients is most critical, due to the low temperatures (210 K and lower) and the high total pressures (30-200 torr).

E.4.2 Heterogeneous Effects

A continuing question in stratospheric modeling is whether or not aerosols perturb the homogeneous chemistry to a significant degree. This question has assumed much greater importance in connection with the possible role of polar stratospheric clouds in Antarctic chemistry. On a global scale, effects have been suggested through the following processes:

(1) Surface catalysis of chemical reactions.

(2) Production or removal of active species.

(3) Effects of aerosol precursors such as SO_2.

In NASA Reference Publications 1010 and 1049, processes 1 and 2 above were discussed in general terms. It was shown that, with a few possibly significant exceptions, surface catalysis of chemical reactions is not expected to compete with the rates of homogeneous gas phase reactions. The essential reason is that the frequency of collision of a gas phase molecule with the aerosol surface is typically of the order of 10^{-5} sec^{-1}, whereas most of the key gas phase reactions occur with much greater frequency, for example, conversion of atomic chlorine to HCl by the Cl + CH_4 reaction (10^{-2} sec^{-1}). Thus, even in the unlikely case of unit reaction efficiency on the aerosol surface the heterogeneous process cannot be significant. Possible exceptions occur for reactions which are extremely slow in the gas phase, such as hydrolysis of an anhydride, as in the reaction $N_2O_5 + H_2O \rightarrow 2HNO_3$. There remains some uncertainty with regard to the role of these latter processes.

It was also shown in NASA Publications 1010 and 1049 that there is no evidence that aerosols serve as significant sources or sinks of the major active species such as chlorine compounds. However, it has been suggested that dust particles of meteoritic origin may scavenge metallic atoms and ions, and in particular may remove Na diffusing from the mesosphere in the form of absorbed NaOH or Na_2SO_4.

Although it appears that aerosols do not greatly perturb the ambient concentrations of active species through direct interaction with the surfaces, the aerosol precursors may significantly perturb the stratospheric cycles through removal of species such as OH radicals. For example, a large injection of SO_2, such as that which occurred in the El Chichon eruption, has the potential of significantly depleting HO_x radical concentrations, as was discussed in the section on SO_x chemistry. It must be reiterated, however, that recent studies of the mechanism of SO_2 oxidation have shown that OH plays a catalytic role, and, therefore, the process does not result in a net loss of OH from the system.

The effects of aerosols on the radiation field and on the temperature may also need to be considered. These effects are probably small, however.

There are two problems with regard to detecting the effects of aerosol injections such as that following the El Chichon eruption. One is that no adequate baseline exists for the unperturbed atmosphere, and therefore a given observation cannot unambiguously be assigned to the enhanced presence of the aerosol loading. A second problem is that, as already discussed, the effects are expected to be subtle and probably of small magnitude. Thus, in spite of large changes that may occur in the aerosol content of the lower stratosphere, effects on the chemical balance will be difficult to detect.

E.5 Rate Constant Data

In Table E-1 (Rate Constants for Second Order Reactions) the reactions are grouped into the classes O_x, $O(^1D)$, HO_x, NO_x, Hydrocarbon Reactions, ClO_x, BrO_x, FO_x, and SO_x. The data in Table E-2 (Rate Constants for Three-Body Reactions), while not grouped by

class, are presented in the same order as the bimolecular reactions. Further, the presentation of photochemical cross section data follows the same sequence.

E.5.1 Bimolecular Reactions

Some of the reactions in Table E-1 are actually more complex than simple two-body reactions. To explain the anomalous pressure and temperature dependences occasionally seen in reactions of this type, it is necessary to consider the bimolecular class of reactions in terms of two subcategories, direct (concerted) and indirect (non-concerted) reactions.

A direct or concerted bimolecular reaction is one in which the reactants A and B proceed to products C and D without the intermediate formation of an AB adduct which has appreciable bonding, i.e., no stable A-B molecule exists, and there is no reaction intermediate other than the transition state of the reaction, $(AB)^{\#}$.

$$A + B \rightarrow (AB)^{\#} \rightarrow C + D$$

The reaction of OH with CH_4 forming $H_2O + CH_3$ is an example of a reaction of this class.

Very useful correlations between the expected structure of the transition state $(AB)^{\#}$ and the A-factor of the reaction rate constant can be made, especially in reactions which are constrained to follow a well- defined approach of the two reactants in order to minimize energy requirements in the making and breaking of bonds. The rate constants for these reactions are well represented by the Arrhenius expression k = A exp(-E/RT) in the 200-300 K temperature range. These rate constants are not pressure dependent.

The indirect or non-concerted class of bimolecular reactions is characterized by a more complex reaction path involving a potential well between reactants and products, leading to a bound adduct (or reaction complex) formed between the reactants A and B:

$$A + B \rightarrow (AB)^{*} \rightarrow C + D$$

The intermediate (AB)* is different from the transition state $(AB)^{\#}$, in that it is a bound molecule which can, in principle, be isolated. (Of course, transition states are involved in all of the above reactions, both forward and backward, but are not explicitly shown.) An example of this reaction type is ClO + NO, which normally produces $Cl + NO_2$ as a bimolecular product, but which undoubtedly involves ClONO (chlorine nitrite) as an intermediate. This can be viewed as a chemical activation process forming (ClONO)* which decomposes to the ultimate products, $Cl + NO_2$. Reactions of the non-concerted type can have a more complex temperature dependence, can exhibit a pressure dependence if the lifetime of (AB)* is comparable to the rate of collisional deactivation of (AB)*. This arises because the relative rate at which (AB)* goes to products C + D vs. reactants A + B is a sensitive function of its excitation energy. Thus, in reactions of this type, the distinction between the bimolecular and termolecular classification becomes less meaningful, and it is especially necessary to study such reactions under the temperature and pressure conditions in which they are to be used in model calculations.

The rate constant tabulation for second-order reactions (Table E-1) is given in Arrhenius form: k(T) = A exp ((- E/R)(1/T)) and contains the following information:

(1) Reaction stoichiometry and products (if known). The pressure dependences are included, where appropriate.

(2) Arrhenius A-factor.

(3) Temperature dependence and associated uncertainty ("activation temperature" E/R +/- ΔE/R).

(4) Rate constant at 298 K.

(5) Uncertainty factor at 298 K.

E.5.2 Termolecular Reactions

Rate constants for 3rd order reactions (Table E-2) of the type A + B $\leftrightarrow$ (AB)* $\rightarrow$ AB are given in the form

$$k_0(T) = k_0^{300}(T/300)^{-n} \text{ cm}^6 \text{ molecule}^{-2} \text{ s}^{-1}$$

(where the value is suitable for air as the third body), together with the recommended value of n. Where pressure fall-off corrections are necessary, an additional entry gives the limiting high pressure rate constant in a similar form:

$$k_\infty(T) = k_\infty^{300}(T/300)^{-m} \text{ cm}^3 \text{ molecule}^{-1} \text{ s}^{-1}$$

To obtain the effective second-order rate constant for a given condition of temperature and pressure (altitude), the following formula is used:

$$k(Z) = k(M,T) = (\{k_0(T)[M]\}/\{1+k_0(T)[M]/k_\infty(T)\})0.6^{1/\alpha}$$

where

$$\alpha = 1 + \{\log_{10}(k_0(T)[M]/k_\infty(T))\}^2$$

The fixed value 0.6 which appears in this formula fits the data for all listed reactions adequately, although in principle this quantity may be different for each reaction.

Thus, a compilation of rate constants of this type requires the stipulation of the four parameters, $k_0(300)$, n, $k_\infty(300)$, and m. These can be found in Table E-2. The discussion that follows outlines the general methods we have used in establishing this table.

E.5.2.1 Low-Pressure Limiting Rate Constant [$k^x_0(T)$]

Troe (J. Chem. Phys. 66, 4745 (1977)) has described a simple method for obtaining low-pressure limiting rate constants. In essence this method depends on the definition:

$$k^x_0(T) = \beta_x k^x_{0,sc}(T)$$

Here sc signifies "strong" collisions, x denotes the bath gas, and β_x is an efficiency parameter ($0 < \beta_x < 1$), which provides a measure of energy transfer.

The coefficient β_x is related to the average energy transferred in a collision with gas x, $\langle\Delta E\rangle_x$, via:

$$\beta_x/(1-\beta_x^{0.5}) = \langle\Delta E\rangle_x/F_E kT$$

Notice that $\langle\Delta E\rangle_x$ is quite sensitive to β. F_E is the correction factor of the energy dependence of the density of states (a quantity of the order of 1.1 for most species of stratospheric interest).

For many of the reactions of possible stratospheric interest reviewed here, there exist data in the low-pressure limit (or very close thereto), and we have chosen to evaluate and unify this data by calculating $k^x_{o,sc}(T)$ for the appropriate bath gas x and computing the value of β_x corresponding to the experimental value. A recent compilation (Patrick and Golden, Int. J. Chem. Kinet. 15, 1189 (1983)) gives details for many of the reactions considered here.

From the β_x values (most of which are for N_2, i.e., β_{N2}), we compute $\langle\Delta E\rangle_x$ according to the above equation. Values of $\langle\Delta E\rangle_{N2}$ of approximately 0.3 - 1.0 kcal mole^{-1} are generally expected. If multiple data exist, we average the values of $\langle\Delta E\rangle_{N2}$ and recommend a rate constant corresponding to the β_{N2} computed in the equation above.

Where no data exist we have estimated the low-pressure rate constant by taking $\beta_{N2} = 0.3$ at T = 300 K, a value based on those cases where data exist.

E.5.2.2 Temperature Dependence of Low-Pressure Limiting Rate Constants: n

The value of n recommended here comes from a calculation of $\langle\Delta E\rangle_{N2}$ from the data at 300 K, and a computation of β_{N2}(200 K) assuming that $\langle\Delta E\rangle_{N2}$ is independent of temperature in this range. This β_{N2}(200 K) value is combined with the computed value of $k_{o,sc}$(200 K) to give the expected value of the actual rate constant at 200 K. This latter in combination with the value at 300 K yields the value of n.

This procedure can be directly compared with measured values of k_o(200 K) when those exist. Unfortunately, very few values at 200 K are available. There are often temperature-dependent studies, but some ambiguity exists when one attempts to extrapolate these down to 200 K. If data are to be extrapolated beyond the measured temperature range, a choice must be made as to the functional form of the temperature dependence. There are two general ways of expressing the temperature dependence of rate constants. Either the Arrhenius expression $k_o(T) = A\exp(-E/RT)$ or the form $k_o(T) = A'T^{-n}$ is employed. Since neither of these extrapolation techniques is soundly based, and since they often yield values that differ substantially, we have used the method explained earlier as the basis of our recommendations.

E.5.2.3 High-Pressure Limit Rate Constants, $k_\infty(T)$

High-pressure rate constants can often be obtained experimentally, but those for the relatively small species of atmospheric importance usually reach the high-pressure limit at inaccessibly high pressures. This leaves two sources of these numbers, the first being guesses based upon some model, and the second being extrapolation of fall-off data up to higher pressures. Stratospheric conditions generally render reactions of interest much closer to the low-pressure limit, and thus are fairly insensitive to the high- pressure value. This means that while the extrapolation is long, and the value of $k_\infty(T)$ not very accurate, a "reasonable guess" of $k_\infty(T)$ will then suffice. In some cases we have declined to guess since the low-pressure limit is effective over the entire range of stratospheric conditions.

E.5.2.4 Temperature Dependence of High-Pressure Limit Rate Constants: m

There are very little data upon which to base a recommendation for values of m. Values in Table E-2 are estimated, based on models for the transition state of bond association reactions and whatever data are available.

E.5.2.5 Isomer Formation

A particular problem with association reactions arises when there are easily accessible isomeric forms of the molecule AB. In this situation, if the laboratory measurement of the rate constant is accomplished by following the disappearance of reactants, the value ascertained may be the sum of two or more processes that should be measured and tabulated independently. A specific example of such a case is found in Table E-2 for the reactions of Cl-atoms with NO_2. These reactants may come together to form either $ClNO_2$ or ClONO. Whether or not isomer formation, such as discussed above, is important depends on the relative stability of the possible products. At the moment the only case that we are sure about is the above example. In the past however, there was some thought that data on the reaction between ClO radicals and NO_2 could be understood only in terms of the formation of both chlorine nitrate ($ClONO_2$) and other isomers (ClOONO, OClONO). Experiments have shown that this is not the case and that chlorine nitrate is the sole product.

There are many other possibilities for isomer formation in the reactions listed in Table E-2. Even for reactions where no mention is made of isomers, because we felt that they could not contribute under atmospheric conditions, extrapolation to higher pressures and lower temperatures should be done with the possibilities kept in mind.

E.5.3 Uncertainty Estimates

For second-order rate constants in Table E-1, an estimate of the uncertainty at any given temperature may be obtained from the following expression:

$$f(T) = f(298)\exp((\Delta E/R)(1/T - 1/298))$$

An upper or lower bound (corresponding approximately to one standard deviation) of the rate constant at any temperature T can be obtained by multiplying or dividing the value of the rate constant at that temperature by the factor f(T). The quantities f(298) and $\Delta E/R$ are,

respectively, the uncertainty in the rate constant at 298 K and in the Arrhenius temperature coefficient, as listed in Table E-1. This approach is based on the fact that rate constants are almost always known with minimum uncertainty at room temperature. The overall uncertainty normally increases at other temperatures, because there are usually fewer data and it is almost always more difficult to make measurements at other temperatures. It is important to note that the uncertainty at a temperature T cannot be calculated from the expression $\exp(\Delta E/RT)$. The above expression for f(T) must be used to obtain the correct result.

The uncertainty represented by f(298) is normally symmetric; i.e., the rate constant may be greater than or less than the central value, k(298), by the factor f(298). In a few cases in Table E-1 asymmetric uncertainties are given in the temperature coefficient.

For three-body reactions (Table E-2) a somewhat analogous procedure is used. Uncertainties expressed as increments to k_0 and k_∞ are given for these rate constants at room temperature. The additional uncertainty arising from the temperature extrapolation is expressed as an uncertainty in the temperature coefficients n and m.

The assigned uncertainties represent the subjective judgment of the Panel. They are not determined by a rigorous, statistical analysis of the data base, which generally is too limited to permit such an analysis. Rather, the uncertainties are based on a knowledge of the techniques, the difficulties of the experiments, and the potential for systematic errors. There is obviously no way to quantify these "unknown" errors. The spread in results among different techniques for a given reaction may provide some basis for an uncertainty, but the possibility of the same, or compensating, systematic errors in all the studies must be recognized. Furthermore, the probability distribution may not follow the normal, Gaussian form. For measurements subject to large systematic errors, the true rate constant may be much further from the recommended value than would be expected based on a Gaussian distribution with the stated uncertainty. As an example, the recommended rate constants for the reactions $HO_2 + NO$ and $Cl + ClONO_2$ have changed by factors of 30-50, occurrences which could not have been allowed for with any reasonable values of σ in a Gaussian distribution.

E.5.4 Units

The rate constants are given in units of concentration expressed as molecules per cubic centimeter and time in seconds. Thus, for first-, second-, and third-order reactions the units of k are s^{-1}, cm^3 $molecule^{-1}$ s^{-1}, and cm^6 $molecule^{-2}$ s^{-1}, respectively. Cross sections are expressed as cm^2 $molecule^{-1}$, base e.

Table E-1. Rate Constants for Second Order Reactions[a]

Reaction	A-Factor[a]	E/R±(ΔE/R)	k(298 K)	f(298)[b]
		O_x Reactions		
$O + O_2 \xrightarrow{M} O_3$	(See Table 2)			
$O + O_3 \rightarrow O_2 + O_2$	8.0×10^{-12}	2060±250	8.0×10^{-15}	1.15
		$O(^1D)$ Reactions		
$O(^1D) + N_2O \rightarrow N_2 + O_2$	4.9×10^{-11}	0±100	4.9×10^{-11}	1.3
$\rightarrow NO + NO$	6.7×10^{-11}	0±100	6.7×10^{-11}	1.3
& $O(^1D) + H_2O \rightarrow OH + OH$	2.2×10^{-10}	0±100	2.2×10^{-10}	1.2
$O(^1D) + CH_4 \rightarrow OH + CH_3$	1.4×10^{-10}	0±100	1.4×10^{-10}	1.2
$\rightarrow H_2 + CH_2O$	1.4×10^{-11}	0±100	1.4×10^{-11}	1.2
$O(^1D) + H_2 \rightarrow OH + H$	1.0×10^{-10}	0±100	1.0×10^{-10}	1.2
$O(^1D) + N_2 \rightarrow O + N_2$	2.8×10^{-11}	-(110±100)	2.6×10^{-11}	1.2
$O(^1D) + N_2 \xrightarrow{M} N_2O$	(See Table 2)			
$O(^1D) + O_2 \rightarrow O + O_2$	3.2×10^{-11}	-(70±100)	4.0×10^{-11}	1.2
$O(^1D) + CO_2 \rightarrow O + CO_2$	7.4×10^{-11}	-(120±100)	1.1×10^{-10}	1.2
$O(^1D) + O_3 \rightarrow O_2 + O_2$	1.2×10^{-10}	0±100	1.2×10^{-10}	1.3
$\rightarrow O_2 + O + O$	1.2×10^{-10}	0±100	1.2×10^{-10}	1.3
& $O(^1D) + HCl \rightarrow$ products	1.5×10^{-10}	0±100	1.5×10^{-10}	1.2
$O(^1D) + HF \rightarrow OH + F$	1.4×10^{-10}	0±100	1.4×10^{-10}	2.0
# $O(^1D) + HBr \rightarrow$ products	1.5×10^{-10}	0±100	1.5×10^{-10}	2.0
# $O(^1D) + Cl_2 \rightarrow$ products	2.8×10^{-10}	0±100	2.8×10^{-10}	2.0
$O(^1D) + CCl_4 \rightarrow$ products	3.3×10^{-10}	0±100	3.3×10^{-10}	1.2

[a] Units are cm^3/molecule-sec.

[b] f(298) is the uncertainty at 298K. To calculate the uncertainty at other temperatures, use the expression: $f(T) = f(298) \exp \left| \frac{\Delta E}{R} \left(\frac{1}{T} - \frac{1}{298} \right) \right|$. Note that the exponent is absolute value.

* Indicates a change from the previous Panel evaluation (JPL 85-37). Small round-off changes have been made for several entries in the table; these are not marked by asterisks.

\# Indicates a new entry that was not in the previous evaluation.

& Indicates a change in the Note.

Table E-1. (Continued)

Reaction	A-Factor[a]	E/R±(ΔE/R)	k(298 K)	f(298)[b]
$O(^1D) + CFCl_3 \rightarrow$ products	2.3×10^{-10}	0±100	2.3×10^{-10}	1.2
$O(^1D) + CF_2Cl_2 \rightarrow$ products	1.4×10^{-10}	0±100	1.4×10^{-10}	1.3
$O(^1D) + CF_4 \rightarrow CF_4 + O$	1.8×10^{-13}	0±100	1.8×10^{-13}	2.0
$O(^1D) + CCl_2O \rightarrow$ products	3.6×10^{-10}	0±100	3.6×10^{-10}	2.0
$O(^1D) + CFClO \rightarrow$ products	1.9×10^{-10}	0±100	1.9×10^{-10}	2.0
$O(^1D) + CF_2O \rightarrow$ products	7.4×10^{-11}	0±100	7.4×10^{-11}	2.0
$O(^1D) + NH_3 \rightarrow OH + NH_2$	2.5×10^{-10}	0±100	2.5×10^{-10}	1.3
		HO_x Reactions		
$H + O_2 \xrightarrow{M} HO_2$	(See Table 2)			
$H + O_3 \rightarrow OH + O_2$	1.4×10^{-10}	470±200	2.9×10^{-11}	1.25
* $H + HO_2 \rightarrow$ products	8.1×10^{-11}	0±200	8.1×10^{-11}	1.3
$O + OH \rightarrow O_2 + H$	2.2×10^{-11}	-(120±100)	3.3×10^{-11}	1.2
& $O + HO_2 \rightarrow OH + O_2$	3.0×10^{-11}	-(200±100)	5.9×10^{-11}	1.2
$O + H_2O_2 \rightarrow OH + HO_2$	1.4×10^{-12}	2000±1000	1.7×10^{-15}	2.0
* $OH + HO_2 \rightarrow H_2O + O_2$	4.6×10^{-11}	-(230±200)	1.0×10^{-10}	1.3
& $OH + O_3 \rightarrow HO_2 + O_2$	1.6×10^{-12}	940±300	6.8×10^{-14}	1.3
$OH + OH \rightarrow H_2O + O$	4.2×10^{-12}	240±240	1.9×10^{-12}	1.4
$\xrightarrow{M} H_2O_2$	(See Table 2)			
$OH + H_2O_2 \rightarrow H_2O + HO_2$	3.3×10^{-12}	$200\pm^{100}_{300}$	1.7×10^{-12}	1.3
$OH + H_2 \rightarrow H_2O + H$	5.5×10^{-12}	2000±400	6.7×10^{-15}	1.2

[a] Units are cm^3/molecule-sec.

[b] f(298) is the uncertainty at 298K. To calculate the uncertainty at other temperatures, use the expression: $f(T) = f(298) \exp\left|\frac{\Delta E}{R}\left(\frac{1}{T} - \frac{1}{298}\right)\right|$. Note that the exponent is absolute value.

* Indicates a change from the previous Panel evaluation (JPL 85-37). Small round-off changes have been made for several entries in the table; these are not marked by asterisks.

\# Indicates a new entry that was not in the previous evaluation.

& Indicates a change in the Note.

Table E-1. (Continued)

Reaction	A-Factor[a]	E/R±(ΔE/R)	k(298 K)	f(298)[b]
& $HO_2 + HO_2 \rightarrow H_2O_2 + O_2$	2.3×10^{-13}	-(600±200)	1.7×10^{-12}	1.3
$\xrightarrow{M} H_2O_2 + O_2$	1.7×10^{-33}[M]	-(1000±400)	4.9×10^{-32}[M]	1.3
* $HO_2 + O_3 \rightarrow OH + 2O_2$	1.1×10^{-14}	$500\pm^{500}_{100}$	2.0×10^{-15}	1.3
		NO_x Reactions		
$N + O_2 \rightarrow NO + O$	4.1×10^{-12}	3200±400	8.9×10^{-17}	1.25
$N + O_3 \rightarrow NO + O_2$	-	-	$<1.0\times10^{-15}$	-
$N + NO \rightarrow N_2 + O$	3.4×10^{-11}	0±100	3.4×10^{-11}	1.3
& $N + NO_2 \rightarrow N_2O + O$	-	-	3.0×10^{-12}	3.0
$O + NO \xrightarrow{M} NO_2$	(See Table 2)			
* $O + NO_2 \rightarrow NO + O_2$	6.5×10^{-12}	-(120±120)	9.7×10^{-12}	1.1
$O + NO_2 \xrightarrow{M} NO_3$	(See Table 2)			
$O + NO_3 \rightarrow O_2 + NO_2$	1.0×10^{-11}	0±150	1.0×10^{-11}	1.5
$O + N_2O_5 \rightarrow$ products	-	-	$<3.0\times10^{-16}$	-
$O + HNO_3 \rightarrow OH + NO_3$	-	-	$<3.0\times10^{-17}$	-
$O + HO_2NO_2 \rightarrow$ products	7.8×10^{-11}	3400±750	8.6×10^{-16}	3.0
$O_3 + NO \rightarrow NO_2 + O_2$	2.0×10^{-12}	1400±200	1.8×10^{-14}	1.2
& $NO + HO_2 \rightarrow NO_2 + OH$	3.7×10^{-12}	-(240±80)	8.3×10^{-12}	1.2
* $NO + NO_3 \rightarrow 2NO_2$	1.7×10^{-11}	-(150±100)	2.9×10^{-11}	1.3
$OH + NO \xrightarrow{M} HONO$	(See Table 2)			
$OH + NO_2 \xrightarrow{M} HNO_3$	(See Table 2)			

[a] Units are cm^3/molecule-sec.

[b] f(298) is the uncertainty at 298K. To calculate the uncertainty at other temperatures, use the expression: $f(T) = f(298) \exp\left|\frac{\Delta E}{R}\left(\frac{1}{T} - \frac{1}{298}\right)\right|$. Note that the exponent is absolute value.

* Indicates a change from the previous Panel evaluation (JPL 85-37). Small round-off changes have been made for several entries in the table; these are not marked by asterisks.

\# Indicates a new entry that was not in the previous evaluation.

& Indicates a change in the Note.

Table E-1. (Continued)

Reaction	A-Factor[a]	E/R±(ΔE/R)	k(298 K)	f(298)[b]
& $OH + HNO_3 \rightarrow H_2O + NO_3$	(See Note C13 and ≠ below)			1.3
& $OH + HO_2NO_2 \rightarrow$ products	1.3×10^{-12}	$-(380\pm^{270}_{500})$	4.6×10^{-12}	1.5
$HO_2 + NO_2 \xrightarrow{M} HO_2NO_2$	(See Table 2)			
$O_3 + NO_2 \rightarrow NO_3 + O_2$	1.4×10^{-13}	2500±140	3.2×10^{-17}	1.15
$O_3 + HNO_2 \rightarrow O_2 + HNO_3$	-	-	$<5.0\times10^{-19}$	-
$NO_2 + NO_3 \xrightarrow{M} N_2O_5$	(See Table 2)			
& $N_2O_5 + H_2O \rightarrow 2HNO_3$	-	-	$<2.0\times10^{-21}$	-
& $OH + NH_3 \rightarrow H_2O + NH_2$	3.6×10^{-12}	930±200	1.6×10^{-13}	1.4
$NH_2 + HO_2 \rightarrow$ products	-	-	3.4×10^{-11}	2.0
& $NH_2 + NO \rightarrow$ products	3.8×10^{-12}	-(450±150)	1.7×10^{-11}	2.0
& $NH_2 + NO_2 \rightarrow$ products	2.1×10^{-12}	-(650±250)	1.9×10^{-11}	3.0
& $NH_2 + O_2 \rightarrow$ products	-	-	$<3.0\times10^{-18}$	-
$NH_2 + O_3 \rightarrow$ products	4.8×10^{-12}	930±500	2.1×10^{-13}	3.0
	Hydrocarbon Reactions			
* $OH + CO \rightarrow CO_2 + H$	$1.5\times10^{-13}(1+0.6P_{atm})$	0±300	$1.5\times10^{-13}(1+0.6P_{atm})$	1.3
$OH + CH_4 \rightarrow CH_3 + H_2O$	2.3×10^{-12}	1700±200	7.7×10^{-15}	1.2
# $OH + {}^{13}CH_4 \rightarrow {}^{13}CH_3 + H_2O$	(See Note)			
$OH + C_2H_6 \rightarrow H_2O + C_2H_5$	1.1×10^{-11}	1100±200	2.8×10^{-13}	1.2

[a] Units are cm^3/molecule-sec.

[b] f(298) is the uncertainty at 298K. To calculate the uncertainty at other temperatures, use the expression: $f(T) = f(298)\ \exp\left|\frac{\Delta E}{R}\left(\frac{1}{T}-\frac{1}{298}\right)\right|$. Note that the exponent is absolute value.

* Indicates a change from the previous Panel evaluation (JPL 85-37). Small round-off changes have been made for several entries in the table; these are not marked by asterisks.

\# Indicates a new entry that was not in the previous evaluation.

& Indicates a change in the Note.

≠ $OH + HNO_3$ pressure and temperature dependence fit by

$$k(M,T) = k_o + \frac{k_3[M]}{1 + \frac{k_3[M]}{k_2}}$$ with $k_o = 7.2 \times 10^{-15}\ \exp(785/T)$, $k_2 = 4.1 \times 10^{-16}\ \exp(1440/T)$, $k_3 = 1.9 \times 10^{-33}\ \exp(725/T)$

Table E-1. (Continued)

Reaction	A-Factor[a]	E/R±(ΔE/R)	k(298 K)	f(298)[b]
* $OH + C_3H_8 \rightarrow H_2O + C_3H_7$	$1.4x10^{-11}$	750±200	$1.1x10^{-12}$	1.3
$OH + C_2H_4 \rightarrow$ products	(See Table 2)			
$OH + C_2H_2 \rightarrow$ products	(See Table 2)			
$OH + H_2CO \rightarrow H_2O + HCO$	$1.0x10^{-11}$	0±200	$1.0x10^{-11}$	1.25
# $OH + CH_3CHO \rightarrow CH_3CO + H_2O$	$6.0x10^{-12}$	-(250±200)	$1.4x10^{-11}$	1.4
$OH + CH_3OOH \rightarrow$ products	$1.0x10^{-11}$	0±200	$1.0x10^{-11}$	2.0
$OH + HCN \rightarrow$ products	$1.2x10^{-13}$	400±150	$3.1x10^{-14}$	3.0
$OH + CH_3CN \rightarrow$ products	$4.5x10^{-13}$	900±400	$2.2x10^{-14}$	2.0
$HO_2 + CH_2O \rightarrow$ adduct	-	-	$4.5x10^{-14}$	10.0
# $O + HCN \rightarrow$ products	$1.0x10^{-11}$	4000±1000	$1.5x10^{-17}$	10.0
$O + C_2H_2 \rightarrow$ products	$3.0x10^{-11}$	1600±250	$1.4x10^{-13}$	1.3
$O + H_2CO \rightarrow$ products	$3.4x10^{-11}$	1600±250	$1.6x10^{-13}$	1.25
# $O + CH_3CHO \rightarrow CH_3CO + OH$	$1.8x10^{-11}$	1100±200	$4.5x10^{-13}$	1.25
$O + CH_3 \rightarrow$ products	$1.1x10^{-10}$	0±250	$1.1x10^{-10}$	1.3
$CH_3 + O_2 \rightarrow$ products	-	-	$<3.0x10^{-16}$	-
$CH_3 + O_2 \xrightarrow{M} CH_3O_2$	(See Table 2)			
* $CH_2OH + O_2 \rightarrow CH_2O + HO_2$	$9.6x10^{-12}$	0±500	$9.6x10^{-12}$	1.3
* $CH_3O + O_2 \rightarrow CH_2O + HO_2$	$3.9x10^{-14}$	900±300	$1.9x10^{-15}$	1.5
$HCO + O_2 \rightarrow CO + HO_2$	$3.5x10^{-12}$	-(140±140)	$5.5x10^{-12}$	1.3
$CH_3 + O_3 \rightarrow$ products	$5.4x10^{-12}$	220±150	$2.6x10^{-12}$	2.0
* $CH_3O_2 + O_3 \rightarrow$ products	-	-	$<3.0x10^{-17}$	-

[a] Units are cm^3/molecule-sec.

[b] f(298) is the uncertainty at 298K. To calculate the uncertainty at other temperatures, use the expression: $f(T) = f(298) \exp\left|\frac{\Delta E}{R}\left(\frac{1}{T} - \frac{1}{298}\right)\right|$. Note that the exponent is absolute value.

* Indicates a change from the previous Panel evaluation (JPL 85-37). Small round-off changes have been made for several entries in the table; these are not marked by asterisks.

\# Indicates a new entry that was not in the previous evaluation.

& Indicates a change in the Note.

Table E-1. (Continued)

Reaction	A-Factor[a]	E/R±(ΔE/R)	k(298 K)	f(298)[b]
* $CH_3O_2 + CH_3O_2 \rightarrow$ products	1.9×10^{-13}	-(220±220)	4.0×10^{-13}	1.5
$CH_3O_2 + NO \rightarrow CH_3O + NO_2$	4.2×10^{-12}	-(180±180)	7.6×10^{-12}	1.2
$CH_3O_2 + NO_2 \xrightarrow{M} CH_3O_2NO_2$	(See Table 2)			
$CH_3O_2 + HO_2 \rightarrow CH_3OOH + O_2$	7.7×10^{-14}	$-(1300\pm^{500}_{1300})$	6.0×10^{-12}	3.0
* $NO_3 + CO \rightarrow$ products	-	-	$<4.0\times10^{-19}$	-
$NO_3 + CH_2O \rightarrow$ products	-	-	6.0×10^{-16}	1.5
# $NO_3 + CH_3CHO \rightarrow$ products	1.4×10^{-12}	1900±300	2.4×10^{-15}	1.3
		<u>ClO_x Reactions</u>		
& $Cl + O_3 \rightarrow ClO + O_2$	2.9×10^{-11}	260±100	1.2×10^{-11}	1.15
$Cl + H_2 \rightarrow HCl + H$	3.7×10^{-11}	2300±200	1.6×10^{-14}	1.25
$Cl + CH_4 \rightarrow HCl + CH_3$	1.1×10^{-11}	1400±150	1.0×10^{-13}	1.1
$Cl + C_2H_6 \rightarrow HCl + C_2H_5$	7.7×10^{-11}	90±90	5.7×10^{-11}	1.1
$Cl + C_3H_8 \rightarrow HCl + C_3H_7$	1.4×10^{-10}	-(40±250)	1.6×10^{-10}	1.5
$Cl + C_2H_2 \rightarrow$ products	(See Table 2)			
* $Cl + CH_3OH \rightarrow CH_2OH + HCl$	5.7×10^{-11}	0±250	5.7×10^{-11}	1.5
$Cl + CH_3Cl \rightarrow CH_2Cl + HCl$	3.3×10^{-11}	1250±200	4.9×10^{-13}	1.2
$Cl + CH_3CN \rightarrow$ products	-	-	$<2.0\times10^{-15}$	-
$Cl + CH_3CCl_3 \rightarrow CH_2CCl_3 + HCl$	-	-	$<4.0\times10^{-14}$	-
$Cl + H_2CO \rightarrow HCl + HCO$	8.1×10^{-11}	30±100	7.3×10^{-11}	1.15
$Cl + H_2O_2 \rightarrow HCl + HO_2$	1.1×10^{-11}	980±500	4.1×10^{-13}	1.5
& $Cl + HOCl \rightarrow Cl_2 + OH$	3.0×10^{-12}	130±250	1.9×10^{-12}	2.0

[a] Units are cm^3/molecule-sec.

[b] f(298) is the uncertainty at 298K. To calculate the uncertainty at other temperatures, use the expression: $f(T) = f(298) \exp\left|\frac{\Delta E}{R}\left(\frac{1}{T} - \frac{1}{298}\right)\right|$. Note that the exponent is absolute value.

* Indicates a change from the previous Panel evaluation (JPL 85-37). Small round-off changes have been made for several entries in the table; these are not marked by asterisks.

\# Indicates a new entry that was not in the previous evaluation.

& Indicates a change in the Note.

Table E-1. (Continued)

Reaction	A-Factor[a]	E/R±(ΔE/R)	k(298 K)	f(298)[b]
$Cl + HNO_3 \rightarrow$ products	-	-	$<1.7\times10^{-14}$	-
& $Cl + HO_2 \rightarrow HCl + O_2$	1.8×10^{-11}	-(170±200)	3.2×10^{-11}	1.5
$\rightarrow OH + ClO$	4.1×10^{-11}	450±200	9.1×10^{-12}	2.0
$Cl + Cl_2O \rightarrow Cl_2 + ClO$	9.8×10^{-11}	0±250	9.8×10^{-11}	1.2
$Cl + OClO \rightarrow ClO + ClO$	5.9×10^{-11}	0±250	5.9×10^{-11}	1.25
$Cl + ClONO_2 \rightarrow$ products	6.8×10^{-12}	-(160±200)	1.2×10^{-11}	1.3
$Cl + NO \xrightarrow{M} NOCl$	(See Table 2)			
$Cl + NO_2 \xrightarrow{M} ClONO\ (ClNO_2)$	(See Table 2)			
* $Cl + NO_3 \rightarrow ClO + NO_2$	5.2×10^{-11}	0±400	5.2×10^{-11}	2.0
# $Cl + N_2O \rightarrow ClO + N_2$	(See Note)			
* $Cl + ClNO \rightarrow NO + Cl_2$	6.0×10^{-11}	$0\pm^{500}_{250}$	6.0×10^{-11}	2.0
$Cl + O_2 \xrightarrow{M} ClOO$	(See Table 2)			
$Cl + ClOO \rightarrow Cl_2 + O_2$	1.4×10^{-10}	0±250	1.4×10^{-10}	3.0
$\rightarrow ClO + ClO$	8.0×10^{-12}	0±250	8.0×10^{-12}	3.0
* $ClO + O \rightarrow Cl + O_2$	3.0×10^{-11}	-(70±70)	3.8×10^{-11}	1.2
$ClO + NO \rightarrow NO_2 + Cl$	6.4×10^{-12}	-(290±100)	1.7×10^{-11}	1.15
$ClO + NO_2 \xrightarrow{M} ClONO_2$	(See Table 2)			
$ClO + NO_3 \rightarrow$ products	4.0×10^{-13}	0±400	4.0×10^{-13}	2.0
& $ClO + HO_2 \rightarrow HOCl + O_2$	4.8×10^{-13}	$-(700\pm^{250}_{700})$	5.0×10^{-12}	1.4
$ClO + H_2CO \rightarrow$ products	$\sim1.0\times10^{-12}$	>2100	$<1.0\times10^{-15}$	-
* $ClO + OH \rightarrow$ products	1.1×10^{-11}	-(120±150)	1.7×10^{-11}	1.5

[a] Units are cm^3/molecule-sec.

[b] f(298) is the uncertainty at 298K. To calculate the uncertainty at other temperatures, use the expression: $f(T) = f(298) \exp\left|\frac{\Delta E}{R}\left(\frac{1}{T} - \frac{1}{298}\right)\right|$. Note that the exponent is absolute value.

* Indicates a change from the previous Panel evaluation (JPL 85-37). Small round-off changes have been made for several entries in the table; these are not marked by asterisks.

\# Indicates a new entry that was not in the previous evaluation.

& Indicates a change in the Note.

Table E-1. (Continued)

Reaction	A-Factor[a]	E/R±(ΔE/R)	k(298 K)	f(298)[b]
$ClO + CH_4 \rightarrow$ products	$\sim 1.0 \times 10^{-12}$	>3700	$<4.0 \times 10^{-18}$	-
$ClO + H_2 \rightarrow$ products	$\sim 1.0 \times 10^{-12}$	>4800	$<1.0 \times 10^{-19}$	-
$ClO + CO \rightarrow$ products	$\sim 1.0 \times 10^{-12}$	>3700	$<4.0 \times 10^{-18}$	-
$ClO + N_2O \rightarrow$ products	$\sim 1.0 \times 10^{-12}$	>4300	$<6.0 \times 10^{-19}$	-
* $ClO + ClO \rightarrow$ products	8.0×10^{-13}	1250±500	1.2×10^{-14}	2.0
$ClO + O_3 \rightarrow ClOO + O_2$	1.0×10^{-12}	>4000	$<1.0 \times 10^{-18}$	-
$\rightarrow OClO + O_2$	1.0×10^{-12}	>4000	$<1.0 \times 10^{-18}$	-
* $OH + Cl_2 \rightarrow HOCl + Cl$	1.4×10^{-12}	900±400	6.7×10^{-14}	1.2
& $OH + HCl \rightarrow H_2O + Cl$	2.6×10^{-12}	350±100	8.0×10^{-13}	1.3
* $OH + HOCl \rightarrow H_2O + ClO$	3.0×10^{-12}	500±500	5.0×10^{-13}	3.0
$OH + CH_3Cl \rightarrow CH_2Cl + H_2O$	1.7×10^{-12}	1100±200	4.3×10^{-14}	1.2
$OH + CH_2Cl_2 \rightarrow CHCl_2 + H_2O$	4.7×10^{-12}	1050±200	1.4×10^{-13}	1.2
$OH + CHCl_3 \rightarrow CCl_3 + H_2O$	3.4×10^{-12}	1050±200	1.0×10^{-13}	1.2
$OH + CHFCl_2 \rightarrow CFCl_2 + H_2O$	8.6×10^{-13}	1000±200	3.0×10^{-14}	1.3
$OH + CHF_2Cl \rightarrow CF_2Cl + H_2O$	8.3×10^{-13}	1550±200	4.6×10^{-15}	1.2
$OH + CH_2ClF \rightarrow CHClF + H_2O$	2.1×10^{-12}	1150±150	4.4×10^{-14}	1.2
$OH + CH_3CCl_3 \rightarrow CH_2CCl_3 + H_2O$	5.0×10^{-12}	1800±200	1.2×10^{-14}	1.3
# $OH + CH_3CF_2Cl \rightarrow CH_2CF_2Cl + H_2O$	1.5×10^{-12}	1800±200	3.6×10^{-15}	1.3
# $OH + CH_3CHF_2 \rightarrow$ products	1.9×10^{-12}	1200±300	3.4×10^{-14}	1.3
# $OH + CHCl_2CF_3 \rightarrow CCl_2CF_3 + H_2O$	1.1×10^{-12}	1050±300	3.2×10^{-14}	1.3
# $OH + CHClFCF_3 \rightarrow CClFCF_3 + H_2O$	7.2×10^{-13}	1250±300	1.1×10^{-14}	1.3

[a] Units are cm^3/molecule-sec.

[b] f(298) is the uncertainty at 298K. To calculate the uncertainty at other temperatures, use the expression: $f(T) = f(298) \exp\left|\frac{\Delta E}{R}\left(\frac{1}{T} - \frac{1}{298}\right)\right|$. Note that the exponent is absolute value.

* Indicates a change from the previous Panel evaluation (JPL 85-37). Small round-off changes have been made for several entries in the table; these are not marked by asterisks.

\# Indicates a new entry that was not in the previous evaluation.

& Indicates a change in the Note.

Table E-1. (Continued)

Reaction	A-Factor[a]	E/R±(ΔE/R)	k(298 K)	f(298)[b]
# $OH + CH_2ClCClF_2 \rightarrow CHClCClF_2 + H_2O$	3.4×10^{-12}	1600±300	1.6×10^{-14}	2.0
# $OH + CH_2FCF_3 \rightarrow CHFCF_3 + H_2O$	6.6×10^{-13}	1300±300	8.4×10^{-15}	1.5
# $OH + CH_3CCl_2F \rightarrow CH_2CCl_2F + H_2O$	3.4×10^{-12}	1800±500	8.0×10^{-15}	3.0
$OH + C_2Cl_4 \rightarrow$ products	9.4×10^{-12}	1200±200	1.7×10^{-13}	1.25
$OH + C_2HCl_3 \rightarrow$ products	4.9×10^{-13}	-(450±200)	2.2×10^{-12}	1.25
$OH + CFCl_3 \rightarrow$ products	$\sim1.0\times10^{-12}$	>3700	$<5.0\times10^{-18}$	-
$OH + CF_2Cl_2 \rightarrow$ products	$\sim1.0\times10^{-12}$	>3500	$<6.0\times10^{-18}$	-
$OH + ClONO_2 \rightarrow$ products	1.2×10^{-12}	330±200	3.9×10^{-13}	1.5
$O + HCl \rightarrow OH + Cl$	1.0×10^{-11}	3300±350	1.5×10^{-16}	2.0
$O + HOCl \rightarrow OH + ClO$	1.0×10^{-11}	2200±1000	6.0×10^{-15}	10.0
$O + ClONO_2 \rightarrow$ products	2.9×10^{-12}	800±200	2.0×10^{-13}	1.5
$O + Cl_2O \rightarrow ClO + ClO$	2.9×10^{-11}	630±200	3.5×10^{-12}	1.4
$O + OClO \rightarrow ClO + O_2$	2.8×10^{-11}	1200±300	5.0×10^{-13}	2.0
# $OH + OClO \rightarrow HOCl + O_2$	4.5×10^{-13}	-(800±200)	6.8×10^{-12}	2.0
$NO + OClO \rightarrow NO_2 + ClO$	2.5×10^{-12}	600±300	3.4×10^{-13}	2.0
* $HCl + ClONO_2 \rightarrow$ products	-	-	$<1.0\times10^{-20}$	-
$HCl + HO_2NO_2 \rightarrow$ products	-	-	$<1.0\times10^{-20}$	-
# $H_2O + ClONO_2 \rightarrow$ products	-	-	$<2.0\times10^{-21}$	-
		BrO_x Reactions		
* $Br + O_3 \rightarrow BrO + O_2$	1.7×10^{-11}	800±200	1.2×10^{-12}	1.2
* $Br + H_2O_2 \rightarrow HBr + HO_2$	1.0×10^{-11}	>3000	$<5.0\times10^{-16}$	-

[a] Units are cm^3/molecule-sec.

[b] f(298) is the uncertainty at 298K. To calculate the uncertainty at other temperatures, use the expression: $f(T) = f(298) \exp\left|\frac{\Delta E}{R}\left(\frac{1}{T} - \frac{1}{298}\right)\right|$. Note that the exponent is absolute value.

* Indicates a change from the previous Panel evaluation (JPL 85-37). Small round-off changes have been made for several entries in the table; these are not marked by asterisks.

\# Indicates a new entry that was not in the previous evaluation.

& Indicates a change in the Note.

Table E-1. (Continued)

Reaction	A-Factor[a]	E/R±(ΔE/R)	k(298 K)	f(298)[b]
$Br + H_2CO \rightarrow HBr + HCO$	1.7×10^{-11}	800±200	1.1×10^{-12}	1.3
* $Br + HO_2 \rightarrow HBr + O_2$	1.5×10^{-11}	600±600	2.0×10^{-12}	2.0
# $Br + Cl_2O \rightarrow BrCl + ClO$	-	-	3.8×10^{-12}	2.0
$BrO + O \rightarrow Br + O_2$	3.0×10^{-11}	0±250	3.0×10^{-11}	3.0
& $BrO + ClO \rightarrow Br + OClO$	6.7×10^{-12}	0±250	6.7×10^{-12}	1.5
$\rightarrow Br + ClOO$	6.7×10^{-12}	0±250	6.7×10^{-12}	1.5
$BrO + NO \rightarrow NO_2 + Br$	8.8×10^{-12}	-(260±130)	2.1×10^{-11}	1.15
$BrO + NO_2 \xrightarrow{M} BrONO_2$	(See Table 2)			
$BrO + BrO \rightarrow 2\ Br + O_2$	1.4×10^{-12}	-(150±150)	2.3×10^{-12}	1.25
$\rightarrow Br_2 + O_2$	6.0×10^{-14}	-(600±600)	4.4×10^{-13}	1.25
$BrO + O_3 \rightarrow Br + 2O_2$	$\sim1.0\times10^{-12}$	>1600	$<5.0\times10^{-15}$	-
$BrO + HO_2 \rightarrow$ products	-	-	5.0×10^{-12}	3.0
$BrO + OH \rightarrow$ products	-	-	1.0×10^{-11}	5.0
* $OH + Br_2 \rightarrow HOBr + Br$	4.2×10^{-11}	0±600	4.2×10^{-11}	1.3
& $OH + HBr \rightarrow H_2O + Br$	1.1×10^{-11}	0±250	1.1×10^{-11}	1.2
$OH + CH_3Br \rightarrow CH_2Br + H_2O$	6.0×10^{-13}	820±200	3.8×10^{-14}	1.25
$O + HBr \rightarrow OH + Br$	6.7×10^{-12}	1550±200	3.7×10^{-14}	1.3
		FO_x Reactions		
$F + O_3 \rightarrow FO + O_2$	2.8×10^{-11}	230±200	1.3×10^{-11}	2.0
$F + H_2 \rightarrow HF + H$	1.5×10^{-10}	520±250	2.7×10^{-11}	1.3
$F + CH_4 \rightarrow HF + CH_3$	3.0×10^{-10}	400±300	8.0×10^{-11}	1.5

[a] Units are cm^3/molecule-sec.

[b] f(298) is the uncertainty at 298K. To calculate the uncertainty at other temperatures, use the expression: $f(T) = f(298) \exp\left|\frac{\Delta E}{R}\left(\frac{1}{T} - \frac{1}{298}\right)\right|$. Note that the exponent is absolute value.

* Indicates a change from the previous Panel evaluation (JPL 85-37). Small round-off changes have been made for several entries in the table; these are not marked by asterisks.

# Indicates a new entry that was not in the previous evaluation.

& Indicates a change in the Note.

Table E-1. (Continued)

Reaction	A-Factor[a]	E/R±(ΔE/R)	k(298 K)	f(298)[b]
* $F + H_2O \rightarrow HF + OH$	4.6×10^{-11}	400±200	1.2×10^{-11}	1.5
$F + O_2 \xrightarrow{M} FO_2$	(See Table 2)			
$F + NO \xrightarrow{M} FNO$	(See Table 2)			
$F + NO_2 \xrightarrow{M} FNO_2(FONO)$	(See Table 2)			
$NO + FO \rightarrow NO_2 + F$	2.6×10^{-11}	0±250	2.6×10^{-11}	2.0
$FO + FO \rightarrow 2\ F + O_2$	1.5×10^{-11}	0±250	1.5×10^{-11}	3.0
$FO + O_3 \rightarrow F + 2\ O_2$	(See Note)			
$\rightarrow FO_2 + O_2$	(See Note)			
$FO + NO_2 \xrightarrow{M} FONO_2$	(See Table 2)			
$O + FO \rightarrow F + O_2$	5.0×10^{-11}	0±250	5.0×10^{-11}	3.0
$O + FO_2 \rightarrow FO + O_2$	5.0×10^{-11}	0±250	5.0×10^{-11}	5.0
$CF_3O_2 + NO \rightarrow CF_3O + NO_2$	3.9×10^{-12}	-(400±200)	1.5×10^{-11}	1.3
$CF_2ClO_2 + NO \rightarrow CF_2ClO + NO_2$	3.1×10^{-12}	-(500±200)	1.6×10^{-11}	1.3
$CFCl_2O_2 + NO \rightarrow CFCl_2O + NO_2$	3.5×10^{-12}	-(430±200)	1.5×10^{-11}	1.3
$CCl_3O_2 + NO \rightarrow CCl_3O + NO_2$	5.7×10^{-12}	-(330±200)	1.7×10^{-11}	1.3
		SO_x Reactions		
& $OH + H_2S \rightarrow SH + H_2O$	5.9×10^{-12}	70±70	4.7×10^{-12}	1.2
* $OH + OCS \rightarrow$ products	1.1×10^{-13}	1200±500	1.9×10^{-15}	2.0
& $OH + CS_2 \rightarrow$ products	(See Note)	-	-	-
$OH + SO_2 \xrightarrow{M} HOSO_2$	(See Table 2)			
$O + H_2S \rightarrow OH + SH$	9.2×10^{-12}	1800±550	2.2×10^{-14}	1.7

[a] Units are cm^3/molecule-sec.

[b] f(298) is the uncertainty at 298K. To calculate the uncertainty at other temperatures, use the expression: $f(T) = f(298)\ \exp\left|\frac{\Delta E}{R}\left(\frac{1}{T} - \frac{1}{298}\right)\right|$. Note that the exponent is absolute value.

* Indicates a change from the previous Panel evaluation (JPL 85-37). Small round-off changes have been made for several entries in the table; these are not marked by asterisks.

\# Indicates a new entry that was not in the previous evaluation.

& Indicates a change in the Note.

Table E-1. (Continued)

Reaction	A-Factor[a]	E/R±(ΔE/R)	k(298 K)	f(298)[b]
$O + OCS \rightarrow CO + SO$	2.1×10^{-11}	2200±150	1.3×10^{-14}	1.2
$O + CS_2 \rightarrow CS + SO$	3.2×10^{-11}	650±150	3.6×10^{-12}	1.2
$S + O_2 \rightarrow SO + O$	2.3×10^{-12}	0±200	2.3×10^{-12}	1.2
$S + O_3 \rightarrow SO + O_2$	-	-	1.2×10^{-11}	2.0
$S + OH \rightarrow SO + H$	-	-	6.6×10^{-11}	3.0
$SO + O_2 \rightarrow SO_2 + O$	2.6×10^{-13}	2400±500	8.4×10^{-17}	2.0
$SO + O_3 \rightarrow SO_2 + O_2$	3.6×10^{-12}	1100±200	9.0×10^{-14}	1.2
$SO + OH \rightarrow SO_2 + H$	-	-	8.6×10^{-11}	2.0
$SO + NO_2 \rightarrow SO_2 + NO$	1.4×10^{-11}	0±50	1.4×10^{-11}	1.2
* $SO + ClO \rightarrow SO_2 + Cl$	2.8×10^{-11}	0±50	2.8×10^{-11}	1.3
$SO + OClO \rightarrow SO_2 + ClO$	-	-	1.9×10^{-12}	3.0
* $SO + BrO \rightarrow SO_2 + Br$	-	-	5.7×10^{-11}	1.4
$SO_2 + HO_2 \rightarrow$ products	-	-	$<1.0\times10^{-18}$	-
$SO_2 + CH_3O_2 \rightarrow$ products	-	-	$<5.0\times10^{-17}$	-
$SO_2 + NO_2 \rightarrow$ products	-	-	$<2.0\times10^{-26}$	-
$SO_3 + NO_2 \rightarrow$ products	-	-	1.0×10^{-19}	10.0
# $SO_2 + NO_3 \rightarrow$ products	-	-	$<7.0\times10^{-21}$	-
$SO_2 + O_3 \rightarrow SO_3 + O_2$	3.0×10^{-12}	>7000	$<2.0\times10^{-22}$	-
* $Cl + H_2S \rightarrow HCl + SH$	5.7×10^{-11}	0±50	5.7×10^{-11}	1.3
& $Cl + OCS \rightarrow SCl + CO$	-	-	$<1.0\times10^{-16}$	-
$ClO + OCS \rightarrow$ products	-	-	$<2.0\times10^{-16}$	-

[a] Units are cm^3/molecule-sec.

[b] f(298) is the uncertainty at 298K. To calculate the uncertainty at other temperatures, use the expression: $f(T) = f(298) \exp\left|\frac{\Delta E}{R}\left(\frac{1}{T} - \frac{1}{298}\right)\right|$. Note that the exponent is absolute value.

* Indicates a change from the previous Panel evaluation (JPL 85-37). Small round-off changes have been made for several entries in the table; these are not marked by asterisks.

\# Indicates a new entry that was not in the previous evaluation.

& Indicates a change in the Note.

Table E-1. (Continued)

Reaction	A-Factor[a]	E/R±(ΔE/R)	k(298 K)	f(298)[b]
$ClO + SO_2 \rightarrow Cl + SO_3$	-	-	$<4.0\times10^{-18}$	-
$SH + H_2O_2 \rightarrow$ products	-	-	$<5.0\times10^{-15}$	-
$SH + O \rightarrow H + SO$	-	-	1.6×10^{-10}	5.0
* $SH + O_2 \rightarrow OH + SO$	-	-	$<4.0\times10^{-19}$	-
* $SH + O_3 \rightarrow HSO + O_2$	9.7×10^{-12}	280±200	3.8×10^{-12}	1.3
* $SH + NO_2 \rightarrow HSO + NO$	2.9×10^{-11}	-(240±100)	6.5×10^{-11}	1.3
$SH + NO \xrightarrow{M} HSNO$	(See Table 2)			
# $HSO + NO \rightarrow$ products	-	-	$<1.0\times10^{-15}$	-
# $HSO + NO_2 \rightarrow HSO_2 + NO$	-	-	9.6×10^{-12}	2.0
# $HSO + O_2 \rightarrow$ products	-	-	$<2.0\times10^{-17}$	-
$HSO + O_3 \rightarrow$ products	-	-	1.0×10^{-13}	5.0
# $HSO_2 + O_2 \rightarrow HO_2 + SO_2$	-	-	3.0×10^{-13}	3.0
* $HOSO_2 + O_2 \rightarrow HO_2 + SO_3$	1.3×10^{-12}	330±200	4.4×10^{-13}	1.2
# $H_2S + NO_3 \rightarrow$ products	-	-	$<3.0\times10^{-14}$	-
$CS + O_2 \rightarrow OCS + O$	-	-	2.9×10^{-19}	2.0
$CS + O_3 \rightarrow OCS + O_2$	-	-	3.0×10^{-16}	3.0
$CS + NO_2 \rightarrow OCS + NO$	-	-	7.6×10^{-17}	3.0
		Metal Reactions		
$Na + O_2 \xrightarrow{M} NaO_2$	(See Table 2)			
& $Na + O_3 \rightarrow NaO + O_2$	5×10^{-10}	0±400	5.0×10^{-10}	1.5
$\rightarrow NaO_2 + O$	$<3\times10^{-11}$	0±400	$<3.0\times10^{-11}$	-

[a] Units are cm^3/molecule-sec.

[b] f(298) is the uncertainty at 298K. To calculate the uncertainty at other temperatures, use the expression: $f(T) = f(298) \exp\left|\frac{\Delta E}{R}\left(\frac{1}{T} - \frac{1}{298}\right)\right|$. Note that the exponent is absolute value.

* Indicates a change from the previous Panel evaluation (JPL 85-37). Small round-off changes have been made for several entries in the table; these are not marked by asterisks.

\# Indicates a new entry that was not in the previous evaluation.

& Indicates a change in the Note.

Table E-1. (Continued)

Reaction	A-Factor[a]	E/R±(ΔE/R)	k(298 K)	f(298)[b]
# $Na + N_2O \rightarrow NaO + N_2$	$2.4x10^{-10}$	1600±400	$1.1x10^{-12}$	1.3
# $Na + Cl_2 \rightarrow NaCl + Cl$	$7.3x10^{-10}$	0±200	$7.3x10^{-10}$	1.3
# $NaO + O \rightarrow Na + O_2$	$3.7x10^{-10}$	0±400	$3.7x10^{-10}$	3.0
# $NaO + O_2 \xrightarrow{M} NaO_3$	(See Table 2)			
# $NaO + O_3 \rightarrow NaO_2 + O_2$	$1.6x10^{-10}$	0±400	$1.6x10^{-10}$	2.0
$\rightarrow Na + 2O_2$	$6x10^{-11}$	0±800	$6.0x10^{-11}$	3.0
# $NaO + H_2 \rightarrow NaOH + H$	$2.6x10^{-11}$	0±600	$2.6x10^{-11}$	2.0
# $NaO + H_2O \rightarrow NaOH + OH$	$2.2x10^{-10}$	0±400	$2.2x10^{-10}$	2.0
# $NaO + NO \rightarrow Na + NO_2$	$1.5x10^{-10}$	0±400	$1.5x10^{-10}$	4.0
# $NaO + CO_2 \xrightarrow{M} NaCO_3$	(See Table 2)			
$NaO + HCl \rightarrow$ products	$2.8x10^{-10}$	0±400	$2.8x10^{-10}$	3.0
# $NaO_2 + NO \rightarrow NaO + NO_2$			$<10^{-14}$	
# $NaO_2 + HCl \rightarrow$ products	$2.3x10^{-10}$	0±400	$2.3x10^{-10}$	3.0
$NaOH + HCl \rightarrow NaCl + H_2O$	$2.8x10^{-10}$	0±400	$2.8x10^{-10}$	3.0
# $NaOH + CO_2 \xrightarrow{M} NaHCO_3$	(See Table 2)			

[a] Units are cm^3/molecule-sec.

[b] f(298) is the uncertainty at 298K. To calculate the uncertainty at other temperatures, use the expression: $f(T) = f(298) \exp\left|\frac{\Delta E}{R}\left(\frac{1}{T} - \frac{1}{298}\right)\right|$. Note that the exponent is absolute value.

* Indicates a change from the previous Panel evaluation (JPL 85-37). Small round-off changes have been made for several entries in the table; these are not marked by asterisks.

\# Indicates a new entry that was not in the previous evaluation.

& Indicates a change in the Note.

Table E-2. Rate Constants for Three-Body Reactions

Reaction	Low Pressure Limit[a] $k_o(T) = k_o^{300}(T/300)^{-n}$		High Pressure Limit[b] $k_\infty(T) = k_\infty^{300}(T/300)^{-m}$	
	k_o^{300}	n	k_∞^{300}	m
& $O + O_2 \xrightarrow{M} O_3$	(6.0±0.5)(-34)	2.3±0.5	-	-
$O(^1D) + N_2 \xrightarrow{M} N_2O$	(3.5±3.0)(-37)	$0.6\pm^{2.0}_{0.6}$	-	-
* $H + O_2 \xrightarrow{M} HO_2$	(5.7±0.5)(-32)	1.6±0.5	(7.5±4.0)(-11)	0±1
$OH + OH \xrightarrow{M} H_2O_2$	(6.9±3.0)(-31)	$0.8\pm^{2.0}_{0.8}$	(1.0±0.5)(-11)	1±1
$O + NO \xrightarrow{M} NO_2$	(9.0±2.0)(-32)	1.5±0.3	(3.0±1.0)(-11)	0±1
$O + NO_2 \xrightarrow{M} NO_3$	(9.0±1.0)(-32)	2.0±1.0	(2.2±0.3)(-11)	0±1
$OH + NO \xrightarrow{M} HONO$	(7.0±2.0)(-31)	2.6±1.0	(1.5±1.0)(-11)	0.5±0.5
& $OH + NO_2 \xrightarrow{M} HNO_3$	(2.6±0.3)(-30)	3.2±0.7	(2.4±1.2)(-11)	1.3±1.3
* $HO_2 + NO_2 \xrightarrow{M} HO_2NO_2$	(1.8±0.3)(-31)	3.2±0.4	(4.7±1.0)(-12)	1.4±1.4
& $NO_2 + NO_3 \xrightarrow{M} N_2O_5$	(2.2±0.5)(-30)	4.3±1.3	(1.5±0.8)(-12)	0.5±0.5
$Cl + NO \xrightarrow{M} ClNO$	(9.0±2.0)(-32)	1.6±0.5	-	-
$Cl + NO_2 \xrightarrow{M} ClONO$	(1.3±0.2)(-30)	2.0±1.0	(1.0±0.5)(-10)	1±1
$\xrightarrow{M} ClNO_2$	(1.8±0.3)(-31)	2.0±1.0	(1.0±0.5)(-10)	1±1
$Cl + O_2 \xrightarrow{M} ClOO$	(2.0±1.0)(-33)	1.4±1.4	-	-
# $Cl + C_2H_2 \xrightarrow{M} ClC_2H_2$	(1.0±0.2)(-29)	3.5±0.5	(5.0±1.5)(-11)	2.6±0.5
# $ClO + ClO \xrightarrow{M} Cl_2O_2$	(4.0±2.0)(-32)	2.0±1.0	(1.0)(-11±1)	2±2
& $ClO + NO_2 \xrightarrow{M} ClONO_2$	(1.8±0.3)(-31)	3.4±1.0	(1.5±0.7)(-11)	1.9±1.9
$BrO + NO_2 \xrightarrow{M} BrONO_2$	(5.0±2.0)(-31)	2.0±2.0	(1.0±0.5)(-11)	1±1

Note: $k(Z) = k(M,T) = \left(\frac{k_o(T)[M]}{1 + k_o(T)[M]/k_\infty(T)}\right) 0.6^{\{1 + [\log_{10}(k_o(T)[M]/k_\infty(T))]^2\}^{-1}}$

The values quoted are suitable for air as the third body, M.

a Units are $cm^6/molecule^2$-sec

b Units are $cm^3/molecule$-sec

* Indicates a change from the previous Panel evaluation (JPL 85-37).

& Indicates a change in the note from the previous evaluation.

# Indicates a new entry that was not in the previous evaluation.

Table E-2. (Continued)

Reaction	Low Pressure Limit[a] $k_o(T) = k_o^{300}(T/300)^{-n}$		High Pressure Limit[b] $k_\infty(T) = k_\infty^{300}(T/300)^{-m}$	
	k_o^{300}	n	k_∞^{300}	m
$F + O_2 \xrightarrow{M} FO_2$	(1.6±0.8)(-32)	1.4±1.0	-	-
$F + NO \xrightarrow{M} FNO$	(5.9±3.0)(-32)	1.7±1.7	-	-
$F + NO_2 \xrightarrow{M}$ Products	(1.1±0.6)(-30)	2.0±2.0	(3.0±2.0)(-11)	1±1
$FO + NO_2 \xrightarrow{M} FONO_2$	(2.6±2.0)(-31)	1.3±1.3	(2.0±1.0)(-11)	1.5±1.5
& $CH_3 + O_2 \xrightarrow{M} CH_3O_2$	(4.5±1.5)(-31)	2.0±1.0	(1.8±0.2)(-12)	1.7±1.7
$CH_3O_2 + NO_2 \xrightarrow{M} CH_3O_2NO_2$	(1.5±0.8)(-30)	4.0±2.0	(6.5±3.2)(-12)	2±2
& $OH + SO_2 \xrightarrow{M} HOSO_2$	(3.0±1.0)(-31)	3.3±1.5	(1.5±0.5)(-12)	$0\pm^{0}_{2}$
$OH + C_2H_4 \xrightarrow{M} HOCH_2CH_2$	(1.5±0.6)(-28)	0.8±2.0	(8.8±0.9)(-12)	$0\pm^{0}_{2}$
$OH + C_2H_2 \xrightarrow{M} HOCHCH$	(5.5±2.0)(-30)	0.0±0.2	(8.3±1.0)(-13)	$-2\pm^{2}_{1}$
* $CF_3 + O_2 \xrightarrow{M} CF_3O_2$	(1.5±0.3)(-29)	4±2	(8.5±1.0)(-12)	1±1
$CFCl_2 + O_2 \xrightarrow{M} CFCl_2O_2$	(5.0±0.8)(-30)	2±2	(6.0±1.0)(-12)	1±1
$CCl_3 + O_2 \xrightarrow{M} CCl_3O_2$	(1.0±0.7)(-30)	2±2	(2.5±2)(-12)	1±1
$CFCl_2O_2 + NO_2 \xrightarrow{M} CFCl_2O_2NO_2$	(3.5±0.5)(-29)	4±2	(6.0±1.0)(-12)	2±2
$HS + NO \xrightarrow{M} HSNO$	(2.4±0.4)(-31)	3±1	(2.7±0.5)(-11)	$0\pm^{0}_{2}$
$Na + O_2 \xrightarrow{M} NaO_2$	(1.9±1)(-30)	1.1±0.5	(2.0±1.8)(-10)	0±1
# $NaO + O_2 \xrightarrow{M} NaO_3$	(3.5±0.7)(-30)	2±2	(5.7±3)(-10)	0±1
# $NaO + CO_2 \xrightarrow{M} NaCO_3$	(8.7±2.6)(-28)	2±2	(6.5±3)(-10)	0±1
# $NaOH + CO_2 \xrightarrow{M} NaHCO_3$	(1.3±0.3)(-28)	2±2	(6.8±4)(-10)	0±1

Note: $k(Z) = k(M,T) = \left(\frac{k_o(T)[M]}{1 + k_o(T)[M]/k_\infty(T)}\right) 0.6^{\{1 + [\log_{10}(k_o(T)[M]/k_\infty(T))]^2\}^{-1}}$

The values quoted are suitable for air as the third body, M.

a Units are $cm^6/molecule^2$-sec

b Units are $cm^3/molecule$-sec

* Indicates a change from the previous Panel evaluation (JPL 85-37).

& Indicates a change in the note from the previous evaluation.

# Indicates a new entry that was not in the previous evaluation.

E.6 Equilibrium Constants

E.6.1 Format

Some of the three-body reactions in Table E-2 form products which are thermally unstable at atmospheric temperatures. In such cases the thermal decomposition reaction may compete with other loss processes, such as photodissociation or radical attack. Table E-3 lists the equilibrium constants, K(T), for seven reactions which may fall into this category. The table has three column entries, the first two being the parameters A and B which can be used to express K(T):

$$K(T)/cm^3\ molecule^{-1} = A\ \exp(B/T),\ (200\ K < T < 300\ K)$$

The third column entry in Table E-3 is the calculated value of K at 298 K.

The data sources for K(T) are described in the individual notes to Table E-3. When values of the heats of formation and entropies of all species are known at the temperature T, we note that:

$$\log(K(T)/cm^3\ molecule^{-1}) = (\Delta S^o_T/2.303R) - (\Delta H^o_T/2.303RT) + \log(T) - 21.87$$

where the superscript "o" refers to a standard state of one atmosphere. In some cases K values were calculated from this equation, using thermochemical data. In other cases the K values were calculated directly from kinetic data for the forward and reverse reactions. When available, JANAF values were used for the equilibrium constants. The following equations were then used to calculate the parameters A and B:

$$B/^\circ K = 2.303(\log(K_{200}/K_{300}))(300x200)/(300-200)$$

$$= 1382(\log(K_{200}/K_{300}))$$

$$\log(A) = \log(K(T)) - B/2.303T$$

Table E-3. Equilibrium Constants

	Reaction	A/cm^3 molecule^{-1}	B±ΔB/^{o}K	K_{eq}(298 K)	f(298 K)[a]
	$HO_2 + NO_2 \rightarrow HO_2NO_2$	2.1×10^{-27}	10,900±1,000	1.6×10^{-11}	5
#	$NO + NO_2 \rightarrow N_2O_3$	3.0×10^{-27}	4,700±100	2.1×10^{-20}	2
*	$NO_2 + NO_3 \rightarrow N_2O_5$	1.1×10^{-27}	11,200±500	2.3×10^{-11}	2
	$Cl + O_2 \rightarrow ClOO$	2.3×10^{-25}	3,000±750	5.4×10^{-21}	20
	$ClO + O_2 \rightarrow ClO \cdot O_2$	$<2.9 \times 10^{-26}$	<5,000±1,500	$<5.6 \times 10^{-19}$	500
#	$ClO + ClO \rightarrow Cl_2O_2$	7.9×10^{-27}	8,600±2,500	2.7×10^{-14}	100
&	$F + O_2 \rightarrow FOO$	5.3×10^{-25}	7,600 -	6.3×10^{-14}	-
		1.1×10^{-25}	3,600 -	1.9×10^{-20}	-
	$CH_3O_2 + NO_2 \rightarrow CH_3O_2NO_2$	1.3×10^{-28}	11,200±1,000	2.7×10^{-12}	10

K/cm^3 molecule^{-1} = A exp(B/T) [200 < T/K < 300]

[a] f(298 K) is the uncertainty at 298 K. To calculate the uncertainty at other temperatures, use the expression: $f(T) = f(298\ K) \exp(\Delta B \left| \frac{1}{T} - \frac{1}{298} \right|)$.

* Indicates a change from the previous Panel evaluation (JPL 85-37).

& Indicates a change in the note from the previous evaluation.

# Indicates a new entry that was not in the previous evaluation.

E.7 Photochemical Data

E.7.1 Discussion of Format and Error Estimates

In Table E-4 we present a list of photochemical reactions considered to be of stratospheric interest. The absorption cross sections of O_2 and O_3 largely determine the extent of penetration of solar radiation into the stratosphere and troposphere. The photodissociation of NO in the O_2 Schumann-Runge band spectral range is another important process requiring special treatment and is not discussed in this evaluation.

For some other species having highly structured spectra, such as CS_2 and SO_2, some comments are given in the text of the complete evaluation, but the photochemical data are not presented. The species CH_2O, NO_2, NO_3 and OClO also have complicated spectra, but in view of their importance for atmospheric chemistry a sample of the data is presented in the evaluation; for more detailed information on their high-resolution spectra and temperature dependence, the reader is referred to the original literature.

Table E-5 gives recommended reliability factors for some of the more important photochemical reactions. These factors represent the combined uncertainty in cross sections and quantum yields, taking into consideration the atmospherically important wavelength regions, and they refer to the total dissociation rate regardless of product identity (except in the case of $O(^1D)$ production from photolysis of O_3).

Table E-4. Photochemical Reactions of Stratospheric Interest

&	$O_2 + h\nu \rightarrow O + O$		$CCl_4 + h\nu \rightarrow$ products
*	$O_3 + h\nu \rightarrow O_2 + O$		$CCl_3F + h\nu \rightarrow$ products
	$O_3 + h\nu \rightarrow O_2 + O(^1D)$		$CCl_2F_2 + h\nu \rightarrow$ products
*	$HO_2 + h\nu \rightarrow$ products		$CHClF_2 + h\nu \rightarrow$ products
	$H_2O + h\nu \rightarrow H + OH$	(1)	$CH_3Cl + h\nu \rightarrow$ products
	$H_2O_2 + h\nu \rightarrow OH + OH$		$CCl_2C + h\nu \rightarrow$ products
	$NO + h\nu \rightarrow N + O$		$CClFO + h\nu \rightarrow$ products
*	$NO_2 + h\nu \rightarrow NO + O$		$CF_2O + h\nu \rightarrow$ products
*	$NO_3 + h\nu \rightarrow$ products		$CH_3CCl_3 + h\nu \rightarrow$ products
	$N_2O + h\nu \rightarrow N_2 + O(^1D)$		# $CBrClF_2 + h\nu \rightarrow$ products
	$N_2O_5 + h\nu \rightarrow$ products		# $CBrF_3 + h\nu \rightarrow$ products
	$NH_3 + h\nu \rightarrow NH_2 + H$	(1)	$BrO + h\nu \rightarrow Br + O$
	$HNO_2 + h\nu \rightarrow OH + NO$		$BrONO_2 + h\nu \rightarrow$ products
	$HNO_3 + h\nu \rightarrow OH + NO_2$		$HF + h\nu \rightarrow H + F$
	$HNO_4 + h\nu \rightarrow$ products		$CO + h\nu \rightarrow C + O$ (1)
	$Cl_2 + h\nu \rightarrow Cl + Cl$		$CO_2 + h\nu \rightarrow CO + O$ (1)
	$ClO + h\nu \rightarrow Cl + O$		$CH_4 + h\nu \rightarrow$ products (2)
	$ClOO + h\nu \rightarrow$ products		$CH_2O \rightarrow$ products
*	$OClO + h\nu \rightarrow O + ClO$		$CH_3OOH + h\nu \rightarrow$ products
	$ClO_3 + h\nu \rightarrow$ products		$HCN + h\nu \rightarrow$ products
#	$Cl_2O_2 + h\nu \rightarrow$ products		$CH_3CN + h\nu \rightarrow$ products
	$HCl + h\nu \rightarrow H + Cl$		$SO_2 + h\nu \rightarrow SO + O$
	$HOCl \rightarrow OH + Cl$		$OCS + h\nu \rightarrow CO + S$
*	$ClNO + h\nu \rightarrow Cl + NO$		$H_2S + h\nu \rightarrow HS + H$ (2)
	$ClNO_2 + h\nu \rightarrow$ products		$CS_2 + h\nu \rightarrow$ products
	$ClONO + h\nu \rightarrow$ products		# $NaCl + h\nu \rightarrow Na + Cl$
	$ClONO_2 + h\nu \rightarrow$ products		$NaOH + h\nu \rightarrow Na + OH$

(1) Hudson and Kieffer, CIAP Monograph 1, 5-156 (1975)
(2) Turco, Geophys. Surveys 2, 153 (1975)
New entry
* Indicates a change in the recommendation from the previous evaluation.
& Indicates a change in the note.

Table E-5. Combined Uncertainties for Cross Sections and Quantum Yields

Species	Uncertainty
O_2 (Schumann-Runge bands)	1.4
O_2 (Continua)	1.3
O_3	1.1
$O_3 \rightarrow O(^1D)$	1.4
NO_2	1.3
NO_3	2.0
N_2O	1.2
N_2O_5	2.0
H_2O_2	1.4
HNO_3	1.3
HO_2NO_2	2.0
CH_2O	1.4
HCl	1.1
HOCl	1.4
$ClONO_2$	1.3
CCl_4	1.1
CCl_3F	1.1
CCl_2F_2	1.1
CH_3Cl	1.1
CF_2O	2.0
CH_3OOH	1.4
$BrONO_2$	1.4

SECTION E - APPENDIX

GAS PHASE ENTHALPY DATA

The following data are adapted mainly from CODATA (1984), although a few entries have been updated.

MOLECULE	$\Delta H_f(298)$ (Kcal/mol)	MOLECULE	$\Delta H_f(298)$ (Kcal/mol)	MOLECULE	$\Delta H_f(298)$ (Kcal/mol)	MOLECULE	$\Delta H_f(298)$ (Kcal/mol)
H	52.1	CH_3O	3.5	HSO	-1±2	CCl_3	19±1
H_2	0.00	CH_3O_2	3.8±2	HSO_3	-92±2	CCl_4	-22.9
O	59.57	CH_2OH	-6.2	CS	65	$CHCl_3$	-24.6
$O(^1D)$	104.9	CH_3OH	-48.0	CS_2	28.0	CH_2Cl	28±1
O_2	0.00	CH_3OOH	-31.3	CH_3S	33±2	CH_2Cl_2	-22.8
$O_2(^1$-DELTA)	22.5	CH_3ONO	-15.6	CH_3SCH_3	-8.9	CH_3Cl	-19.6
$O_2(^1$-SIGMA)	37.5	CH_3ONO_2	-28.6	CH_3SSCH_3	-5.8	ClCO	-4.1
O_3	34.1	$CH_3O_2NO_2$	-10.6±2	OCS	-34	$COCl_2$	-52.6
HO	9.3	C_2H	135	F	18.98	CFCl	7±6
HO_2	3±1	C_2H_2	54.35	F_2	0.00	CH_2F	-8±2
H_2O	-57.81	C_2H_3	68.1	HF	-65.34	$CHCl_2$	23.5±1
H_2O_2	-32.6	C_2H_4	12.45	HOF	-23.4±1	$CFCl_2$	-22.9
N	113.00	C_2H_5	28.4	FO	26±2	$CFCl_3$	-68.1
N_2	0.00	C_2H_6	-20.0	FO_2	12±3	CF_2Cl	-64.3
NH	82.0	CH_2CN	58.6	FONO	-15.2	CF_2Cl_2	-117.9
NH_2	45.3	CH_3CN	19.1	FNO_2	-25.4	CF_3Cl	-169.2
NH_3	-10.98	CH_2CO	-14.23	$FONO_2$	2.4	$CHFCl_2$	-68.1
NO	21.57	CH_3CO	-5.8	CF_2	-44±2	CHF_2Cl	-115.6
NO_2	7.9	CH_3CHO	-39.7	CF_3	-112±1	COFCl	-102±8
NO_3	17±1	C_2H_5O	-4.1	CF_4	-223.0	C_2Cl_4	-3.0
N_2O	19.61	CH_2CH_2OH	-13.2	FCO	-41±14	C_2HCl_3	-1.9
N_2O_3	19.8	C_2H_5OH	-56.2	COF_2	-151.7	CH_2CCl_3	11±7
N_2O_4	2.2	CH_3CO_2	-49.6	Cl	28.9	CH_3CCl_3	-34.0
N_2O_5	2.7	$C_2H_5O_2$	-1.8	Cl_2	0.00	Br	26.7
HNO	23.8	CH_3OOCH_3	-30.0	HCl	-22.07	Br_2	7.39
HNO_2	-19.0	C_3H_5	39.4	ClO	24.4	HBr	-8.70
HNO_3	-32.3	C_3H_6	4.8	ClOO	22.5±1	HOBr	-19±2
HO_2NO_2	-11±2	n-C_3H_7	22.6±2	OClO	23±2	BrO	30
CH	142.0	i-C_3H_7	18.2±2	$ClOO_2$	>13.4	BrNO	19.7
CH_2	92.3	C_3H_8	-24.84	ClO_3	37	$BrONO_2$	5±7
CH_3	35.1	C_2H_5CHO	-44.8	Cl_2O	19.5	BrCl	3.5
CH_4	-17.88	CH_3COCH_3	-51.9	Cl_2O_2	31±5	CH_2Br_2	-2.6±2
CN	104.0	CH_3CHCH_2OH	-18.0	HOCl	-18.6±3	CH_2Br	41±2
HCN	32.3	S	66.22	ClNO	12.4	CH_3Br	-9.0
NCO	38	S_2	30.72	$ClNO_2$	3.0	$CHBr_2$	45±3
CO	-26.42	HS	34±1	ClONO	19.8	I	25.52
CO_2	-94.07	H_2S	-4.93	$ClONO_2$	6.3	I_2	14.92
HCO	9.0	SO	1.2	FCl	-12.1	HI	6.30
CH_2O	-26.0	SO_2	-70.96	CCl	120±5	IO	41.1
HCOOH	-90.5	SO_3	-94.6	CCl_2	56.9±5	INO	29.0
						INO_2	14.4

SECTION F

CONTRIBUTORS

F.1. OZONE TRENDS REPORT

PANEL

Albritton, D.	NOAA Aeronomy Laboratory, Boulder, CO
Bloomfield, P	North Carolina State University, Raleigh, NC
Bojkov, R.	Atmospheric Environment Service, Downsview, Ontario, Canada
Ehhalt, D.	Institut fur Chemie, Julich, West Germany
Fraser, P.	CSIRO, Aspendale, Australia
Gille, J.	National Center for Atmospheric Research, Boulder, CO
Hartmann, D.	University of Washington, Seattle, WA
Hudson, R.	NASA Goddard Space Flight Center, Greenbelt, MD
Isaksen, I.S.A.	University of Oslo, Oslo, Norway
Johnston, H.	University of California, Berkeley, CA
Mahlman, J.	NOAA Geophysical Fluid Dynamics Lab, Princeton, NJ
Margitan, J.J.	Jet Propulsion Lab/NASA Headquarters, Washington, DC
McCormick, M.P.	NASA Langley Research Center, Hampton, VA
McFarland, M.	E.I. Du Pont de Nemours & Company, Wilmington, DE
Ormond, F., **Executive Secretary**,	ORI, Inc/NASA, Washington, DC
Rodgers, C.	Oxford University, Oxford, UK
Rowland, F. S.	University of California, Irvine, CA
Schoeberl, M.	NASA/Goddard Space Flight Center, Greenbelt, MD
Stolarski, R., **Vice Chairman**,	NASA/Goddard Space Flight Center, Greenbelt, MD
Turco, R.	R&D Associates, Marina del Rey, CA
Watson, R. T., **Chairman**,	NASA Headquarters, Washington, DC

REVIEWERS

Barnett, J.	Oxford University, Oxford, UK
Cicerone, R.	NCAR, Boulder, CO
Fels, S.	NOAA Geophysical Fluid Dynamics Laboratory, Princeton, NJ
Krull, N.	Federal Aviation Administration, Washington, DC
Kurylo, M.J.	NBS/NASA Headquarters, Washington, DC
McIntyre, M.	University of Cambridge, Cambridge, UK
Megie, G.	Service d'Aeronomie, CNRS, Verrieres, Le Bussion, France
Prather, M. J.	Goddard Institute for Space Studies, N.Y., NY
Rodhe, H.	University of Stockholm, Stockholm, Sweden
Schmeltekopf, A.	NOAA, Environmental Research Laboratory, Boulder, CO
Sundararaman, N.	World Meteorological Organization, Geneva, Switzerland
Visconti, G.	University Aquila, Aquila, Italy
Wofsy, S	Harvard University, Cambridge, MA

WORKING GROUPS

Executive Summary

Robert T. Watson, NASA Headquarters, Washington, DC, Chairman

Ozone Trend Panel Members
Ozone Trend Panel Reviewers

1 - Introduction

Robert T. Watson, Chairman, Ozone Trends Panel

2 - Spacecraft Instrument Calibration and Stability

J. Gille, Chairman, National Center for Atmospheric Research, Boulder, CO

P. Feldman	Johns Hopkins University, Baltimore, MD
R. Hudson	NASA GSFC, Greenbelt, MD
J. Lean	Naval Research Laboratory, Washington, DC
R. Madden	National Bureau of Standards, Gaithersburg, MD
L. McMaster	NASA Langley Research Center, Hampton, VA
G. Mount	NOAA, Boulder, CO
G. Rottman	LASP, University of Colorado, Boulder, CO
P.C. Simon	Institute d'Aeronomie Spatiale de Belgique, Brussels, Belgium

3 - Information Content of Ozone Retrieval Algorithms

C. Rodgers, Chairman, Oxford University, Oxford, England

P.K. Bhartia	Science Applications Research, Lanham, MD
W.P. Chu	NASA Langley Research Center, Hampton, VA
R. Curran	NASA Headquarters, Washington, DC
J. DeLuisi	NOAA, Boulder, CO
J. Gille	NCAR, Boulder, CO
R. Hudson	NASA Goddard Space Flight Center, Greenbelt, MD
C. Mateer	Atmospheric Environment Service, Downsview, Ontario, Canada
D. Rusch	University of Colorado, Boulder, CO
R.J. Thomas	University of Colorado, Boulder, CO
R. Turco	R&D Associates, Marina del Rey, CA
W. Wiscombe	NASA Goddard Space Flight Center, Greenbelt, MD

4 - Trends in Total Column Ozone Measurements

F.S. Rowland, Chairman, University of California, Irvine

J. Angell	NOAA, Rockville, MD
W. Attmannspacher	Deutscher Wetterdienst, Hohenpeissenberg, FRG
P. Bloomfield	North Carolina State University, Raleigh, NC
R. Bojkov	Atmospheric Environment Service, Downsview, Ontario, Canada
N. Harris	University of CA, Irvine
W. Komyhr	NOAA, Boulder, CO
M. McFarland	E.I. DuPont de Nemours & Company, Wilmington, DE
R. McPeters	NASA Goddard Space Flight Center, Greenbelt, MD
R. Stolarski	NASA Goddard Space Flight Center, Greenbelt, MD

5 - Trends in Ozone Profile Measurements

H. Johnston, Chairman, University of California, Berkeley

A. Aikin	NASA Goddard Space Flight Center, Greenbelt, MD
R. Barnes	Chemal, Inc., Wallops Island, VA
S. Chandra	NASA Goddard Space Flight Center, Greenbelt, MD
D. Cunnold	Georgia Institute of Technology, Atlanta, GA
J. DeLuisi	NOAA, Boulder, CO
J. Gille	NCAR, Boulder, CO
R. Hudson	NASA Goddard Space Flight Center, Greenbelt, MD
A.J. Miller	NOAA, National Meteorological Service, Washington, DC
M.P. McCormick	NASA Langley Research Center, Hampton, VA
L. McMaster	NASA Langley Research Center, Hampton, VA
W. Planet	NOAA NESDIS, Washington, DC
E. Remsberg	NASA Langley Research Center, Hampton, VA
D. Rusch	University of Colorado, Boulder, CO
C. Trepte	STX, Inc., Hampton, VA
R. Veiga	NRC/NSF, Hampton, VA
P. Wang	STC, Hampton, VA
C. Wellemeyer	ST Systems, Lanham, MD
J. Zawodny	NASA Langley Research Center, Hampton, VA

6 - Trends in Stratospheric Temperature

M. Schoeberl, Chairman, NASA Goddard Space Flight Center, Greenbelt, MD

J. Angell	NOAA, Rockville, MD
J. Barnett	Oxford University, Oxford, England
B. Boville	NCAR, Boulder, CO
S. Chandra	NASA Goddard Space Flight Center, Greenbelt, MD
S. Fels	NOAA, Geophysical Fluid Dynamics Laboratory, Princeton, NJ
E. Fleming	ARC Corporation, Landover, MD
K. Labitzke	Free University of Berlin, FRG
A.J. Miller	NOAA, Rockville, MD
J. Nash	British Meteorological Office, England
P.A. Newman	NASA Goddard Space Flight Center, Greenbelt, MD
V. Ramaswamy	Princeton University, Princeton, NJ
J. Rosenfield	NASA Goddard Space Flight Center, Greenbelt, MD
F. Schmidlin	NASA Wallops Island, VA
M. Schwartzkopf	NOAA, Geophysical Fluid Dynamics Laboratory, Princeton, NJ
K. Shine	Oxford University, Oxford, England

7 - Theory and Observations

I.S.A. Isaksen, Chairman, University of Oslo, Oslo, Norway

R. Eckman	University of Cambridge, Cambridge, England
A. Lacis	Goddard Institute for Space Studies, NY, NY
M. Ko	AER, Inc, Cambridge, MA
M. Prather	Goddard Institute for Space Studies, NY, NY
J. Pyle	University of Cambridge, Cambridge, England
H. Rodhe	University of Stockholm, Stockholm, Sweden
F. Stordal	University of Oslo, Oslo, Norway
R. Stolarski	NASA Goddard Space Flight Center, Greenbelt, MD
R. Turco	R&D Associates, Marina del Rey, CA
D. Wuebbles	Lawrence Livermore National Laboratories, Livermore, CA

8 - Trends in Source Gases

D. Ehhalt, Chairman, Institute for Chemistry, Julich, FRG
P. Fraser, Co-Chairman, CSIRO, Aspendale, Australia

D. Albritton	NOAA, Boulder, CO
R.J. Cicerone	NCAR, Boulder, CO
M.A.K. Khalil	Oregon Graduate Center, Beaverton, OR
M. Legrand	CNRS, France
Y. Makide	University of Tokyo, Tokyo, Japan
F.S. Rowland	University of CA, Irvine
L.P. Steele	CIRES, University of Colorado/NOAA, Boulder, CO
R. Zander	University of Liege, Liege-Ougree, Belgium

9 - Trends in Stratospheric Minor Constituents

R. Stolarski, Chairman, NASA Goddard Space Flight Center, Greenbelt, MD

W. P. Chu	NASA Langley Research Center, Hampton, VA
M. T. Coffey	NCAR, Boulder, CO
W.S. Heaps	NASA Goddard Space Flight Center, Greenbelt, MD
J.A. Kaye	NASA Goddard Space Flight Center, Greenbelt, MD
M.P. McCormick	NASA Langley Research Center, Hampton, VA
R. Zander	University of Liege, Liege-Ougree, Belgium

10 - Trends in Aerosol Abundances and Distributions

R.P. Turco, Chairman, R&D Associates, Marina del Rey, CA
M.P. McCormick, Co-Chairman, NASA Langley Research Center, Hampton, VA

R.T. Clancy	LASP, University of Colorado, Boulder, CO
R. Curran	NASA Headquarters, Washington, DC
J. DeLuisi	NOAA/ERL, Boulder, CO
P. Hamill	San Jose State University, San Jose, CA
G. Kent	STC, Hampton, VA
J.M. Rosen	University of Wyoming, Laramie, WY
O.B. Toon	NASA Ames, Moffett Field, CA
G. Yue	NASA Langley Research Center, Hampton, VA

11 - Observations and Theories Related to Antarctic Ozone Changes

D. Hartmann, Co-Chairman, University of Washington, Seattle, WA
R.T. Watson, Co-Chairman, NASA Headquarters, Washington, DC

R.A. Cox	AERE, Harwell, England
C. Kolb	Aerodyne Research, Billerica, MA
J. Mahlman	NOAA Geophysical Fluid Dynamics Laboratory, Princeton, NJ
M. McElroy	Harvard University, Cambridge, MA
A. Plumb	CSIRO, Aspendale, Australia
V. Ramanathan	University of Chicago, Chicago, IL
M. Schoeberl	NASA Goddard Space Flight Center, Greenbelt, MD
S. Solomon	NOAA, Boulder, CO
N.D. Sze	AER, Inc., Cambridge, MA
A. Tuck	NOAA, Boulder, CO

Appendix - Statistical Approaches to Ozone Trend Detection

P. Bloomfield, Chairman. North Carolina State University, Raleigh, NC

D.R. Brillinger	University of CA, Berkeley, CA
D. Nychka	North Carolina State University, Raleigh, NC
R. Stolarski	NASA Goddard Space Flight Center, Greenbelt, MD

F.2. PREDICTIONS OF FUTURE OZONE CHANGE

AD HOC THEORY PANEL

Michael J. Prather, Chairman, Goddard Institute for Space Studies, NY

D. Fisher	E.I. Dupont de Nemours & Company, Wilmington, DE
R. Garcia	National Center for Atmospheric Research, Boulder, CO
P. Guthrie	NASA Goddard Space Flight Center, Greenbelt, MD
M. Hitchman	National Center for Atmospheric Research, Boulder, CO
I. S. A. Isaksen	University of Oslo, Oslo, Norway
C. Jackman	NASA Goddard Space Flight Center, Greenbelt, MD
M. Ko	Atmospheric and Environmental Research, Inc., Cambridge, MA
J. Pyle	University of Cambridge, Cambridge, England
R. Seals	NASA Langley Research Center, Hampton, VA
N. D. Sze	Atmospheric and Environmental Research, Inc., Cambridge, MA
D. Wuebbles	Lawrence Livermore National Laboratory, Livermore, CA
Y. Yung	California Institute of Technology, Pasadena, CA

F.3. CHEMICAL KINETICS AND PHOTOCHEMICAL DATA FOR USE IN STRATOSPHERIC MODELING

NASA PANEL FOR DATA EVALUATION

W. B. DeMore, Chairman, Jet Propulsion Laboratory, Pasadena, CA

D. M. Golden	SRI International, Menlo Park, CA.
R. F. Hampson	National Bureau of Standards, Gaithersburg, MD
C. J. Howard	NOAA Environmental Research Laboratory, Boulder, CO
M. J. Kurylo	National Bureau of Standards/NASA Hqts., Washington, DC
M. J. Molina	Jet Propulsion Laboratory, Pasadena, CA
A. R. Ravishankara	NOAA Environmental Research Laboratory, Boulder, CO
S. P. Sander	Jet Propulsion Laboratory, Pasadena, CA

SECTION G

LIST OF TABLES AND FIGURES

G.1: LIST OF FIGURES

C-3

G.2: LIST OF TABLES

NASA
National Aeronautics and Space Administration

Report Documentation Page

1. Report No.	2. Government Accession No.	3. Recipient's Catalog No.
NASA RP-1208		

4. Title and Subtitle	5. Report Date
PRESENT STATE OF KNOWLEDGE OF THE UPPER ATMOSPHERE 1988: AN ASSESSMENT REPORT	August 1988
	6. Performing Organization Code: EE

7. Author(s)	8. Performing Organization Report No.
R.T. Watson and Ozone Trends Panel, M.J. Prather and Ad Hoc Theory Panel, and M.J. Kurylo and NASA Panel for Data Evaluation	
	10. Work Unit No.

9. Performing Organization Name and Address	11. Contract or Grant No.
NASA Office of Space Science and Applications Earth Science and Applications Division	
	13. Type of Report and Period Covered: Reference Publication

12. Sponsoring Agency Name and Address	14. Sponsoring Agency Code
National Aeronautics and Space Administration Washington, D.C. 20546	

15. Supplementary Notes

16. Abstract

This document is issued in response to the Clean Air Act Amendments of 1977, Public Law 95-95, which mandates that the National Aeronautics and Space Administration (NASA) and other key agencies submit biennial reports to Congress and the Environmental Protection Agency. NASA is charged with the responsibility to report on the state of our knowledge of the Earth's upper atmosphere, particularly the stratosphere. This is the sixth ozone assessment report submitted to Congress and the concerned regulatory agencies. Part I of this report contains an outline of the NASA Upper Atmosphere Research Program and summaries of the individual research efforts supported during the last two years.

This report presents an assessment of the state of knowledge as of March 15, 1988 when the Ozone Trends Panel, organized by NASA and co-sponsored by the World Meteorological Organization, the National Oceanic and Atmospheric Administration, the Federal Aviation Administration and the United Nations Environment Program released an executive summary of its findings from a critical in-depth study involving over 100 scientists from 12 countries. Chapter summaries of the international Ozone Trends Panel Report form the major part of this report. Two other sections are Model Predictions of Future Ozone Change and Chemical Kinetics and Photochemical Data for Use in Stratospheric Modeling. Each of these sections and the report in its entirety were peer reviewed.

17. Key Words (Suggested by Author(s))	18. Distribution Statement
stratosphere, ozone, chlorofluorocarbons, model results, assessment, Antarctic ozone hole.	Unclassified - Unlimited Subject Category 46

19. Security Classif. (of this report)	20. Security Classif. (of this page)	21. No. of pages	22. Price
Unclassified	Unclassified	208	A10

NASA FORM 1626 OCT 86

Available from the National Technical Information Service, Springfield, VA 22161

NASA-Langley, 1988

National Aeronautics and
Space Administration
Code NTT-4

Washington, D.C.
20546-0001

SPECIAL FOURTH-CLASS RATE
POSTAGE & FEES PAID
NASA
Permit No. G-27

NASA